# CONSTRUCTIVE TISSUE REMODELING OF BIOLOGIC SCAFFOLDS: A PHENOMENON ASSOCIATED WITH SCAFFOLD CHARACTERISTICS AND DISTINCTIVE MACROPHAGE PHENOTYPES

by

Bryan Nicklaus Brown

Bachelor of Science in Mechanical Engineering, University of Pittsburgh, 2005

Submitted to the Graduate Faculty of

Swanson School of Engineering in partial fulfillment

of the requirements for the degree of

Doctor of Philosophy

University of Pittsburgh

2010

UNIVERSITY OF PITTSBURGH

SWANSON SCHOOL OF ENGINEERING

This dissertation was presented

by

Bryan Nicklaus Brown

It was defended on

July 14th, 2010

and approved by

Thomas W. Gilbert, PhD, Assistant Professor, Department of Surgery

Fadi G. Lakkis, MD, Professor, Department of Surgery

Michael T. Lotze, MD, Professor, Department of Surgery

William R. Wagner, PhD, Professor, Department of Bioengineering

Dissertation Director: Stephen F. Badylak, DVM, PhD, MD, Professor, Department of Surgery

**CONSTRUCTIVE TISSUE REMODELING OF BIOLOGIC SCAFFOLDS: A PHENOMENON ASSOCIATED WITH SCAFFOLD CHARACTERISTICS AND DISTINCTIVE MACROPHAGE PHENOTYPES**

Bryan Nicklaus Brown, PhD

University of Pittsburgh, 2010

Scaffolds composed of extracellular matrix (ECM) have been shown to promote formation of site-specific, functional host tissue following implantation in a number of preclinical and clinical settings. However, the exact mechanisms by which ECM scaffolds are able to promote this type of "constructive tissue remodeling" are unknown. Further, the ability of ECM scaffolds to promote constructive tissue remodeling appears to be dependent on the methods used in their production and the applications in which they are utilized. Therefore, a comprehensive understanding of ECM scaffold characteristics and their effects upon the host response and subsequent tissue remodeling outcome is essential to the design of intelligent scaffolds for specific clinical applications.

The present work investigated the effects of tissue source and chemical cross-linking upon the resulting ECM scaffolds, showing that ECM scaffold materials have distinct ultrastructural and compositional characteristics which are dependant on the anatomic location from which the scaffolds are derived and the methods used in their production. These characteristics were associated with distinct patterns of cell behavior *in vitro.*

Distinct tissue remodeling outcomes were observed following implantation of a subset of these scaffold materials in a rat abdominal wall musculature reconstruction model. Acellular, non-cross-linked ECM was associated with constructive tissue remodeling while scaffolds that

contained cellular components or were chemically cross-linked resulted in dense connective tissue deposition or encapsulation, respectively.

Despite differences in the tissue remodeling outcome, a histologically similar population of macrophages was observed following implantation in each of these cases. Therefore, the phenotype of the macrophage population participating in the host response was investigated. It was shown that scaffolds which resulted in constructive tissue remodeling were associated with an increase in the M2 (regulatory, pro-wound healing) macrophage population, while scaffolds which resulted in the deposition of dense collagenous connective tissue or encapsulation were associated with an increase in the M1 (pro-inflammatory) macrophage population, suggesting that different macrophage populations are associated with different tissue remodeling outcomes following ECM scaffold implantation. *In vitro* work showed that M1 and M2 macrophages had distinct paracrine effects upon other cell populations, further suggesting distinct roles for M1 and M2 macrophages in tissue remodeling.

## TABLE OF CONTENTS

## LIST OF TABLES

## LIST OF FIGURES

## PREFACE

This dissertation is dedicated to my wife, Meg Goehrig for all her love and support. Thank you for understanding all of the long hours, conference trips, and stressful days. I love you. Thank you as well to my family and friends for their love and encouragement. It is their support which carried me through everything.

Thank you to my committee members: Stephen Badylak, Thomas Gilbert, Fadi Lakkis, Michael Lotze, and William Wagner. Each of you has helped to shape the work contained within this dissertation. I appreciate all of your advice, support, and willingness to help me get what I wanted out of my graduate studies. Dr. Badylak, thank you for taking me in to your lab and it has been great to work with you for the last 8 years, both as an undergraduate and a graduate student. You have provided me with every opportunity I could have hoped for during the course of my graduate studies.

I would like to thank everyone who has helped me in the Badylak Lab over the many years. Not only for your help with my work, but also for making the lab a fun place to work. Special thanks to Ann Stewart-Akers and John Freund for keeping the lab running and well stocked. Thank you to Thomas Gilbert and Danny Freytes for their help with material production. Thank you to Scott Johnson and Hongbin Jiang for their help with my many rat surgeries. Thank you to Li Zhang for her help with Boyden chamber assays. Thank you to Neill Turner for helping me with microscopy. Thank you to Jennifer DeBarr and Deanna Rhodes for their help with histology. Thank you to to Rena Kasick and Kathryn Kukla for their help with

summer projects. And, a special thank you to Renee Atikinson, Dawn Robertson, Jocely Runyon, and Eve Blasko for their help with my many requests and for helping keep track of Dr. Badylak.

I would like to thank Buddy Ratner, David Castner, and Chris Barnes of the University of Washington for their help with the time of flight work. I would like to thank Masauki Yamato and Teruo Okano of Tokyo Womens Medical University for accepting me into their lab for a summer fellowship and Dehua Chang for helping me with projects while I was there. Thank you to Donna Stolz, Mark Rubin, Ana Bursick and Mara Sullivan of the Center for Biologic Imaging at the University of Pittsburgh for all of their help with SEM. Thank you to Joe Hanke, Terri Gasser, Buffie Kerstetter, Mike Firda, and Shawn Bengston of the McGowan Institute Animal Facility.

I would like to say a special thank you to Harvey Borovetz, who has always been there to support me and to provide advice on many subjects. Thank you to the Department of Bioengineering staff Lynette Spataro, Joan Williamson, Judy Repp, Jason Vey, and Glenn Peterson for your assistance.

I would also like to thank the National Science Foundation and the National Institutes of Health for providing me with financial support for my graduate studies.

To everyone listed here, and to anyone who I may have forgotten, thank you for everything.

# 1.0 INTRODUCTION AND SPECIFIC AIMS

The work presented in this dissertation examines the effects of the tissue source and methods used to produce extracellular matrix (ECM) scaffold materials upon the structural and compositional characteristics of the resultant scaffold. The effects of these characteristics upon the ability of the material to support and modulate cell growth *in vitro* as well as to act as an inductive template for the formation of functional site-specific host tissues *in vivo* are also investigated. Lastly, the role of macrophages in determining the ability of an ECM based scaffold material to promote the observed, "constructive tissue remodeling", outcome was investigated. The introductory materials below are intended to provide background on ECM scaffold materials, their production and their use in tissue engineering and regenerative medicine. Additional background is provided on the host response following tissue injury and its role in tissue engineering and regenerative medicine, and on selected aspects of the role of macrophages in the host response and tissue remodeling which occurs following injury.

## 1.1 EXTRACELLULAR MATRIX AS A SCAFFOLD FOR TISSUE ENGINEERING AND REGENERATIVE MEDICINE

The ECM is composed of the secreted molecules produced by the resident cells of each tissue or organ. Thus, the composition and three-dimensional ultrastructure of the ECM is highly related to resident cell phenotype and the required functions of the tissue or organ from which it is

derived. The exact composition of the ECM is dependant on a number of factors that influence resident cell phenotype including mechanical forces, biochemical milieu, oxygen requirements, pH, and gene expression patterns. The ECM, in turn, influences the phenotype, migration, and proliferation of resident cells, and serves as a medium for signal transfer between cells (2-5). For these reasons, the ECM is considered to be in a state of dynamic reciprocity (3) with the resident cell population and to play an important role in normal tissue and organ morphogenesis (6).

The components of the ECM include collagen, fibronectin, elastin, laminin, glycosaminoglycans, and growth factors, among others. Collagen comprises nearly 90% of the dry weight of most ECM (7), with collagen type I being the predominant type found in most tissues and organs. Other types of collagen are known to exist within the ECM depending on the tissue or organ of interest (7). Among them are collagen type II, III, IV, V, VI, and VII (1, 8-10). Each collagen type plays a specific role in maintaining the structure and function of the tissue or organ of interest. Collagen can also be associated with a number of other proteins and molecules related to the structural and functional requirements of the tissue. Among the functional molecules found within ECM are growth factors including vascular endothelial growth factor (VEGF), members of the fibroblast growth factor (FGF) family, stromal derived growth factor (SDF-1), epidermal growth factor (EGF), transforming growth factor beta (TGF-β), keratinocytes growth factor (KGF), hepatocyte growth factor (HGF), platelet derived growth factor (PDGF), and bone morphogenetic protein (BMP) (11-13). The exact type and amount of each component within the ECM are highly tissue dependant and related to the specific functional requirements of the tissue.

Individual components of the ECM, such as collagen I, collagen IV, laminin, and fibronectin, have been used as surface coatings for biomaterials to facilitate cell attachment and

growth and to promote biocompatibility (14, 15). The advantages of using whole, intact, acellular, non-cross-linked ECM as a scaffold for cell growth or tissue reconstruction as opposed to individual components of the ECM include the presence of tissue-specific ECM constituents in the same relative amounts that exist in nature and in their native ultrastructure. In some respects, an ECM scaffold can be thought of as a reservoir of tissue-specific structural and functional proteins. Many groups have attempted to create ECM analogues using individual ECM components and/or synthetic materials (16-18); however, the diversity and complex structure of the molecules that make up the ECM predict the difficulty of creating such a scaffold *in vitro*. It is for these reasons that the isolation of ECM through the decellularization of tissues and organs is an effective method for the production of materials to be used in tissue engineering and regenerative medicine approaches to tissue reconstruction.

ECM based scaffold materials have been derived from numerous xenogeneic and allogeneic source tissues and organs including cardiac tissues, blood vessels, skin, nerves, skeletal muscle, tendons, ligaments, small intestine, urinary bladder, trachea, and liver (Table 1). These scaffolds have been used successfully as templates for tissue reconstruction in a similarly wide variety of preclinical tissue engineering and regenerative medicine applications including orthopedic, esophageal, tracheal, cartilage, lower urinary tract, dermal, cardiovascular, central nervous system, and skeletal muscle (Table 1). Biologic scaffolds composed of various types of ECM are also commercially available for use in human clinical applications, and ECM scaffolds derived from porcine small intestinal submucosa (SIS) alone have been implanted in more than 2 million human patients to date. A partial list of the sources from which ECM scaffold materials have been derived, the configurations into which they have been processed, and the tissue engineering and regenerative medicine applications in which they have been used is provided in

Table 1. A list of commercially available ECM scaffolds, their source material, and configuration is provided in Table 2.

**Table 1 A** partial list of ECM scaffold donor sources, configurations, and applications.

| Donor | Configuration | Application |
|---|---|---|
| *Source* | Sheet | Abdominal Wall (19, 20) |
| | Multilaminate Sheet (21) | Artery (22, 23) |
| Allogeneic | Powder (24) | Bladder (25-27) |
| Xenogeneic | Gel (28) | Bone (29, 30) |
| | 3D Construct (31, 32) | Cartilage (33, 34) |
| *Species* | Intact Decellularized Organ (35, 36) | Dura Mater (37, 38) |
| | | Esophagus (32, 39) |
| Bovine | | Heart (40) |
| Equine | | Liver (41) |
| Porcine | | Nerve (42, 43) |
| Human | | Skin (44-47) |
| | | Tendon (48-51) |
| *Age* | | Thoracic Wall (52) |
| | | Trachea (53, 54) |
| Fetal | | Tympanic Membrane (55) |
| Adult | | Vocal Fold (56, 57) |
| *Organ* | | |
| Bladder (26, 58, 59) | | |
| Heart (35, 60) | | |
| Liver (41) | | |
| Muscle (61) | | |
| Nerve (42, 62) | | |
| Skin (63, 64) | | |
| Small Intestine (22) | | |
| Tendon (65, 66) | | |

**Table 2** A partial list of commercially available scaffold materials composed of extracellular matrix.

| *Product* | *Company* | *Material* | | *Form* | *Use* |
|---|---|---|---|---|---|
| AlloDerm | Lifecell | Human skin | Cross-linked | Dry Sheet | Abdominal wall, breast, ENT/head & neck reconstruction, grafting |
| AlloPatch® | Musculoskeletal Transplant Foundation | Human fascia lata | Cross-linked | Dry Sheet | Orthpedic applications |
| Axis™ dermis | Mentor | Human dermis | Natural | Dry Sheet | Pelvic organ prolapse |
| CollaMend® | Bard | Porcine dermis | Cross-linked | Dry Sheet | Soft tissue repair |
| CuffPatch™ | Arthrotek | Porcine small intestinal submucosa (SIS) | Cross-linked | Hydrated Sheet | Reinforcement of soft tissues |
| DurADAPT™ | Pegasus Biologicals | Horse pericardium | Cross-linked | | Repair dura matter after craniotomy |
| Dura-Guard® | Synovis Surgical | Bovine pericardium | | Hydrated Sheet | Spinal and cranial repair |
| Durasis® | Cook SIS | Porcine small intestinal submucosa (SIS) | Natural | Dry Sheet | Repair dura matter |
| Durepair® | TEI Biosciences | Fetal bovine skin | Natural | Dry Sheet | Repair of cranial or spinal dura |
| FasLata® | Bard | Cadaveric fascia lata | Natural | Dry Sheet | Soft tissue repair |
| Graft Jacket® | Wright Medical Tech | Human skin | Cross-linked | Dry Sheet | Foot ulcers |
| Oasis® | Healthpoint | Porcine small intestinal submucosa (SIS) | Natural | Dry Sheet | Partial & full thickness wounds; superficial and second degree burns |
| OrthADAPT™ | Pegasus Biologicals | Horse pericardium | Cross-linked | | Reinforcement, repair and reconstruction of soft tissue in orthopedics |
| Pelvicol® | Bard | Porcine dermis | Cross-linked | Hydrated Sheet | Soft tissue repair |
| Peri-Guard® | Synovis Surgical | Bovine pericardium | | | Pericardial and soft tissue repair |
| Permacol™ | Tissue Science Laboratories | Porcine skin | Cross-linked | Hydrated Sheet | Soft connective tissue repair |
| PriMatrix™ | TEI Biosciences | Fetal bovine skin | Natural | Dry Sheet | Wound management |
| Restore™ | DePuy | Porcine small intestinal submucosa (SIS) | Natural | Sheet | Reinforcement of soft tissues |
| Stratasis® | Cook SIS | Porcine small intestinal submucosa (SIS) | Natural | Dry Sheet | Treatment of urinary incontinence |
| SurgiMend™ | TEI Biosciences | Fetal bovine skin | Natural | Dry Sheet | Surgical repair of damaged or ruptured soft tissue membranes |
| Surgisis® | Cook SIS | Porcine small intestinal submucosa (SIS) | Natural | Dry Sheet | Soft tissue repair and reinforcement |
| Suspend™ | Mentor | Human fascia lata | Natural | Dry Sheet | Urethral sling |
| TissueMend® | TEI Biosciences | Fetal bovine skin | Natural | Dry Sheet | Surgical repair and reinforcement of soft tissue in rotator cuff |
| Vascu-Guard® | Synovis Surgical | Bovine pericardium | | | Reconstruction of blood vessels in neck, legs, and arms |
| Veritas® | Synovis Surgical | Bovine pericardium | | Hydrated Sheet | Soft tissue repair |
| Xelma™ | Molnlycke | ECM protein, PGA, water | | Gel | Venous leg ulcers |
| Xenform™ | TEI Biosciences | Fetal bovine skin | Natural | Dry Sheet | Repair of colon, rectal, urethral, and vaginal prolapse, pelvic reconstruction, urethral sling |
| Zimmer Collagen Patch ® | Tissue Science Laboratories | Procine dermis | Cross-linked | Dry Sheet | Orthpedic applications |

### 1.1.1 Production of ECM Scaffolds

The production of ECM scaffolds requires the use of mechanical, chemical, and enzymatic, processing methods that decellularize and terminally sterilize the scaffold (67). These methods can affect the composition, ultrastructure, and mechanical properties of the resulting scaffold, thus potentially affecting the host response associated with its use. The goal of a decellularization protocol is to remove as much of the cellular material as possible with minimal effects upon the tissue-specific structural and functional components of the scaffold. The efficacy of a decellularization protocol is dependent upon the tissue being decellularized as well as the methods used to decellularize it. It has been shown that ECM scaffolds, almost regardless of the methods used in their production, retain small amounts of DNA and cellular debris following processing (68). The consequences of these small amounts of cellular material that remain in an ECM scaffold are as of yet unclear. However, as will be discussed in subsequent sections, it is logical to assume that large quantities of cellular material may be associated with an adverse host immune response to an implanted ECM scaffold.

Chemical cross-linking is used in the production of many ECM scaffolds to slow or prevent degradation, to inhibit recognition of surface epitope by the host, and to increase strength. While slowed degradation due to cross-linking may be beneficial in some cases where additional mechanical support from the scaffold is required, inhibiting scaffold degradation via chemical cross-linking may alter the presentation and conformation of ligands on the surface of an ECM scaffold, potentially altering ligand-receptor interactions that may be important in determining the outcome of cell-scaffold interactions. In general, the *in vivo* consequence of inhibiting scaffold degradation via chemical cross-linking has been shown to be less constructive tissue remodeling than has been observed with the use of non-cross-linked ECM scaffolds (69).

### 1.1.2 ECM Configuration

Following the decellularization of a tissue or organ, the resulting ECM may take on a variety of shapes and sizes which are dependant on the particular architecture of the decellularized organ of interest or the methods used in the decellularization process (67). Many tissues and organs such as dermis, small intestine, and urinary bladder are typically processed into a sheet-like configuration prior to decellularization. However, the sheet form may be insufficient in its mechanical properties and/or three-dimensional morphology (i.e., shape and size) depending on the application of interest. Therefore, a number of methods have been utilized for the processing of decellularized ECM scaffolds into a variety of application-specific shapes and sizes. Intact ECM scaffolds have been molded and vacuum pressed into shapes that include tubes (39), cones (70), and multi-laminate sheets among others (21) (Table 1). These scaffolds have been utilized in applications ranging from esophageal repair (tubular) (39), to gastro-esophageal junction repair (cone-shaped) (70), and orthopedic applications (multilaminate sheets) (50). ECM materials have also been comminuted to create a powder form of the scaffold which is of interest for injectable and space filling applications (24). A hydrogel form of ECM has also been produced via enzymatic degradation of ECM scaffolds (28). The ability of ECM scaffolds to be formed into varied shapes and sizes further adds to their utility as scaffolds for tissue engineering and regenerative medicine applications.

### 1.1.3 Mechanisms by which ECM Scaffolds Promote Constructive tissue remodeling

While the exact mechanisms which underlie the ability of ECM based scaffold materials to promote constructive tissue remodeling remain largely unknown, there are a number of elements which are believed to play key roles. Among these elements are the ability of the scaffold material to degrade rapidly with concomitant release of bioactive matricryptic peptides, the ability of the scaffold material to recruit progenitor and other tissue-specific cell populations to sites of tissue remodeling, the ability of the scaffold material to respond to local environmental stimuli, and the ability of the scaffold material to elicit a host response which does not result in a foreign body response or immunologic rejection of the implant. Each of these elements is outlined below, and multiple elements are explored in further detail in the studies which follow.

#### 1.1.3.1 Degradation of ECM Scaffolds

ECM scaffolds degrade rapidly *in vivo*. A recent study showed that 10-layer scaffolds composed of $^{14}C$ labeled ECM were 60% degraded at 30 days post implantation and 100% degraded by 90 days in a model of canine Achilles tendon repair (48). During this period, the scaffold was populated and degraded by host-derived cells and resulted in the formation of site-specific functional host tissue which was histologically indistinguishable from native tissue. The major mechanism of excretion of the degraded scaffold was found to be via hematogenous circulation and elimination by the kidneys, urine and exhaled $CO_2$. The mechanisms of *in vivo* degradation of ECM scaffolds are complex and include both cellular and enzymatic pathways. The process is mediated by inflammatory cells, such as macrophages, which produce oxidants as well as proteolytic enzymes that aid in the degradation of the matrix (71). A recent study showed that peripheral blood monocytes are required for the early and rapid degradation of both

ECM scaffolds and autologous body wall control tissues, and that chemically cross-linked ECM scaffolds are resistant to macrophage-mediated degradation (72).

ECM scaffolds have also been degraded *in vitro* by chemical and physical methods. Recent findings suggest that the degradation products of ECM scaffolds are bioactive (73-78). Studies have shown antimicrobial activity associated with the degradation products of ECM scaffolds; however, in the absence of degradation, antimicrobial activity was not seen, suggesting that some of the bioactive properties of the ECM are derived from its degradation products rather than from whole molecules present within the ECM (73, 77, 79). Degradation products of ECM scaffolds have also been shown to be chemoattractants for progenitor and non-progenitor cell populations (74-76, 78). An ECM scaffold that cannot degrade (i.e. is chemically cross-linked) may not release bioactive degradation products, including those bioactive molecules that may be responsible for modulating the host response towards a constructive tissue remodeling response.

#### 1.1.3.2 Chemoattraction of Progenitor Cells By Remodeling ECM Scaffolds

One of the biologic effects of the degradation of ECM scaffolds is the ability to recruit progenitor cells to sites of ECM degradation during *in vivo* remodeling (49, 80, 81). A study of ECM scaffold remodeling in a model of mouse Achilles tendon repair examined the ability of ECM scaffolds and autograft tissue to recruit bone marrow derived cells (49). Bone marrow derived cells were observed in the sites of remodeling associated with both ECM scaffolds and autograft control tissue among what appeared to be predominantly mononuclear cells at early time points (1 and 2 weeks) post surgery. Both scaffold types remodeled into tissue resembling the native Achilles tendon; however, by 16 weeks the presence of bone marrow derived cells was observed only in the ECM treated group. Another study, also utilizing a model of mouse

Achilles tendon repair, examined the ability of ECM scaffold explants to cause the chemotaxis of progenitor cells after 3, 7, and 14 days of *in vivo* remodeling (81). The results of the study showed greater migration of progenitor cells towards tendons repaired with ECM scaffolds compared to tendons repaired with autologous tissue and uninjured normal contralateral tendon. These results suggest that ECM scaffolds are capable of recruiting progenitor cells to the site of implantation to participate in constructive tissue remodeling over the long-term. The exact components of the ECM which are responsible for the recruitment of progenitor cells, the mechanisms by which ECM scaffolds recruit progenitor cell populations during *in vivo* remodeling, and the specific phenotype of the cells recruited remains largely unknown.

#### 1.1.3.3 Angiogenesis and New ECM Deposition

Angiogenesis is implicit in the success of many tissue engineering and regenerative medicine strategies involving biomaterials. The in-growth of vessels into a tissue-engineered construct provides a means for nourishing the tissue growing on or within the implanted material. In the absence of angiogenesis, many implanted biomaterials may fail to integrate with the surrounding tissue and/or fail to support cell populations that have been seeded onto or migrate into the material. Angiogenesis has been shown to be a prominent feature of ECM scaffold remodeling and is commonly observed within the first 1-3 days following scaffold implantation (69, 82). These vessels remain within the implantation site and continue to provide a blood supply to the remodeling tissue throughout the remodeling process. It has been shown that certain ECM scaffolds contain bioactive VEGF (a potent angiogenic factor) and bFGF (83). Factors such as these may account, in part, for the ability of ECM scaffolds promote angiogenesis at early time points following implantation.

#### 1.1.3.4 Response to Mechanical Stimuli

ECM scaffolds derived from a number of different sources have been used to promote site-specific formation of functional host tissue (Table 1). It is unknown whether there is an advantage to the use of ECM derived from the same tissue as that being reconstructed; however, it is known that ECM scaffold materials derived from a single tissue, urinary bladder (urinary bladder matrix; UBM) for example, can remodel into a variety of site-specific tissues. UBM has been shown capable of supporting the formation of bladder, trachea, myocardium, and fibrocartilage, among others (25, 40, 53). This suggests that there are environmental cues which direct site-specific tissue formation following the implantation of ECM scaffolds. These cues likely include pH, local gene expression, and oxygen tension, among others. However, of these cues, mechanical stimuli has been shown to be essential to the formation of a constructive tissue remodeling response in a number of applications (25, 51, 84).

A recent study utilized UBM to reconstruct the bladder following partial cystectomy in a canine model (25). Following implantation, animals were exposed either to short-term catheterization (24 hours post-surgery or to long-term catheterization (4 weeks post-surgery). In those animals which were subjected to only short-term catheterization, remodeling of the UBM scaffold material resulted in the formation of a urothelial layer, angiogenesis, smooth muscle actin and smooth muscle myosin heavy chain expressing cells and neuronal processes within the site of implantation at early time points (4 weeks) and the formation of a highly differentiated urothelium and islands of smooth muscle within the site of remodeling in the long-term (12 weeks). In contrast, in those animals which were subjected to long-term catheterization, remodeling of the UBM scaffold resulted in the presence of myofibroblasts and the formation of granulation tissue at early time points (4 weeks) and a response consistent with fibrosis in the

long-term (12 weeks). These results show that early mechanical loading is essential to the formation of a constructive tissue remodeling response and that the mechanical stimulation which occurred following removal of the catheter was insufficient to overcome the lack of early mechanical stimuli.

Another study investigated the role of mechanical forces in a model Achillie's tendon repair (84). Rabbits were subjected to 1.5 cm ligament repair using SIS with and without post-surgical immobilization. In those animals which were allowed to return to partial or full range of motion shortly after surgery, replacement of the scaffold with organized connective tissue resembling that of the native tendon was observed. Limiting the range of motion resulted in degradation of the scaffold with limited cellular infiltration and limited extracellular matrix deposition. Again, showing that mechanical forces have an impact upon the type and quality of tissue which results from the tissue remodeling process.

Many studies have examined the effects of mechanical stimulation upon the phenotype of a wide variety of cells, including progenitor cells. The mechanical forces experienced by the progenitor cell populations recruited to sites of extracellular matrix mediated tissue remodeling, in combination with other microenvironmental factors, may guide their differentiation into tissue-specific phenotypes.

#### 1.1.3.5 Host Response to Extracellular Matrix Scaffolds

The effects of the host response in general, and the host macrophage response in particular, which occurs following the implantation of ECM scaffolds is a central theme of this dissertation and is explored in-depth in the studies which follow. Therefore, the following section is intended to give the reader a basic understanding of the aspects of the host response to ECM scaffolds which are not examined in great detail hereafter.

The mechanisms of the host cell and humoral response to whole organ transplantation are reasonably well understood. Xenogeneic and allogeneic cellular antigens are recognized by the host, elicit immune activation, and cause the production of pro-inflammatory mediators with downstream cytotoxicity and transplant tissue rejection. The mechanisms of the host immune response to acellular scaffolds derived from ECM, either allogeneic or xenogeneic, are neither as well studied nor as well understood as whole organ and tissue transplantation (85). The preparation of ECM scaffolds for tissue engineering and regenerative medicine applications involves the decellularization of the tissue or organ from which the ECM is to be harvested (40). The removal of the cellular component produces a different type of 'tissue graft' than is typically presented with autogeneic, allogeneic, or xenogeneic whole organ grafts. An acellular ECM scaffold consists primarily of the ECM constituent molecules, the majority of which have been found to be conserved across species (7), thus mitigating many adverse components of host the immune response (86).

While the majority of the components which remain following decellularization are conserved across species and largely non-immunogenic, many ECM scaffolds have been shown to contain a number of components that are known to induce adverse host immune and/or rejection type responses when present in large quantities. These components include the Galα1-3Galβ1-4GlcNAcβ-R (α-Gal) epitope and DNA. The α-Gal epitope is known to cause hyperacute rejection of organ transplants (87-90). However, studies of α-Gal positive ECM scaffold implantation have not shown adverse responses that can be attributed to the α-Gal epitope (91, 92). A recent study investigated the effects of the presence of the α-Gal epitope upon the remodeling of ECM scaffolds in a nonhuman primate model (91). The study compared the host response to ECM derived from allogeneic, xenogeneic porcine, and xenogeneic α-Gal -

/- porcine sources. The results of the study showed that although those animals implanted with ECM scaffolds containing the α-Gal epitope exhibited an increase in serum anti-α-Gal antibodies, there were no adverse effects of the α-Gal epitope upon the tissue remodeling response. Several studies have shown the presence of DNA fragments remaining within ECM scaffolds following the decellularization and sterilization processes (13, 93, 94). A recent study examined the presence of DNA within a number of commercially available ECM scaffolds (95). The results of the study showed that, although all of the products tested contained small amounts of DNA, the remnants generally consisted of fragments of less than 300 bp. Despite the presence of small amounts of both the α-Gal epitope and DNA within ECM scaffolds, adverse clinical effects have not been observed. This is likely due to the minute amounts of these components present within efficiently decellularized materials and the rapid degradation of the ECM scaffold. However, it is probable that there is a threshold amount of these components required to induce adverse effects upon the remodeling response.

In general, innate immune cells (i.e. neutrophils and macrophages) are the first cells to encounter and respond to implanted biomaterials. The immediate cellular response observed following the implantation of an ECM scaffold consists almost exclusively of neutrophils but there is also a significant mononuclear cell component as well. In the absence of large amounts of cellular debris within the scaffold, chemical cross-linking, or contaminants such as endotoxin, the neutrophil infiltrate diminishes almost entirely within 72 hours and is replaced by a mononuclear cell population. As will be discussed in the following section, this type of response, characterized by a large infiltration of innate immune cells, has been conventionally interpreted as either acute or chronic inflammation with associated negative implications (i.e. downstream encapsulation and fibrosis). However, the presence of these cells, especially

mononuclear macrophages, has been shown to be essential to the formation of the type of constructive tissue remodeling response that has been observed following the implantation of ECM scaffolds (69, 72, 96, 97). These and other aspects of macrophage involvement in tissue remodeling are the subject of the following sections as well as a central theme of this dissertation.

A histologically similar population of neutrophils and macrophages is observed at early time points following the implantation of ECM scaffolds which either have or have not been processed using chemical cross-linking agents such as glutaraldehyde or carbodiimide; however, the tissue remodeling outcome observed following the implantation of chemically cross-linked ECM scaffolds is distinctly different than that observed following the implantation of non-cross-linked scaffolds (69). The host tissue response typically observed following implantation of an acellular ECM scaffold that has not been chemically cross-linked is characterized by a dense infiltration of neutrophils at early time points changing to primarily mononuclear cells thereafter. This infiltrate of innate immune cells is accompanied by rapid degradation of the ECM scaffold and replacement with organized, site-specific, functional host tissue (69, 82, 98). If the scaffold has been processed using chemical cross-linking agents such as glutaraldehyde or carbodiimide, the host response is characterized by a similar presence of a large number of neutrophils and macrophages, but results in a more typical pro-inflammatory, foreign body type response resulting in dense fibrous tissue encapsulation and the prolonged presence of a multinucleate cell population (69). Thus, while ECM scaffolds may elicit what appears to be a chronic inflammatory tissue response, the outcome is not necessarily scar tissue formation or encapsulation of the material. Rather, non-cross-linked acellular ECM scaffolds appear to elicit an innate immune response which is not pro-inflammatory in nature.

In addition to eliciting a robust, but apparently not detrimental, host innate immune response, acellular non-cross-linked ECM scaffolds have been shown to evoke a Th2 type T-lymphocyte response (86, 99). One study utilized a mouse model of subcutaneous implantation to examine the T-lymphocyte response to xenogeneic muscle tissue, syngeneic muscle tissue, and an acellular ECM scaffold (86). Results showed that the xenogeneic tissue implant was associated with a response consistent with rejection. That is, the xenogeneic muscle implant showed signs of necrosis, granuloma formation and encapsulation. The syngeneic tissue and the ECM scaffold elicited an acute inflammatory response that resolved with time and resulted in organized tissue morphology at the remodeling site. Tissue cytokine analysis revealed that the ECM group elicited expression of interleukin (IL)-4 and suppressed the expression of interferon (IFN)-γ as compared to the xenogeneic tissue implant group. The ECM group elicited the production of an ECM specific antibody response, however it was restricted to the immunoglobulin G (IgG) 1 isotype. Re-implantation of the mice with another ECM scaffold led to a secondary anti-ECM antibody response that was also restricted to the IgG1 isotype and there was no evidence of the formation of a Th1 type response. Further investigation confirmed that the observed responses were in fact T-lymphocyte dependant. Finally, it has been shown that, while both T and B cells respond to ECM scaffolds, they are not required for constructive tissue remodeling of an ECM implant (86). This finding further indicates the importance of the host innate immune response in driving/determining the downstream remodeling outcome following implantation of an ECM scaffold.

## 1.2 THE HOST RESPONSE FOLLOWING INJURY AND IMPLANTATION OF BIOMATERIALS

As will be seen in the examples which follow, the host response to ECM scaffolds is highly complex and does not seem to follow the classic paradigms set forward for the default wound healing response or the response to non-degradable metallic or polymeric biomaterials intended for long-term implantation. ECM scaffolds appear to be subject to what can be described as chronic inflammation under a classical definition (i.e. the presence of mononuclear cells within newly deposited ECM over time). However, as has been shown in a number of studies (69, 96, 100) and as will be demonstrated in the studies presented herein, this response does not necessarily result in the encapsulation and fibrosis of ECM scaffold materials. In particular, acellular, non-chemically cross-linked ECM scaffolds have been shown to promote constructive tissue remodeling, even in the presence of what can be described as chronic inflammation. Therefore, the default wound healing response and the host response following the implantation of non-degradable biomaterials are reviewed here and the role of the host response to the components of tissue engineered constructs which may not fall into either of these categories is discussed as a base from which to understand the host response to ECM based scaffold materials.

### 1.2.1 The Host Response to Tissue Injury

The default mammalian host response following tissue injury is a well-documented series of events that typically result in the deposition of dense fibrous connective tissue within the site of injury (101-103). Very few tissues in adult mammals have the ability for regeneration. Those which possess the ability to regenerate are known to include the bone marrow, liver, intestinal

epithelium, and epidermis of the skin. The default response to tissue injury has been described as occurring in four stages: hemostasis, inflammation, proliferation and remodeling (102).

#### 1.2.1.1 Homeostasis

Following tissue injury and resultant damage to the vasculature, platelets contact the damaged tissues resulting in the release of clotting factors that initiate hemostasis. A provisional matrix forms consisting largely of fibrin and entrapped erythrocytes. The provisional matrix provides a substrate for further cell migration into the site of injury and a medium for cell signaling (104). In addition to their role in hemostasis and provisional matrix formation, platelets also release cytokines including PDGF, TGF-β, chemokine C-X-C motif ligand 4 (CXCL4), and IL-1 (105-107). These factors contribute to initial repair process via recruitment of multiple cell types including neutrophils, macrophages, fibroblasts, and other tissue specific cells to the injury site (107).

#### 1.2.1.2 Inflammation

Neutrophils are the first inflammatory cell type to arrive at the wound site. Neutrophils phagocytose and destroy foreign material, bacteria, or dead cells which may have entered the wound site as a result of the injury and also provide further signaling molecules that recruit macrophages to the injury site (106). Mast cells also participate in the early stages of wound healing by releasing granules containing enzymes, histamine, and other factors that modulate the inflammatory response (102, 108). By 48 to 72 hours post injury, macrophages begin to dominate the cell population at the site of injury (109). Activated macrophages secrete cytokines and chemokines which promote the further recruitment of leukocytes to the site of injury (106, 107). Macrophages also clear apoptotic neutrophils, the phagocytosis of which leads to a change

towards a more reparative macrophage phenotype and the resolution of the inflammatory phase of wound healing (110). The T-lymphocyte population plays an important late regulatory role in the resolution of the inflammatory process through local secretion of cytokines and chemokines (111).

#### 1.2.1.3 Proliferative Phase

The proliferative phase of wound healing involves cellular proliferation, angiogenesis, new extracellular matrix deposition and the formation of granulation tissue - processes which are largely mediated via the effects of the local microenvironment including pH and oxygen tension, and cytokines secreted by macrophages, T-lymphocytes, and other cells within the wound site (107, 112, 113). These cytokines include EGF, basic FGF, TGF-α, TGF-β, VEGF, and others depending on the nature of the injured tissue (107).

#### 1.2.1.4 Remodeling Phase

Following the deposition of significant amounts of extracellular matrix (predominantly collagens type I and III) during the proliferative phase, the remodeling phase of wound healing begins. This phase is characterized by matrix metalloproteinase (MMP) and tissue inhibitor of metalloproteinase (TIMP) mediated degradation and remodeling of the newly deposited collagen, generally resulting in scar tissue formation/maturation (102, 114). In some cases, prolonged remodeling leading to fibrosis or hypertrophic scar formation may occur due to dysregulation of the healing process (102). Although these wound healing events are described as part of the default response to tissue injury, many of these events, as will be discussed in the sections which follow, also occur as part of a regenerative process. The selective activation of components of the inflammatory, proliferation and remodeling phase can result in a constructive

and functional outcome as opposed to scar tissue formation. In particular, the role of macrophages in promoting a constructive tissue remodeling outcome following implantation of biomaterial scaffolds will be discussed in further detail in following sections.

In Figure 1, an example of the default host remodeling response following injury of the abdominal wall musculature in a rat is shown. By 28 days post-injury, an increasingly dense layer of collagenous connective tissue can be seen forming over the injured musculature. This connective tissue contains spindle-shaped cells, likely fibroblasts. Numerous mononuclear cells, consisting of macrophages and T-lymphocytes can also be seen within the area of the disrupted musculature and an angiogenic process can be observed, indicating that the inflammatory process is not entirely complete at this stage of tissue remodeling. With time, the collagenous tissue being deposited at the site of injury will mature into dense scar tissue and the presence of inflammatory cells will subside, signaling complete repair of the wound by the host. However, this repair does not result in the restoration of the function of the injured tissue. This default response to tissue injury is important and necessary to understand if one hopes to appreciate a variant of the inflammatory response; specifically, the foreign body response that occurs following the implantation of a non-degradable or slowly degradable biomaterial.

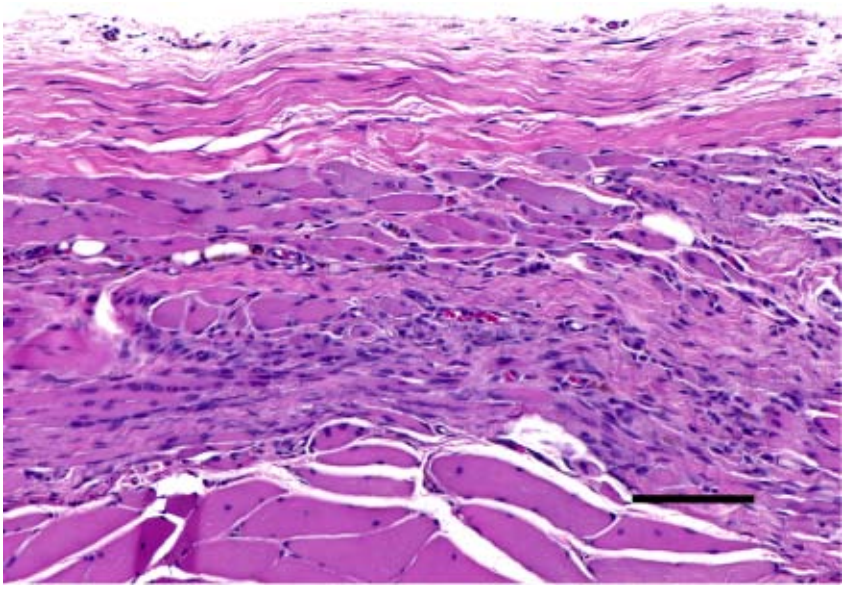

**Figure 1. Hematoxylin and eosin (H&E) stained section showing host remodeling response at 28 days post-injury of abdominal wall musculature. Spindle shaped cells, likely fibroblasts, within increasingly dense connective tissue can be observed forming at the periphery of the site of remodeling (top). A mononuclear cell response is observed within the area of the injured musculature (middle) and angiogenesis is observed. Uninjured muscle tissue can also be observed (bottom). Image magnification = 20X, scale bar = 100 μm.**

### 1.2.2 Host Response Following Biomaterial Implantation

The host response following the long-term implantation of a non-degradable synthetic or metallic biomaterial involves a series of overlapping processes which include: 1) blood-material interaction with deposition of a protein film on the biomaterial, 2) provisional matrix formation, 3) acute inflammation, 4) chronic inflammation, 5) granulation tissue formation, 6) foreign body reaction, and 7) fibrosis and tissue capsule development (115, 116). While many of these processes are similar to those described above for the default host response to tissue injury, there are a number of key differences.

The surgical implantation of a biomaterial is invariably associated with tissue damage and disruption of the vasculature at the surgical site. Release of blood into the wound site results in degranulation of platelets, formation of a provisional matrix and signaling which recruits inflammatory cells (i.e. neutrophils and macrophages) to the surgical site. Blood contact also results in adsorption of proteins to the surface of the biomaterial within seconds of implantation (117). The proteins which adsorb to a biomaterial may include components of the coagulation system (fibrinogen and tissue factors), complement cascade (C5), and other plasma derived proteins (albumin and IgG) (116, 118). These proteins provide a substrate through which the inflammatory cells arriving at the site of injury interact with the surface of the biomaterial. The specific proteins which attach and the behavior of the attached cells are dependent on the nature of the biomaterial surface and on an adsorption/desorption process, which is governed by the affinity of the proteins for the biomaterial surface (known as the Vroman Effect) (117, 118). As will be described briefly below, interactions of cells with the proteins adsorbed to the surface of the biomaterial may lead to a variety of cellular responses including adherence, activation, or triggering of phagocytic pathways, among others, depending on the cell type and the proteins involved (119, 120).

Acute inflammation, consisting of the emigration of neutrophils from the vasculature into the implant site, follows formation of the provisional matrix and the release of chemoattractant factors by platelets and other cells within the inflammatory site, much like the process described above for default wound healing. However, upon arrival within the wound site, neutrophils interact with the proteins adsorbed onto the biomaterial surface through integrin receptors specific for the adsorbed proteins (116). For example, the adsorption of fibronectin and IgG play significant roles in the Mac-1 mediated attachment of neutrophils and macrophages to

biomaterial surfaces during the acute phase of inflammation (121). Complement and serum immunoglobulin adsorption to a pathogen (termed opsonization) leads to phagocytosis by neutrophils and or macrophages, or destruction of the pathogen via the complement pathway. In comparison, an opsonized biomaterial elicits phagocytosis from neutrophils (and later macrophages), or is subjected to frustrated phagocytosis, depending on the nature of the biomaterial and its size (116). The process of frustrated phagocytosis involves the extracellular release of microbicidal contents at the surface of a foreign body. This release may cause the erosion of implanted materials which are not intended to degrade, and may eventually lead to failure of the material to perform as intended.

The chronic inflammation phase associated with the implantation of a biomaterial is typically characterized by the presence of activated macrophages. This process of macrophage accumulation may occur for a period of days to months depending on the nature of the implanted material and the adsorbed proteins. A meshwork of new extracellular matrix usually is deposited around the biomaterial and the accompanying angiogenic process is prominent. The continued presence of macrophages at the site of biomaterial implantation is often the precursor to the formation of granulation tissue, the foreign body giant cell response, and the eventual encapsulation of the biomaterial within a dense layer of collagenous connective tissue.

Chronic inflammation can progress to a granulation tissue phase, in which the deposition of new extracellular matrix and the growth of vasculature into the implantation site through the process of angiogenesis are conspicuous. The persistence of granulation tissue combined with the presence of a non-degradable biomaterial eventually leads to the formation of foreign body giant cells (116). The classic histologic description of a foreign body reaction consists of macrophages and multinucleated foreign body giant cells, formed through the fusion of the

macrophages, which are typically located at the surface of the biomaterial. There are a number of factors including the chemical composition and surface topography, which play a role in determining the degree to which a material elicits a foreign body giant cell response, predominantly through the modulation of protein adsorption (122-124). As previously stated, macrophages generally interact with protein adsorbed surfaces through cell surface integrin receptors, the ligation of which induces intracellular signaling cascades that regulate macrophage behavior. Depending on the type of signaling elicited and the immunologic microenvironment, macrophages may undergo fusion, thus forming foreign body giant cells. The exact mechanisms of foreign body giant cell formation are highly complex and have yet to be fully described. An in-depth discussion of the process of foreign body giant cell formation is beyond the scope of this chapter, however the topic of foreign body giant cell formation as it relates to biomaterials has been reviewed elsewhere (116). In the final stage of the host response following the implantation of a biomaterial, an increasingly dense layer of collagenous connective tissue is deposited around the surface of the material, thus isolating or "encapsulating" it from the surrounding healthy tissue.

Many approaches have been investigated to coat or modify the surface of a biomaterial to minimize the potentially detrimental processes of platelet activation, coagulation, and protein adsorption (125, 126). Similarly, a number of other approaches have attempted to develop material coatings or other strategies that reduce the foreign body giant cell and fibrotic responses to non-degradable biomaterials intended for long-term implantation (127, 128). All attempts to date have resulted in only modest success at best.

### 1.2.3 Role of the Host Response in Tissue Engineering and Regenerative Medicine

The biomaterials most suitable for tissue engineering and regenerative medicine applications are typically degradable, manufactured from either synthetic or naturally occurring materials and are commonly combined with bioactive molecules or living cells. Therefore, the host tissue response tends to be distinctly different from that just described for metallic or polymeric biomaterials intended as permanent implants. While an in-depth consideration of how each of the components (degradable materials, bioactive factors and cells) of tissue engineered constructs affects the host response is beyond the scope of this chapter, a short discussion of each and examples of the host response elicited by commonly used degradable materials are provided below.

In general, tissue engineering strategies utilize naturally or synthetically derived materials which are degradable, either in the short-term or the long-term, following implantation. These materials include degradable polymers such as poly-lactic co-glycolic acid and poly-caprolactone, among many others. While these materials are subject to the same processes of protein adsorption as the non-degradable materials described above, their transient nature can affect both the severity and the duration of the host response. An example of this process is provided in Figure 2. In this instance, a Vicryl (Polyglactin 910) mesh has been placed in the abdominal wall musculature of a rat following creation of a surgical defect. By 14 days post implantation, the Vicryl mesh is still largely intact and is subject to an intense foreign body giant cell response at the surface of the material (Figure 2a and 2b). This multinucleate cell response is accompanied by the deposition of large amounts of granulation tissue consisting of newly deposited extracellular matrix, mononuclear cells, and blood vessels. By 35 days post-implantation, the Vicryl mesh is largely degraded, however is still present within the implantation site (Figure 2c and 2d). The portion of the mesh which remains is surrounded by

foreign body giant cells, with increasingly dense collagenous tissue formation at the periphery. The foreign body giant cell response, while reduced as compared to the response observed at 14 days, will only resolve after the material has been completely degraded. However, resolution of the inflammatory response will not result in constructive tissue remodeling in this case. Rather, dense collagenous connective tissue resembling scar tissue will remain at the site of implantation.

One of the advantages to the use of polymeric materials is the ability to form the material into specific shapes and sizes using a variety of techniques such as weaving, extrusion, or electrospinning, among others. The use of such processes allows for highly accurate tuning of many factors associated with the biomaterial construct. These factors include three-dimensional configuration, mechanical and material properties, porosity and degradability. These factors are known to have important effects upon the migration, proliferation, and differentiation of tissue specific cells when cultured during the creation of tissue-engineered constructs *in vitro*. However, the impact of these factors upon the eventual success of a biomaterial device following *in vivo* implantation appears to be limited to the immediate time period surrounding the surgical implantation of the construct. Surface chemistry, surface topography, and porosity have all been shown to have an effect upon the *in vitro* response of macrophages to biomaterials but few studies have investigated the effects of these factors upon the *in vivo* host response (122, 124, 129-131).

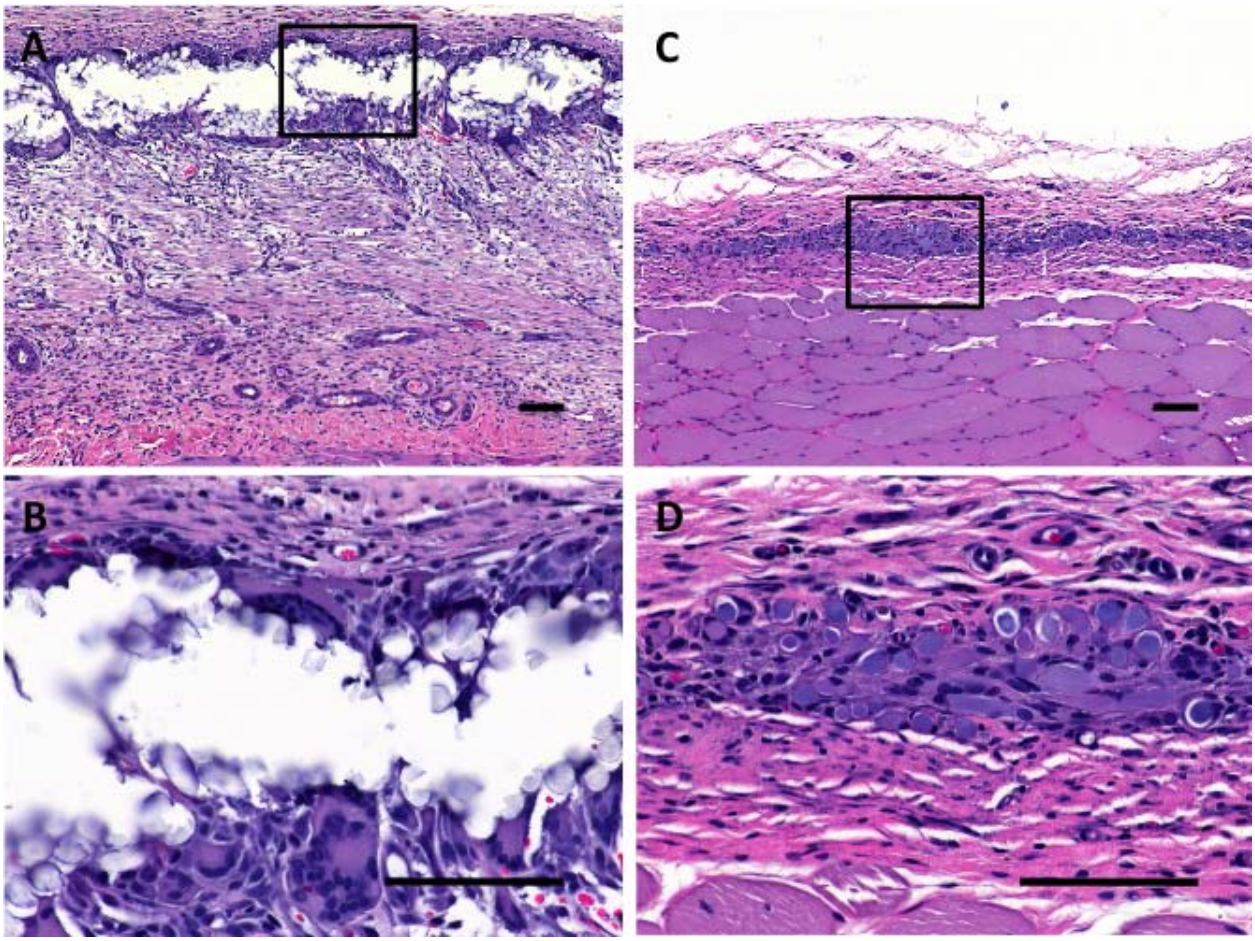


**Figure 2. H&E stained sections showing the host remodeling response following implantation of a degradable synthetic biomaterial (Vicryl mesh). The material can be observed within the site of remodeling at 14 days post implantation (panels A and B) and is surrounded by a multinucleate giant cell population indicating a foreign body response. Angiogenesis, a robust mononuclear cell response, and the deposition of new extracellular matrix (granulation tissue) can be observed further from the surface of the implanted material. At 35 days post-implantation (panels C and D), a significant portion of the material has been degraded. However, remnants of the material can still be observed within the site of implantation and a chronic inflammatory response including foreign body giant cells persists. Increasingly dense connective tissue can be observed separating the implant from the native musculature (bottom). Magnification of panels A and C = 10X, magnification of panels of B and D = 40X, scale bars =100 μm.**

Other approaches to tissue engineering and regenerative medicine utilize naturally derived biologic materials such as the ECM of mammalian tissues or those of plant origin. These materials may elicit a distinctly different type of host response than those of a synthetic origin due to differences in the surface topology and the ligand landscape present on the surface of the material. Naturally derived materials likely experience adsorption of a different repertoire of molecules than do synthetically derived materials and also often possess an inherent surface functionality which is related to the function of the biologic structure from which they are isolated. There are a number of factors which influence the host response to naturally derived materials including the rate at which the material degrades and the molecular weight or composition of the material in the case of biopolymers such as chitosan. For example, the degree of deacetylation of chitosan has been shown to affect the rate of degradation and the host response it elicits upon implantation (132). Figure 3 shows an example of a 4-layer biologic material composed of UBM. The material is surrounded by mononuclear cells, which are also observed to infiltrate the degrading material, at 14 days post-implantation into a rat abdominal wall musculature defect. This cellular response is accompanied by the deposition of new extracellular matrix within the implantation site, as well as angiogenesis, similar to the example provided in Figure 2, although notably no foreign body giant cells are present. However, the host response to the material at 35 days post-implantation is quite different than that observed in Figure 1. By 35 days post-implantation, the material has degraded and is replaced with well-organized collagen, blood vessels, and new islands of skeletal muscle. While the response shown in Figure 3 represents only the beginning of the constructive tissue remodeling process, studies have shown that similar ECM scaffold materials are capable of promoting the formation of functional, innervated muscle tissue at later time points (25, 133, 134).

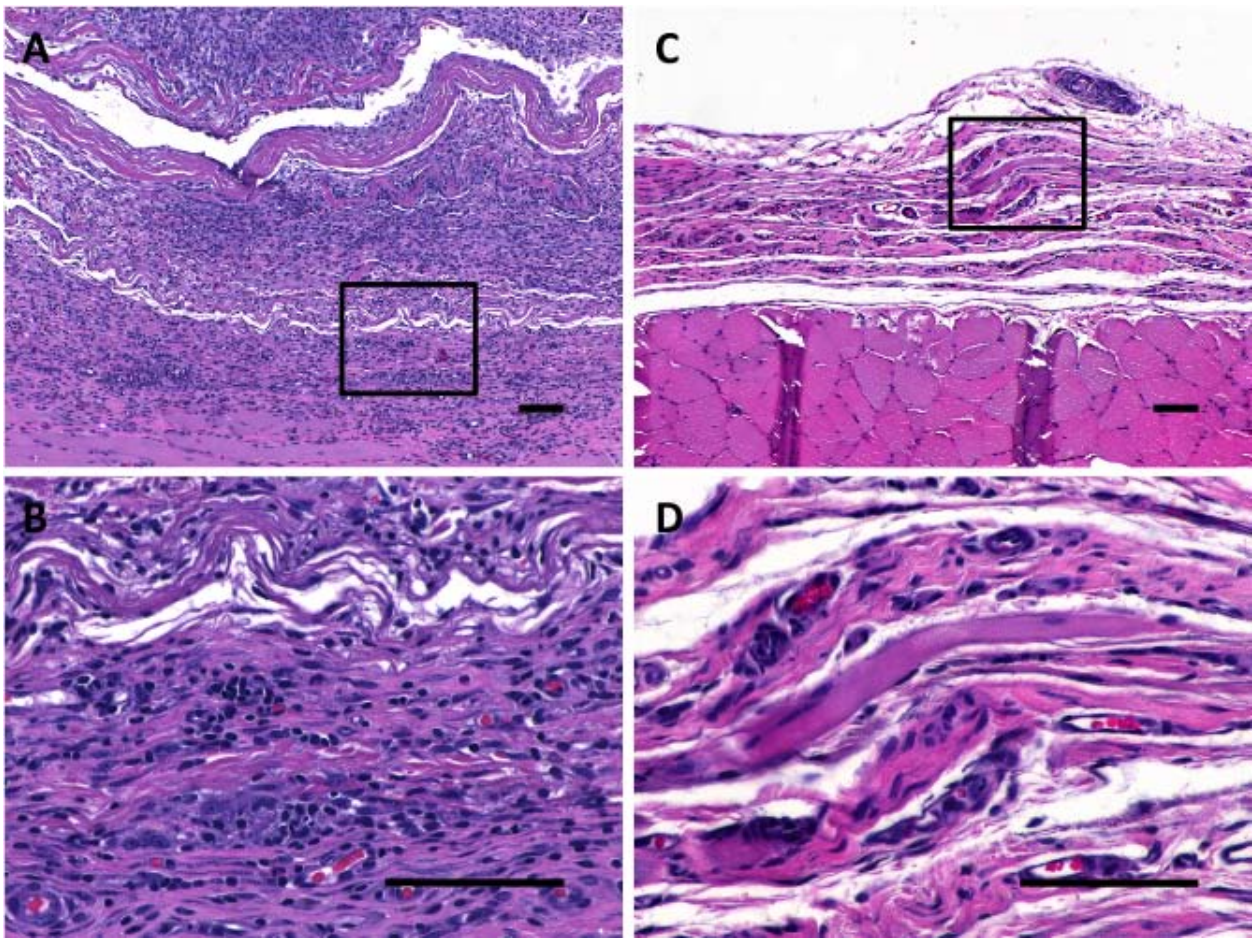


**Figure 3. Hematoxylin and eosin stained sections showing the host remodeling response following implantation of a degradable biologic scaffold material (UBM). At 14 days post-implantation (panels A and B) a robust mononuclear cell response accompanied by angiogenesis and deposition of new extracellular matrix are observed within and surrounding the degrading scaffold material. Of note, no foreign body giant cells are observed at the surface of the material. By 35 days post-implantation (panels C and D), the material is no longer identifiable in a histologic section and has been replaced by organized collagenous tissue, blood vessels, and bundles of skeletal muscle – a response which can be characterized as constructive tissue remodeling. Magnification of panels A and B = 10X, magnification of panels of C and D = 40X, scale bars =100 μm.**

The two examples provided here are intended to show the diverse responses which may be elicited by the materials used in tissue engineering and regenerative medicine and not to imply that synthetic based approaches do not result in constructive tissue remodeling. Indeed, there are numerous examples of tissue-engineered constructs containing polymeric components that facilitate what can be described as constructive tissue remodeling. Similarly, there are numerous examples of biologically derived scaffold materials which do not promote constructive tissue remodeling. For example, chemical cross-linking of ECM based scaffold materials similar to those used in Figure 3 has been shown to result in fibrous tissue encapsulation as opposed to the constructive tissue remodeling outcome which was achieved using non-cross-linked forms of the same material (69). It is also interesting to note that, although the outcome of tissue remodeling was different for the materials used in the examples provided in Figures 2 and 3, there are many similarities in the early host response to both materials. That is, both materials elicited a robust mononuclear cell response and both elicited the formation of new extracellular matrix within the wound site. Phenotypic differences in the cells which make up the observed mononuclear cell population which participates in the host response and their roles in determining the ability of a tissue engineered construct to promote constructive tissue remodeling will be examined in more detail in the studies which follow.

Classic approaches to tissue engineering often dictate that cells be seeded into a carrier material and then cultured until reaching mechanical and biochemical properties which are similar to the tissue of interest. Other strategies involve the culture of scaffold free constructs containing only cells, which can then be stacked or otherwise shaped prior to implantation. These strategies have achieved varying levels success in a number of applications. However, there is little evidence that cell based approaches result in new tissues that include the originally

implanted cells. There may be important and beneficial paracrine effects that initially promote the integration of tissue-engineered constructs or the formation of new tissue, but it is highly unlikely that the entire implanted cell population will survive in the host long-term. The process of cell death and subsequent phagocytosis of cellular debris by neutrophils and macrophages can modulate the host response to a tissue engineered construct. In particular, the mechanism of cell death (i.e. necrosis versus apoptosis) may play a role in determining how immune cells respond to cells implanted as part of a tissue engineered construct. The cells used in tissue engineering and regenerative medicine strategies are generally of an autologous or allogeneic nature, with few approaches utilizing xenogeneic cell sources. These cells may be recognized by the adaptive immune system through mechanisms similar to those which have been described in detail for organ transplantation and rejection. Recent evidence suggests that certain cell sources may be capable of evading the adaptive immune system or elicit less immune activation (135, 136). A number of strategies for the provision of cells that produce therapeutic molecules, such as insulin production by transplanted islet cells, have utilized hydrogels as encapsulating materials to prevent the recognition of cells by the host immune system (137, 138). However, these approaches do not promote the integration of such cells into the tissue or organ of interest nor do they prevent the influx of potentially damaging small molecules and are, therefore, often only effective in the short-term. An in depth discussion of all of the factors affecting host recognition of cells of an allogeneic or xenogeneic nature is beyond the scope of this chapter. However, such recognition by the host and immune activation will obviously have deleterious effects upon the ability of the tissue-engineered construct to integrate within the host tissues and otherwise perform as intended.

The inclusion of bioactive factors such as cytokines, chemokines, and peptides within scaffold materials for tissue engineering and regenerative medicine have been shown to have wide ranging effects upon the ability of the material to the promote migration, proliferation, and differentiation of the cells which are seeded onto the scaffold and cultured prior to implantation . These same factors, when included on scaffolds prior to implantation have been shown to have similarly wide ranging effects, which are often dependant on the tissue or organ into which the constructs are implanted. Each of these factors, especially those that have immunomodulatory properties will logically have an effect upon the host response to the construct and, thus, affect the subsequent tissue remodeling outcome associated with its implantation.

Regardless of its components (cells, biomaterials, signaling molecules), the host response to the implanted construct will play a much more important role in the ultimate functionality than the properties of the construct at the time of surgery. Therefore, strong emphasis should be placed upon those factors that influence the host recognition of the engineered construct and subsequent cellular response. Following implantation, the engineered construct will acquire a surface coating of adsorbed proteins, the nature of which will affect the subsequent host response and the interaction with the first responding cell types (neutrophils and macrophages). Further, the type of cells that are included may elicit recognition by the host immune system, and the bioactive factors may alter the nature of this host response. The complex interplay between these events and others will determine whether the implanted construct is infiltrated with cells, degraded, integrated with the surrounding native tissue, or encapsulated.

## 1.3 MACROPHAGES

The studies presented in this dissertation focus upon one major aspect of the host response to biologic materials used in tissue engineering and regenerative medicine, the macrophage response. It is hypothesized that the phenotype of the macrophage population which participates in the host response following the implantation of a biologic scaffold material may be a predictor of the downstream outcome associated with its use. The following section provides a brief background on macrophage origin, heterogeneity, plasticity, and role of the macrophage in the host response following tissue injury. These concepts are then applied to the evaluation of the host response to ECM scaffold materials in an abdominal wall musculature defect model.

### 1.3.1 Origin

Macrophages are monocyte derived myeloid cells that develop from a common myeloid progenitor cell residing within the bone marrow of adult mammals (139). This same myeloid progenitor cell also gives rise to the other cells of the myeloid lineage including neutrophils, eosinophils, basophils and dendritic cells depending upon the cytokines to which the cell is exposed during its development. Monocytes are derived from the common myeloid progenitor cell through a cascade that includes the cytokines granulocyte-macrophage colony stimulating factor (GM-CSF), granulocyte colony stimulating factor (G-CSF), and macrophage colony stimulating factor (M-CSF). These signals induce differentiation of the common myeloid progenitor to monoblasts, pro-monocytes, and finally monocytes. Mature monocytes then leave the bone marrow and enter the blood stream where may they reside for several days before

entering tissues to become macrophages, either in a process of steady-state turnover or due to chemoattractant factors produced as part of a local inflammatory process.

Prior to entering tissues and differentiating into macrophages, circulating blood monocytes are known to be heterogeneous with at least two general populations having been identified (139). These consist of $CD14^{hi}CD16^{-}$ and $CD14^{+}CD16^{+}$ populations in humans and Ly-$6c^{high}$ ($Gr1^{+}$) and Ly-$6c^{low}$($Gr1^{-}$) subsets in mice, and have been grouped into two basic categories termed 'inflammatory' and 'resident', respectively . Inflammatory ($CD14^{hi}CD16^{-}$/Ly-$6c^{high}$) monocytes are characterized by their ability to migrate to sites of injury or infection and to propagate chronic inflammatory diseases, while resident monocytes are characterized by their ability to patrol the vasculature, populate normal tissues, and to act as regulators of the inflammatory response. Similar cell populations to the two described above have been identified in other species, however species dependant differences in characteristic markers do exist.

During normal tissue turnover monocytes differentiate into macrophages upon emigration from the vasculature into the tissue. Once within the tissue, macrophages may undergo differentiation into a number of distinct phenotypes depending on the tissue and the immunologic microenvironment. Native tissue-resident macrophage populations include those of the bone (osteoclast), lung (alveolar macrophage), the nervous system (microglia), connective tissues (histiocytes), the gut, liver (Kupffer cells), the spleen, and the peritoneum. Each tissue-specific macrophage performs a specific function and may be associated with specific patterns of gene expression and functional activity (139). For example, macrophages present within the gut perform a specialized function which requires high levels of phagocytosis and low production of pro-inflammatory cytokines, a phenotype which is distinct from the other macrophage populations listed above. It has been shown that this phenotype can be induced in other

macrophage populations through exposure to intestinal stromal cell products (140), showing that the local microenvironment plays a large role in determining the phenotype and activity of various macrophage populations. This is also an example of the remarkable plasticity exhibited by macrophages, which will be further examined in the following section.

### 1.3.2 Macrophage Polarization

Macrophages, like the monocytes from which they derive, are a heterogeneous cell population with different markers and functions depending upon the signals to which they are exposed (71, 139, 141, 142). Upon leaving the blood stream and migration into sites of inflammation, macrophages become activated in response to tissue damage or infection, causing an increase in the production of cytokines, chemokines, and other inflammatory molecules (139, 141, 143-145). Macrophages have been characterized based on their distinct functional properties as well as their microenvironment. Polarized macrophages are referred to as either M1 or M2 cells, mimicking the Th1/Th2 nomenclature (143). M1, classically activated pro-inflammatory, macrophages are known to be induced by IFN-γ alone or in combination with LPS or TNF. In general, M1 activated macrophages express IL-12$^{high}$, IL-23$^{high}$, IL-10$^{low}$; metabolize arginine, produce high levels of inducible nitric oxide synthase (iNOS); secrete toxic reactive oxygen and nitric oxygen intermediates and inflammatory cytokines such as IL-1β, IL-6, and tumor necrosis factor (TNF); and are inducer and effector cells in Th1 type inflammatory responses (146). In contrast, M2, alternatively activated, macrophages are induced by exposure to a variety of signals including the cytokines IL-4, IL-13, and IL-10, immune complexes, and glucocorticoid or secosteroid (vitamin D3) hormones. M2 activated macrophages express IL-12$^{low}$, IL23-$^{low}$, and IL-10$^{high}$; have high levels of scavenger, mannose, and galactose receptors; produce arginase in

the place of arginine, subsequently producing ornithine and polyamines; and are involved in polarized Th2 reactions (146). It should be noted, however, that M2 alternatively activated macrophages have also been shown to be a heterogenous subset with three well-recognized subpopulations (M2a, M2b, and M2c), each with its own inducers, markers, and function. The characteristics of each macrophage subtype are outlined in Figure 4.

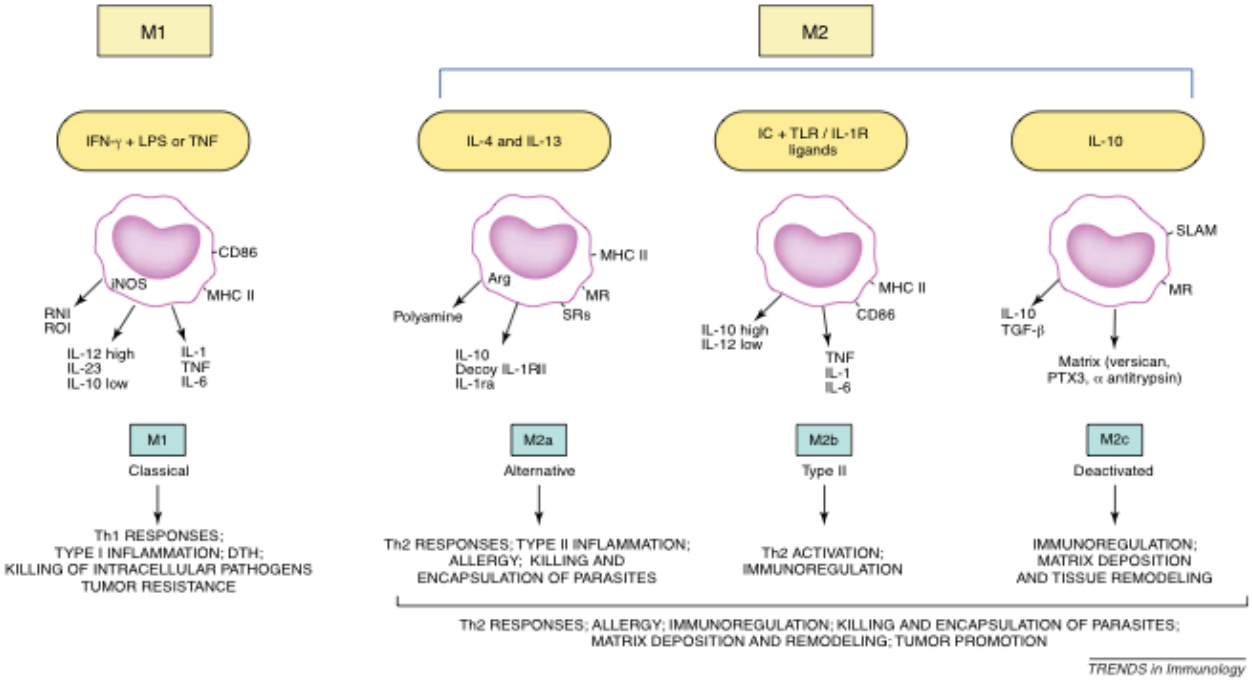


**Figure 4. Inducers and selected markers, secreted products and functionality of polarized macrophage populations. Reprinted from (141) with permission from Elsevier.**

### 1.3.3 Role of Macrophage Polarization in Wound Healing

To date, the causes and the effects of macrophage polarization towards an M1 or M2 phenotype have been studied largely in the context of the host response to pathogens and in cancer biology. However, a number of recent studies have shown that macrophages, and macrophage polarization in particular, play an essential role in the healing response following tissue injury

(147-149). While the overall role of macrophages following tissue injury is well described, these studies show that macrophages with specific phenotypes have distinct roles in tissue remodeling, and that the phenotype of the macrophages which participate in tissue remodeling may play a role in determining the downstream outcome of the remodeling process (i.e. scar tissue formation vs. constructive tissue remodeling).

A recent study examined gene expression during cutaneous wound healing following skin biopsies of human patients (147). Results showed upregulation of a wide variety of genes throughout the duration of wound healing. Of note, however, investigators identified two clusters of genes associated with macrophage M1/M2 polarization, which were upregulated transiently during the wound healing process. The first was upregulated during the early, inflammatory stage of wound healing and contained a mixture of M1 and M2 associated genes (11 M1 genes and 7 M2 genes). The second was upregulated in the later tissue remodeling and angiogenesis stages of healing and contained predominantly M2 associated genes (1 M1 gene and 9 M2 genes). The results of this study suggest evidence for the involvement of M1/M2 polarization in the process of cutaneous wound healing. Similar patterns of macrophage polarization have been described in the myocardium following injury.

Another study investigated the role of macrophages and macrophage polarization in the processes of tissue repair following injury of the spinal cord (148). The results of the study showed that a predominantly M1 phenotype was induced immediately following injury and persisted within spinal cord lesions. A small number of M2 macrophages were also seen in the site of injury at early time points; however, these cells were not observed at later time points in the remodeling process, suggesting that the M1 to M2 phenotype shift does not occur in the same way in the spinal cord as it does in some tissues following injury. This study also showed that

M1 and M2 macrophages had distinct effects upon the survival of neurons and upon and neurite outgrowth. Neurons which were exposed to media conditioned by M1 macrophages were shown to exhibit a decrease in viability as well as a decrease in neurite length, while those cells exposed to media conditioned by M2 macrophages showed improved survival and a greater degree of neurite extension. This suggests that the default response following CNS injury is a chronic pro-inflammatory, M1 type response which leads to decreased viability of the neurons within the site of injury, and that induction of a more M2 type response may be capable of promoting a more constructive tissue remodeling type environment.

Polarized macrophages have also been shown to play an important role in muscle tissue regeneration following injury. In one study, the role of M2 macrophages was investigated in a mouse model of necrotic muscle injury repair (149). In this study it was shown that the deletion of two of the binding sites in the CREB-C/EBPβ pathway blocked the induction of M2 associated genes, while M1 gene expression was not affected. Necrotic injury was induced through the injection of cardiotoxin, an injury which results in rapid recovery of the injured muscle tissue in unaltered mice, and mice were then monitored for up to 10 days following injection. In those mice in which the CREB-C/EBPβ pathway was blocked (i.e. lacked expression of genes associated with the M2 macrophage phenotype), the tissue which formed within the site of tissue remodeling was highly fibrotic and associated with a decrease in myofiber size, which was in direct contrast to control mice which exhibited full recovery of the injured muscle. Representative images of muscle morphology from this study are shown in Figure 5. This shows the importance of the M2 macrophage phenotype in promoting a constructive tissue remodeling type response following skeletal muscle injury.

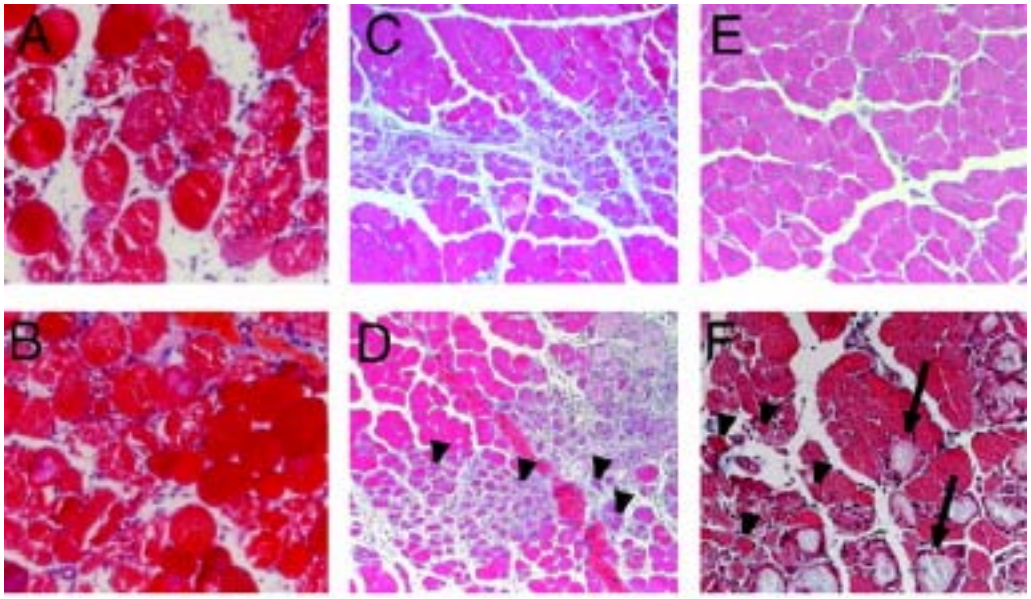


**Figure 5. Muscle tissue remodeling following cardiotoxin injection in normal (C57BL6 – A,C,E) and CREB-C/EBPβ (B, D, F) mice at 2 (A, B), 5 (C, D), and 10 days (E, F) post-injection. Myofibers with eosinophil cytoplasm indicated by arrowheads. Myofibers with decreased size were observed at 10 days in the knockout mice (arrows). Modified from (149) with permission from National Academy of Sciences, USA.**

In this dissertation, concepts of macrophage M1/M2 phenotype are applied to the study of tissue remodeling following the implantation of extracellular matrix scaffold materials in an abdominal wall musculature defect model to determine whether differences in the phenotype of the macrophage population which responds following ECM scaffold implantation may be, in part, a predictor of the downstream tissue remodeling outcome.

## 1.4 CENTRAL HYPOTHESIS

The central hypothesis of this dissertation is that methods used in the production ECM scaffolds have distinct effects upon the characteristics of the resultant scaffold, and that these

characteristics play an important role in determining the ways in which the scaffold materials interact with cells both *in vitro* and *in vivo*, and that ECM scaffold-macrophage interactions play an important role in determining the ability of ECM scaffolds to promote constructive tissue remodeling.

## 1.5 SPECIFIC AIMS

**Aim 1:** To determine the effects of tissue source and chemical cross-linking upon the structure and composition of ECM scaffold materials, and to show that these characteristics have effects upon patterns of cell behavior *in vitro*.

**Aim 2:** To determine the effects of the presence of a cellular component within an extracellular matrix scaffold and the use of carbodiimide during scaffold production upon the capacity of extracellular matrix scaffolds to elicit a constructive tissue remodeling versus encapsulation or scar tissue type remodeling response in model of rat abdominal wall musculature reconstruction.

**Sub-Aim:** To determine whether the host remodeling response to one ECM scaffold material affects the outcome of the host remodeling response to a second material implanted concurrently in the same animal.

**Aim 3:** To show that extracellular matrix scaffolds are capable of altering the default host macrophage response following implantation, and that the modulation of the host macrophage response is related to the ability of the scaffold to promote the constructive versus encapsulation or scar tissue type remodeling responses observed in **Aim 2.**

**Sub-Aim:** To evaluate the effects of polarized macrophages upon the *in vitro* behavior of other cell types.

# 2.0 SPECIFIC AIM 1: EFFECTS OF TISSUE SOURCE AND CHEMICAL CROSS-LINKING UPON EXTRACELLULAR MATRIX SCAFFOLDS

## 2.1 BACKGROUND

The extracellular matrix (ECM) is composed of the secreted molecules produced by the resident cells of each tissue or organ. Thus, the composition and three-dimensional ultrastructure of the ECM is highly related to cell phenotype and the required functions of the tissue or organ from which it is derived. The exact composition of the ECM is dependant on a number of factors that influence resident cell phenotype including mechanical forces, biochemical milieu, oxygen requirements, pH, and gene expression patterns, among others. The ECM, in turn, influences the phenotype, migration, and proliferation of its resident cells, and serves as a medium for signal transfer between cells (2-5). For these reasons, the ECM is considered to be in a state of dynamic reciprocity (3) with the cells which reside within it and to play an important role in normal tissue and organ morphogenesis (6).

For these same reasons, biologic scaffolds composed of ECM have been investigated as inductive templates for functional tissue reconstruction in a number of anatomic locations including the lower urinary tract, skin, musculotendinous tissues, dura mater, esophagus and cardiovascular structures in both preclinical animal studies and in human clinical applications (51, 150-159). ECM scaffolds prepared from different tissue sources or prepared using different

methods have been shown to have distinctive effects upon cell adhesion patterns (1, 160, 161), the ability to support and maintain a differentiated cell phenotype (2, 162, 163), oxygen diffusivity (68), and water permeability (164, 165). It is unknown whether the bulk (or average) composition of the ECM, the surface chemistry, or the ultrastructural morphology, especially the surface ultrastructure, plays a greater role in determining the phenotype of the cells with which it comes into contact.

The process of host tissue remodeling following implantation of a biologically derived scaffold is dependant upon the immediate and subsequent events that occur at the surface of the material following *in vivo* implantation. The surface topography and ligand landscape of the scaffold material will determine the host molecules that bind and the type and behavior of cells that mediate the host response. The production of biologic scaffolds composed of ECM requires the use of processing methods that decellularize and terminally sterilize the material (67). These methods can affect the composition, ultrastructure, mechanical properties, and surface topography of the resulting scaffold, thus potentially affecting the host response associated with its use (67). Similarly, chemical cross-linking is a method used in the production of many commercially available ECM scaffolds that may affect the surface characteristics of the resulting material as well as alter the host response following implantation (69, 166). Therefore a comprehensive understanding of surface characteristics and their effects upon cellular behavior both *in vitro* and *in vivo* is essential for the design of intelligent scaffolds for specific clinical applications.

The objectives of the studies presented in this section were fourfold: (1) to determine and compare by scanning electron microscopy (SEM) and time of flight secondary ion mass spectrometry (ToF-SIMS) the ultrastructure and molecular composition of the surfaces of

extracellular matrix (ECM) scaffolds derived from porcine UBM, SIS, and liver (LECM); (2) to determine the effects of two commonly used methods of chemical cross-linking (carbodiimide and glutaraldehyde) upon the surface characteristics of one of these ECM scaffold materials, specifically UBM; (3) to determine the presence of an intact basement membrane complex on the surfaces of three types of ECM scaffold described above; and (4) to determine the effects of the ECM scaffold surface characteristics upon the *in vitro* growth of NIH 3T3 fibroblasts, human microvascular endothelial cells (HMECs), and embryonic rat spinal cord neurons.

## 2.2 METHODS

### 2.2.1 Preparation of Extracellular Matrix Scaffold Materials

The ECM materials for this study were harvested and prepared using methods previously described (80, 167-169). The urinary bladder, small intestine and liver were harvested from market weight pigs (approximately 110-120 kg) immediately after sacrifice.

#### 2.2.1.1 Urinary Bladder Matrix

Excess adipose tissue and collagenous connective tissue were removed from the outside of the bladder with scissors. The urothelial cells were removed by soaking the bladder tissue in 1.0 N saline. Intraluminal water pressure was used to expand and stretch the bladder to facilitate the removal of the muscle layer and the tunica submucosa. The apex of the bladder was removed using scissors. The bladder was then bisected on one side from the opening to the apical region, forming a rectangular shaped sheet. The luminal side of the bladder was placed downward and

the tunica serosa, tunica muscularis externa, tunica submucosa, and the muscularis mucosa were removed by mechanical delamination. The remaining tissue was then soaked in phosphate buffered saline (PBS, pH 7.4) and represented UBM (21).

#### 2.2.1.2 Small Intestinal Submucosa

The jejunum of the porcine intestine was isolated and the mesentery removed by sharp dissection. The lumen of the isolated segment of jejunum was then flushed with running tap water for 2-5 minutes. The intestine was then split longitudinally and mechanically delaminated to remove the luminal portions of tunica mucosa including the majority of the lamina propria and the entirety of the tunica muscularis externa and serosa. The remaining tunica submucosa and the basilar layers of the tunica mucosa, specifically the muscularis mucosa and stratum compactum, represented SIS (22, 80).

#### 2.2.1.3 Liver Extracellular Matrix

The four lobes of the porcine liver were separated using a scalpel and then trimmed to a uniform shape. The liver lobes were allowed to freeze completely at -80°C for at least 24 hours. The frozen lobes were cut into 5 mm slices using a commercial meat slicer. Because the structure of liver tissue is complex and does not exhibit a layered structure, it was not possible to mechanically delaminate the desired tissue layers as in the case of intestinal and urinary bladder scaffolds. Instead, the liver slices were chemically treated to remove undesired content. The slices were placed in deionized (DI) water and shaken vigorously for 30 minutes at room temperature. This process was repeated with clean DI water for a total of three rinses. The slices were then massaged to hasten the lysis of hepatocytes and the removal of cell remnants, and then were placed in a container of 0.02% trypsin / 0.05% EDTA at 37°C for one hour. The solution

was decanted, the slices rinsed in DI water, and the massaging was repeated. The liver slices were then placed back on the shaker at room temperature for one hour in 3% Triton X-100. The water rinses and massaging process were then repeated as necessary to lyse and remove any remaining cellular elements. The slices were then placed in 4% sodium deoxycholic acid for one hour on a shaker and then rinsed in water. The remaining decellularized connective tissue matrix was referred to as LECM (41).

#### 2.2.1.4 Disinfection and Cell Lysis

Following removal of the appropriate tissue layers and bulk cellular contents from the three organs as described above, the remaining tissue was treated with a 0.1% peracetic acid/4% ethanol solution for two hours at room temperature on a shaker (170). Traces of peracetic acid were removed and the pH was returned to approximately 7.4 by rinsing the ECM at room temperature, with shaking, in PBS one time, then in water twice, and then again in PBS one time. Each rinse lasted 15 minutes. Samples to be examined by time of flight secondary ion mass spectrometry were subjected to three additional 1-hour long water rinses and one overnight water rinse to remove as much of the residual contamination which might affect ToF-SIMS data collection (e.g., Na, K, Si, PDMS) remaining from the production process as possible. The resulting decellularized and disinfected ECM scaffolds were then lyophilized prior to any cross-linking or sterilization treatments as described below.

#### 2.2.1.5 Cross-linking of Urinary Bladder Matrix

Scaffolds composed of UBM were cross-linked by immersion in solutions of either carbodiimide (10 mM; CDI-UBM) or glutaraldehyde (0.625%; GLUT-UBM) for 8-10 hours at room temperature. The cross-linked scaffolds were subjected to three separate 1 hour water

washes as well as an overnight water wash to remove any residual cross-linking solution or contamination that may have remained following the cross-linking process.

#### 2.2.1.6 Terminal Sterilization

The resulting decellularized and disinfected ECM scaffolds were terminally sterilized by exposure to ethylene oxide gas for 16 hours.

### 2.2.2 Characterization of Extracellular Matrix Scaffolds

#### 2.2.2.1 Scanning Electron Microscopy

Samples to be utilized in the characterization of ultrastructure were dehydrated by sequential immersion in 30, 50, 70, 90, and 100 percent ethanol. The immersion in 100 percent ethanol was repeated three times. Residual ethanol in the samples was exchanged with hexamethyldisilazane (HMDS) and then the samples were allowed to air dry. Samples were attached to aluminum specimen mounting stubs and sputter coated with gold palladium alloy. The samples were then analyzed using a JEOL 6330F field emission gun SEM with an accelerating voltage of 3 kV.

#### 2.2.2.2 Time of Flight Secondary Ion Mass Spectrometry

ToF-SIMS is an analytically sensitive surface technique that can be used to create a detailed mass spectrum of the outermost 10-20 Å of a sample (171). ToF-SIMS is performed by bombarding the surface of the sample with a beam of primary ions and then measuring the

intensities of the individual masses of the positive and negative secondary ions emitted (Figure 7A and B). Analysis of the type and amount of secondary ions generated can provide important information about the material from which they were emitted including the composition, structure, orientation and spatial distribution of the molecules on the surface (Figure 7B).

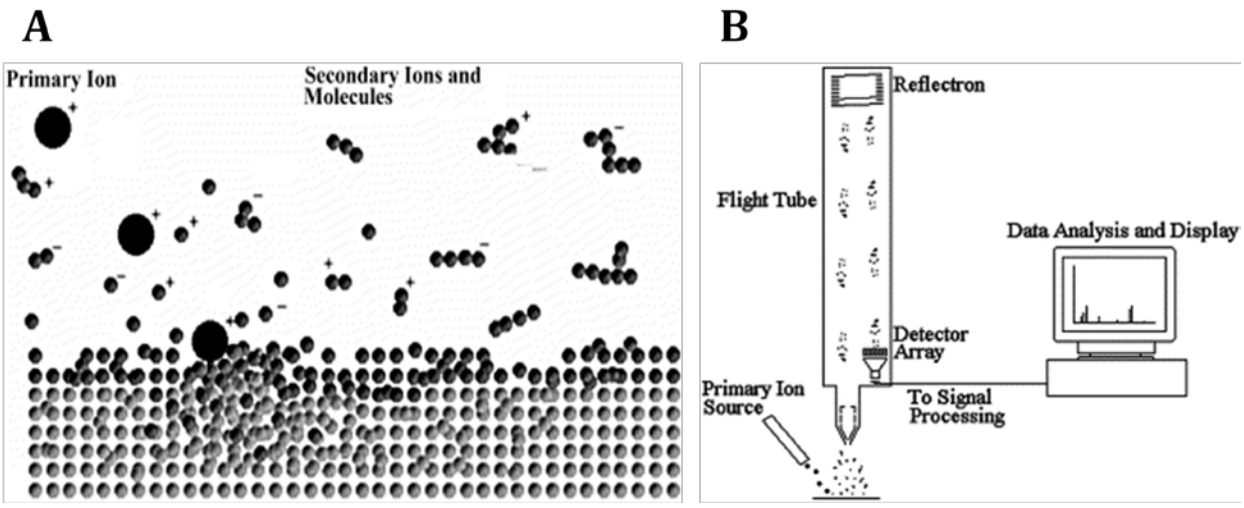


**Figure 6. (A) A schematic drawing of the secondary ion emission process initiated by the impact of a primary ion. Extensive fragmentation occurs near the collision site producing mainly atomic particles. Away from the point of impact collisions become less energetic resulting in the emission of larger molecular fragments. (B) Schematic drawing of a SIMS instrument with a TOF analyzer. The primary ion source, sample, and flight tube are kept under ultrahigh vacuum. The mass of the detected ions is determined by the flight time of the ion between the extractor and the detector. The reflectron helps compensate for energy and angular dispersion that can occur during the emission process. Reprinted from (171) with permission from Elsevier.**

In the present study, ToF-SIMS spectra were acquired on an ION-TOF ToF.SIMS 5-100 spectrometer using an 25 keV Bi+ ion source in the pulsed mode, at a pulse width of approximately 2 ns based on the hydrogen peak width, to enhance mass resolution of the spectra. Spectra were acquired for both positive and negative secondary ions over a mass range of mass to charge ratio (m/z) = 0 to 700. The primary ion current was 0.8 pA. Secondary ions of a given

polarity were extracted and detected using a reflectron time-of-flight mass analyzer. Spectra were acquired using an analysis area of 0.005-0.01 $mm^2$. Positive ion spectra were mass calibrated using the $CH_3$+, $C_2H_3$+, and $C_3H_5$+ peaks. Negative ion spectra were not considered in this study as they lacked characteristic peaks. Mass calibration errors were kept below 10 ppm. Mass resolution (m/Dm) for a typical spectrum was 3000 - 7000 at m/z = 27.

Multivariate analysis was conducted by selecting peak sets from the samples analyzed by ToF-SIMS. The selected peaks were then normalized to the total ion intensity of all peaks selected to account for fluctuations in secondary ion yield between different spectra. Principal components analysis (PCA) was then employed to analyze the positive ToF-SIMS data using a Matlab based algorhithm. All spectra were mean-centered before running PCA. PCA was used to determine the linear combination of peaks that captured the highest degree of variation in a dataset (172).

#### 2.2.2.3 Immunolabeling

Immunolabeling was performed using the Vectastain advin-biotin peroxidase (ABC) method. Tissues were frozen in optimal cutting temperature solution and sectioned on a cryostat at 8μm and placed on slides. The cryosections were thawed to room temperature, fixed in acetone for five minutes at room temperature, rinsed in PBS, treated with 0.3% hydrogen peroxide in methanol at room temperature for 30 minutes to quench endogenous peroxidase activity, rinsed in PBS, and then incubated in 1.5% serum for 30 minutes in a 37°C humidified chamber to block binding of antibodies to nonspecific proteins. Serum for blocking was horse serum or rabbit serum, depending on the host species of the secondary antibody. Following incubation in blocking serum, sections were incubated in primary antibody in a 37°C humidified chamber for 30 minutes and then rinsed in PBS. Sections were then incubated in the appropriate

secondary antibody for 30 minutes in a humidified 37°C chamber and again rinsed in PBS. Sections were then incubated in Vectastain ABC reagent for 30 minutes in a humidified 37°C chamber, rinsed 3 times in PBS for a total of five minutes, incubated in 4% diaminobenzadine (DAB) substrate solution at room temperature while being viewed on a microscope until slides showed the desired darkness of antigen labeling. Finally slides were rinsed in DI water to stop the development of the DAB substrate prior to coverslipping. Each PBS rinse in the protocol was for 5 minutes at room temperature, replacing the PBS 3 times, with occasional agitation.

The primary antibodies used were rabbit anti-human laminin at 1:100, rabbit anti-human collagen IV at 1:200, and mouse anti-human collagen VII, which was used undiluted. All primary antibodies cross-reacted with porcine tissue. The secondary antibodies used were biotinylated goat anti-rabbit IgG at 1:200 and biotinylated horse anti-mouse IgG at 1:200.

For collagen IV staining, formalin fixed paraffin embedded tissue samples were sectioned, dewaxed and treated as the frozen sections, beginning with the hydrogen peroxide step.

### 2.2.3 Cell Culture on Extracellular Matrix Scaffolds

#### 2.2.3.1 NIH 3T3 Mouse Fibroblasts

NIH 3T3 fibroblasts were cultivated in Dulbecco's modified eagle medium (DMEM) containing 10% fetal bovine serum. Cells were grown at 37°C in a 5% $CO_2$/95% air humidified incubator, and were harvested for seeding when they were approximately 70-80% confluent. All scaffolds were placed in 100mm cell culture dishes, one sample per dish, and stainless steel tissue culture rings with inner diameters of 1.5 cm were placed on the scaffolds. Pressure was applied to create a seal and to hold the sheets of ECM on the bottom of the Petri dish. The

scaffolds were incubated in 1mL of the appropriate media at 37°C and 5% $CO_2$ for approximately 15 minutes prior to cell seeding, at which point the media was removed just before adding the cells. Cells were trypsinized, counted and placed on the ECM scaffolds within the tissue culture rings at concentrations of either $0.5X10^6$ or $1X10^6$ cells per ring. Growth media was added to the cell culture dishes and dishes were incubated at 37°C and 5% $CO_2$. After 4 hours, two-thirds of the media was replaced with fresh media. After four additional hours at 37°C and 5% $CO_2$, the stainless steel rings were removed. The cells were grown on the scaffolds for 10 days at 37°C and 5% $CO_2$.

#### 2.2.3.2 Human Microvascular Endothelial Cells

HMECs were cultivated in MCDB-131 medium containing 10% fetal bovine serum, 2mM L-glutamine, 100 units/ml penicillin/100 ug/ml streptomycin, and 1 ug/ml hydrocortisone. Cells were grown at 37°C in 5% $CO_2$/95% air humidified incubator, and were harvested for seeding when they were approximately 70-80% confluent. The same cell seeding procedure described above for NIH 3T3 cells was used for the culture of HMEC cells upon ECM scaffolds.

#### 2.2.3.3 Histologic Staining

After the 10-day growth period, ECM scaffolds seeded with either NIH 3T3 cells or HMECs were placed in 10% neutral buffered formalin, embedded in paraffin, and then sectioned and stained with hematoxylin and eosin prior to being viewed under a light microscope.

#### 2.2.3.4 Primary Rat Embryonic Spinal Cord Neurons

Spinal cord neurons were isolated from embryonic day 14 Sprague–Dawley rat pups. Spinal cords were isolated under a dissection microscope and placed in cold Hank's buffered salt

solution (HBSS) without $Ca^{2+}$ and $Mg^{2+}$, minced into pieces approximately 0.5 $mm^2$ in size and enzymatically dissociated in 2 ml 0.25% trypsin solution containing 0.05% collagenase L1 at 37° C for 20 min. Cell digestion was inhibited by adding 2 ml SBTI-DNAse solution (0.52 mg/ml soybean trypsin inhibitor, 3.0 mg/ml BSA, 0.04 mg/ml bovine pancreas DNAse). The cell suspension was gently mixed with a Pasteur pipette and centrifuged at 800 × g for 5 min. The resulting pellet was then re-suspended in plating medium and gently mixed. The plating medium consisted of 20% horse serum, 2 mM L-glutamine, 5 ml HBSS without $Ca^{2+}$ and $Mg^{2+}$ and 9.8ml DMEM.

Single sheets of UBM were cut with a 1.5 cm diameter circular punch and sterilized to create discs for use in cell culture experiments. Using sterile stainless steel rings to anchor the UBM discs, spinal cord neurons were seeded on the abluminal surface of the discs in plating medium at a plating density of $3 \times 10^5$ cells/$cm^2$ and allowed to adhere for 4 h in culture conditions of 5% $CO_2$ and 37 °C in a humidified environment. After 4 h, the medium was exchanged with 1 ml serum-free culture medium containing Neurobasal-A, 1× B27 supplement and 1 mM Glutamax. The cells were maintained in a humidified 5% CO2 atmosphere at 37°C, with 50% of the culture medium changed every 4 days. Cells were seeded at the same concentration on poly-L-lysine-coated coverslips (12.5 μg/ml in $H_2O$) as a control.

#### 2.2.3.5 Immunolabeling

Rat primary spinal cord neurons seeded on control coverslips were maintained in culture for 5 days and were then washed three times with PBS warmed to 37°C, fixed with 4% formaldehyde at 37°C for 15 min and incubated in permeablization buffer (0.5% Triton X) for 15 min at room temperature. All antibodies were diluted in a modified PBS solution (0.3 M NaCl

PBS, 0.3% Triton X). All primary antibodies were diluted to a working dilution of 1:100 in PBS and incubated overnight at 4°C. All secondary antibodies, also at a working dilution of 1:100, were incubated for 1 h at 37°C. After each stage of antibody incubation, the samples were gently washed three times for 5 min in PBS. Samples were examined using antibodies against β-tubulin III and GFAP and appropriate secondary antibodies, FITC-conjugated goat anti-mouse IgG and TRITC-conjugated goat anti-rabbit IgG, respectively. All samples were mounted in Vectashield mounting medium containing 4',6-diamidino-2-phenylindole (a nuclear stain, DAPI) prior to being viewed under a fluorescence microscope.

UBM cell-seeded discs were harvested after 5 days and fixed with 10% neutral buffered formalin for 24 h. Sections of the discs were trimmed, embedded in paraffin and then cut in into 5 μm thick sections. All sections were deparaffinized by immersion in a xylenes and a graded series of ethanol before being immersed in permeablization buffer (0.5% Triton X) for 15 min at room temperature. Sections were then triple-stained as described above for samples grown on coverslips.

#### 2.2.3.6 Scanning Electron Microscopy

ECM scaffolds seeded with primary spinal cord neurons were fixed for 2 h with 2.5% glutaraldehyde. After three 15 min washes in PBS, the samples were dehydrated through a graded series of ethanol washes, followed by chemical drying with 100% HMDS overnight. Samples were sputter-coated with a 4 nm thick layer of gold-palladium alloy and then examined using a JEM 6335F field emission gun SEM with an excitation voltage of 4 kV.

## 2.3 RESULTS

### 2.3.1 Characterization of Extracellular Matrix Scaffolds

#### 2.3.1.1 Scanning Electron Microscopy

Scanning electron micrographs showed morphological and structural differences between the luminal and abluminal sides of SIS and UBM but not LECM, which did not appear to possess a distinct sidedness. In brief, a network of collagen, reticular fibers, and elastic fibers with varying diameters ranging from submicron to micron scale were observed on the abluminal sides of SIS and UBM while the luminal sides were characterized by a relatively smooth surface comprised of tightly compacted fibers in the case of SIS or a smooth surface characteristic of a basement membrane structure in the case of UBM. This is in contrast with LECM, which consisted of a dense meshwork of predominantly submicron fibers throughout the entirety of the material. The inter-fiber distance on the abluminal sides of SIS and UBM was observed to be greater than the distance between the fibers present in LECM. Furthermore, on the abluminal sides of SIS and UBM, smaller fibers characteristic of reticular and elastic fibers (173) were found to be interlaced with the larger bundles of collagen I, creating a more porous extracellular matrix microenvironment compared to that observed in LECM. Representative SEM images of the surfaces of the non-cross-linked UBM, SIS, and LECM scaffolds are shown in Figure 7 and a cross sectional view of the same scaffolds is shown in Figure 8.

The CDI-UBM demonstrated distinct structural differences in the arrangement of collagen fibers from those observed for GLUT-UBM and non-cross-linked UBM. Fibers on the abluminal side of the CDI-UBM appeared to coalesce to form a more dense, compact mesh of collagen with smaller pore sizes compared to non-cross-linked UBM and GLUT-UBM. The

abluminal side of GLUT-UBM showed thicker bundles of collagen than were found in UBM; however, GLUT-UBM maintained a similar pore size to that observed on the abluminal side of non-cross-linked UBM. Fewer individual reticular and elastic fibers were observed in both CDI-UBM and GLUT-UBM than were observed in non-cross-linked UBM. The luminal sides of both CDI-UBM and GLUT-UBM exhibited a more fibrous surface topography as compared to non-cross-linked UBM. Representative SEM images of the surfaces of the cross-linked UBM scaffolds are shown in Figure 9.

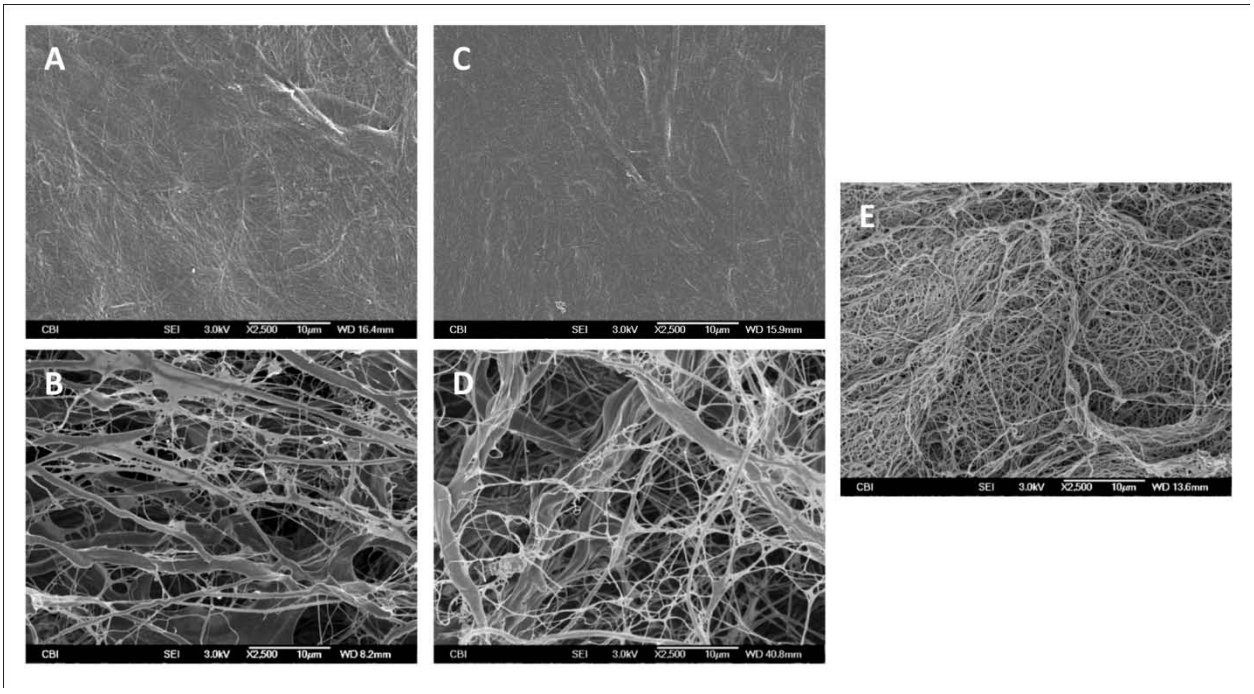


**Figure 7. SEM images of the luminal surface of SIS (A), the abluminal surface of SIS (B), the luminal surface of UBM (C), the abluminal surface of UBM (D), and the surface of LECM (E). All images are 2500X magnification and scale bar = 10 μm. Reprinted from (174) with permission from Elsevier.**

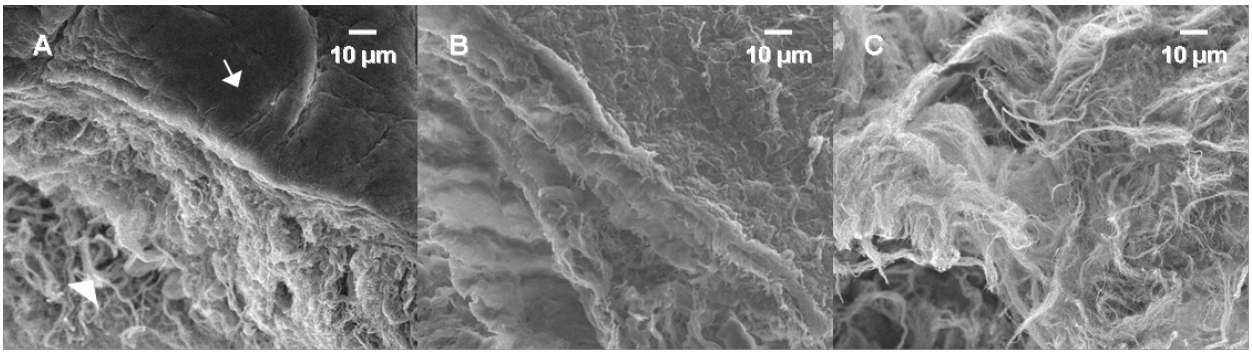


**Figure 8. SEM showing a cross sectional view of UBM, SIS, and LECM scaffolds. The presence of a smooth surface ultrastructure which is consistent with a basement membrane (arrow) and underlying connective tissue of the tunica propria (arrowhead) was observed in UBM (A). SIS (B) and LECM (C) do not contain a smooth surface ultrastructure which is consistent with non-basement membrane surfaces. (400X). Reprinted from (1) with permission from Elsevier.**

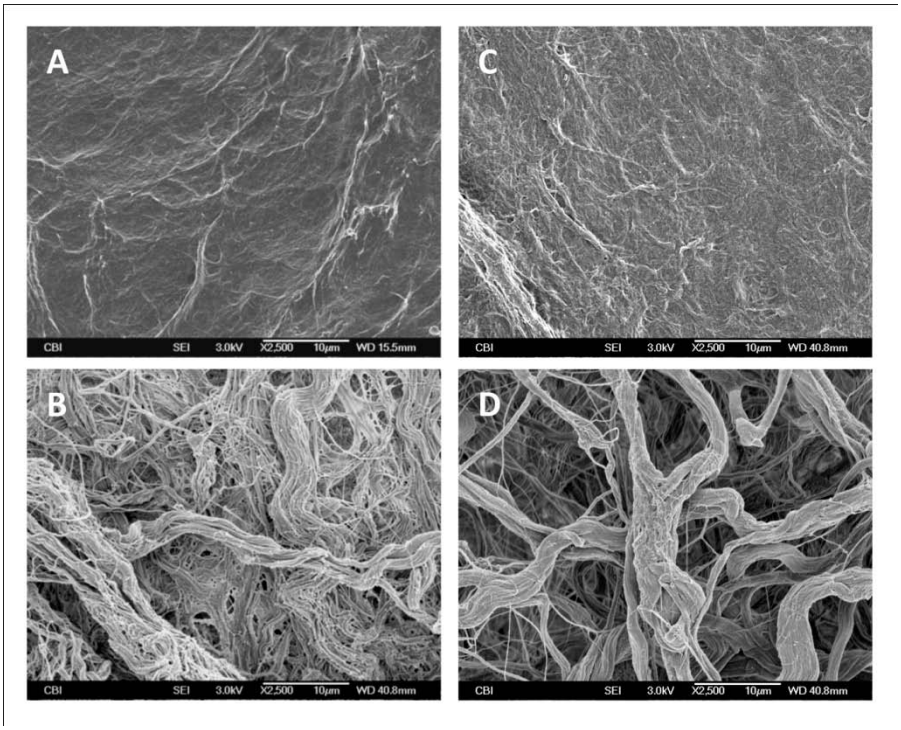


**Figure 9. SEM images of the luminal surface of CDI-UBM (A), the abluminal surface of CDI-UBM (B), the luminal surface of GLUT-UBM (C), and the abluminal surface of GLUT-UBM. All images are 2500X magnification and scale bar = 10 µm. Reprinted from (174) with permission from Elsevier.**

#### 2.3.1.2 Time of Flight Secondary Ion Mass Spectrometry

In all of the samples investigated, the majority of the total ion yield was observed in the mass (m/z) 0-150 range with the exception of large peaks at m/z 166.06, 184.07, and 224.11, which were observed in the SIS and UBM as well as the cross-linked UBM samples but not the LECM samples. Representative positive ion spectra from the abluminal and luminal sides of the SIS and UBM samples along with spectra from the single sided LECM samples are shown in Figure 10. Figure 11 shows representative positive ion spectra for the luminal and abluminal sides of the CDI-UBM and GLUT-UBM samples.

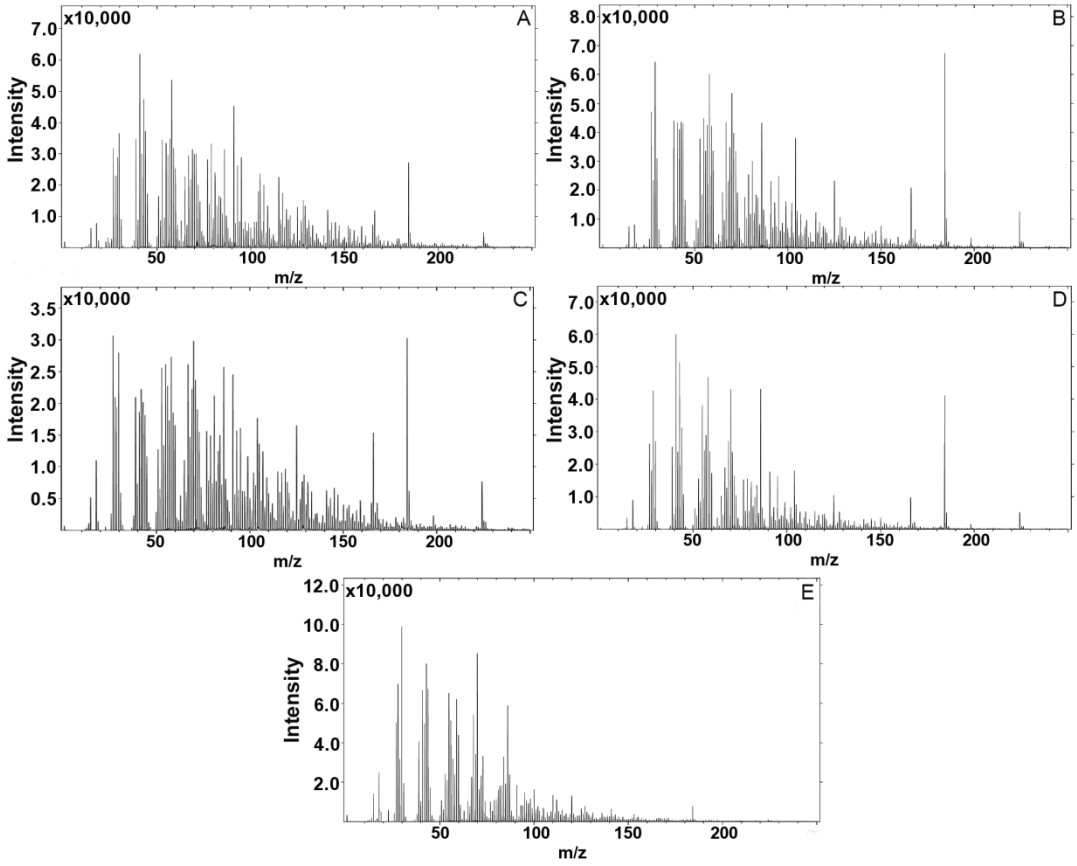


**Figure 10. Representative positive ion spectra from the luminal surface of SIS (A), the abluminal surface of SIS (B), the luminal surface of UBM (C), the abluminal surface of UBM (D), and the surface of LECM (E). Reprinted from (174) with permission from Elsevier.**

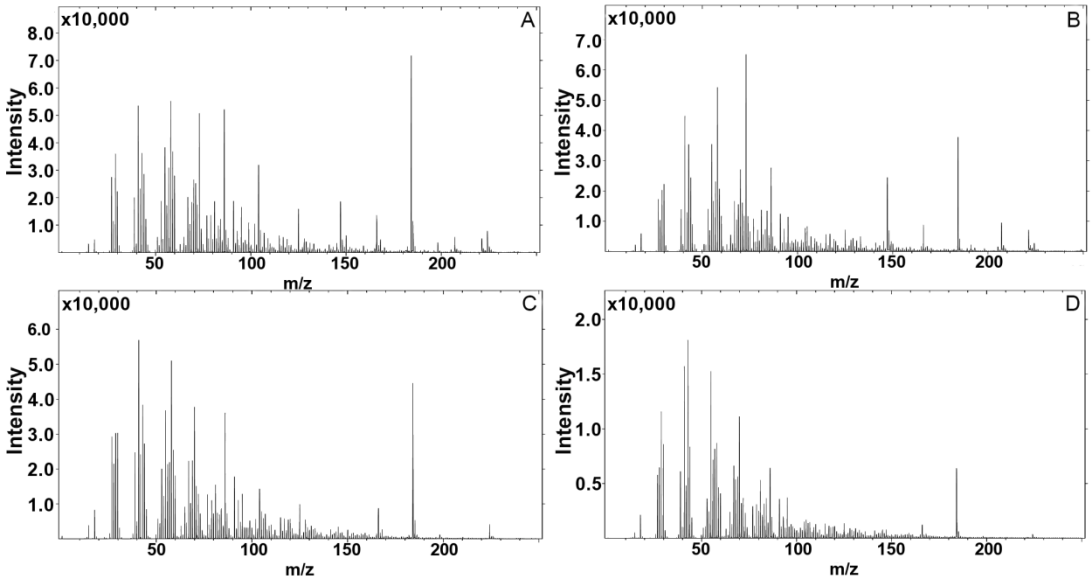


**Figure 11. Representative positive ion spectra from the luminal surface of CDI-UBM (A), the abluminal surface of CDI-UBM (B), the luminal surface of GLUT-UBM (C), and the abluminal surface of GLUT-UBM. Reprinted from (174) with permission from Elsevier.**

The peak list used for PCA (Table 3) in the present study is a slightly abbreviated version of a previously published peak list (175, 176). This list is comprised of peaks characteristic of unique amino acid mass fragmentation patterns created from model extracellular matrix protein surfaces analyzed with ToF-SIMS (175). All PCA data is presented with 95% confidence intervals (176).

**Table 3. Positive Ion Fragment List for Multivariate Analysis with Amino Acids Adapted from Previous Work. (175, 176) Reprinted from (174) with permission from Elsevier.**

| Molecular Fragment | Mass | Prevalent Amino Acid | Extracellular Matrix Protein Association |
|---|---|---|---|
| $CH_4N$ | 30.036 | Gly | Collagen I |
| $CH_3N_2$ | 43.029 | Arg | Laminin |
| $C_2H_6N$ | 44.052 | Ala/Cys | |
| $C_3H_3O$ | 55.020 | Tyr | Fibronectin |
| $C_2H_4NO$ | 58.029 | Gly | Collagen I |
| $CH_5N_3$ | 59.048 | Arg | Laminin |
| $C_2H_6NO$ | 60.045 | Ser | Fibronectin |
| $C_2H_5S$ | 61.011 | Met | Collagen I |
| $C_4H_6N$ | 68.068 | Pro | Collagen I |
| $C_4H_5O$ | 69.039 | Thr | Fibronectin |
| $C_3H_4NO$ | 70.035 | Asn | Laminin |
| $C_3H_3O_2$ | 71.013 | Ser | Fibronectin |
| $C_3H_6NO$ | 72.047 | Gly | Collagen I |
| $C_4H_{10}N$ | 72.088 | Val | Fibronectin |
| $C_2H_7N_3$ | 73.070 | Arg | Laminin |
| $C_3H_8NO$ | 74.065 | Thr | Fibronectin |
| $C_2H_6NS$ | 76.028 | Cys | Laminin |
| $C_4H_5N_2$ | 81.037 | His | |
| $C_5H_7O$ | 83.053 | Val | Fibronectin |
| $C_4H_6NO$ | 84.048 | Glu | Fibronectin |
| $C_5H_{10}N$ | 84.086 | Lys | |
| $C_3H_5N_2O$ | 85.051 | Gly | Collagen I |
| $C_3H_7N_2O$ | 87.062 | Asn/Gly | |
| $C_3H_6NO_2$ | 88.047 | Asn/Asp | |
| $C_5H_7N_2$ | 95.060 | His | |
| $C_4H_4NO_2$ | 98.024 | Asn | Laminin |
| $C_4H_{10}N_3$ | 100.091 | Arg | Laminin |
| $C_4H_{11}N_3$ | 101.038 | Arg | Laminin |
| $C_4H_{10}NS$ | 104.070 | Met | Collagen I |
| $C_7H_7O$ | 107.060 | Tyr | Fibronectin |
| $C_5H_8N_3$ | 110.027 | Arg/His | |
| $C_4H_5N_2O_2$ | 113.052 | Gly | Collagen I |
| $C_4H_7N_2O_2$ | 115.059 | Gly | Collagen I |
| $C_5H_9OS$ | 117.074 | Met | Collagen I |
| $C_8H_{10}N$ | 120.099 | Phe | |
| $C_6H_5N_2O$ | 121.068 | His | |
| $C_5H_{11}N_4$ | 127.096 | Arg | Laminin |
| $C_9H_8O$ | 132.092 | Phe | |
| $C_8H_{10}NO$ | 136.078 | Tyr | Fibronectin |
| $C_{10}H_{11}N_2$ | 159.122 | Trp | Fibronectin |
| $C_{11}H_8NO$ | 170.086 | Trp | Fibronectin |

Figure 12a shows principal component (PC) 1 vs. PC 2 for the non-cross-linked UBM, SIS, and LECM samples. Distinct differences were observed between the LECM samples and the luminal and abluminal surfaces of UBM and SIS. These differences were predominantly observed in PC 1, which accounted for 60% of the statistical separation of the total variance between all samples. It was observed that the peaks at m/z 30.036 ($CH_4N$), 59.048 ($CH_5N_3$), and 68.068 ($C_4H_6N$) accounted for the majority of the loading on the LECM side of the PC 1 axis while peaks at m/z 72.088 ($C_4H_{10}N$), 115.059 ($C_4H_7N_2O_2$), and 117.074 ($C_5H_9OS$) accounted for the majority of the loading on the side of the PC 1 axis attributed to the UBM and SIS samples (Figure 12b).

It was further observed that PC 2, which accounts for 18% of the total sample variance, was predominantly associated with differences between the luminal and abluminal surfaces of the UBM and SIS samples. More specifically, clear sample separation is seen in Figure 12a between the abluminal and the luminal surfaces of UBM. More overlap of the data in PC2 was observed in the luminal and abluminal surfaces of SIS than was observed for the UBM samples making clear differentiation of the peaks associated with each SIS surface difficult (Figure 12b).

To better assess differences in the spectra taken from the luminal and abluminal sides of UBM, PCA was performed on ToF-SIMS data taken from only the luminal and abluminal sides of UBM (i.e. data from SIS or LECM was not included). The scores and loadings for this comparison can be seen in Figure 13. Only PC 1 is shown as PC 2 for the abluminal and luminal sides of UBM did not capture discernable trends in the data (Figure 13a). It was observed that PC 1, which accounted for 47% of the total sample variance, was associated with differences between the luminal and abluminal surfaces of UBM. Peaks at m/z 73.070 ($C_2H_7N_3$), 115.059

($C_4H_7N_2O_2$), and 117.074 ($C_5H_9OS$) were observed to account for the majority of the loading on the portion of the PC 1 axis associated with the luminal surface of UBM, while peaks at m/z 44.052 ($C_2H_6N$), 55.020 ($C_3H_3O$), and 72.088 ($C_4H_{10}N$) accounted for the majority of the loading associated with the abluminal surface of UBM (Figure 13b). A similar analysis was performed for the abluminal and luminal surfaces of SIS; however, distinct peaks were not distinguishable due to overlap in the PCA data affiliated with the SIS surfaces (data not shown).

For the analysis of the differences between the surfaces of cross-linked and non-cross-linked UBM samples, spectra obtained from the CDI and GLUT treated UBM samples were compared to those obtained from the non-cross-linked samples used above. Overlapping of the data was observed in the PCA analysis when performed on the luminal and abluminal surfaces of UBM, CDI-UBM, and GLUT-UBM together. However, more distinct trends were observed when the luminal sides of UBM, CDI-UBM, and GLUT-UBM were examined separately. The scores and loadings for this analysis are shown in Figure 14.

In Figure 14a, separation associated with the non-cross-linked samples as compared to the two cross-linked samples can be observed. PC 1, which captures 51% of the total variance, can be used to clearly differentiate the CDI cross-linked sample from the non-cross-linked sample while there is some overlap of the glutaraldehyde cross-linked sample with non-cross-linked UBM surface. In PC 2, which captures 30% of the variance, the samples are not statistically distinct, but the graphical locations of the 95% confidence intervals suggest that differences may exist and further characterization of these distinctions could be done in future work. A similar analysis was performed on the abluminal sides of UBM, CDI-UBM, and GLUT-UBM, but the comparisons are not included as trends were difficult to extract due to overlapping loadings.

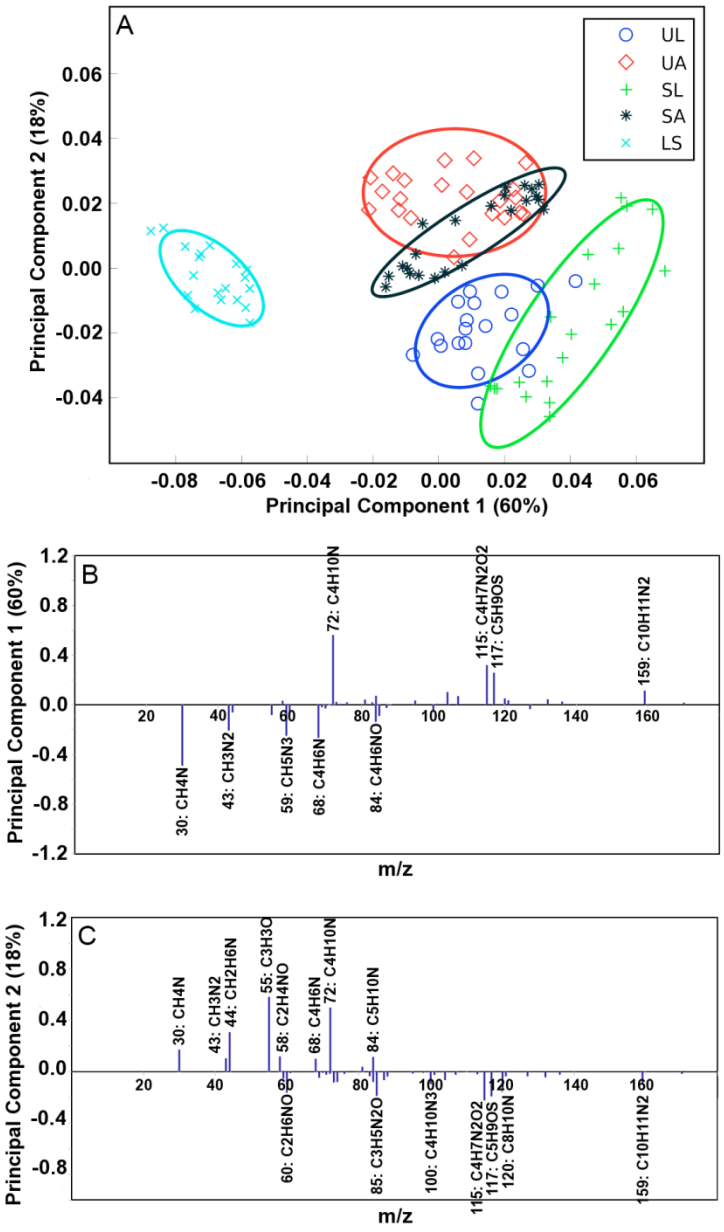


**Figure 12. Principal component scores and loadings for UBM, SIS, and LECM samples. (A) PC1 vs. PC2 scores plot for the luminal surface of UBM (UL; circle), the abluminal surface of UBM (UA; diamond), the luminal surface of SIS (SL; cross), the abluminal surface of SIS (SA; asterisk), and the surface of LECM (LS; x). All results are presented with 95% confidence interval (35). (B) Loadings for PC1. (C) Loadings for PC2. Peaks with loadings greater than 0.1 are labeled with their respective ion. Reprinted from (174) with permission from Elsevier.**

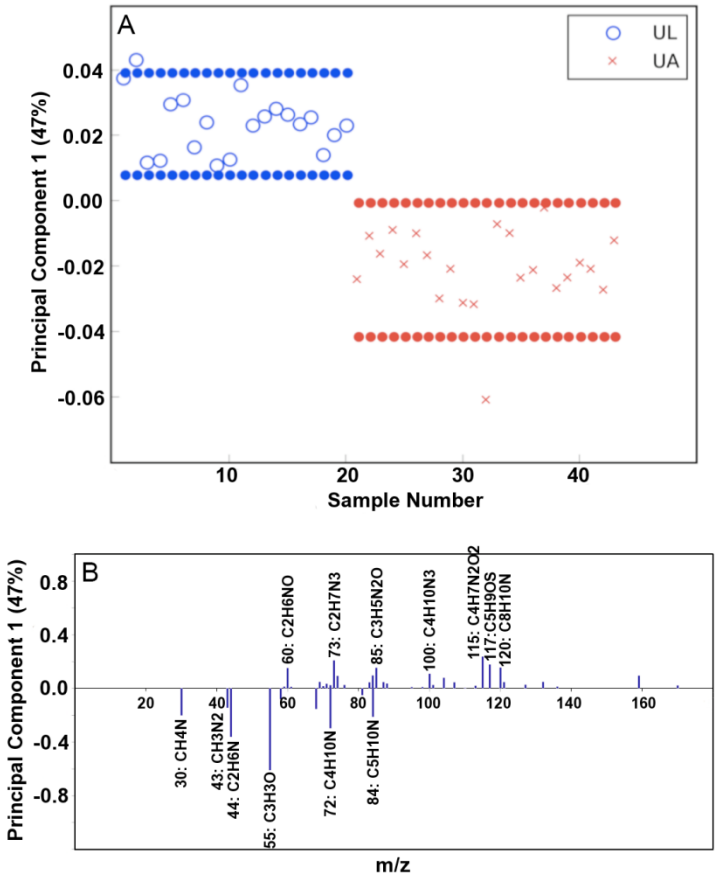


**Figure 13. Principal component 1 scores and loadings for the luminal surface of UBM (UL; circle) and the abluminal surface of UBM (UA; x). Only PC1 is presented. All results are presented with 95% confidence interval (35). (B) Loadings for PC1. Peaks with loadings greater than 0.1 are labeled with their respective ion. Reprinted from (174) with permission from Elsevier.**

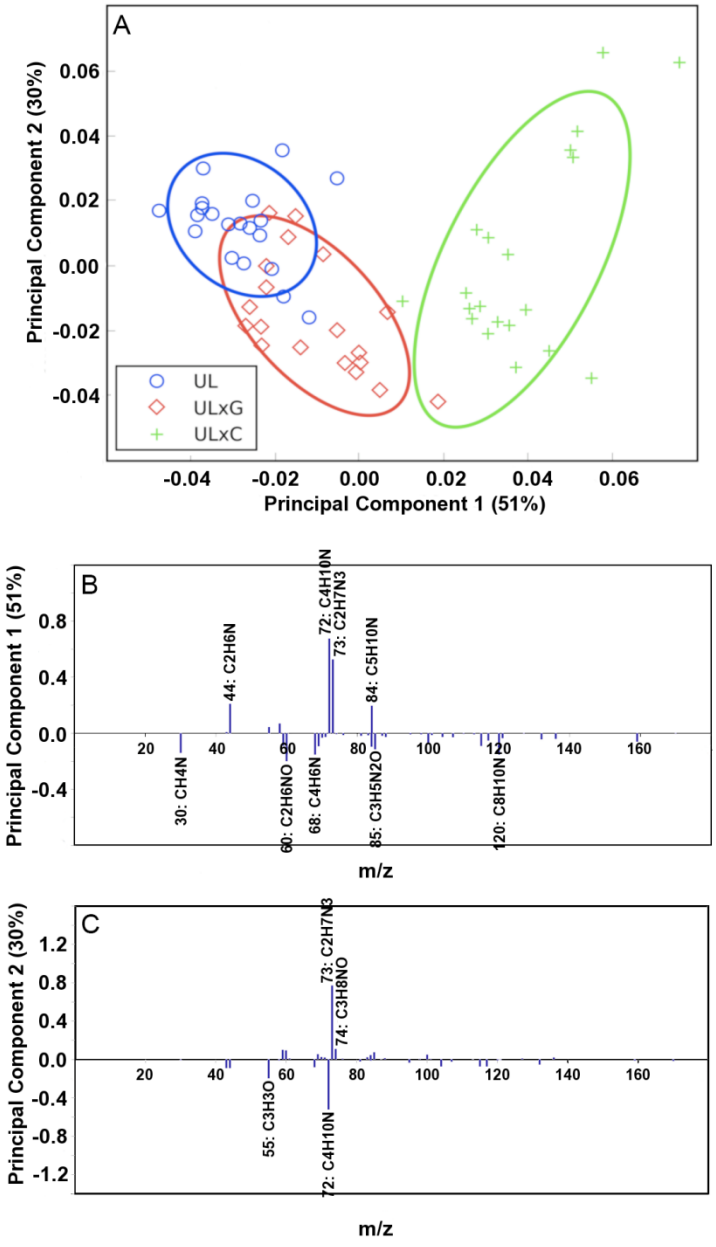


**Figure 14. Principal component scores and loadings for the luminal sides of UBM, UBM-CDI (ULxC) and UBM-GLUT (ULxG) samples. (A) PC1 vs. PC2 scores plot for the luminal surface of UBM (circle), the luminal surface of UBM-GLUT (diamond), and the luminal surface of UBM-CDI (cross). All results are presented with 95% confidence interval (35). (B) Loadings for PC1. (C) Loadings for PC2. Peaks with loadings greater than 0.1 are labeled with their respective ion. Reprinted from (174) with permission from Elsevier.**

#### 2.3.1.3 Immunolabeling

Positive staining for collagen IV (Figure 15) was observed in the vasculature of all of the scaffold materials examined in this study. For the UBM scaffold material, collagen IV staining was also localized at the surface of the tissue in a contiguous pattern consistent with the presence of a basement membrane complex. There was dense positive staining for collagen IV also noted near the surface of SIS consistent with the stratum compactum layer of this ECM. Positive staining for laminin (Figure 16) was localized to the vasculature of all scaffold materials examined and in a contiguous pattern at the surface of UBM material. UBM was the only ECM that stained positive for collagen VII (Figure 17). Positive staining for collagen VII in UBM was localized with the collagen IV and laminin on the luminal surface of the tissue, consistent with the presence of an intact basement membrane complex.


**Figure 15. Immunoperoxidase staining showed the presence of collagen IV in UBM (A), SIS (B) and LECM (C) (40X). Scale bar = 100 μm. Reprinted from (1) with permission from Liebert Publishing.**

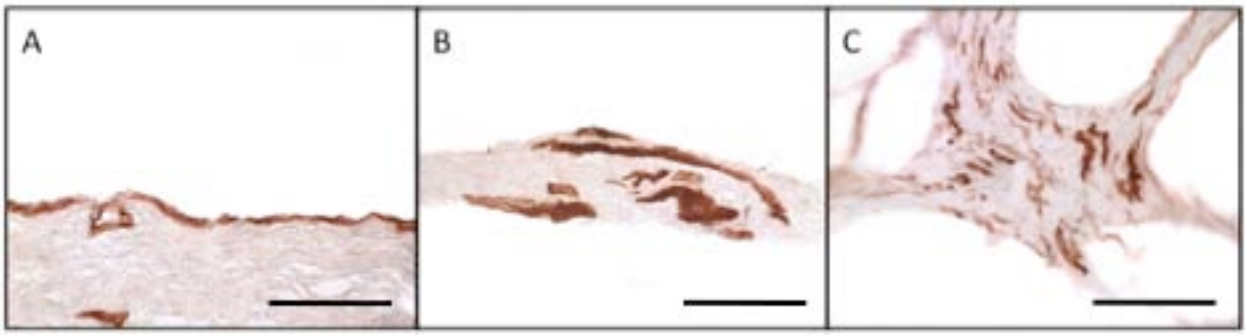


**Figure 16. Immunoperoxidase staining showed the presence of laminin in UBM (A), SIS (B) and LECM (C) (40X). Scale bar = 100 μm. Reprinted from (1) with permission from Liebert Publishing.**

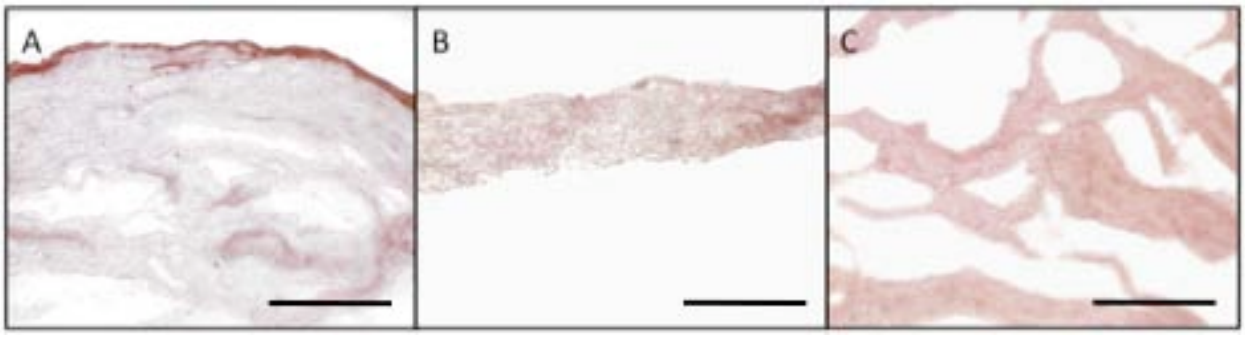


**Figure 17. Immunoperoxidase staining showed the presence of collagen VII in UBM (A), SIS (B) and LECM (C) (40X). Scale bar = 100 μm. Reprinted from (1) with permission from Liebert Publishing.**

### 2.3.2 *In Vitro* Cell Behavior and Phenotype

#### 2.3.2.1 NIH 3T3 Fibroblasts and HMECs

NIH 3T3 cells invaded below the surface and extended into the underlying connective tissues when seeded on UBS, SIS and LECM and when seeded on the abluminal surface of UBM. However, NIH 3T3 cells formed confluent layers on, but did not invade, the luminal

(basement membrane containing) surface of the UBM. The same growth patterns were observed when either a concentration of 0.5 X 10^6 or 1 X 10^6 cells was used as the cell seeding density. The characteristic patterns of growth of NIH 3T3 when seeded on the abluminal and on the luminal surfaces of UBM as well as SIS and LECM scaffolds are illustrated in Figure 15. Patterns of cell growth for HMECs were the same as those listed above for NIH 3T3 fibroblasts.

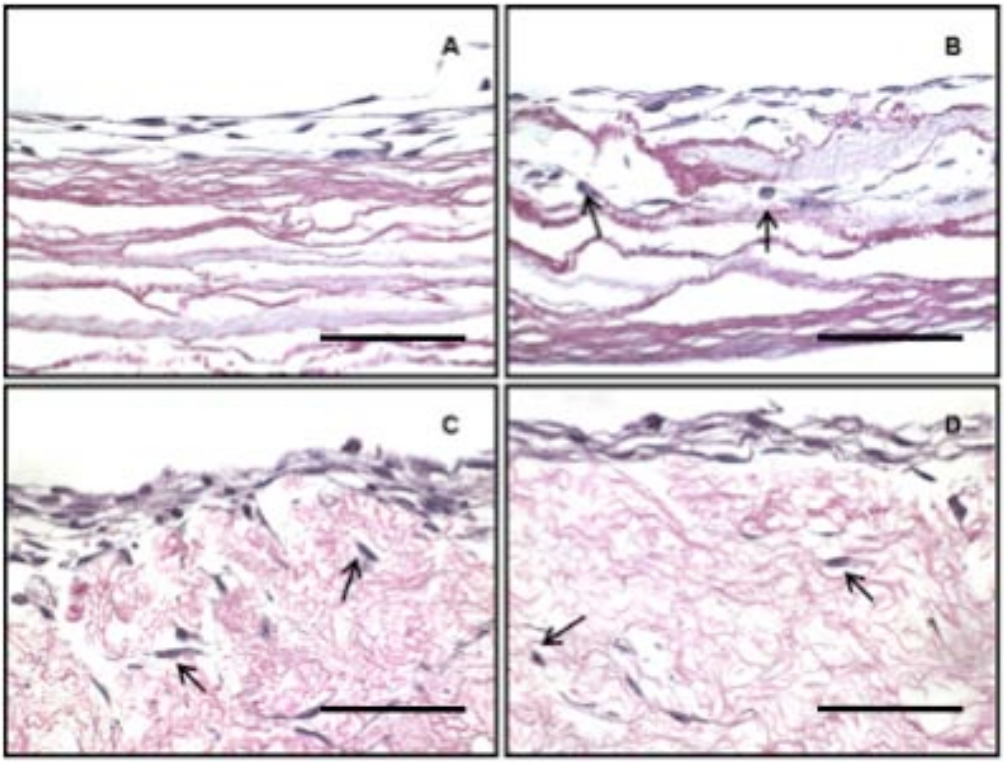


**Figure 18. H&E staining of cell seeded UBM showing that NIH 3T3 cells (A) were not able to invade below the luminal surface of UBM, but were able to invade the abluminal side (B). Staining also showed that NIH 3T3 had an invasive pattern of growth when seeded on SIS (C) and LECM (D). Scale bar = 100 μm. (40X). Reprinted from (1) with permission from Liebert Publishing.**

#### 2.3.2.2 Primary Rat Embryonic Spinal Cord Neurons

Approximately 90% of cells isolated from the spinal cord tissue of embryonic Sprague Dawley rat pups and grown on control coverslips were positively labeled for the neuron-specific cytoskeletal marker β-tubulin-III and were therefore classified as neurons (Figure 19).

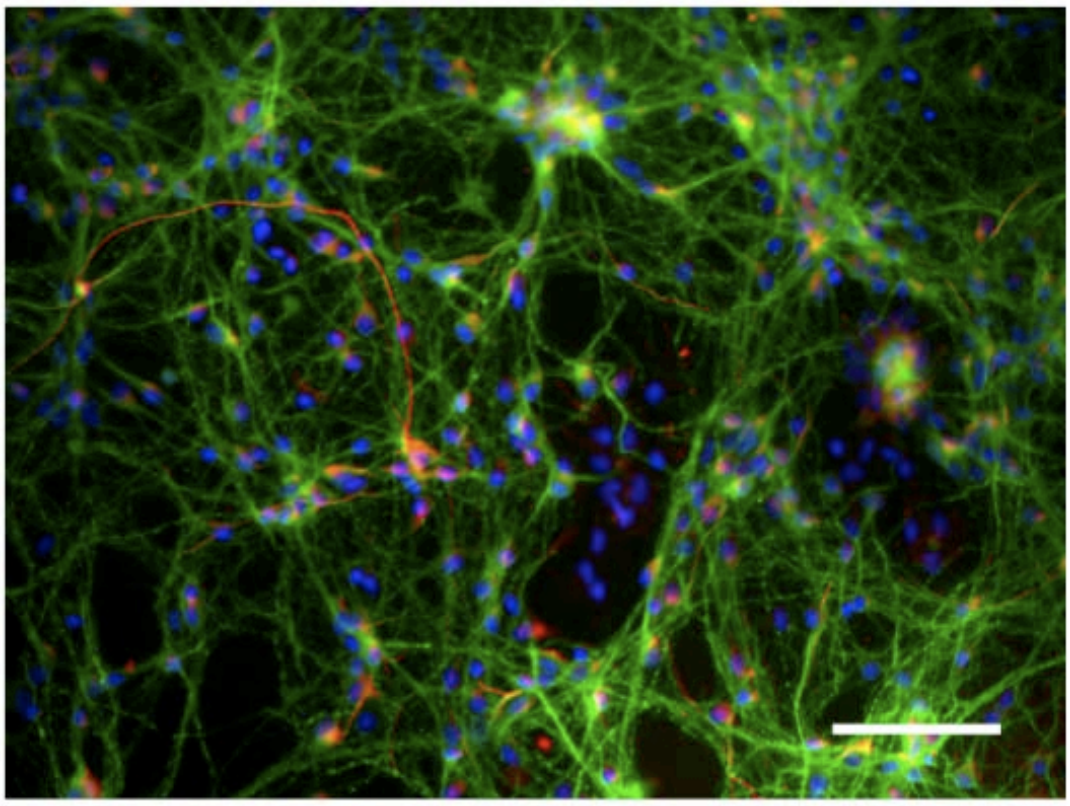

**Figure 19. Immunofluorescent staining of cells seeded on poly-L-lysine control coverslips after 5 days in culture. β-tubulin III (green), glial fibrillary acidic protein (GFAP) (red) and DAPI (blue). Scale bar = 100 μm. Reprinted from (134) with permission from John Wiley and Sons.**

These same cells were seeded onto the luminal and abluminal surfaces of UBM. Investigation by SEM showed that cells which were seeded onto the luminal side of UBM scaffolds were few in number and exhibited a rounded appearance with under developed cellular processes (Figure 20). Cellular debris was also observed. Cells which were seeded onto the abluminal side of the

UBM scaffold were more numerous and were also observed to attach to the collagen fibrils of the UBM scaffold both at the surface and within collagen meshwork (Figure 21). Cellular processes were observed both interacting with the collagen fibers of the ECM scaffold and spanning the spaces between fibers.

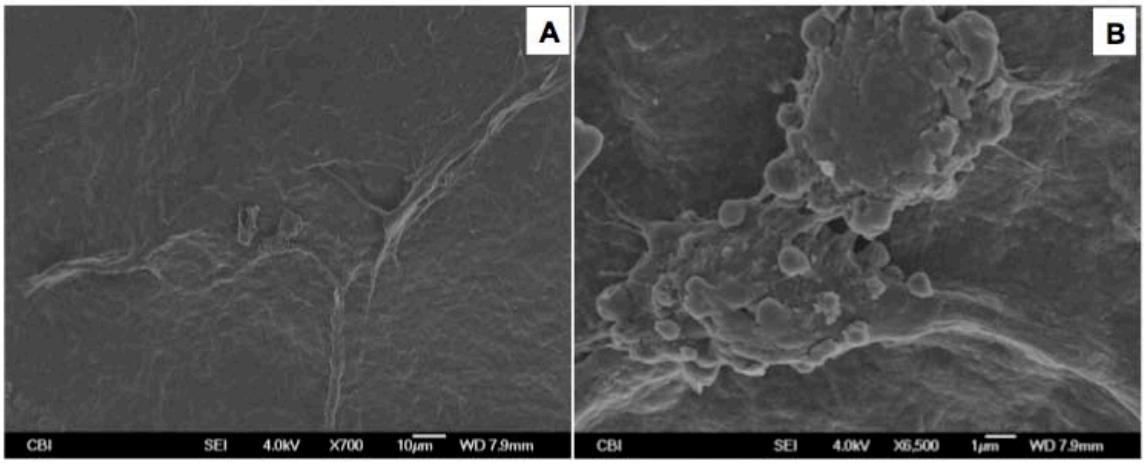


**Figure 20. SEM images of embryonic spinal cord neurons cultured on the luminal surface of UBM for 5 days. (A = 700x, B = 6500x).**

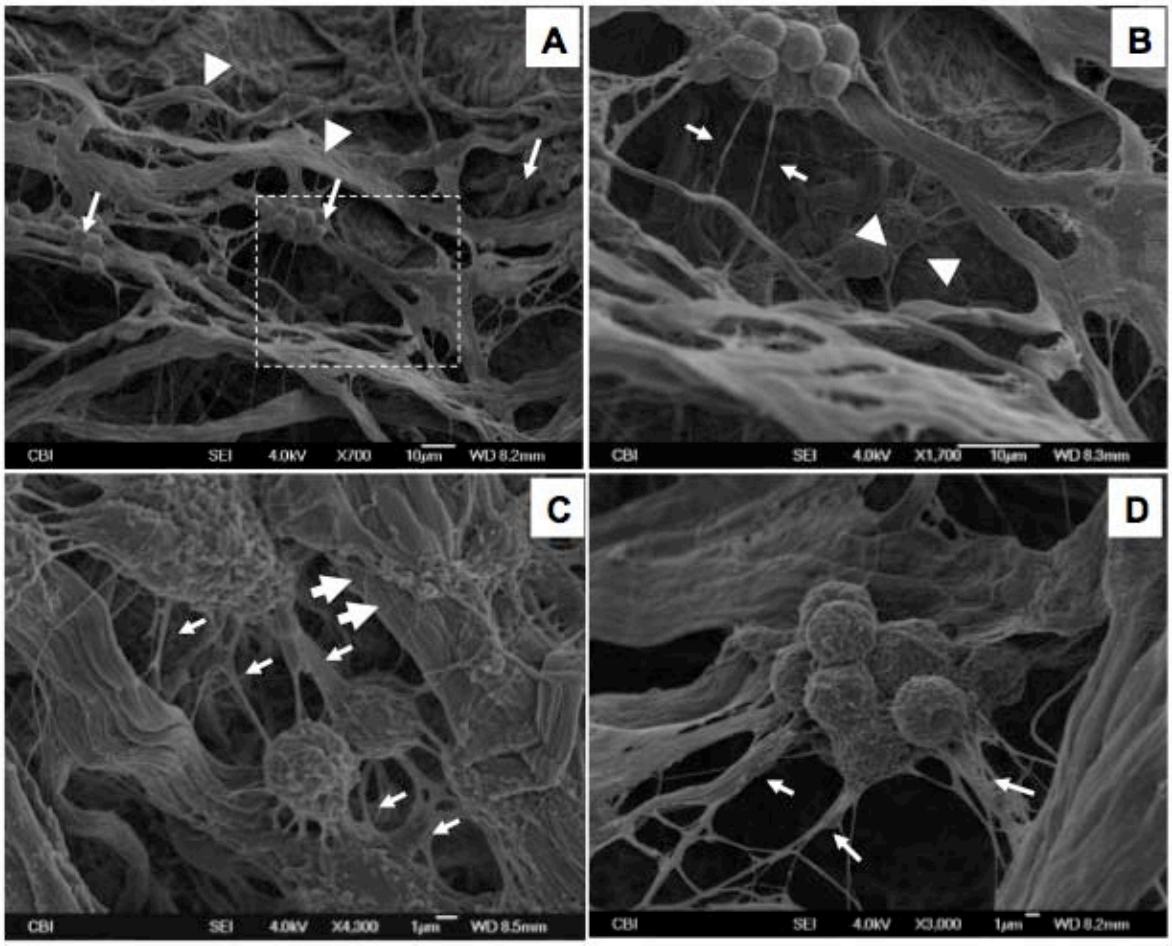


**Figure 21. SEM images of embryonic spinal cord neurons culture on the abluminal surface of UBM for 5 days. Arrowheads in image A denote the collagen fibers of the UBM scaffold. Smaller arrows in image A denote cells attached to the scaffold material (700x). Image B shows a higher magnification of the area denoted in image a by the white box (1700x). Large arrowheads in image B denote cells growing beneath the surface of the scaffold and smaller arrows denote cellular processes spanning the collagen fibers of the UBM scaffold. Image C shows cells growing within the UBM scaffold at high magnification (4300x). Large arrows denote cellular processes interacting with the collagen fibers of the UBM scaffold and smaller arrows denote cellular processes spanning spaces within the scaffold. Image D shows a high magnification example of cells growing on the outer fibers of the UBM scaffold. Small arrows denote cellular processes spanning collagen fibers.**

To confirm that the cells and corresponding cell processes attached to the abluminal surface of the UBM scaffold were neurons, sections were labeled for β-tubulin-III and glial marker GFAP. Cells seeded on the scaffold surface stained positive for both cytoskeletal markers (β-tubulin-III and GFAP; Figure 23).

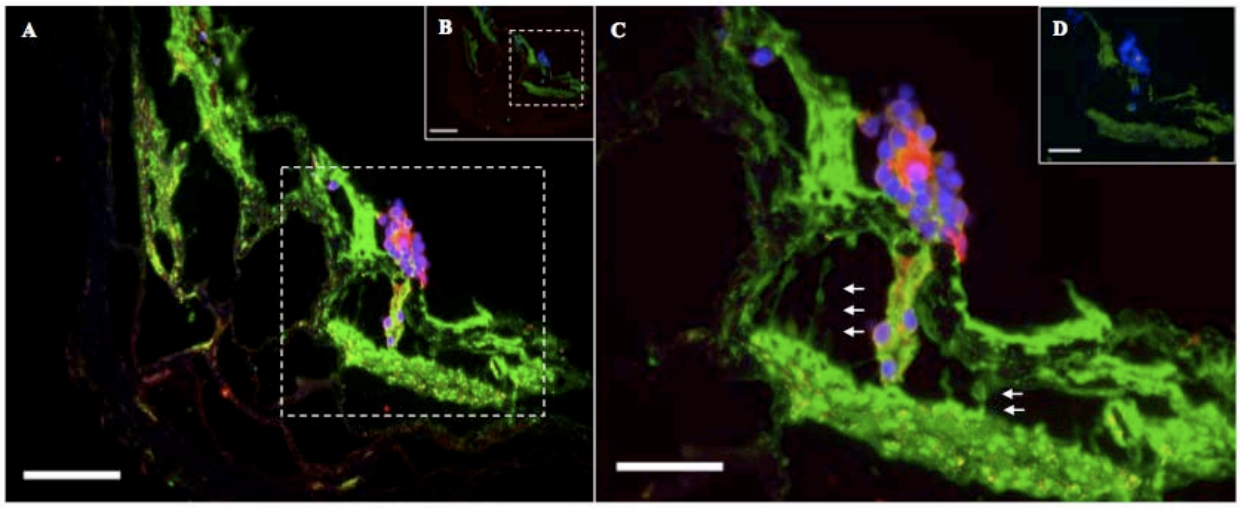


**Figure 22. Immunofluorescent images of cells seeded on the abluminal surface of the UBM scaffolds (A and C). Immunofluorescent images of seeded sections stained with secondary antibodies only (B and D, inset). Arrows indicate cellular processes seen spanning pores of the ECM scaffold material. β-tubulin III (green), glial fibrillary acidic protein (GFAP) (red) and DAPI (blue). Scale bars = 50 µm. (40X)**

## 2.4 DISCUSSION

In tissue engineering and regenerative medicine applications, the cells that participate in the processes of tissue reconstruction require "instruction" for proliferation, morphogenesis, and differentiation. The sources of this "instruction" are the cellular microenvironment and the scaffold or matrix surfaces with which these cells interact. Factors known to influence the

outcome of cell-scaffold interactions include surface topography (18, 177-180), hydrophilicity/hydrophobicity (181-184), ligand presence and presentation (58, 185-189), and mechanical properties (190-194), among others. Further, the success of a given cell-scaffold combination may be highly dependant on the type of cell being examined. Therefore, it is essential to characterize and to consider the surface of a scaffold as well as its effects upon cell phenotype when designing a strategy to facilitate the reconstruction of complex three-dimensional tissues and organs.

Scaffolds composed of single purified ECM components as well as scaffolds composed of intact ECM have been investigated in a large number of *in vitro* and *in vivo* tissue engineering and regenerative medicine applications with varying degrees of success. The advantage of using intact acellular ECM as a scaffold for cell growth or reconstructive tissue remodeling as opposed to the individual components of the ECM includes the presence of all the ECM constituents in the same relative amounts as exist in nature and in an ultrastructure similar to that of native ECM. It remains unclear, however, whether the molecular composition or the ultrastructure of these scaffolds plays a greater role in determining the outcome of the interaction of cells with the scaffold material. Likely, it is the diverse combination of both the structural and the functional components present within ECM scaffolds that accounts for the success of ECM based materials in multiple organ systems.

The studies presented here examined the ultrastructural and compositional characteristics of the surfaces of porcine ECM scaffolds harvested from three different anatomical locations: (1) urinary bladder, (2) small intestine, and (3) liver. SEM showed that the ECM derived from each of the three anatomical locations possessed a distinct ultrastructure. Further evaluation of these same scaffolds using ToF-SIMS showed that that UBM and SIS had more similar surface

compositions when compared to each other than when compared to LECM. There is evidence that these differences, which appear to be related to the tissue source from which an ECM scaffold is derived, may play a role in modulating or maintaining the phenotype of cells that have been seeded into the matrix (1, 41, 163, 195). A recent study investigated the ability of the same three porcine derived ECM scaffolds that were used in the present study to maintain the phenotype of a hepatic sinusoidal endothelial cell population during *in vitro* cell culture (163). The results showed that the LECM scaffolds were capable of maintaining the specialized endothelial cell phenotype in culture both to a greater degree and for a longer duration than were the UBM or SIS scaffolds.

In the present study, it was also observed that certain ECM scaffolds (UBM and SIS) exhibited distinct ultrastructural differences depending on the sidedness (i.e. luminal versus abluminal) of the scaffold while others exhibited an ultrastructure that was more homogeneous throughout (LECM). Evaluation of the scaffolds by ToF-SIMS showed that UBM exhibited significant differences in the composition of the luminal and abluminal surfaces, while SIS exhibited overlapping composition of the luminal and abluminal surfaces.

These results parallel the results of the immunolabeling studies which showed that UBM, but not SIS or LECM, scaffolds possessed an intact basement membrane on its luminal surface, although all three of the scaffolds evaluated did show basement membrane proteins present at sites where vascular structures existed beneath the surface of the materials. The presence of the surface basement membrane on UBM prevented both HMEC and NIH 3T3 fibroblasts from invading the luminal side of the UBM scaffold and this basement membrane served as a substrate for confluent layered growth of these cells. Differences in the behavior of primary spinal cord neurons seeded onto either the luminal or abluminal sides of UBM scaffolds were

also observed. Those cells which were seeded on the luminal side displayed a rounded morphology and did not extend cellular processes while those cells which were seeded onto the abluminal side were more numerous and extended numerous cellular processes. It is unknown whether the differences observed were due to differences in the molecular composition or the ultrastructure of the surface, both of which are well known to play a role the maintenance of neuronal cell phenotype.

Chemical cross-linking is a process commonly used in the production of ECM scaffolds to slow or prevent degradation of the resultant scaffold, to inhibit the recognition of surface epitope by the host, and to provide improved mechanical properties for load bearing applications. The present study examined the effects of chemical cross-linking upon the surface characteristics of the urinary bladder derived extracellular matrix scaffold. It was observed that chemical cross-linking caused changes in the ultrastructure of both the luminal and abluminal sides of UBM. However, chemical cross-linking appeared to cause only minimal changes in the molecular composition of the scaffold surface as observed by ToF-SIMS. It is logical to assume that cross-linking may alter the presentation and conformation of ligands on the surface of an ECM scaffold, thus altering ligand-receptor interactions which may be important in determining the outcome of cell-scaffold interactions; however, it was not possible to fully assess these changes in the present study. Further characterization of the surface of cross-linked ECM scaffolds by ToF-SIMS and other methods may provide insights into the effects of cross-linking upon the cellular response. The *in vivo* response to non-cross-linked and carbodiimide cross-linked ECM scaffolds is examined in the section which follows.

The studies presented in the following sections of this dissertation will examine the effects of cross-linking upon the host tissue remodeling and macrophage responses to ECM scaffolds following implantation.

## 2.5 CONCLUSIONS

The results of the present study demonstrated that each surface of an ECM scaffold is associated with distinct ultrastructural and compositional characteristics and that these surface characteristics are dependant on both the anatomic location from which the material is derived as well as the methods used in its production (i.e. decellularization and chemical cross-linking). These characteristics were shown to affect patterns of *in vitro* cell behavior. It is likely that a complex combination of the structural and functional components of the ECM scaffolds investigated was responsible for the cellular behavior observed. The effects of chemical cross-linking upon the *in vivo* response to ECM scaffolds will be further investigated in the sections which follow.

It was also demonstrated that ToF-SIMS is a highly sensitive method for the detection and differentiation of the molecular composition of the outermost surface of an ECM scaffold. Further, ToF-SIMS may represent a method for future identification of previously unknown surface species as well as for the prediction of cell-scaffold interactions and subsequent remodeling events. Finally, the richness of molecular detail in the ToF-SIMS spectra suggests that ToF-SIMS may be useful for quality control of commercialized ECM-based regenerative scaffold products and for standardization of these scaffolds.

## 2.6 LIMITATIONS AND FUTURE DIRECTIONS

ToF-SIMS as a tool for studying the surface of protein based materials is recent concept, and the present study represents the first attempt to use ToF-SIMS as a tool for compositional analysis and differentiation of the surfaces of highly complex ECM based scaffolds. In the present study, ToF-SIMS was capable of identifying differences in the compositions of the various surfaces investigated and the results obtained paralleled those of obtained in the immunolabeling studies. There are, however, a number of limitations in the application of ToF-SIMS to the analysis of the surface of a biologically derived material.

Due to the inherent mass range limitation of ToF-SIMS, it is not possible to assess whole proteins or peptide sequences. Rather, the method relies on analysis of mass fragmentation patterns. Previous studies have shown successful correlations between such fragmentation patterns and protein surfaces (175, 176). In one such study, known amino acid mass fragmentation patterns generated from ToF-SIMS were compared to the mass spectra obtained for extracellular matrix proteins remaining on a polyNIPAM surface following the removal of cultured bovine aortic endothelial cells. The mass spectra obtained for single purified ECM components adsorbed onto the polyNIPAM surface were the reference spectra for the present study (175). The results showed that ToF-SIMS was capable of detecting protein fragment fingerprints for laminin, fibronectin, and collagen within the film remaining on the culture surface by comparing the protein remnants to single protein film controls. A slightly variant version of this peak list was utilized for this study (Table 3).

In the present study, the complexity of the surfaces makes it difficult to report a one-to-one correlation between fragment and implied protein association. Therefore, it is likely more useful to report the data obtained as a list of prominent fragments as opposed to suggesting that

the fragments indicate specific proteins. The complicated surface milieu of these materials and the relative lack of data on specific fragmentation patterns of many purified ECM components justify this approach. On the other hand, this approach suggests that identification of unknown molecules may be achievable. This possibility for the unique identification of surface structures and features was part of the original hypothesis that was the impetus for this study. Traditional antibody-based immunolabeling requires prior knowledge of the surface proteins as a prerequisite for their identification. In the present approach, the potential to identify molecules both expected and unexpected exists, aiding in the creation of a unique picture of the material surface chemistry and functionality on a molecular level.

In addition to using amino acid mass fragmentation peaks identified in the studies relating ToF-SIMS spectra to protein films, spectra taken from the surfaces in this study were cross-examined with previously published lipid peak lists (196). The identification of large peaks at m/z 166.06, 184.07, and 224.11 in the spectra for SIS and UBM as well as cross-linked UBM indicates lipid structures and likely cell membrane components. Interestingly, these peaks were not observed to the same extent in the LECM scaffolds. This may be due to the different methods used for the decellularization of the SIS/UBM and LECM in this study. The existence of peaks found in the high mass region was not limited to the large peaks mentioned above. Low intensity lipid peaks were identified throughout the high mass region that matched previously published lipid work. However, the focus of this work was to create a fingerprint of the protein remnants and future work will be necessary to more completely characterize the lipid fragments observed here.

Finally, it should be noted that the studies presented here are a continuation of several studies intended to characterize the surfaces of ECM scaffolds and their effects upon cell

phenotype (1, 68, 163, 195). The present studies sought only to characterize the ultrastructure and molecular composition of the surfaces of ECM scaffolds. Further work will be required relate the data shown here to cell behavior both *in vitro* and *in vivo*. Previous studies have used methods such as partial least squares regression to relate data to subsequent *in vitro* cell culture observations (197). Similar studies could be performed to compare the present data to the morphologic or phenotypic profiles of cells cultured on ECM scaffolds or following *in vivo* implantation.

# 3.0 SPECIFIC AIM 2: EFFECTS OF CELLULAR COMPONENTS AND CROSS-LINKING UPON THE CAPACITY OF AN EXTRACELLULAR MATRIX SCAFFOLD TO PROMOTE CONSTRUCTIVE TISSUE REMODELING

## 3.1 BACKGROUND

The success of ECM scaffolds in tissue engineering and regenerative medicine applications may be attributed in large part to their ability to modulate the default mechanisms of tissue repair. In general, the response following implantation of an acellular non-chemically cross-linked ECM scaffold has been described as "constructive tissue remodeling". That is, ECM scaffolds are capable of inducing the formation of new tissue structures that are arranged in a spatially appropriate pattern for the tissue of interest. This is in direct contrast to the default mechanisms of mammalian response to tissue injury, which involve inflammation and scarring. An example of an application in which constructive tissue remodeling was observed following implantation of an ECM scaffold material is provided in detail in Appendix A of this dissertation. Briefly, an acellular non-cross-linked ECM scaffold composed of UBM was used to reconstruct the temporomandibular joint meniscus following either unilateral or bilateral meniscectomy in a canine model. The scaffold material was seen to degrade rapidly and was replaced by new tissue which both grossly and microscopically resembled the native meniscus. The remodeled tissue consisted not only of the fibrocartilaginous tissue and scant vasculature

which comprise the bulk of the meniscus, but also the muscular attachments at the periphery of the meniscus. These results show that a single ECM scaffold composed only of UBM was able to promote the formation of multiple tissue types including fibrocartilage, muscle, connective tissue, and vasculature, which were arranged into an appropriate tissue specific architecture. Biomechanical and biochemical testing was performed on the remodeled tissues, showing that both the composition and the mechanical properties of the remodeled tissue were approaching that of native tissue.

ECM scaffolds such as the ones described above, and such as those used in the studies presented in this dissertation, are produced by the removal of cellular components (i.e. decellularization) prior to their use in tissue engineering and regenerative medicine applications (67). The removal of the cellular component provides a substrate which is ostensibly free of antigenic cellular epitope, leaving only ECM components which have been shown to be highly conserved across species (7). However, a number of studies have shown that potentially antigenic substances such as the α-Gal epitope and DNA remain in ECM scaffolds following the decellularization process (95, 198). The presence of these molecules in small quantities, however, does not appear to affect the ability of ECM scaffolds to promote constructive tissue remodeling (92, 199). The effects of larger quantities of cellular components remaining within an ECM scaffold and the effects of viable cells upon the remodeling outcome associated with their use is unclear. Some studies have shown improved tissue remodeling outcomes when site appropriate autologous cells are either seeded onto the ECM scaffold prior to implantation or placed in contact with the scaffold in-situ (27, 31, 39). However, the survival and fate of such a cellular component during the remodeling process and the effects of cell death upon the tissue

remodeling response following *in vivo* implantation is largely unknown and remains an important question in the fields of tissue engineering and regenerative medicine as a whole.

A number of studies have utilized chemical cross-linking during the processing and production of ECM based scaffold materials as a method to mask cellular epitope which may remain within a scaffold material, either due to the use of intact (i.e. not decellularized) tissues or due to inefficient decellularization. While chemical cross-linking may mask cellular epitope present at the surface of the scaffold material, its effects upon the ability of the material to function in the long-term have not always been positive (69). Other strategies utilize cross-linking in applications where increased mechanical properties or slowed degradation of the scaffold material is desirable. While the use of cross-linking does serve a purpose in some applications (i.e those requiring the scaffold to remain without degradation or loss of mechanical properties over long periods of time), it was shown in the previous chapter that cross-linking causes changes in scaffold architecture and surface composition which may affect the host remodeling response following implantation.

The objectives of the studies presented in this section were two fold: (1) to determine the effects of the presence of a cellular component and the use of carbodiimide cross-linking during scaffold production upon the capacity of extracellular matrix scaffolds to elicit constructive tissue remodeling versus encapsulation or scar tissue formation in a well described model of rat abdominal wall musculature reconstruction, and (2) to determine whether the host tissue remodeling response to one ECM scaffold material affects the outcome of the host tissue remodeling response to a second material implanted concurrently in the same animal.

## 3.2 METHODS

### 3.2.1 Overview

The present studies were split into two separate *in vivo* studies. In the first study, a unilateral model of rat abdominal wall defect repair was used to evaluate the effects of the presence of viable intact cells or cellular components within a test article upon its ability to promote constructive tissue remodeling. A qualitative histomorphologic analysis was performed, as was immunolabeling for evidence of innervation within the remodeled tissue. In the second study, a bilateral model of rat abdominal wall defect repair was used to evaluate the effects of chemical cross-linking with carbodiimide upon the ability of an ECM test article to promote constructive tissue remodeling. The use of a bilateral defect model also allowed for the comparison of remodeling responses when two different test articles were implanted concurrently within the same animal. In the second study, a qualitative histomorphologic analysis was again performed. Staining with Herovici's Polychrome was also performed in order to evaluate the type and maturity of the collagen within the remodeling site to assess differences the quality of the tissue being deposited following implantation of each test article. Finally, quantitative real time PCR was performed to examine the expression of four matrix metalloproteinases (MMP 2, 3, 7, and 9), to examine differences in the remodeling process associated with each test article.

### 3.2.2 Preparation of Extracellular Matrix Scaffolds

#### 3.2.2.1 Rat Body Wall Muscle Extracellular Matrix

The rat body wall tissue for this study was harvested from Sprague-Dawley rats of approximately 200-500g immediately following sacrifice and frozen at -80 ºC. The tissue consisted of all three muscle layers of the ventral abdominal wall without the overlying skin. The body wall tissue was thawed in PBS at room temperature before being placed in 0.02% trypsin/0.05% EDTA at room temperature for 2 h on a shaker. Following soaking in trypsin/EDTA, the body wall tissue was washed in PBS on a shaker for 1 h. The body wall tissue was then placed in 3% (v/v) Triton X-100 at room temperature on an orbital shaker for 2 h. The Triton X-100 treated samples were then washed in water. Following the water wash, the body wall tissue was placed in 4% (w/v) deoxycholic acid for 2 h at room temperature on an orbital shaker and then washed in water. The tissue was then treated with a 0.1% peracetic acid/4% ethanol solution for 2 h at room temperature on a shaker to further decellularize and disinfect the tissue. The peracetic acid solution was decanted and the pH of the material was returned to approximately 7.4 by rinsing in PBS at room temperature, with shaking, then in water twice, and then again in PBS. Each rinse lasted 15 min. The remaining tissue consisted of acellular allogeneic rat body wall ECM (rat body wall ECM). The absence of cell nuclei in this test article was confirmed by DAPI staining (Figure 23a).

The rats used in this study were an outbred strain. As the tissue for the rat body wall ECM was both harvested and implanted into the same outbred rat strain, the intra-strain transplants performed in this study were indeed allografts and cannot be considered isografts.

#### 3.2.2.2 Cellular and Acellular Urinary Bladder Matrix

The porcine bladders for this study were harvested and prepared using methods previously described. The urinary bladders were harvested from market weight pigs of approximately 260 pounds immediately following sacrifice. Two different constructs were prepared from the urinary bladder: 1) cellular xenogeneic bladder tissue, and 2) and acellular xenogeneic bladder ECM.

Excess adipose tissue and collagenous connective tissue were removed from the exterior of the bladder using scissors and the urothelial cells were removed by soaking the bladder tissue in water. The apex of the bladder was then removed and a full thickness cut from the neck of the bladder to the apical opening was made to create a rectangular-shaped sheet. The tunica serosa, tunica muscularis externa, tunica submucosa, and the majority of the muscularis mucosa were removed by mechanical delamination of the abluminal side of the bladder, leaving the basement membrane, tunica propria, and the resident cells intact. The remaining tissue was soaked in PBS and represented cellular urinary bladder matrix (cUBM).

A portion of the cellular urinary bladder matrix prepared as described above was subjected to the 0.1% peracetic acid/4% ethanol treatment as described for the acellular allograft. The peracetic acid treated material consisted of only the basement membrane and tunica propria without the resident cells and represented acellular urinary bladder matrix (UBM). The presence or absence of cell nuclei in the cUBM and UBM test articles was confirmed by DAPI staining (Figure 23b and 23c).

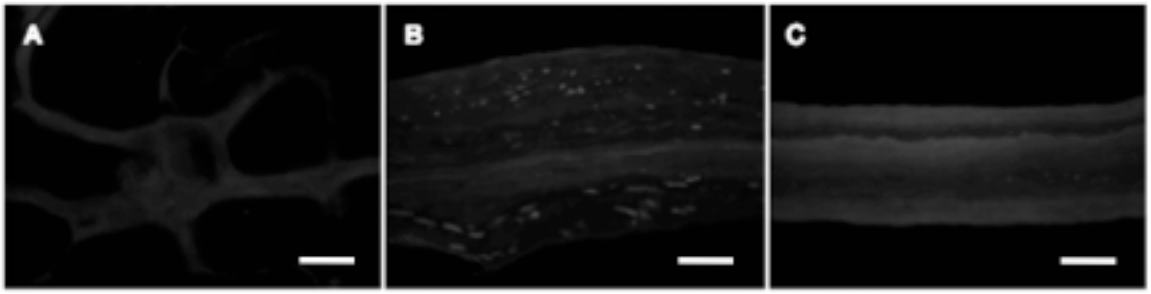


**Figure 23. DAPI staining confirms removal of cell nuclei in the rat body wall ECM (A), maintenance of cell nuclei in the cUBM (B), and removal of cell nuclei in the UBM (C). The cellular autograft test article is not shown as it was replaced immediately following defect creation in the sterile setting of the operating room. Scale bar = 100 μm (20X). Reproduced from (100) with permission from Elsevier.**

#### 3.2.2.3 Preparation of Four Layer Constructs

Single sheets of the cUBM and UBM tissue had insufficient strength to serve as a body wall replacement device in the rat model. Therefore, multilaminate (4-layer) sheets were constructed. In brief, four hydrated sheets of either the cUBM or the UBM were placed on top of one another, each at 90° orientations to the adjacent layers to create a device with isotropic mechanical properties. The constructs were then placed into plastic pouches and attached to a vacuum pump (Leybold, Export, PA) with a condensate trap inline. The constructs were subjected to a vacuum of 28 inches Hg until dried, leaving a multilaminate construct.

#### 3.2.2.4 Chemical Cross-linking

Four-layer scaffolds composed of UBM were cross-linked by immersion in solutions of carbodiimide (10 mM; CDI-UBM) for 8-10 hours at room temperature. The cross-linked scaffolds were then subjected to three separate 1 hour water washes as well as an overnight water wash to remove any residual cross-linking solution that may have remained following the cross-linking process.

#### 3.2.2.5 Terminal Sterilization

The rat body wall ECM, cUBM, UBM, and CDI-UBM were terminally sterilized using ethylene oxide gas. The cellular autografts required no terminal sterilization as they were harvested in sterile fashion and replaced during the surgical procedure.

### 3.2.3 Rat Abdominal Wall Defect Model

Female Sprague-Dawley rats, age 8-12 weeks, were purchased from Charles River Laboratories (Wilmington, MA). The rats were housed individually in shoebox cages. Room temperature was maintained at 68-76 ºC and the rats were fed Purina Iso Pro throughout the study period. Cage bedding was changed at least once per week. All animals were examined by a veterinarian prior to surgery and were determined to be in good health.

#### 3.2.3.1 Unilateral Defect Surgical Procedure

Sixty-four Sprague-Dawley rats were randomly divided into four separate groups of sixteen each. Each rat was subjected to the surgical procedure listed below and one of the four test articles listed in Table 4 was implanted in each animal. The treatment groups were the subdivided into four groups of four each that were sacrificed and explanted at 3, 7, 14, or 28 days post surgery (n=5 for each test article at each time point).

A previously described abdominal wall defect model was used (69, 82). Each rat was anesthetized and maintained at a surgical plane of anesthesia with 2% isoflurane in oxygen. The surgical site was prepared in sterile fashion using a betadine (providone-iodine) solution followed by placement of sterile drapes. A ventral midline incision was made and the adjacent

subcutis bluntly dissected to expose the ventral lateral abdominal wall including the musculotendinous junction of the oblique musculature.

A 1 cm x 1 cm defect was created in the exposed musculature, leaving the underlying peritoneum and transversalus fascia and the overlying skin intact. The defects were then repaired with one of the test articles listed in Table 4. The autologous tissue test article was harvested from the defect site and then replaced immediately thereafter in the sterile setting of the operating room. Each implant was sutured to the adjacent abdominal wall with 4-0 Prolene non-absorbable suture at each corner to secure the test article and to allow for identification of the device boundaries at the time of euthanasia and explantation. A minimal amount of suture material was used to avoid eliciting a host response to the suture that would obscure the host response to the test article. The skin was closed using absorbable 4-0 Vicryl suture. The animals were recovered from anesthesia on a heating pad and allowed normal activity and diet for the remainder of the study period

Each rat received Buprinex (buprenorphine hydrochloride, 0.02 mg) postoperatively as needed for discomfort as evidenced by failure to eat, drink, or resume normal activity. Gentamicin was given subcutaneously (2 mg) postoperatively and once daily for an additional three days. The animals were monitored daily for signs of infection or inflammation at the surgical site. All animals survived the surgical procedure and their predetermined study period without complications.

An example of a device following placement in the unilateral body wall defect model is provided in Figure 24a.

**Table 4. Test articles implanted in the unilateral body wall defect model.**

| Test Article | Composition | Graft Origin |
|---|---|---|
| Autologous Rat Body Wall | Autologous ECM + Autologous Cells | Rat Body Wall |
| Rat Body Wall ECM | Allogenic ECM without cells | Rat Body Wall |
| Cellular UBM | Xenogeneic ECM + Xenogeneic Cells | Porcine Urinary Bladder |
| Acellular UBM | Xenogeneic ECM without cells | Porcine Urinary Bladder |

#### 3.2.3.2 Bilateral Defect Surgical Procedure

Thirty Sprague-Dawley rats were randomly divided into three separate groups of 10 each. Each rat was subjected to the surgical procedure listed below and two of the three test articles listed in Table 5 were implanted in each animal, one on each side of the ventral midline. The treatment groups were the subdivided into five groups of two each that were sacrificed and explanted at 1, 3, 7, 14, or 28 days post surgery (n=2 for each combination of test articles and n=4 for each individual test article at each time point).

The surgical procedure used to create the bilateral defect utilized in the present study was similar to the procedure described above, except that two incisions were made either side of the ventral midline. Two defects of the abdominal wall musculature were then created beneath the incisions on either side of the ventral midline as described above. The defects encompassed of the same tissue structures described above (removal of the internal and external oblique muscles) and were repaired using the same procedure as described for the bilateral model. Defects in the bilateral rat body wall model were repaired with combinations of the three test articles listed in Table 5. Post-surgical care was the same as described above for the unilateral defect model.

All animals survived the surgical procedure and the post surgical study period with no complications.

An example of two devices inserted in the bilateral body wall defect model is given in Figure 24b.

**Table 5. Test articles implanted in the bilateral body wall defect model.**

| Test Article | Composition | Graft Origin |
|---|---|---|
| Autologous Rat Body Wall | Autologous ECM + Autologous Cells | Rat Body Wall |
| Acellular UBM | Xenogeneic ECM without cells | Porcine Urinary Bladder |
| Cross-linked Acellular UBM | Xenogeneic ECM without cells + Carbodiimide | Porcine Urinary Bladder |

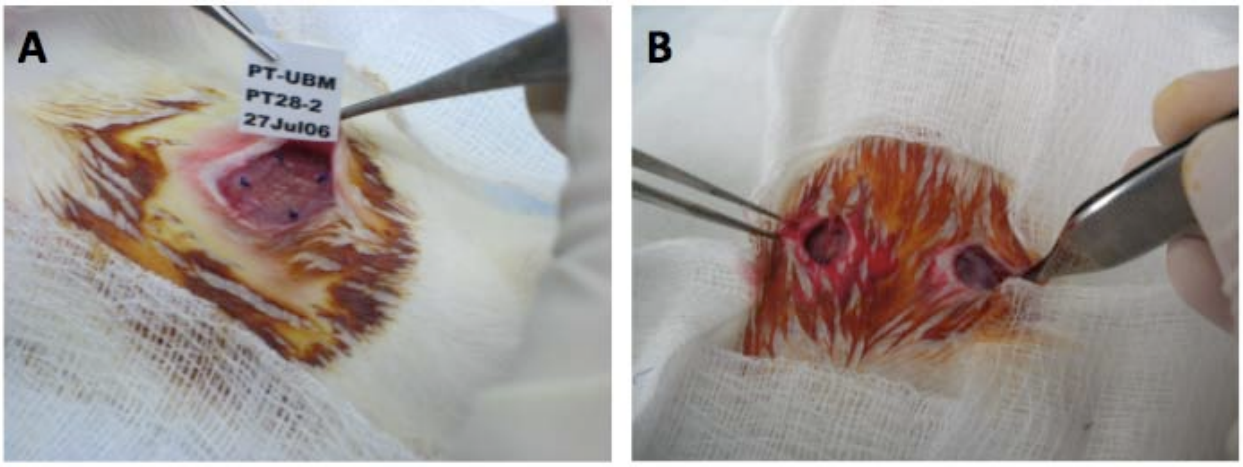


**Figure 24. Photomicrographs of the unilateral (A) and bilateral (B) surgical defect models.**

### 3.2.4 Characterization of the Host Tissue Remodeling Response

#### 3.2.4.1 Sample Collection

On the predetermined sacrifice date, each animal was anesthetized using isoflurane (5% in oxygen) and then euthanized by intracardiac injection of potassium chloride to induce cardiac arrest. The grafts were explanted with a small amount (approximately 2 mm) of the surrounding native tissue. Tissue was fixed in 10% neutral buffered formalin and then embedded in paraffin. The other half of each specimen was preserved in RNAlater for RNA extraction.

#### 3.2.4.2 Histologic Staining

The explanted wound site specimens were fixed in formalin and embedded in paraffin prior to being cut into 6 μm thick sections and mounted on glass slides. The specimens were deparaffinized with xylenes followed by exposure to a graded series of ethanol solutions (100-70%). Sections were stained with Masson's trichrome (unilateral defect model) or H&E (bilateral defect model) for morphological assessment. Selected slides from the bilateral defect model were also stained with Herovici's Polychrome stain, a stain which allows for differentiation of newly synthesized (type III) and mature collagen (type I). The slides were then dehydrated using the reverse of the deparaffinization treatment described above prior to coverslipping.

A qualitative analysis of the histological morphology of each specimen was performed by a pathologist and a trained investigator. The analysis included an assessment of the intensity and type of cellular infiltration, the presence and extent of vascularity, and the organization of host tissue within and around the wound site. The suture sites were avoided in the morphologic evaluation.

#### 3.2.4.3 Immunolabeling for Evidence of Innervation

Paraffin-embedded specimens from the unilateral defect study studies were cut into 6 μm thick sections and mounted onto glass slides. The specimens were deparaffinized by treatment with xylenes and exposure to a graded series of ethanol solutions (100–70%). Following deparaffinization, the slides were placed in citrate antigen retrieval buffer (10 mM citric acid monohydrate, pH 6.0) at 95 – 100 ◦ C for 20 min. The buffer was allowed to cool to room temperature on ice and the slides were washed twice in Tris-buffered saline/Tween 20 solution, pH 7.4, and twice in PBS. The sections were then incubated in 2% normal horse serum for 1 h at

room temperature in a humidified chamber to inhibit non-specific binding of the primary antibody. Following incubation in blocking serum, the sections were incubated in primary antibody in a humidified chamber at 4°C overnight. Each tissue specimen was exposed to antibodies to the light chain of neurofilament, to a marker that localizes to the growth cones of regenerating neurons (GAP43) or to a marker that is known to localize to Schwann cells in the peripheral nervous system following injury (GFAP). Following overnight incubation, the slides were washed three times in PBS. The sections were then incubated in a solution of 3% $H_2O_2$ in methanol for 30 min at room temperature to quench any endogenous peroxidase activity. Following $H_2O_2$ treatment, the slides were washed three times in PBS and incubated in secondary antibody for 30 min in a humidified chamber at room temperature prior to three more washes in PBS. The sections were then incubated in Vectastain ABC reagent for 30 min in a humidified 37°C chamber, rinsed three times in PBS and incubated in 4% DAB substrate solution at room temperature until the slides showed the desired staining affinity. Finally, the slides were rinsed in water to stop the development of the DAB substrate and counterstained using Harris's acidified hematoxylin stain. The slides were then dehydrated using the reverse of the deparaffinization treatment described above and then coverslipped. Each PBS rinse in the protocol was for 3 minutes at room temperature, with occasional agitation.

Anti-neurofilament antibody was used at a concentration of 1:100. Anti-GAP43 was used at a concentration of 1:250. Anti-GFAP antibody was used at a concentration of 1:500. Corresponding secondary antibodies were used at a concentration of 1:100 for biotinylated anti-mouse IgG and 1:200 for biotinylated anti-rabbit IgG (PK-4001, Vector Labs). All antibodies were diluted in filtered PBS, pH 7.4. Native rat abdominal wall was used as positive control tissue samples for staining.

#### 3.2.4.4 Quantitative Real Time Polymerase Chain Reaction

Total RNA was isolated from the explanted tissues from the bilateral defect model using TRI-Reagent according to the manufacturer's instructions. The isolated RNA was then purified using an RNAeasy Mini Kit and a vacuum system. cDNA was synthesized from 1 μg of total RNA in a volume of 20 μL using a iScript cDNA synthesis kit according to the manufacturer's instructions.

Quantitative real-time PCR was then performed using primers specific for four different MMPs (MMP2, 3, 7, 9). Primers were custom designed using Primer-BLAST (NCBI, http://www.ncbi.nlm.nih.gov/tools/primer-blast/; Table 6). Primers for housekeeping genes were purchased as part of a housekeeping gene primer kit, and housekeeping gene expression was used to normalize reactions. 1 μL of cDNA was mixed with the appropriate primers and 2X SYBR Green Master Mix in a total volume of 25 μL. All reactions were performed in triplicate and were monitored using an iQ5 Real-Time Detection System.

Relative expression of the MMP genes as compared to the housekeeping gene was calculated using the $2^{-(\Delta Ct)}$ method (200, 201). The difference between the value of the threshold cycle ($\Delta C_t$) for the gene of interest (GOI) and the value of the threshold cycle for the housekeeping gene (HSKG) was calculated for each specimen as follows:

$$\Delta C_{tGOI} = C_{tGOI} - C_{tHSKG}$$

Fold increase or decrease in gene expression compared to native abdominal wall muscle for each sample type was then calculated using the following equation:

$$Fold\ Expression = \frac{Mean\ \Delta C_{tGOI} Sample}{Mean\ \Delta C_{tGOI} Native}$$

**Table 6. Primers used for MMP gene expression analysis of bilateral body wall samples.**

| Gene | Forward Primer (5' -> 3') | Reverse Primer (5' -> 3') |
|---|---|---|
| MMP2 | AAGAGGCCTGGTTACCCTGT | AAGTAGCACCTGGGAGGGAT |
| MMP3 | ACCCCACTCACATTCTCCAG | ATGAGCCAAGACCATTCCAG |
| MMP7 | CGGAGATGCTCACTTTGACA | TGGGAACAGAAGAGTGACCC |
| MMP9 | TAATAAACACGGATCCCCCA | GGTCAGAACCGACCCTACAA |

### 3.2.5 Statistical Methods

A two way analysis of variance was performed on the gene expression data obtained as part of the bilateral defect model to determine statistical significance of the factors of type of scaffold (autograft, CDI-UBM, and UBM) and the factor of days (1, 3, 7, 14, and 28 days). For the gene expression analysis, the variables analyzed were MMP2, 3, 7, and 9 expression. Because the distributions of these variables were strongly skewed, log-transformed values were used for the statistical analysis and results were transformed back to the original scale for presentation. This transformation corresponds to using geometric means in place of arithmetic means. The Tukey multiple comparison procedure was then employed to determine which pairs of levels of factors were significantly different when a main effect was statistically significant. Additional student's t-tests were used to determine whether there were statistically significant differences within scaffold groups which were related to the contralateral implant. A p-value of $p<0.05$ was used to determine statistical significance.

## 3.3 RESULTS

### 3.3.1 Unilateral Defect Model

#### 3.3.1.1 Histopathologic Findings

The host response to the autologous body wall tissue test article showed necrosis of the skeletal muscle which was apparent as early as the three day post surgery time point. Neutrophils and mononuclear cells were present within the wound site at day 3 and showed a marked increase in number at 7 days post surgery (Figure 25a). By day 14, the cell population was decreased in number, the necrotic muscle fibers were decreased in size, and there was deposition of neomatrix at the site of remodeling. By day 28, dense partially organized connective tissue consistent with scar tissue and a small population of randomly distributed mononuclear cells were present within the remodeled site (Figure 25b).

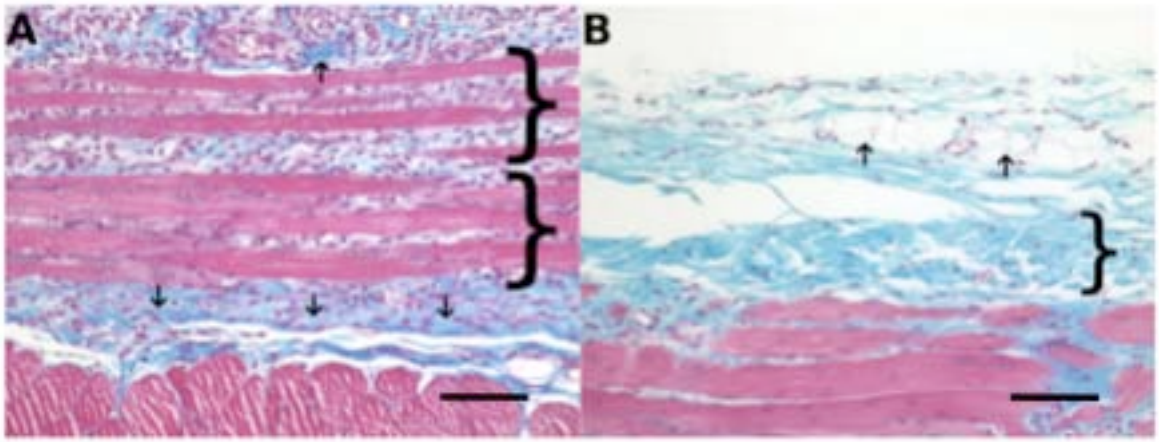


**Figure 25. (A) Histologic appearance of the autograft tissue test article at 7 days post surgery. Necrotic skeletal muscle (brackets), early neomatrix deposition (arrows), neutrophils, and macrophages were present. (B) Histologic appearance of the autograft tissue test article at 28 days post surgery. Autograft muscle tissue has been completely resorbed and replaced by dense poorly organized connective tissue (bracket), adipose tissue (arrows), and a small number of randomly distributed macrophages. Red staining tissue bundles at the bottom of the images represent the underlying transversalis muscle. Scale bar = 100 μm. (Masson's Trichrome, 20X). Reproduced from (100) with permission from Elsevier.**

The host response to the acellular allogeneic rat body ECM test article was characterized by a dense cellular infiltrate of equal numbers of neutrophils and mononuclear cells at day 3. Angiogenesis was also observed at 3 days post surgery and remained a feature of the remodeling wound site throughout the study period. The cellular infiltrate increased in number and was primarily composed of mononuclear cells on day 7 accompanied by a small amount of neomatrix deposition, especially at the periphery of the implant (Figure 26a). By day 14, the rat body wall ECM material was still discernable, but was diffusely and uniformly infiltrated with host mononuclear cells that were embedded within new ECM. By day 28, the rat body wall ECM material was no longer visible and was replaced by moderately well organized collagenous and

adipose tissue containing blood vessels, a small number of randomly dispersed mononuclear cells, and small islands of skeletal myoblasts growing in from the periphery (Figure 26b).

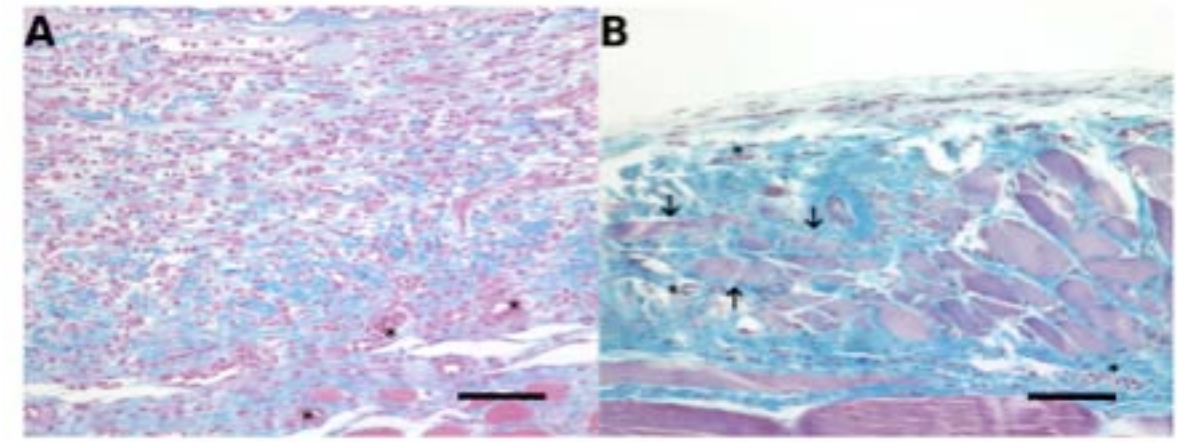


**Figure 26. (A) Histologic appearance of the rat body wall ECM at 7 days post-surgery. A dense cell population consisting of primarily macrophages was present. New blood vessels (asterisks) and neo-matrix (blue staining) deposition were also present. (B) Histologic appearance of the rat body wall ECM at 28 days post surgery. The rat body wall ECM was no longer discernable and was replaced by moderately well organized collagenous tissue, containing blood vessels (asterisks), islands of skeletal myoblasts (arrows) and a small number of randomly distributed mononuclear cells. Red staining tissue bundles at the bottom of the images represent the underlying transversalis muscle. Scale bar = 100 μm. (Masson's Trichrome, 20X). Reproduced from (100) with permission from Elsevier.**

The host response to the cellular xenogeneic cUBM test article was characterized by a dense accumulation of neutrophils with a lesser number of mononuclear cells at day 3. Maximum cellularity occurred at 7 days (Figure 27a) with extension of the inflammatory response into the surrounding normal tissue. The multilaminate device was still visible at day 14 and neomatrix could be identified. The cellular infiltrate at day 14 was characterized by a mixture of mononuclear cells and a lesser number of neutrophils. By day 28, the implant was no longer visible, and there was an accumulation of dense, poorly organized collagenous connective tissue and a small amount of adipose tissue including a randomly distributed population of mononuclear cells (Figure 27b).

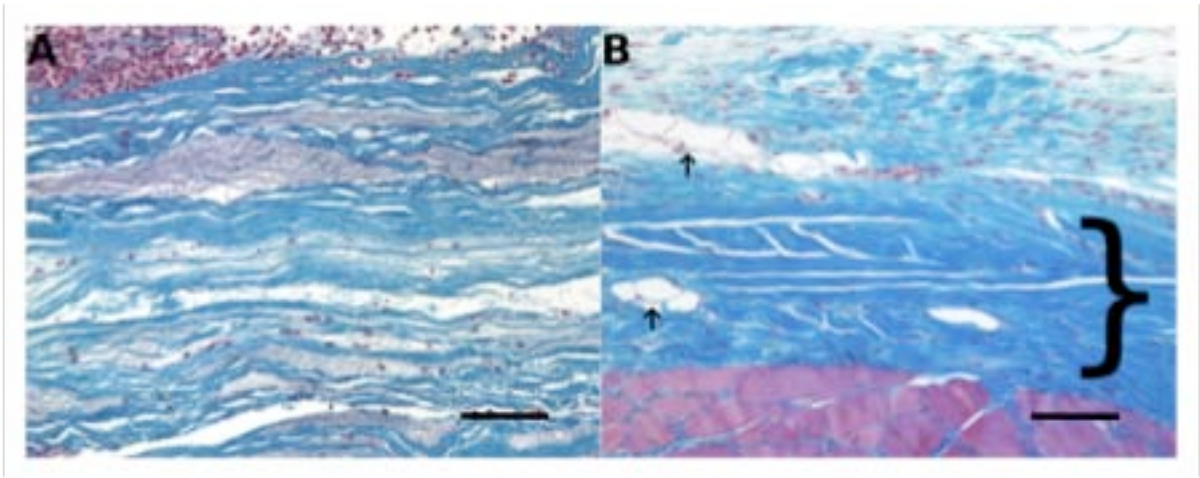


**Figure 27. (A) Histologic appearance of the cUBM at 7 days post surgery. The cUBM (blue staining) appeared minimally degraded at 7 days post surgery. A dense population of both neutrophils and mononuclear cells were present in the operative site; however, there was minimal invasion of the cells into the cUBM. (B) Histologic appearance of the cUBM at 28 days post surgery. The cUBM was no longer discernable at 28 days and was replaced with dense poorly organized collagenous connective tissue (dark blue staining, bracket), a small amount of adipose tissue (arrows), and a randomly distributed population of mononuclear cells. The red staining tissue bundles at the bottom of the image represent the underlying transversalis muscle. Scale bar = 100 μm. (Masson's Trichrome, 20X). Reproduced from (100) with permission from Elsevier.**

The host response to the acellular xenogeneic UBM test article was characterized by a dense infiltration of both neutrophils and mononuclear cells that surrounded the implant and separated the individual layers of the multilaminate device at 3 days post surgery. Angiogenesis was prominent as early as 3 days post surgery and remained a prominent feature of the host response throughout the 28 day study period. Degradation of the UBM was most obvious at 7 and 14 days post surgery at which times there was a uniformly distributed population of mononuclear cells accompanied by neomatrix and a notable absence of neutrophils (Figure 28a). By day 28, the implant was no longer visible and was replaced by organized host connective

tissue. Fibroblasts, blood vessels, aligned collagen, and small islands of skeletal myoblasts growing in from the periphery were observed at the site of remodeling (Figure 28b).

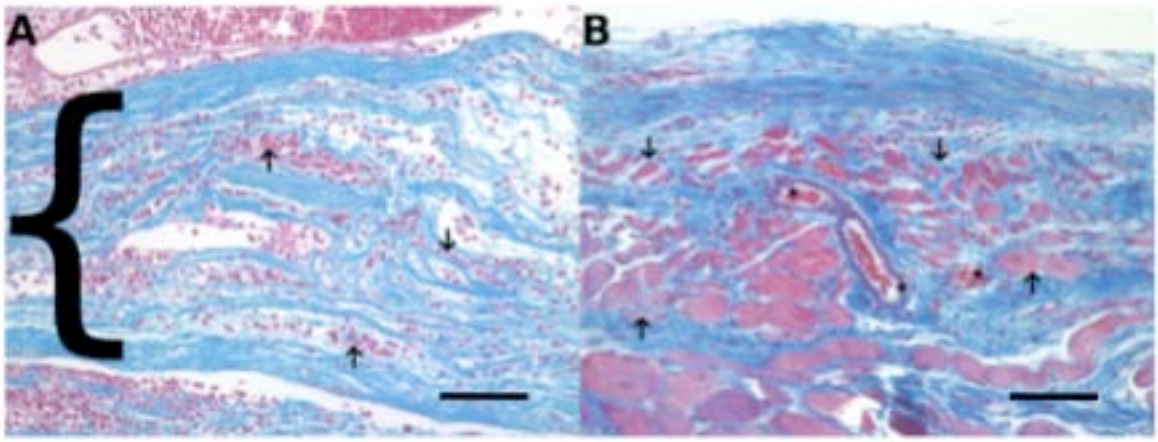


**Figure 28. (A) Histologic appearance of the UBM at 7 days post surgery. A dense cellular infiltrate consisting of mostly mononuclear cells was seen surrounding and within (arrows) the layers of the UBM (blue staining, bracket) at 7 days post surgery. (B) Histologic appearance of the UBM at 28 days post surgery. The UBM was no longer discernable by 28 days post surgery and was replaced by fibroblasts, blood vessels (asterisks), aligned collagen and small islands of skeletal myoblasts (arrows). The red staining tissue bundles at the bottom of the image represent the underlying transversalis muscle. Scale bar = 100 μm. (Masson's trichrome, 20X). Reproduced from (100) with permission from Elsevier.**

The temporal and spatial infiltration of host cells and the degradation of the scaffold material was very similar between the acellular allogeneic body wall ECM and the acellular xenogeneic ECM test groups.

#### 3.3.1.2 Evidence of Innervation

Following unilateral abdominal wall repair in the rodent model, the UBM scaffold showed progressive remodeling with time. Histological examination showed a mixture of skeletal muscle cells and organized collagenous connective tissue at the site of UBM placement

at day 28. No positive labeling for neurons or Schwann cells was present at days 3, 7 and 14. At day 28, positive labeling for neurons was observed in the remodeled UBM scaffold adjacent to the leading edge of growth of the adjacent native external oblique muscle. Nerves were localized to regions of neo-muscular growth. Positive labeling for GAP-43 confirmed that these nerves were actively growing (202-204). Positive labeling for Schwann cells co-localized with positive labeling for nerves within the pockets of neo-muscular growth (Figure 29). The specificity of neurofilament, GFAP and GAP-43 stains was confirmed via staining of nerve in native rat abdominal wall muscle.

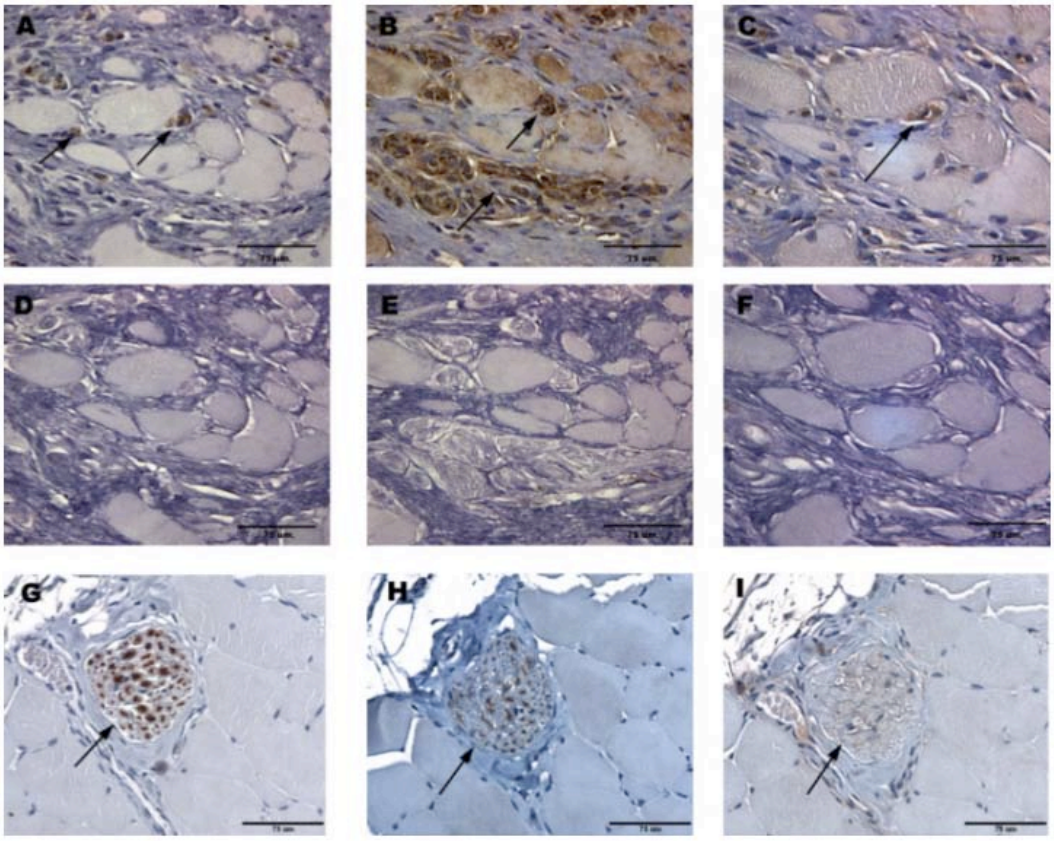


**Figure 29. Histological images of remodeled UBM 28 days after repair of a 1 cm × 1 cm defect in the rat abdominal wall, with specific staining for (A) neurofilament, (B) GAP43 and (C) GFAP. Specificity of staining was confirmed by primary delete negative controls for (D) neurofilament, (E) GAP43 and (F) GFAP. Positive control staining was confirmed in native rat abdominal wall muscle for (G) neurofilament, (H) GAP43 and (I) GFAP. All scale bars are 75 µm. Reprinted from (134) with permission from John Wiley and Sons.**

### 3.3.2 Bilateral Defect Model

#### 3.3.2.1 Histopathologic Findings

In the bilateral model, the host response to the autologous tissue test article consisted of necrotic skeletal muscle and a dense infiltration of mononuclear cells with some neutrophils at the one day post-implantation time point. This was followed by a progression of tissue

remodeling which was similar to that observed for the autograft test article in the unilateral model (Figure 30a and b). Briefly, the host response was characterized by necrosis of the majority of the skeletal muscle tissue accompanied by an angiogenic response and the deposition of abundant neo-matrix with time. Evidence of survival of some of the autograft muscle fibers was observed. By 28 days post-implantation, the remodeling site was characterized by the necrosis of most of the graft material with few islands of skeletal muscle remaining, minimal vascularity, deposition of a layer of dense collagenous connective tissue, and a reduction in the number of inflammatory cells present within the wound site as compared to earlier time points (Figure 30c and d). A qualitatively similar histologic response and tissue remodeling outcome was observed for autograft tissues that were implanted in the same animal as non-cross-linked UBM (Figure 30a and c) and cross-linked UBM (Figure 30b and d) test articles.

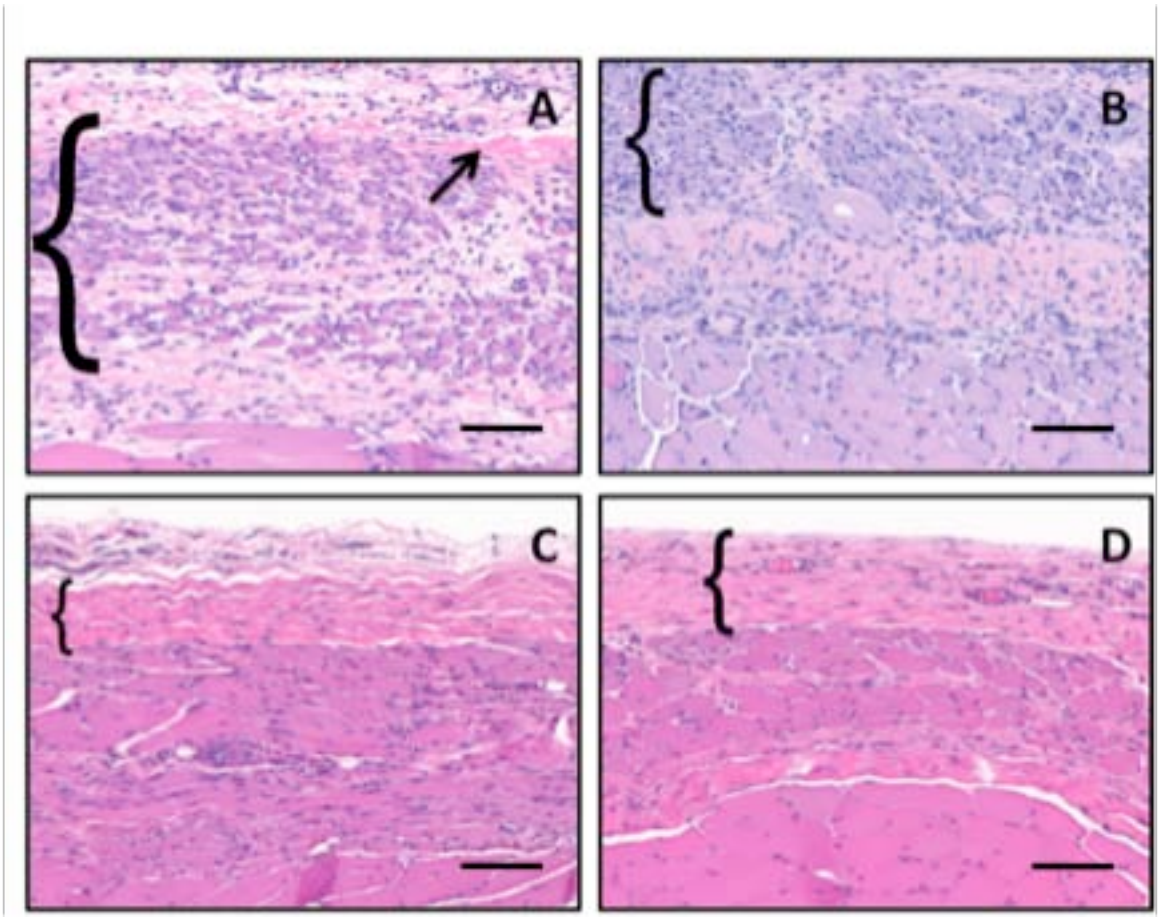


**Figure 30. (A, B) Histologic appearance of the autologous tissue test article at 7 days post-implantation (A, B). Necrotic skeletal muscle (brackets), early neo-matrix deposition (arrow), and a dense infiltration of macrophages were observed. (C, D) Histologic appearance of the autologous tissue test article at 28 days post-implantation. Autograft tissue has been resorbed and has been replaced with dense collagenous connective tissue (brackets), and a small number of spindle shaped cells. Pink tissue at bottom of images is native muscle tissue. A and C are autologous tissue test articles implanted with contralateral implantation of UBM. B and D are autologous tissue test articles implanted with contralateral implantation of CDI-UBM. Scale bar = 100 μm. (Hematoxylin and eosin, 20X)**

The host response to the carbodiimide cross-linked UBM test article was characterized by an accumulation of primarily neutrophils at the surface of the scaffold material at early time points. Some necrotic muscle fibers were observed at within the superficial layer of the native host muscle tissue. By three days post-implantation, the majority of the cells within the wound site were neutrophils with a lesser number of mononuclear cells within the remodeling site. At the three day time point, few of the cells within the remodeling site were seen to be interacting with the surface of the cross-linked test article. By seven days post-implantation, the neutrophil population had changed to a population consisting of predominantly mononuclear cells, few of which were observed to have infiltrated the surface of the test article (Figure 31a and b). Angiogenesis and areas of neo-matrix deposition were observed in the tissues adjacent to the test article. By 14 days post-implantation a more defined connective tissue layer was observed surrounding the test article and a small degree of cellular infiltration was observed at the periphery of the test article. The cells within the remodeling site were predominantly mononuclear with a number of foreign body giant cells observed at the superficial surface of the test article. By 28 days the site of remodeling was characterized by little to no evidence of infiltration of the scaffold material with mononuclear cells, the formation of an increasingly dense layer of disorganized collagenous connective tissue at the host-test article interface, and a significant foreign body giant cell response at the superficial surface of the test article (Figure 31c and d). Again, no qualitative differences in the course of tissue remodeling were observed for those test articles which were implanted with non-cross-linked UBM (Figure 31a and c) or autologous tissue test articles (Figure 31b and d).

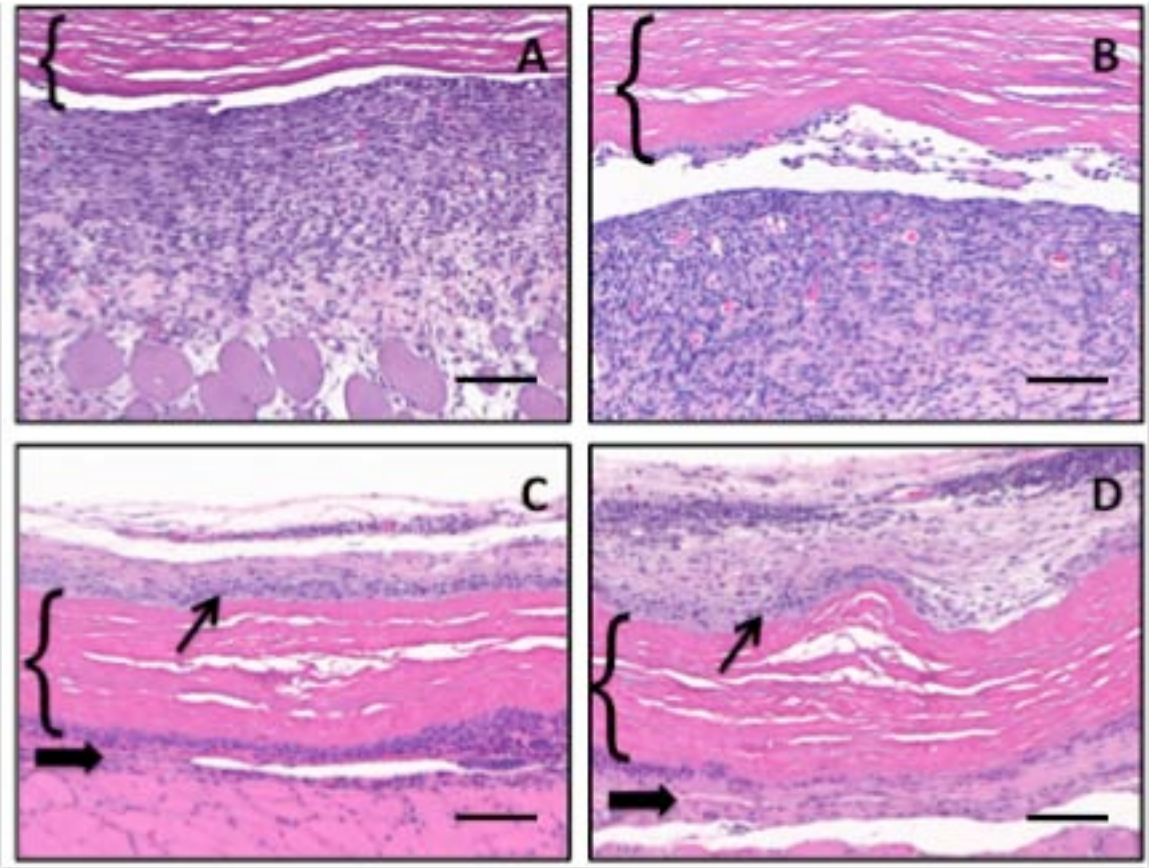


**Figure 31. (A, B) Histologic appearance of CDI-UBM at 7 days post-implantation. The test article is visible (brackets) and no infiltration of mononuclear cells was observed. (C, D) Histologic appearance of the CDI-UBM test article at 28 days post-implantation. The test article is still clearly visible (brackets) and a foreign body giant cell response is observed at the superficial surface of the implant (arrows). Deposition of dense, poorly organized connective tissue was observed at the host-material interface (block arrow). Pink tissue at bottom of images is native muscle tissue. A and C are CDI-UBM test articles implanted with contralateral implantation of UBM. B and D are CDI-UBM test articles implanted with contralateral implantation of autologous tissue. Scale bar = 100 μm. (Hematoxylin and eosin, 20x).**

The host response to the non-cross-linked UBM test article was similar to that observed in the unilateral body wall study. The host response at one day post-implantation was characterized by the accumulation of neutrophils at the surface of the test article, with a small number of cells infiltrating into the interior of the test article. By three days post-implantation the cellular population was predominantly composed of neutrophils with a lesser number of mononuclear cells observed, mostly at the periphery of the test article. More obvious infiltration of neutrophils into the test article was observed than at one day post-implantation. By seven days post-implantation, significant disruption of the architecture of the UBM test article was observed and cellular infiltration was observed throughout the full thickness of the test article (Figure 32a and b). The cells within the remodeling site and infiltrating the scaffold were predominantly mononuclear in nature. Angiogenesis was observed mainly at the periphery of the implant with a smaller number of vessels within the test article itself. Neo-matrix deposition was also observed, predominantly at the periphery of the test article with lesser amounts of neo-matrix deposition observed within the UBM test article. By 14 days post-implantation, the remodeling site was characterized by extensive degradation of the test article accompanied by robust deposition of neo-matrix within the remodeling site. The cellular population at the 14 day time point was almost exclusively mononuclear with few multinucleated cells observed. It was not clear whether these cells represented foreign body giant cells, early muscle cells, or satellite cells. By 28 days post-implantation the scaffold material was not distinguishable in histologic sections, except for a small amount of scaffold material which was distinguishable in one sample (Figure 32c and d). The rapid degradation of the scaffold material was accompanied by a marked decrease in cellularity, scattered islands of muscle tissue located largely at the periphery of the scaffold material, and partially organized connective tissue within the site of remodeling.

Again, no qualitative differences in the outcome of tissue remodeling were observed to occur when the UBM test article was implanted with either the autologous tissue test article (Figure 32a and c) or the CDI-UBM (Figure 232b and d) test articles.

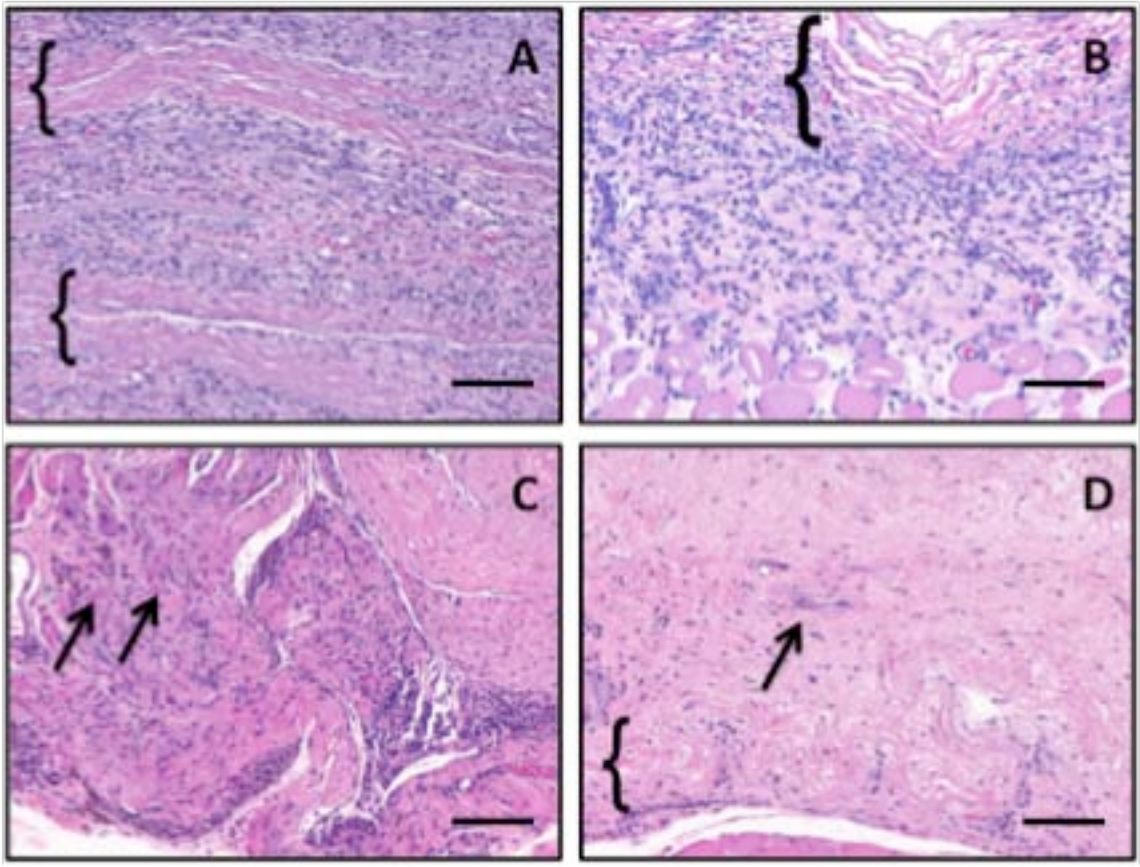


**Figure 32. (A, B) Histologic appearance of UBM at 7 days post-implantation. A dense infiltration of mononuclear cells is observed within and surrounding the layers of the UBM test article (brackets). (C, D) Histologic appearance of the UBM test article at 28 days post-implantation. The test article was largely degraded and was replace with newly deposited extracellular matrix, fewer mononuclear cells and some spindle shaped cells, and small islands of skeletal muscle at the periphery of the implantation site (arrows). In one sample (D), a small amount of the test article was observed (bracket). Pink tissue at bottom of images is native muscle tissue. A and C are UBM test articles implanted with contralateral implantation of autologous tissue. B and D are UBM test articles implanted with contralateral implantation of CDI-UBM tissue. Scale bar = 100 μm. (Hematoxylin and eosin, 20x).**

#### 3.3.2.2 Herovici's Polychrome Staining

Herovici's polychrome allows for the identification of immature (type III; blue) collagen and mature (type I; dark purple/pink) collagen. Each test article type was investigated at 7 (early) and 28 day (late) time points for the type and maturity of collagen deposited. Each test article was associated with a qualitatively different pattern of immature and mature collagen deposition (Figure 33). The autologous tissue test article showed deposition of immature collagen within the implant site and between the necrotic skeletal muscle bundles of the autograft at 7 days. By 28 days, the necrotic bundles of skeletal muscle were no longer visible and were replaced by a dense layer of mature collagenous connective tissue surrounded by immature collagen. The CDI-UBM test article was visible at 7 days and the intact scaffold material remaining within the site of implantation was characterized by predominantly mature collagen type I. The surrounding tissue was characterized by the deposition of immature collagen. By 28 days, the test article was still present within the remodeling site and again stained positive for mature collagen. The surrounding implant site was characterized by the deposition of mostly immature collagen and with a small band of more mature encapsulating collagen at the implant surface. At 7 days the UBM test article was partially degraded and appeared to be composed of a mixture of mature and immature collagen. Immature collagen was observed within the layers of the degrading UBM test article. By 28 days, the UBM test article was largely degraded and the implant site was characterized by the deposition of mature collagen intermixed with a smaller amount of immature collagen throughout the site of implantation.

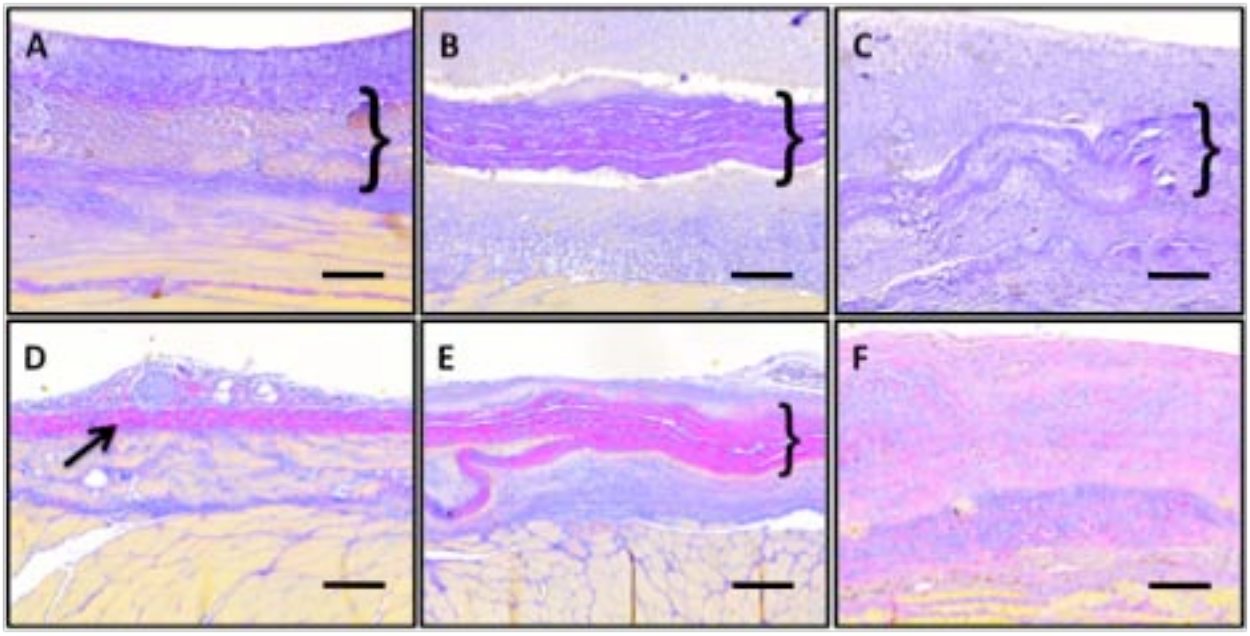


**Figure 33. Herovici staining of autologous tissue (A, D), CDI-UBM (B, E), and UBM (C, F) test articles at 7 (A, B, C) and 28 (D, E, F) days post-implantation. Brackets indicate visible remnants of test articles and arrow indicates dense layer of mature collagen deposition. Light blue staining is indicative of immature collagen (type III) deposition, purple/pink staining is indicative of mature collagen (type I) deposition, yellow staining indicates muscle bundles. Scale Bar = 200 μm. (Herovici's Polychrome, 10x).**

#### 3.3.2.3 MMP Gene Expression Analysis

MMP expression was evaluated by real-time quantitative PCR. With few exceptions, increased expression of all genes examined (MMP2, 3, 7, and 9) was observed in all samples as compared to native tissue. An increase in MMP2 expression (Figure 34a) was observed for all remodeling test articles between 1 and 7 days post-implantation, with similar expression levels for all test articles at the 1 and 3 day time points. At 7 days the autologous test article exhibited higher expression of MMP2 than did UBM or CDI-UBM; however, the results were not statistically significant. MMP2 expression decreased between 7 and 14 days, with all test articles expressing similar levels of MMP2 at 14 days post-implantation. By 28 Days MMP2 expression

was slightly elevated in the autologous tissue and CDI-UBM test articles as compared to native tissue. However, MMP2 levels in the UBM test article were seen to increase between 14 and 28 days post-implantation, again this result was not statistically significant. No significant interactions between scaffold type and time point were found.

MMP3 expression levels (Figure 34b) were elevated in all test articles as compared to native tissue, with the exception of UBM at 1 day post-implantation. Levels in autologous tissue test articles were elevated at 1 day post-implantation as compared to CDI-UBM and UBM test articles, although not statistically significant. Levels in all test articles decreased from 3 days to 7 days, then increased at 14 days. By 28 days post-implantation levels had decreased as compared to 14 days, however were elevated as compared to native tissue. No significant interactions between scaffold type and time were found

MMP7 expression levels (Figure 34c) were found to be slightly elevated at early time points (1 and 3 days post-implantation) in all scaffold materials. At 7 days post-implantation, MMP7 expression was significantly higher in the CDI-UBM test article, while levels remained only slightly elevated in the autologous tissue and UBM test articles. At 14 days both the CDI-UBM and UBM test articles were found to have statistically significant elevated MMP7 expression as compared to the autologous tissue test article, which dropped below the level found in native tissue. By 28 days post-implantation, MMP7 levels were elevated as compared to native tissue in the autologous and CDI-UBM test articles, with higher levels observed for the UBM test article, although not statistically significant. Only scaffold type was found to be a statistically significant factor ($F=5.2451$, $p<0.01$). Statistically significant differences in MMP7 expression between scaffold types were observed at 7, and 14 days post-implantation.

MMP9 expression levels (Figure 34d) were found to be elevated in all scaffold types throughout the study period as compared to native tissue. At 1 day post-implantation, both the CDI-UBM and UBM test articles showed statistically significant higher expression of MMP9 than the autologous tissue test article. Expression levels were seen to decrease at 3 and 7 days post-implantation, and increase at 14 and 28 days post-implantation. The largest increase was observed in the UBM test articles and was highest at 28 days, although not statistically significant. No significant interactions between scaffold type and time were found. Both scaffold type ($F=7.9702$, $p<0.001$) and time ($F=7.8561$, $p<0.01$) were found to be statistically significant factors. Statistically significant differences in MMP9 expression between scaffold types were observed at 1, 7, and 14 days post-implantation.

Statistically significant differences were found for MMP2 (at 3 days) and MMP7 (at 28 days) expression for autologous tissue which was implanted concurrently with either UBM or CDI-UBM test articles. However, these differences were few and no distinct pattern was observed.

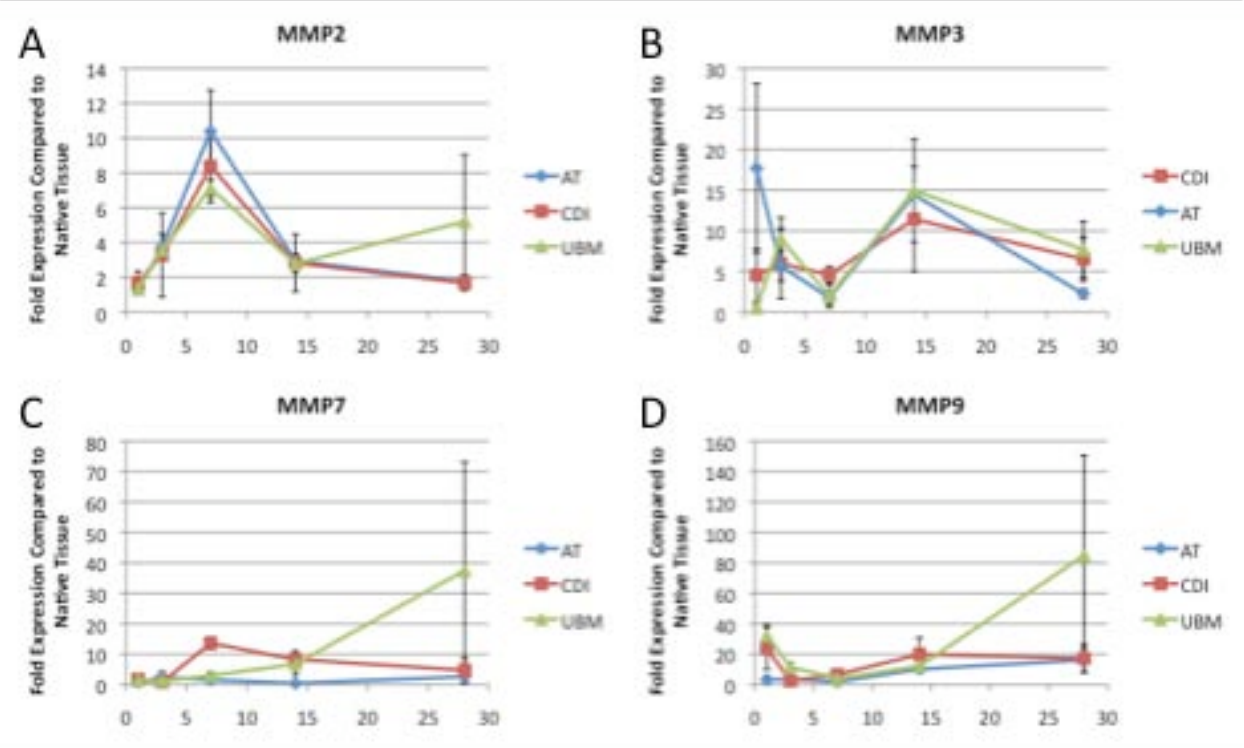


**Figure 34. MMP gene expression compared to expression in native tissues for samples from the bilateral defect study. (A) MMP2 expression was not shown to have statistically significant relationships with scaffold type or time. (B) MMP 3 expression was not shown to have statistically significant relationships with scaffold type or time. (C) Scaffold type was found to be a statistically significant (F=5.2451, p=<0.01) factor in MMP7 expression with statistically significant differences observed at 7, and 14 days post implantation. (D) MMP9 expression showed the most significant differences for all MMP genes investigated. Both scaffold type and time were found to be significant factors (F=7.9702, p=<0.001 and F=7.8561, p<0.01, respectively).**

## 3.4 DISCUSSION

The results of the present studies show that each of the implanted test articles was associated with a distinct tissue remodeling outcome. In both the unilateral and bilateral body wall models,

the implantation of autograft tissue resulted in necrosis of the skeletal muscle and replacement with dense, mature collagenous connective tissue within the remodeling site. Implantation of UBM, both in the unilateral and bilateral body wall defect models, resulted in early stages of constructive tissue remodeling (i.e. innervated islands of skeletal muscle, angiogenesis, and deposition of mature, well organized collagen). In contrast, UBM that contained a cellular component or was chemically cross-linked with carbodiimide resulted in either degradation of the scaffold material resulting in deposition of a dense layer of poorly organized collagenous connective tissue or a foreign body reaction and encapsulation, respectively. Herovici's polychrome staining showed that the composition of the tissues deposited within the remodeling site were different for the autograft, CDI-UBM, and UBM groups and MMP gene expression analysis showed that there were significant differences in MMP expression between scaffold materials. Most notably, UBM test articles appeared to have increased MMP expression as compared to other test articles occurring between the 14 and 28 day time points. Although, not necessarily statistically significant, this change in MMP expression also coincided with the most noticeable differences in the histologic response.

These results show that, despite a response which is histologically similar at early time points (1 to 7 days post-implantation) in the tissue remodeling process, the outcome of the tissue remodeling process is distinctly different at later time points (14 days and beyond). In each case, however, a large population of mononuclear cells was observed starting at 3 days post-implantation and continued to persist to varying degrees throughout the course of the study period. A robust mononuclear cell response has been observed following the implantation of ECM scaffold materials in a wide variety of applications (85). This response, although it often results in constructive tissue remodeling, has been characterized by some as chronic

inflammation. However, as the results of the present study show, this response does not necessarily result in the deposition of granulation tissue, a foreign body response, or the deposition of collagenous connective tissue within the site of remodeling. Rather, the response resolves and results in what can be described as constructive tissue remodeling. This would suggest that, although the majority of the cells present in the early stages of remodeling are polymorphonuclear and mononuclear in nature, there may be phenotypic differences which are dependant on the nature of the scaffold implanted and that these differences may be predictive of the tissue remodeling outcome.

The present studies also showed that the presence of cellular material within an ECM scaffold prior to implantation led to inability of the ECM scaffold material to promote constructive tissue remodeling. This is not surprising in the case of large amounts of xenogeneic cellular components, which may be recognized by the host immune system and elicit host immune response following implantation. Porcine cells express such cell associated epitope as α-Gal, which is known to play a role in transplant rejection in humans (88, 89). Other molecules, including those associated with cell death, have also been shown to have potent immunomodulatory effects (205, 206). These cell death associated molecules, termed damage associated molecular pattern molecules (DAMPs), include extracellular DNA, high mobility group box 1, S100, and heat shock proteins among numerous others. In general, these molecules are recognized by pattern recognition receptors on cells of the innate immune system. Therefore, it is logical to assume that large amounts of these molecules resulting from inefficient removal during processing or due to cellular death upon implantation may have detrimental effects upon the ability of ECM scaffold materials to promote a constructive tissue remodeling response. DAMPs including HMGB1, S100, and multiple heat shock proteins have been shown to be

present within ECM scaffold materials (unpublished data), even those which have been efficiently decellularized. The presence of these molecules within decellularized matrices is logical when one considers that most decellularization processes include cell lysis. However, the amounts of these molecules which remain following decellularization has not been shown to have detrimental effects upon tissue remodeling.

The present studies also show that the presence of autologous cellular components within a test article may prevent constructive tissue remodeling. In the present study, healthy autologous tissue harvested during the creation of the surgical defect was re-implanted within minutes of defect creation. Tissue remodeling, however, resulted in necrosis of the cellular component and deposition of dense mature collagenous scar tissue. The process of muscle necrosis is well understood, and the results in the present study are not surprising. Likely, disruption of the vascular supply leads to necrosis of the skeletal muscle tissue, causing a pro-inflammatory tissue response which results in the deposition of collagenous connective tissue. The fate and contribution of seeded cells in tissue engineering is a subject which has not been well addressed. While cells may have positive paracrine effects following implantation, it is not clear that seeded cells participate in constructive tissue remodeling in the long-term. However, if one thinks of autologous tissue as a target for tissue engineering approaches to muscular reconstruction, the results of the present study may suggest that seeding of a scaffold with autologous cells, even if viable and arranged in a tissue-specific three dimensional architecture with a vascular network, prior to implantation may not promote constructive tissue remodeling.

The exact mechanisms by which non-cross-linked ECM scaffolds are capable of modulating the host tissue response towards constructive tissue remodeling are not fully understood; however, the results presented here clearly show that chemical cross-linking has

detrimental effects upon this ability. Similar results were observed in a study which investigated the short (2 days) and long-term (up to 112 days) host tissue remodeling responses elicited by 5 commercially available ECM based scaffold materials commonly used for rotator cuff repair (69). Results showed that constructive tissue remodeling occurred in those ECM scaffolds which were not chemically cross-linked. This was in contrast to materials which were chemically cross-linked, which elicited a chronic foreign body response similar to that observed in the present study. As was shown in the previous studies, chemical cross-linking changes both the ultrastructure and, to a smaller degree, the composition of the surface of ECM scaffold materials. Therefore, it is logical to assume that interactions between the surface of the material and the cells which participate in the host tissue remodeling response may be responsible for determining the downstream tissue remodeling outcome associated with the implantation of ECM scaffold materials.

In the present studies, it was also observed that the host tissue remodeling response to one test article did not appear to affect the host tissue remodeling of another scaffold material implanted concurrently within the same animal. These results suggest that scaffold remodeling is a localized phenomenon which occurs at the site of implantation. Likely this is a result of cellular interactions with the surface of the material.

## 3.5 CONCLUSIONS

Despite a similar histologic response at early time points in the remodeling process (up to 7 days post-implantation), the outcomes observed following the implantation of each scaffold type were distinct. The present study showed that the presence of a cellular component within an

extracellular matrix scaffold impaired the ability of the scaffold material to support constructive tissue remodeling. It was observed that those test articles that contained a cellular component, even viable autologous cells, resulted in the deposition of dense connective tissue and/or scarring. Those test articles that did not contain a cellular component, however, were observed to result in a more constructive type remodeling response including the formation of islands of new skeletal muscle within organized, mature collagen. Chemical crosslinking was also shown to affect the ability of and ECM scaffold material to promote constructive tissue remodeling. Scaffolds which were crosslinked resulted encapsulation of the material within increasingly dense collagenous connective tissue with no signs of constructive tissue remodeling. Lastly, the remodeling of one ECM scaffold material did not appear affect the remodeling of a second ECM scaffold material implanted in the same animal, suggesting that ECM scaffold remodeling is a localized and not a systemic phenomenon. The results of these studies demonstrate the importance of the methods used in ECM scaffold production and an understanding of how scaffold characteristics affect downstream tissue remodeling. The section which follows will investigate differences in the phenotype of the macrophages which participate in the response to each of the materials described above and their role in determining the downstream tissue remodeling outcome associated with their implantation.

## 3.6 LIMITATIONS AND FUTURE DIRECTIONS

The present study utilized a rat abdominal wall musculature defect model to investigate the host tissue remodeling response to ECM scaffold materials. This model has been used to successfully evaluate the ability of a wide variety of ECM scaffold materials to promote constructive tissue

remodeling (44, 69, 133). In the present study, ECM materials derived from two separate tissue sources were investigated. Implantation of both acellular rat body wall ECM (allogeneic source) and acellular ECM derived from porcine urinary bladder (xenogeneic source) were observed to result in early signs of constructive tissue remodeling of the abdominal wall musculature. However, due to the short time period utilized in the present study, it was not possible to determine if the source of the ECM scaffold material would have affected the long-term outcome of tissue remodeling and the functionality of the remodeled muscle tissue. A number of *in vitro* studies have shown that ECM derived from tissue-specific sources may be better for the support of specialized cell populations derived from the same tissue (207-209). However, the effects of tissue, or species, specific ECM scaffolds has not been well investigated *in vivo*.

The effects of both viable autologous cells and xenogeneic cellular components were investigated. In both cases, tissue remodeling resulted in the deposition of dense collagenous connective tissue with no signs of constructive tissue remodeling. The exact mechanism by which cellular components affect tissue remodeling in the case of ECM based scaffold materials has not been fully elucidated, but likely includes pro-inflammatory responses to cellular components such as DNA and DAMPs. Previous studies have shown that ECM scaffold materials contain small amounts of DNA, α-Gal, and DAMPs, even when intact nuclei are not present in histologic sections. Despite the presence of these molecules, acellular non-cross-linked ECM scaffold materials are capable of eliciting an immune response which does not appear to affect the ability of the material to promote constructive tissue remodeling. In the present study, it was shown that large amounts of cellular material, even viable autologous cells, affected the ability of the scaffold to remodel. Thus, there may be a threshold for potentially

immunogenic molecules, beyond which the ability of an ECM scaffold to promote constructive tissue remodeling is impaired. Further studies are needed to determine this threshold.

The present study examined the effects of one commonly used method of chemical cross-linking. In the previous chapter, both glutaraldehyde and carbodiimide cross-linking were shown to affect the surface ultrastructure and, to a lesser degree, the surface composition of UBM. A variety of other chemical cross-linking methods are available and may result in a different tissue response than was observed in the present studies. In particular, genipin, a cross-linking agent derived from gardenia, has been shown to have anti-inflammatory properties (210-212). Cross-linking of ECM scaffolds with genipin may result in a more constructive host tissue remodeling response than was observed with the carbodiimide cross-linked ECM scaffolds used in the present study. Additionally, in the present study, the mechanisms by which cross-linking inhibited constructive tissue remodeling were unclear. The inability of the ECM scaffold material to degrade may have prevented the release of bioactive matricryptic peptides which have been shown to have antibacterial, and chemotactic properties in previous studies. Alternatively, cross-linking, as was suggested in the studies presented previously, may have altered the presentation of ligands on the surface of the material. Differences in surface chemistry may have also resulted the adsorption of a different repertoire of proteins following implantation and contact with blood. It is also possible that the observed differences were due to inability of the macrophage population participating in the host response to degrade or phagocytose the material within the site of tissue remodeling resulting in the formation of foreign body giant cells and encapsulation.

Finally, the results of the present studies suggest that the tissue remodeling response to one test article was not affected by the implantation of a second test article implanted

concurrently within the same animal. This suggests that the remodeling of an ECM scaffold material is a localized phenomenon. However, as the data presented as part of the above studies was largely qualitative and study populations were small (n=2 for each combination of scaffolds, and n=4 for each scaffold type), additional work may be necessary to detect smaller differences in the tissue remodeling outcome which may not be readily observed through histologic staining alone. However, it is clear that the implantation of either autologous tissue or CDI-UBM did not significantly inhibit constructive tissue remodeling of UBM. And, conversely, that the implantation of UBM did not result in constructive tissue remodeling of autologous tissue or CDI-UBM. The studies which follow will investigate the host response to each of the scaffolds implanted as part of these studies and quantitatively assess differences in the host macrophage response which may occur as a result of the implantation of two ECM scaffold materials within the same animal.

# 4.0 SPECIFIC AIM 3: EXTRACELLULAR MATRIX SCAFFOLDS ALTER THE DEFAULT HOST MACROPHAGE RESPONSE

## 4.1 BACKGROUND

The extracellular matrix (ECM) represents the secreted products, both structural and functional, of the resident cells of each tissue and organ. The composition and ultrastructure of the ECM is determined by factors that influence the phenotype of its resident cells including mechanical forces, biochemical milieu, oxygen requirements, pH and inherent gene expression patterns, among others. In turn, the ECM influences cell attachment, migration, proliferation and three-dimensional organization, serving as an "information highway" between cells (3-5). For these reasons, multiple forms of allogeneic and xenogeneic ECM from sources such as small intestine, urinary bladder, and skin have been investigated as biologic scaffolds for tissue reconstruction in both preclinical studies and human clinical applications (213).

Macrophages are a heterogeneous subset of the mononuclear cell population (139, 142-144, 146) involved in the host response to implanted materials. Macrophages are generally activated in response to tissue damage or infection, causing an increase in the production of cytokines, chemokines, and other inflammatory molecules to which they are exposed (141, 143, 144). Recently, macrophage phenotype has been characterized based on distinct functional properties, surface markers, and the cytokine profile of the microenvironment (141, 143, 146).

Polarized macrophages are referred to as either M1 or M2 cells, mimicking the Th1/Th2 nomenclature (143). However, M1 and M2 represent extremes along a continuum that includes multiple macrophage phenotypes (M1, M2a, M2b and M2c). M1, classically activated pro-inflammatory, macrophages are known to be induced by IFN-γ alone or in combination with LPS, TNF and GM-CSF. In general, M1 activated macrophages express IL-$12^{high}$, IL-$23^{high}$, IL-$10^{low}$; metabolize arginine, produce high levels of inducible nitric oxide synthase (iNOS); secrete toxic reactive oxygen and nitric oxygen intermediates and inflammatory cytokines such as IL-1β, IL-6, and TNF; and are inducer and effector cells in Th1 type inflammatory responses. In contrast, M2, alternatively activated, macrophages are induced by exposure to a variety of signals including the cytokines IL-4, IL-13, and IL-10, immune complexes, and glucocorticoid or secosteroid (vitamin D3) hormones. M2 activated macrophages express IL-$12^{low}$, IL-$23^{low}$, and IL-$10^{high}$; have high levels of scavenger, mannose, and galactose receptors; produce arginase in the place of arginine, subsequently producing ornithine and polyamines; are involved in polarized Th2 reactions; and possess the ability to facilitate tissue repair and regeneration.

Macrophages are a plastic cell population capable of sequentially changing their polarization in response to local stimuli during the process of wound healing (214-216). The macrophages participating in the host response to an implanted material are exposed to multiple stimuli including cytokines and effector molecules secreted by cells including other macrophages that are participating in the host response, microbial agents, epitope associated with the implanted biomaterial, and the degradation products of the biomaterial, among others. Therefore, it is logical to assume that the host macrophage response after implantation of a biomaterial is modulated via “cross-talk” between macrophages and the other cells involved in the host response as well as factors within the local microenvironment. The effects of

macrophage phenotype upon the tissue remodeling outcome following the implantation of a biomaterial are largely unknown, but recognition of the predominant phenotypic profile of the macrophages which participate in the host response to an implanted material may provide a tool by which a constructive and functional tissue remodeling outcome can be predicted and/or promoted.

The objectives of the present studies were three fold: (1) to shown that extracellular matrix scaffolds are capable of altering the default host macrophage response following implantation, (2) to show that modulation of the host macrophage response is related to the ability scaffold to promote the constructive versus encapsulation or scar tissue type remodeling responses observed in **Aim 2,** and (3) to evaluate the effects of polarized macrophages upon the *in vitro* behavior of other cell types in vitro.

## 4.2 METHODS

### 4.2.1 Evaluation of Macrophage Phenotype in Explanted Extracellular Matrix Scaffolds

The samples evaluated in the present studies were the same samples examined in the studies presented as part of Aim 2 above. The evaluation methods used for immunolabeling and quantification of macrophage phenotype in samples from the unilateral model and samples from the bilateral model differ in some respects which are listed below.

#### 4.2.1.1 Sample Collection

On the predetermined sacrifice date, each animal was anesthetized using isoflurane (5% in oxygen) and then euthanized by intracardiac injection of potassium chloride to induce cardiac arrest. The grafts were explanted with a small amount (approximately 2 mm) of the surrounding native tissue. One half of the tissue was fixed in 10% neutral buffered formalin and then embedded in paraffin. The other half of each specimen was preserved in RNAlater (Ambion, Austin, TX) for RNA extraction.

#### 4.2.1.2 Immunolabeling

##### (a) Unilateral Model

Immunolabeling was performed on consecutive 6 μm sections of each specimen in order to assess the macrophage phenotype within and surrounding the implant wound site. Following deparaffinization, the slides were placed in citrate antigen retrieval buffer (10mM citric acid monohydrate, pH 6.0, Spectrum) which was then brought to a boil (95-100ºC) for 20 min. The buffer was allowed to cool and the slides were then washed twice in TRIS buffered saline/Tween 20 (Trizma Base, Sigma; Tween 20, Sigma) solution (pH 7.4) and twice in PBS. The sections were incubated in 1.5% normal horse serum (Vector) for 1 h at room temperature in a humidified chamber to inhibit non-specific binding of the primary antibody. Following incubation in blocking serum, the sections were incubated in primary antibody in a humidified chamber at 4°C overnight. Each tissue specimen was exposed to antibodies to a pan-macrophage marker (CD68), an M1 phenotype marker (CCR7), and an M2 phenotype marker (CD163). Following the overnight incubation, the slides were washed three times in PBS. Sections were then incubated in a solution of 3% $H_2O_2$ in methanol for 30 min at room temperature to quench

endogenous peroxidase activity. Following $H_2O_2$ treatment, the slides were washed three times in PBS prior to incubation in secondary antibody for 30 min in a humidified chamber, at either room temperature (CD68) or 37°C (CD163, CCR7), and then subjected to three more washes in PBS. The sections were then incubated in Vectastain ABC (Elite ABC kit, Vector) reagent for 30 min in a humidified 37°C chamber, rinsed 3 times in PBS, and incubated in 4% DAB substrate solution (Vector) at room temperature. The slides were rinsed in water to stop the development of the DAB substrate and counterstained using Harris hematoxylin stain (Thermo Electron Corporation-Shandon, Pittsburgh, PA). The slides were then dehydrated using the reverse of the deparaffinization treatment described above prior to coverslipping. Each PBS rinse in the protocol was for 3 minutes at room temperature, with occasional agitation.

The primary antibodies used were mouse anti-rat CD68 (Serotec, Raleigh, NC) at a dilution of 1:50, rabbit anti-CCR7 (Cell Applications, San Diego, CA) at a dilution of 1:100, and mouse anti-rat CD163 (Serotec) at a dilution of 1:50. The secondary antibodies used were biotinylated horse anti-mouse IgG (Vector, CD68 and CD163) at a dilution of 1:50 and goat anti-rabbit IgG (Vector, CCR7) at a dilution of 1:100. All antibodies were diluted in filtered PBS (pH 7.4).

Representative images of the immunolabeling for each surface marker at 7 days post implantation are shown in Figure 35.

The immunostained slides were examined and imaged by a blinded investigator using a Nikon e600 microscope. The images were then evaluated quantitatively in a blinded fashion by two independent investigators. Quantitative analysis was performed by counting the number of immunopositive cells in six matched microscope fields at 40X magnification. Cell counts from negative controls (no primary antibody) were subtracted from the cell counts of the test articles

and the percentage of M1 and M2 macrophages was determined by dividing the number of CCR7+ (M1) and CD163+ (M2) cells by the number of CD68+ (pan-macrophage) cells in each field. A ratio of the percentage of M1 cells to M2 cells was also calculated for each field as follows:

$$M_1 : M_2 = \frac{Percent\ M_1\ Cells}{Percent\ M_2\ Cells}$$

The ratioa were then plotted on a log scale such that values grater than 1.0 were representative of the predominance of M1 cells among those cells staining positive for either M1 or M2 surface markers. Conversely, a value of less than 1.0 was representative of a predominance of M2 cells.

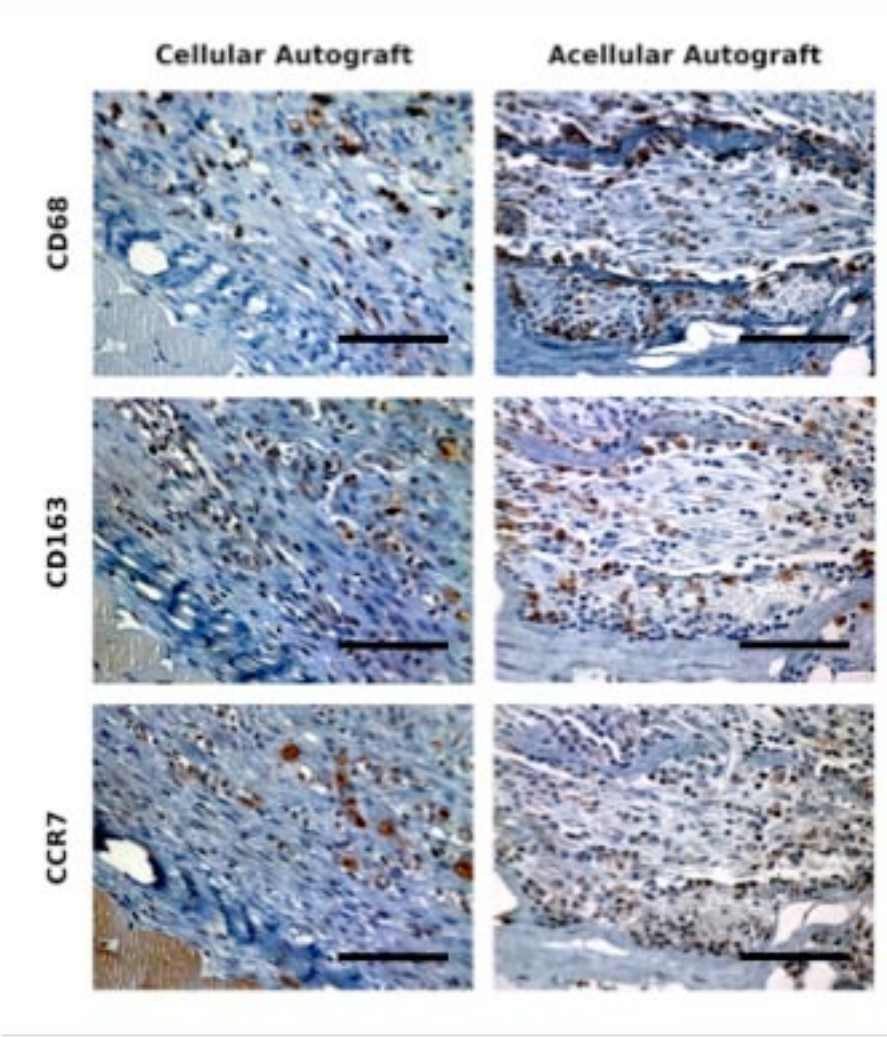


**Figure 35. Representative images of immunohistochemical staining for CD68, CD163, and CCR7 in the cellular autograft and acellular allograft test articles at 7 days post surgery. Scale bar = 100 μm (40X). Reproduced from (100) with permission from Elsevier.**

### (b) Bilateral Model

Immunofluorescence was utilized in place of immunoperoxidase methods in the bilateral study in order to allow for the evaluation of both the phenotype of the macrophages participating in the host response and their temporal and spatial distribution throughout the site of remodeling. As the analysis was performed using immunofluorescent triple labeling, which required the use

of rat-specific primary antibodies from three different species, the antibodies and markers used for macrophage polarization analysis in the bilateral study were somewhat different from those used in the unilateral defect study due to the commercial availability of antibodies which react with rat markers at the time the study was performed.

Immunolabeling was performed on 6 μm sections. Following deparaffinization, the slides were placed in citrate antigen retrieval buffer (10 mm citric acid monohydrate, pH 6.0) which was then brought to a boil (95–100 °C) for 20 min. The buffer was allowed to cool and the slides were then washed twice in TRIS buffered saline/Tween 20 (Trizma Base, Sigma; Tween 20, Sigma) solution (pH 7.4) and twice in PBS. The sections were incubated in 2% normal horse serum, 1% BSA, 0.1% Triton X-100, and 0.1% Tween 20 in PBS (pH 7.4) for 1 h at room temperature in a humidified chamber to inhibit non-specific binding of the primary antibody. Following incubation in blocking serum, the sections were incubated in primary antibodies in a humidified chamber at 4 °C overnight. Each tissue specimen was exposed to antibodies to a pan-macrophage marker (CD68), an M1 macrophage phenotype marker (CCR7), and an M2 macrophage phenotype marker (CD206). Following the overnight incubation, the slides were washed three times in PBS prior to incubation in fluorescently labeled secondary antibodies for one hour in a humidified chamber at room temperature, and then subjected to three more washes in PBS. Slides were then exposed to a DRAQ5 nuclear stain for 30 minutes at 37°C prior to being washed three times in PBS. The slides were then coverslipped using aqueous mounting media prior to visualization under a fluorescent microscope. Each PBS rinse in the protocol was for 3 min at room temperature, with occasional agitation.

The primary antibodies used were mouse anti-CD68 (Serotec) at a dilution of 1:50, rabbit anti-CCR7 (Epitomics) at a dilution of 1:200, and goat anti-CD206 (Santa Cruz) at a dilution of

1:50. The secondary antibodies used were AlexaFluor donkey anti-mouse IgG (350 nm) at a dilution of 1:25, donkey anti-rabbit IgG (568 nm) at a dilution of 1:100 and donkey anti-goat IgG (488 nm) at a dilution of 1:100. All antibodies were diluted in blocking serum as described above.

The immunolabeled slides were examined and imaged by a blinded investigator using a Nikon e600 microscope. The images were then evaluated quantitatively in a blinded fashion by a separate independent investigator. Quantitative analysis was performed by selecting three areas of approximately 90 x 60 μm at the surface of the test article and encompassing the 2-3 cell layers closest to the test article surface from within a high power microscope field (40x magnification). The number of cells labeled positively for each marker within the three boxes was then counted and summed for each image. The mean of the sums for all three high power images was then calculated for each sample. Examples of immunolabeling of UBM and CDI-UBM at 14 days post-implantation are provided in Figures 32 and 33.

A ratio of the percentage of M1 cells to M2 cells was also calculated for each field as follows:

$$M_1 : M_2 = \frac{Number\ M_1\ Cells}{Number\ M_2\ Cells}$$

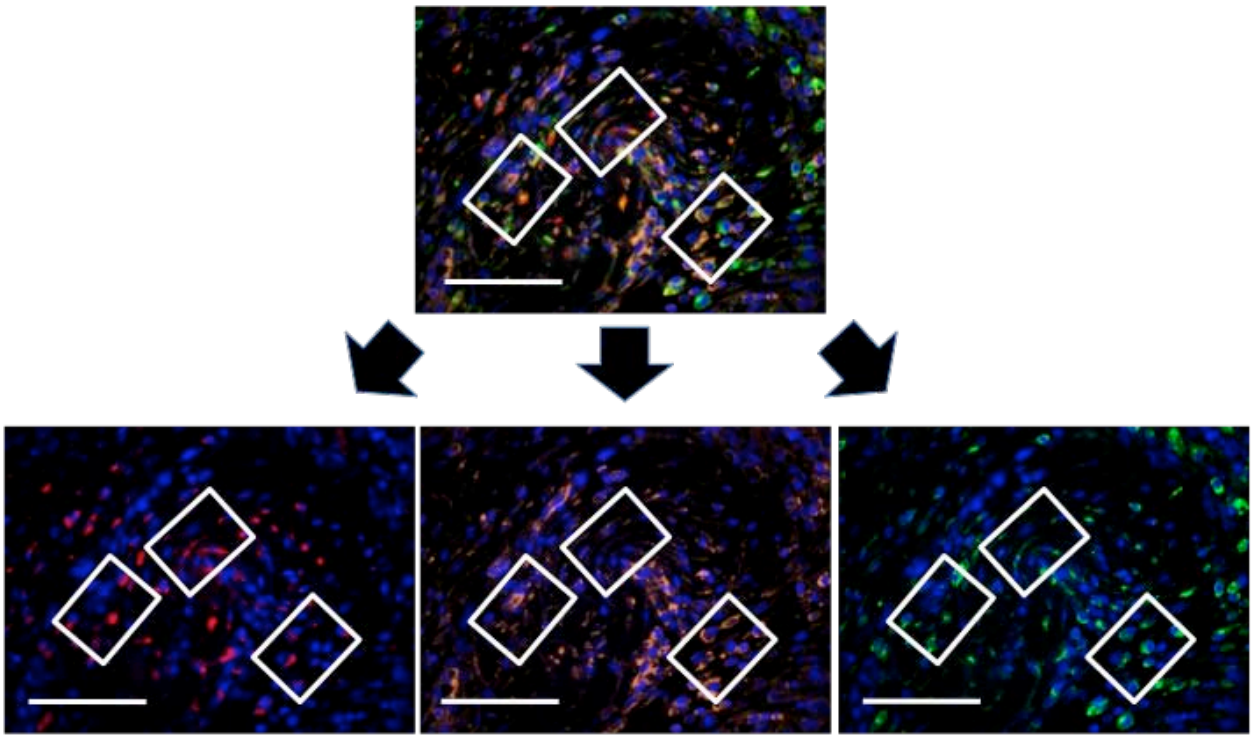

**Figure 36. Example of immunolabeling in UBM at 14 days post-implantation. (A) 40x magnification image of immunolabeling. Red labeling is CD68 (pan-macrophage); orange labeling is CCR7 (M1); green labeling is CD206 (M2); blue labeling is nuclei (DRAQ5). (B) Three areas of 90 μm x 60 μm at the surface of the test article were randomly selected from each high power image. (C, D, E) The number of CD68+ (C), CCR7+ (D), and CD206+ (E) within each box were counted and summed for each image. Reproduced from (100) with permission from Elsevier.**

#### 4.2.1.3 Quantitative Real Time Polymerase Chain Reaction

##### (a) Unilateral Model

Total RNA was isolated from the explanted tissues using TRI-Reagent (Molecular Research Center Inc., Cincinnati, OH) according to the manufacturer's instructions. The isolated RNA was then purified using an RNAeasy Mini Kit (Qiagen, Valencia, CA) and a vacuum

system (Qiagen). cDNA was synthesized from 1 μg of total RNA in a volume of 20 μL using a Superscript RT III kit (Invitrogen, Carlsbad, CA) according to the manufacturer's instructions.

Quantitative real-time PCR was then performed using primers specific for genes known to be strong indicators of either an M1 (inducible nitric oxide synthase, iNOS) or an M2 (arginase, ARG) type macrophage response. Both primers were custom designed using Beacon Designer 7.2 primer design software (PREMIER Biosoft International, Palo Alto, CA) (Table 7). Primers for housekeeping genes were purchased as part of a housekeeping gene primer kit (Rat Housekeeping Gene Primer Set, Real Time Primers, LLC, Elkins Park, PA), and housekeeping gene expression was used to normalize reactions. 1 μL of cDNA was mixed with the appropriate primers and 2X SYBR Green Master Mix (BioRad, Hercules, CA) in a total volume of 25 μL. All reactions were performed in triplicate and were monitored using an iQ5 Real-Time Detection System (BioRad).

Relative expression of the M1 and M2 genes was calculated using the $2^{-(\Delta Ct)}$ method (200, 201). The difference between the value of the threshold cycle for the gene of interest and the value of the threshold cycle for the housekeeping gene ($\Delta C_t$) was calculated for each specimen as follows:

$$\Delta C_{tGOI} = C_{tGOI} - C_{tHSKG}$$

Expression relative to the housekeeping gene was then expressed as $2^{-(\Delta C_t)}$. The relative expression of M1 and M2 genes in each specimen was then compared using the following equation:

$$\frac{2^{-(\Delta C_{tM1})}}{2^{-(\Delta C_{tM2})}}$$

Values were then plotted on a log scale such that values greater than 1.0 represented a predominance of iNOS gene expression and values less than 1.0 represented a predominance of ARG gene expression.

It should be noted that fold expression as compared to native muscle tissue was not calculated for samples harvested in the unilateral model as native tissue was not collected.

**Table 7. Primers used for M1 and M2 gene expression analysis of unilateral body wall samples.**

| Gene | Forward Primer (5' -> 3') | Reverse Primer (5' -> 3') |
|---|---|---|
| iNOS | GAGACGCACAGGCAGAGG | CAGGCACACGCAATGATGG |
| Arginase | CATATCTGCCAAGGACATCG | GGTCTCTTCCATCACTTTGC |

### (b) Bilateral Model

Real time PCR was also performed on the samples from the bilateral defect model. However, for the bilateral defect model an expanded panel of M1 (iNOS, CXCL10, IL1β, IL6, IL12B) and M2 (Arg, IL1r-a, IL-10, E-Cadherin) gene markers was used (Table 8). Primers were designed using Primer-BLAST (NCBI, http://www.ncbi.nlm.nih.gov/tools/primer-blast/) and cDNA was synthesized using an iScript cDNA synthesis kit (BioRad). All other methods remained the same as those described for gene expression analysis in samples harvested from the bilateral defect model in Section 3.2.4.4 above.

**Table 8. Primers used for M1 and M2 gene expression analysis of bilateral body wall samples.**

| Gene | Forward Primer (5' -> 3') | Reverse Primer (5' -> 3') |
|---|---|---|
| M1 Genes | | |
| iNOS | CACCTTGGAGTTCACCCAGT | ACCACTCGTACTTGGGATGC |
| CXCL10 | GCTTATTGAAAGCGGTGAGC | GGGTAAAGGGAGGTGGAGAG |
| IL-1 | GCAGCTATGGCAACTGTCCCTGA | TGGACAGCCCAAGTCAAGGGCT |
| IL-6 | TCTCGAGCCCACCAGGAACGA | AGGGAAGGCAGTGGCTGTCA |
| IL-12 | TGCCATGGTTTTGCTGGTGTCT | AGGGTCACCGTTTCTCCAGGGG |
| M2 Genes | | |
| Arg | AGCGCCTTTCTCTAAGGGAC | ACAGACCGTGGGTTCTTCAC |
| IL1r-a | TCTACCGCCATGGTCTGCTTCC | TCTACCGCCATGGTCTGCTTCC |
| IL-10 | GAGTGAAGACCAGCAAAGGC | TTGTCCAGCTGGTCCTTCTT |
| CDH1 | ACACAGTAGTGCCTGGGCCCTT | CGCAGCTTGCATAGTGGTCCCA |

### 4.2.2 Evaluation of Chemotaxis Towards Macrophage Conditioned Medias

#### 4.2.2.1 RAW 264.7 Mouse Macrophage Culture

RAW 264.7 macrophages were cultivated in Dulbecco's minimal essential medium containing 10% fetal bovine serum and 1% penicillin/streptomycin. Cells were grown at 37$^{o}$C in 5% $CO_2$/95% air, and were split when they were approximately 80% confluent. Macrophages were passaged once following thawing and then allowed to reach 80% confluence. Cells were then removed from the cell culture flask using a rubber cell scraper and re-suspended at a concentration of 1 x $10^6$ cells/mL of cell culture media.

Macrophages were then subjected to one of three well-described polarization protocols as follows prior to being placed into a 6 well cell culture plate at a concentration of 2 x $10^6$ cells/well (2 mL/well). M0 (un-polarized) macrophages were cultured in DMEM with 10% fetal bovine serum. M1 macrophages were cultured in DMEM with 10% fetal bovine serum supplemented with 20 ng/mL IFN-$\gamma$ and 100 ng/mL LPS. M2 macrophages were cultured in DMEM with 10% fetal bovine serum supplemented with 20 ng/mL IL-4. Macrophages were

cultured in polarization media for 24 hours post-plating. Following the 24 hour polarization period, the polarization media was aspirated from all wells and the cells were rinsed once using 37$^{o}$C PBS and once using 37$^{o}$C serum free DMEM. Following rinsing, 2 mL of serum free DMEM was placed in each well and the polarized macrophages were allowed to condition the media for 4, 8, 12, and 24 hours. At each specified time point, the conditioned media was removed from each plate and stored at -80$^{o}$C until use in the Boyden chamber chemotaxis assay described below.

#### 4.2.2.2 Effects of Macrophage Polarization Upon Cell Chemotaxis

##### (a) C2C12 Mouse Myoblast Culture

C2C12 mouse myoblasts were cultivated in Dulbecco's minimal essential medium containing 10% fetal bovine serum and 1% penicillin/streptomycin. Cells were grown at 37$^{o}$C in 5% $CO_2$/95% air, and were harvested for Boyden chamber analysis when they were approximately 80% confluent.

##### (b) MG-71 Pericyte Culture

MG-71 pericytes (217) were cultivated in Dulbecco's minimal essential containing 20% fetal bovine serum and 1% penicillin/streptomycin. Cells were grown at 37$^{o}$C in 5% $CO_2$/95% air, and were harvested for Boyden chamber analysis when they were approximately 80% confluent.

### (c) Boyden Chamber Assay

Migration of C2C12 myoblasts and MG71 pericytes towards macrophage-conditioned medias was investigated using a Boyden chamber assay. C2C12 myoblasts and MG71 pericytes were placed into starvation media (DMEM with 0.5% heat-inactivated fetal calf serum) in a 37$^{o}$C in 5% $CO_2$/95% air incubator for 16 hours prior to use in the Boyden chamber assay. Cells were then trypsinized and re-suspended in serum free media and incubated in a conical tube for 1 hour in suspension in a humidified 95% air/5% $CO_2$ incubator. Polycarbonate chemotaxis filters with a pore size of 8μm were coated with 0.05 mg/mL collagen type I. Macrophage conditioned medias (M0, M1, and M2) as well as positive (media + 10% fetal calf serum) and negative (serum free media) control medias were added to the lower wells of a Neuro Probe 48-well micro chemotaxis chamber. The collagen coated chemotaxis filter was then placed over top of the macrophage conditioned media and 50,000 cells were added to each of the upper wells of the chemotaxis chamber. Cells were then allowed to migrate across the chemotaxis filter for 3 hours in a 37ºC humidified 95% air/5% $CO_2$ incubator. Following the 3 hour migration period, non-migrating cells on the upper side of the filter were removed with a rubber scraper and migrating cells on the underside of the filter were stained with DiffQuick prior to imaging under a bright field microscope. Images of three 20x fields corresponding to the top left, top right, and bottom center side of each well were taken for each well. The number of cells in each image was counted and an average for each well was determined. Each sample was tested in quadruplicate and the mean number of migrated cells for each of the macrophage-conditioned medias was determined. Each experiment was repeated at least twice and the results reported are the combined average for all assays performed.

### 4.2.3 Statistical Methods

A two way analysis of variance (ANOVA) was performed on the immunolabeling quantification data and the gene expression data obtained as part of the unilateral and bilateral defect models to determine statistical significance of the factors of type of scaffold (unilateral: autograft, rat body wall ECM, cUBM, UBM; bilateral: autograft, CDI-UBM, UBM) and the factor of days (unilateral: 3, 7, 14, and 28 days; bilateral:1, 3, 7, 14, and 28 days). For the immunolabeling data, the variables analyzed were the percentage of M1 and M2 cells (unilateral) or the number of M0, M1 and M2 cells (bilateral). For the gene expression data, the variables analyzed were the expressions of the genes listed in Tables 7 (unilateral) and 8 (bilateral). Because the distributions of these variables were strongly skewed, log-transformed values were used for the statistical analysis and results were transformed back to the original scale for presentation. This transformation corresponds to using geometric means in place of arithmetic means. The Tukey multiple comparison procedure was then employed to determine which pairs of levels of factors were significantly different when a main effect was statistically significant. Additional student's t-tests were used to determine whether there were statistically significant differences within scaffold groups which were related to the contralateral implant Results of the Boyden chamber assays were evaluated using a students T-test. A p-value of $p<0.05$ was used to determine statistical significance.

## 4.3 RESULTS

### 4.3.1 Macrophage Response Following Implantation of Extracellular Matrix Scaffolds

#### 4.3.1.1 Immunolabeling

**(a) Unilateral Model**

The results of the immunolabeling evaluation showed that mononuclear macrophages (CD68+) were present in all four of the test article implantation sites at each of the time points investigated throughout the study period.

A quantitative analysis of the phenotype of the macrophages present in the remodeling cellular autograft tissue test article showed that the polarized macrophages (those expressing either CCR7 or CD163) present in the remodeling cellular autograft were predominantly CCR7+ (M1) at 3, 7, 14, and 28 days post implantation (Figure 37A). Conversely, the macrophages present in the remodeling rat body wall ECM test article were predominantly CD163+ (M2) at 3, 7, 14, and 28 days (Figure 37B). The macrophages present in the remodeling cUBM were observed to be predominantly CCR7+ at 3, and 7 days post implantation, with a mixed CCR7+/CD163+ population at 14 days followed by a predominantly CCR7+ population thereafter (Figure 37C). The macrophages present in the UBM were observed to be predominantly CD163+ at 3 days post surgery with a mixed CCR7+/CD163+ thereafter (Figure 37D).

It was observed that the patterns of macrophage polarization were similar for the cellular autograft and cUBM test articles, which elicited a CCR7:CD163 ratio that was skewed towards the CCR7+ phenotype at most of the time points examined during the present study. In contrast,

the acellular test articles elicited a CCR7:CD163 ratio that was skewed towards the CD163+ phenotype at most of the time points throughout the study period. Figure 37 shows the phenotypic profile of the macrophages responding to each test article at each time point as well as the ratio of M1 to M2 cells in each test article.

No significant interactions between scaffold type and time point were found. For percent of M1 cells, both scaffold type and time were statistically significant ($F=2.93$, $P<0.05$ and $F=5.26$, $P<0.003$, respectively). For percent of M2 cells only scaffold type was found to be statistically significant ($F=17.22$, $P<0.0001$). For M1, there was a statistically significant difference between the mean at 7 and 14 days and the mean at 21 days; the mean for acellular body wall was significantly different from the mean for autologous body wall. For M2, all pairs of scaffold type means exhibited statistically significant differences with the exception of cellular UBM versus autologous body wall.

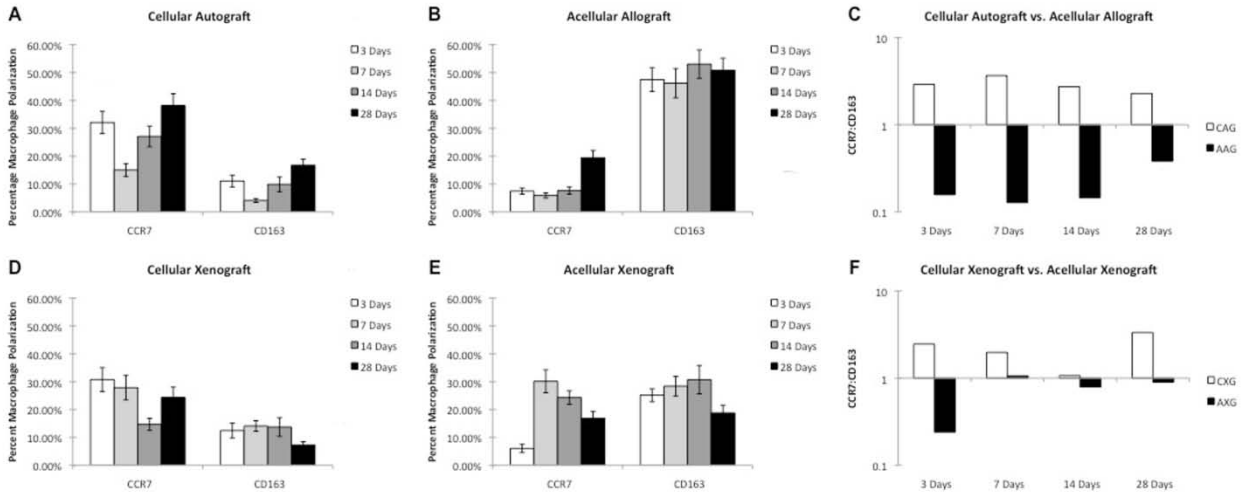


**Figure 37. Percentage macrophage polarization at 3, 7, 14, and 28 days post implantation of cellular autograft (A), rat body wall ECM (B), cUBM (D), or UBM (E). All values are presented as mean ± SEM. For percent of M1 cells, scaffold type and time were statistically significant ($F=2.93$, $P<0.05$ and $F=5.26$, $P<0.003$). For percent of M2 cells, scaffold type was statistically significant ($F=17.22$, $P<0.0001$). Ratio of the percentage of CCR7+:CD163+ macrophages present in the remodeling cellular autograft and rat body wall ECM (C) as well as the remodeling cUBM and UBM (F) at 3, 7, 14, and 28 days post implantation. Values above 1.0 are indicative of an M1 type response while values less than 1.0 are indicative of an M2 type response. Reproduced from (100) with permission from Elsevier.**

### (b) Bilateral Model

As in the unilateral body wall model, immunolabeling showed that there were CD68+ cells present within the sites of remodeling associated with all test articles at all of the time points examined.

Immunofluorescent labeling was used in the bilateral defect study, allowing not only for quantification of the phenotype of the macrophages within the sites of remodeling, but also for the evaluation of the spatial distribution CCR7+ (M1) and CD206+ (M2) macrophages throughout the site of remodeling. Few CD68+ cells were observed in remodeling site associated with any test article at 1 day post-implantation. As was observed in the histologic

assessment in the previous section, the cells present at 1 day post-implantation were predominantly neutrophils. By three days post-implantation, the autologous test article was characterized by a predominance of CCR7+ cells and a smaller number of CD206+ cells throughout the area of the necrotic skeletal muscle (Figure 38a). A similar response was observed at seven days post implantation. By 14 days post-implantation, the number of CCR7+ cells within the site of remodeling was decreased and the number of CD206+ cells had increased from the 7 day time point (Figure 38b). CCR7+ cells were found to be located predominantly within the area of necrosis, with CD206+ cells present within the superficial border of the site of remodeling as well as within the underlying native muscular tissue. By 28 days post-implantation the number of both CCR7+ and CD206+ cells was greatly decreased as compared to other time points (Figure 38c). The CDI-UBM test article was characterized by a strong CCR7+ macrophage response at all time points, especially at the interface between the test article and the host muscular tissue and at the superficial surface of the test article. Few macrophages of either CCR7+ or CD206+ phenotype were send to invade the scaffold material. At 3 days post-implantation, predominantly CCR7+ macrophages were observed within the site of remodeling with few cells interacting with the surface of the material (Figure 38d). A small number of CD206+ cells were observed at the periphery of the site of remodeling and within the native musculature. A similar response was observed at 7 days post-implantation. However, in contrast to day 3, CCR7+ macrophages were observed to be present at the surface of the material. By 14 days a strongly polarized CCR7+ response was observed at the surface of the implanted material (Figure 38e). This response coincided with the start of the foreign body giant cell response observed in the histologic analysis in the previous section. Multinucleate giant cells were observed and stained positive for CCR7+ markers. CD206+ macrophages were

present within the site of remodeling, however were only found at the periphery and within areas encapsulating collagenous tissue deposition. A similar distribution of cells was observed within the site of remodeling at 28 days post-implantation, with fewer CD206+ cells observed within the encapsulating layer (Figure 38f). The UBM test article was characterized by a similar macrophage response as was observed for the CDI-UBM test article at 3 days post-implantation (Figure 38g). By 7 days post-implantation, a mixed population of both CCR7+ and CD206+ cells was seen invading between the layers of the scaffold material and the number of CD206+ cells was higher than at 1 or 3 days. By 14 days, the number of CD206+ macrophages began to decrease. However, both CCR7+ and CD206+ macrophages were observed throughout the scaffold material (Figure 38h). By 28 days, the number of both CCR7+ and CD206+ cells was decreased with a mixed population observed within the middle of the site of remodeling and a predominance of CD206+ macrophages at the interface with the native musculature as well as at the periphery of the remodeling site (Figure 38i). Figure 38 shows the macrophage response to each test articles at early (3 days), middle (14 days), and late stages (28 days) of the remodeling process.

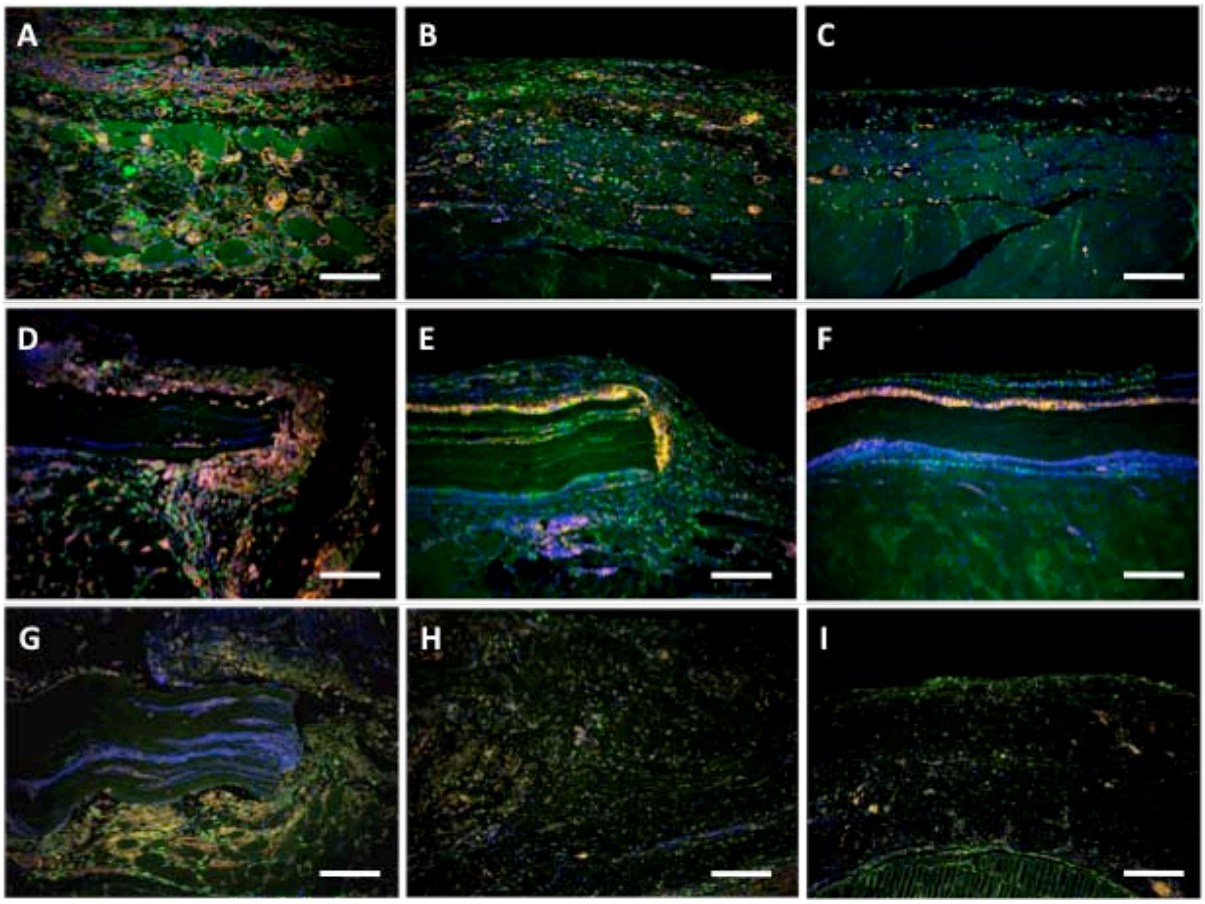


**Figure 38. Immunolabeled images of macrophage response to the autograft tissue test article (A-C), the CDI-UBM test article (D_F) and the UBM test article (G-I). Images shown are from 3 day (A,D,G), 14 day (B,E,H) and 28 day (C,F,I) post-implantation time points. Orange=CCR7 (M1), Green=CD206 (M2), Blue=DRAQ5 (nuclei). Image magnification = 10X, scale bar = 100 μm.**

The number of each type of macrophage observed at the surface of each scaffold material was quantified for each time point and a ratio of CCR7+:CD206+ cells was calculated. Figure 39 shows the counts of the number of macrophages staining positive for each surface marker as well as the CCR7+:CD206+ ratio for each scaffold material. For M0 cells, time was shown to be a statistically significant factor ($F=4.5623$, $p=<0.04$), and significant interactions between time and scaffold material were found ($F=4.5330$, $p<0.02$). Statistically significant differences were observed at the 14 and 28 day time points. For M1 cells, neither scaffold type or time were found to be statistically significant, however statistically significant interactions between

scaffold type and time were found to exist ($F=6.1341$, $p<0.004$). Statistically significant differences between scaffold type were observed at the 28 day time point. For M2 cells, only scaffold type was found to be a statistically significant factor ($F=7.9981$, $p<0.001$). Statistically significant differences between scaffold types were observed at 28 days post-implantation. For M1:M2 ratio, material was found to be a statistically significant factor ($F=13.7723$, $p<0.0001$) and significant interactions were found between scaffold type and time ($F=6.8027$, $p<0.003$). Statistically significant differences in the M1:M2 ratio between scaffold materials was observed at 1, 14, and 28 days post implantation.

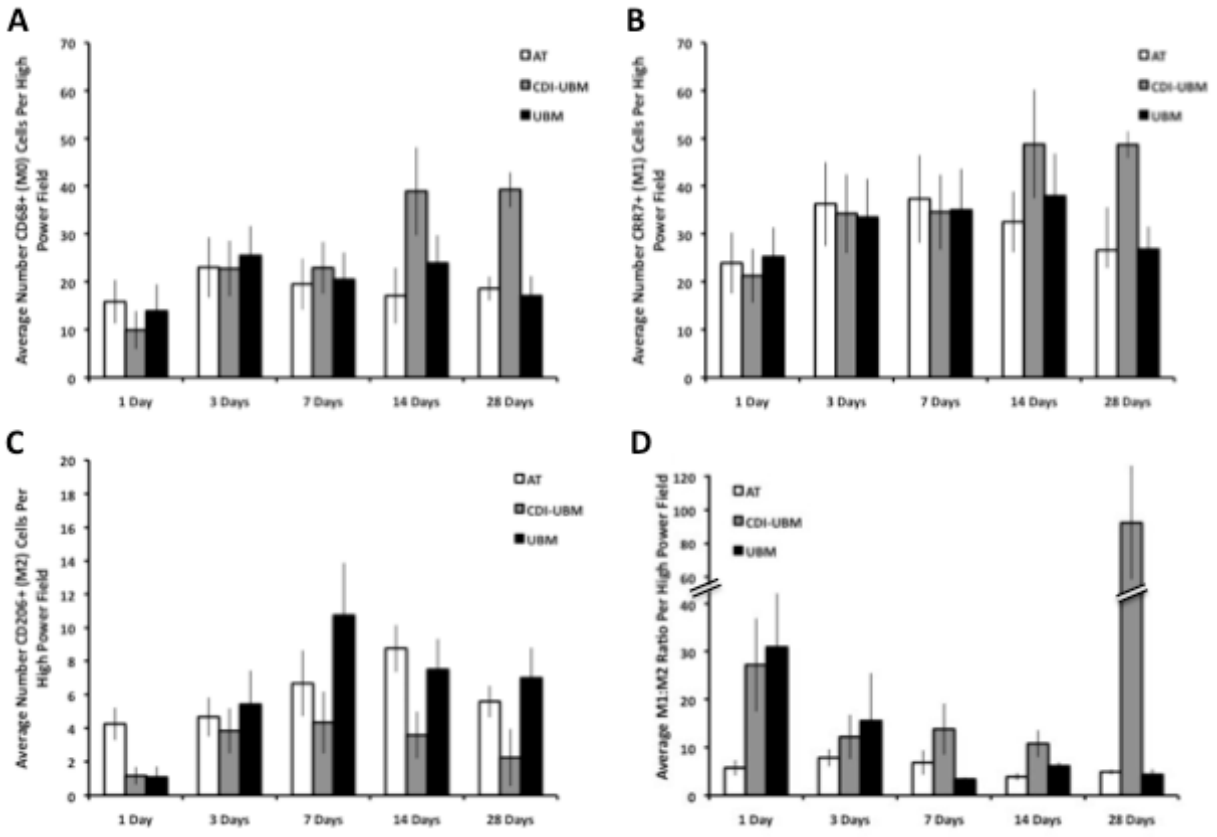


**Figure 39. Average number of CD68+ (pan-macrophage, A) in each 40X field. Time was found to be a significant factor (F=4.5623, p<0.04), and a significant interaction was found between time and scaffold type (F=4.533, p<0.02). Statistically significant differences were observed at 14 and 28 days post-implantation. Average number of CCR7+ (M1, B) cell per 40X field. Significant interactions between time and scaffold were found (F=6.1341, P<0.004). Statistically significant differences were observed at 28 days. Average number of CD206+ (M2, C) cells in each 40x field. Scaffold type was found to be a significant factor (F=7.9981, p<0.001). Statistically significant differences were observed at 28 days. Average ratio of M1 to M2 cells present within each 40x field (D). Both scaffold type was found to be statistically significant factor (F= 13.7723, P<0.0001) and significant interactions between time and material were observed (F=13.7723, p<0.003). Statistically significant differences between test articles were observed at 1, 14, and 28 days. All data is presented as mean ± SEM. White bar is autologous tissue, grey bar is CDI-UBM, black bar is UBM.**

#### 4.3.1.2 Gene Expression

##### (a) Unilateral Model

Varying levels of iNOS (M1) and ARG (M2) gene expression were observed in all test articles throughout the course of the study. However, expression levels in the cellular test articles were higher than expression levels in the acellular test articles for both of the genes examined at all time points with the exception of the 3 day time point in the rat body wall ECM test article. The fold difference in gene expression between the cellular and acellular scaffolds ranged from 5.45 to 1904.91 depending on the time point and gene. Interestingly, it was observed that the fold increase in iNOS expression was larger than the fold increase in ARG expression in the cellular test articles at all time points.

The expression of iNOS versus ARG was also compared in each individual test article. There was a mix of iNOS and ARG gene expression in the cellular autograft group, with a ratio of iNOS:ARG that was skewed towards iNOS expression at all time points with the exception of 14 days (Figure 40A). A mix of iNOS and ARG gene expression was also observed in the acellular allograft test article group (Figure 40B). However, in the rat body wall ECM group the ratio of iNOS:ARG was skewed towards ARG gene expression at all time points (Figure 40C). Similarly, the cUBM group exhibited mixed iNOS and ARG gene expression with a skewing of the iNOS:ARG ratio towards iNOS expression at 3, 7, and 14 days post surgery changing to ARG gene expression at day 28 while the UBM group exhibited a iNOS:ARG ratio that was skewed towards ARG gene expression at all of the time points investigated (Figure 40D, 40E, 40F).

The gene expression profiles in both of the acellular test articles were similar with an increasing predominance of ARG expression from 3 to 14 days and a slight decrease at 28 days.

Conversely, in the cellular test articles, the gene expression ratio was skewed towards the expression of CCR7 at most of the time points investigated in this study. Figure 40 shows the gene expression levels as well as the iNOS:ARG expression ratio in each of the test articles.

No significant interactions between scaffold type and time point were found. For M1 gene expression, both scaffold type and time were statistically significant ($F=2.98$, $P=<0.05$ and $F=21.11$, $P=<0.0001$, respectively). For M2 gene expression, only scaffold type was found to be statistically significant ($F=44.33$, $P<0.0001$). For M1, expression was found to be significantly higher at 28 days than at 3 days. For both iNOS and ARG, the expression in the cellular test articles was significantly higher than in the acellular test articles.

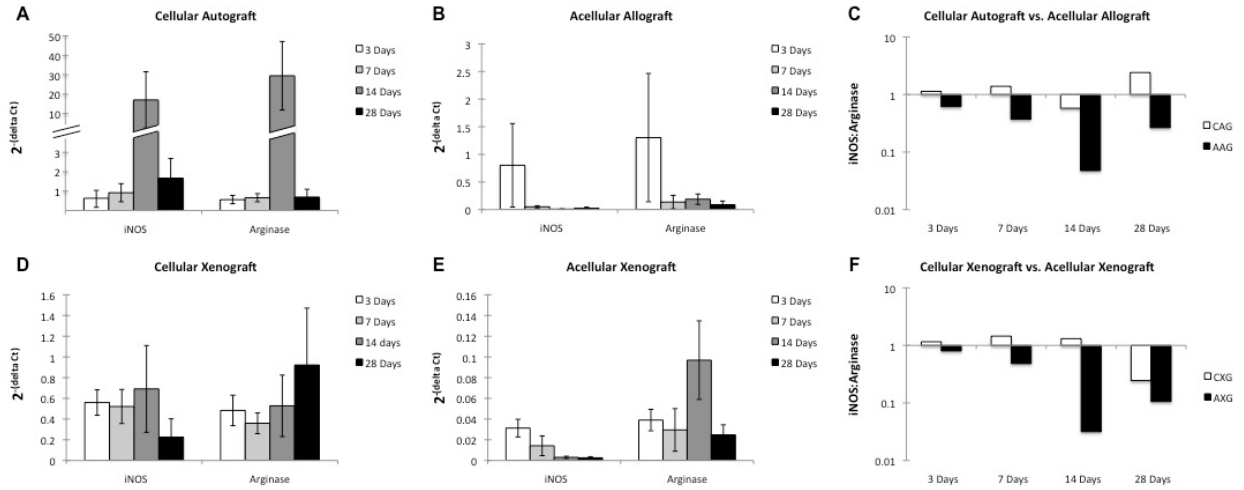


**Figure 40. Gene expression relative to housekeeping gene at 3, 7, 14, and 28 days post implantation of cellular autograft (A), rat body wall ECM (B), cUBM (D), UBM (E). All values are presented as mean ± SEM. For iNOS expression, scaffold type and time were statistically significant ($F=21.11$, $P<0.0001$ and $F=2.98$, $P<0.05$). For arginase expression, scaffold type was statistically significant ($F=44.33$, $P<0.0001$). Ratio of iNOS:arginase expression in the remodeling cellular autograft and rat body wall ECM (C) as well as the remodeling cUBM and UBM (F) at 3, 7, 14, and 28 days post implantation. Values above 1.0 are indicative of a predominance of iNOS expression while values less than 1.0 are indicative of a predominance of arginase expression. Reproduced from (100) with permission from Elsevier.**

**(b) Bilateral Model**

Varying levels were observed for both the M1 (iNOS, CXCL10, IL1β, IL6 and IL12) and M2 (ARG, IL1receptor antagonist, IL10, and E-Cadherin) genes examined in this study. iNOS levels were observed to be greatly increased as compared to native tissue at the one day time point, especially in the CDI-UBM test article. Levels were also observed to be elevated to a lesser degree in the UBM test article. Expression of iNOS decreased at 3 and 7 days, but remained elevated as compared to native tissue. At 14 days the expression of iNOS was shown to increase in the autologous tissue test article, but not in the CDI-UBM or UBM test articles. By 28 days, iNOS expression remained elevated in the CDI-UBM and UBM test articles, but expression in the autologous tissue test article had dropped below the level observed for native tissues. Time was found to be a significant factor in iNOS expression ($F=14.751$, $p<0.0005$), and no interactions were found between scaffold type and time. Statistically significant differences in expression between test articles were found at 1 and 7 days post-implantation.

CXCL10 Expression was shown to increase from one to three days in all test articles examined. Levels in UBM and AT test articles continued to increase until 7 days and decrease at 14 days; however, levels in the CDI-UBM test article decreased steadily from 3 to 14 days. At 14 days expression in all test articles was similar, but elevated as compared to native tissue. Increased expression was seen for the UBM and CDI-UBM test articles, however a slight decrease was observed for the autologous tissue test article. Time was found to be a statistically significant factor ($F=4.6570$, $p<0.04$), and no interactions between scaffold type and time were found. No statistically significant differences in CXCL10 expression between scaffold types were observed at any time point.

IL1β expression showed the largest number of statistically significant differences of any of the M1 genes investigated. At 1 day, increased expression was observed in the CDI-UBM test article and UBM test article as compared to the autologous tissue test article, which while elevated as compared to native tissue, remained relatively steady throughout. Expression in the UBM test article was found to be slightly higher than was observed for the autologous tissue or CDI-UBM test articles at 3 days post implantation. Expression in all samples was seen to remain relatively steady thereafter. Material was found to be a statistically significant factor ($F=3.4206$, $p<0.05$). Statistically significant differences in expression between test articles was observed at 1 and 3 days post-implantation.

IL6 expression was slightly elevated in all samples as compared to native tissue. Expression remained relatively steady with the exception of an increase in expression in the UBM test article at 3 days post-implantation. Neither time nor scaffold type were found to be significant factors and no interactions between scaffold type and time were found.

IL12 expression was elevated in all test articles as compared to native tissue throughout the study period. Expression was increased in all test articles at the 7 day time point, however the results were not statistically significant. Levels were seen to decrease thereafter, with the exception of a small increase in expression in the UBM test article at 28 days. Neither time nor scaffold type were found to be significant factors and no interactions between scaffold type and time were found.

As with MMP expression in Aim 2, small differences were observed within groups for implantation with a different contralateral material. However, again as in Aim 2, these instances were few and did not occur in any discernable pattern. Figure 41 shows M1 gene expression for each scaffold type at each of the time points investigated in the study.

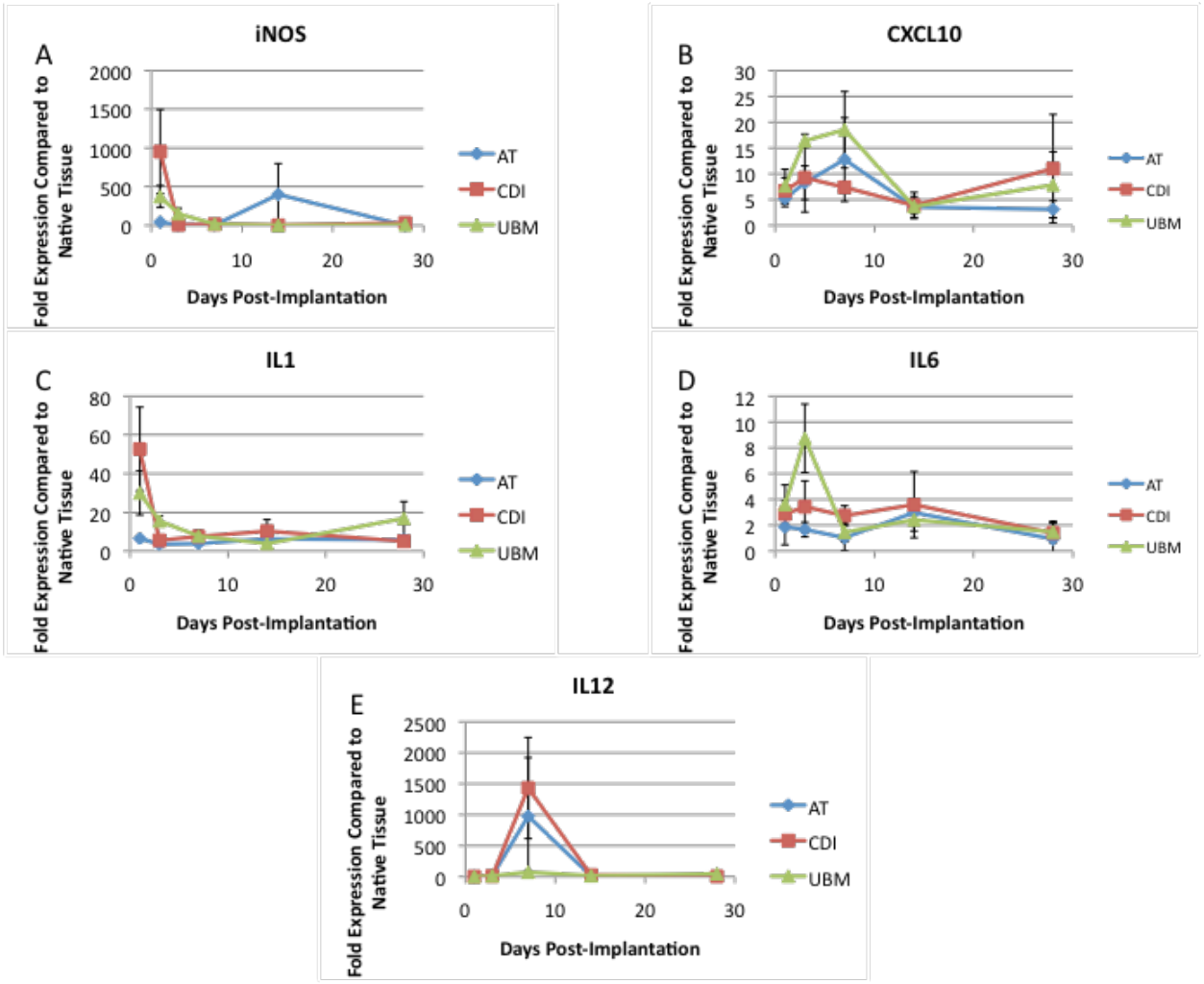


**Figure 41. M1 gene expression. (A) Expression of iNOS. Time was found to be a significant factor ($F=14.751$, $p<0.0005$). Significant differences between scaffold materials were observed at 1 and 3 days. (B) Expression of CXCL10. Time was found to be a significant factor ($F=4.6570$, $p<0.04$). Significant differences between scaffold materials were not observed at any time point. (C) Expression of IL1β. Scaffold material was found to be a significant factor ($F=3.4206$, $p<0.05$). Significant differences between scaffold materials were observed at 1 and 3 days. (D) Expression of IL6. Neither scaffold material or time was found to be a significant factor. Significant differences between scaffold materials were not observed. (E) Expression of IL12. Neither scaffold material or time was found to be a significant factor. Significant differences between scaffold materials were not observed.**

ARG levels were observed to be greatly increased as compared to native tissue at the one day time point, especially in the CDI-UBM and UBM test articles. Levels were also observed to be elevated to a lesser degree in the autograft test article. Expression of ARG decreased at 3 and 7 days, but remained elevated as compared to native tissue. At 14 days the expression of ARG was to be similar for all test articles. At 28 days, ARG expression in the CDI and UBM test articles was seen to increase, but expression in the autologous tissue test article remained at similar levels to those observed at earlier time points. Both time and material were found to be a significant factors in ARG expression ($F=10.9215$, $p<0.002$ and $F=4.0982$, $p<0.03$, respectively), and no interactions were found between scaffold type and time. Statistically significant differences in expression between test articles were found at 1, 3 and 7 days post-implantation.

IL1ra expression showed the largest number of statistically significant differences of any of the M2 genes investigated. At 1 day, increased expression was observed in the CDI-UBM test article and UBM test article as compared to the autologous tissue test article, which while elevated as compared to native tissue, remained relatively steady throughout. By 3 days expression in the CDI-UBM test article were seen to drop to levels similar to those observed for autologous tissue. CDI-UBM did not increase significantly thereafter. UBM test articles showed a more gradual decrease from 1 to 14 days, and an increase at 28 days. Both material and time were found to be a statistically significant factors ($F=11.8361$, $p<0.0001$ and $F=8.3442$, $P<0.006$, respectively). Statistically significant differences in expression between test articles was observed at 1, 3, 7 and 14 days post-implantation.

IL10 expression was elevated in all samples as compared to native tissue from one to 14 days post-implantation. Expression was then observed to increase at 28 days for the UBM and CDI-UBM test articles with a greater increase in the UBM test article. Neither time nor scaffold

type were found to be significant factors and no interactions between scaffold type and time were found.

E-Cadherin expression was elevated in all test articles as compared to native tissue throughout the study period. Expression was increased in all test articles at the 3 day time point, however the results were not statistically significant. Levels were seen to decrease at 7 days, and then increase at 14 days. Levels were decreased at 28 days, however were still elevated as compared to native tissues. Neither time nor scaffold type were found to be significant factors and no interactions between scaffold type and time were found.

Again, small differences were observed within groups for implantation with a different contralateral material. However, again, these instances were few and did not occur in any discernable pattern. Figure 42 shows M2 gene expression for each scaffold type at each of the time points investigated in the study.

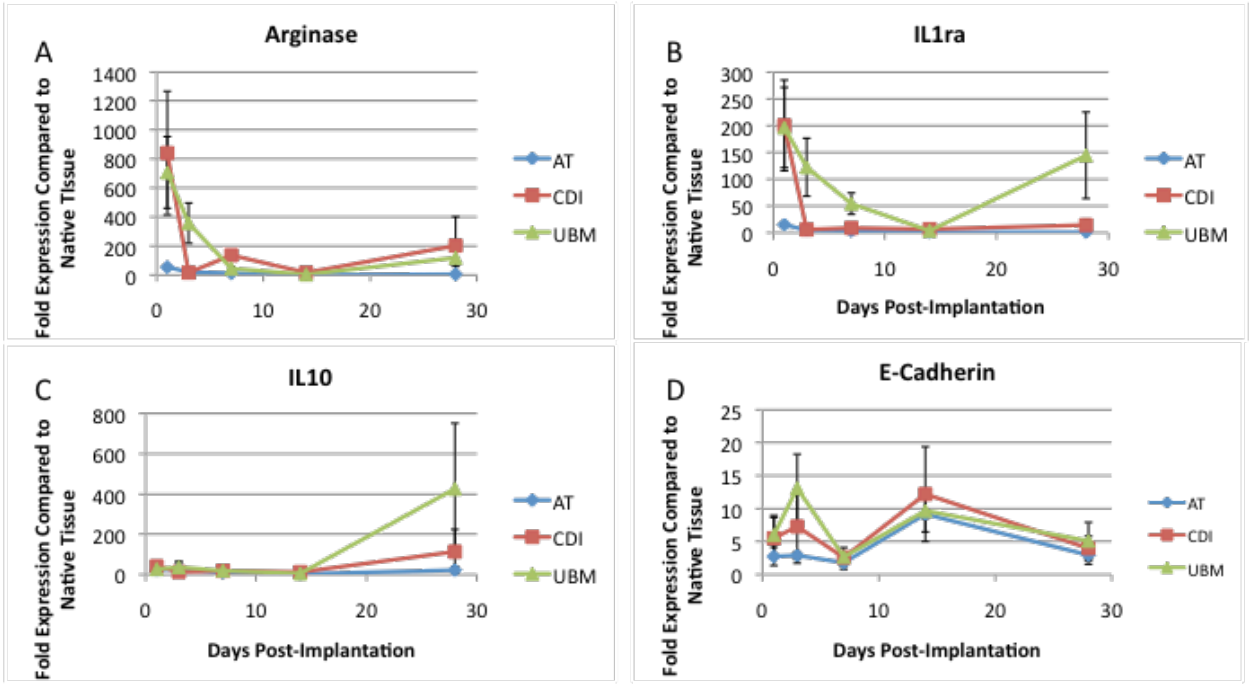


**Figure 42. M2 gene expression. (A) Expression of ARG. . Both time and material were found to be a significant factors in ARG expression (F=10.9215, p<0.002 and F=4.0982, p<0.03, respectively), and no interactions were found between scaffold type and time. Statistically significant differences in expression between test articles were found at 1, 3 and 7 days post-implantation. (B) Expression of IL1ra. Both material and time were found to be a statistically significant factors (F=11.8361, p<0.0001 and F=8.3442, P<0.006, respectively). Statistically significant differences in expression between test articles was observed at 1, 3, 7 and 14 days post-implantation. (C) Expression of IL10. Neither time nor scaffold type were found to be significant factors and no interactions between scaffold type and time were found. (D) Expression of E-Cadherin. Neither scaffold material or time was found to be a significant factor. Significant differences between scaffold materials were not observed.**

### 4.3.2 *In Vitro* Effects of Macrophage Phenotype Upon Cell Chemotaxis

#### 4.3.2.1 C2C12 Myoblasts

The number of myoblasts which migrated in the Boyden chamber assay were quantified for medias conditioned by M0, M1 and M2 macrophages at varying time points (4, 8, 12, and 24

hours). Results showed that myoblast migration which was similar for media from cultures of all macrophage types harvested at 4 hours. Results from medias harvested at 8, 12, and 24 hours show that both M0 and M2 conditioned medias caused greater myoblast migration than did M1 conditioned media. However, all media types were observed to cause migration which was greater than or equal to that of the positive control at 8 hours. M1 conditioned media caused migration which was less than the positive control at 12 and 24 hours. The greatest migration response was seen in 8 hour conditioned medias from M0 and M2 cells. No significant differences were found between M0 and M2 conditioned medias at any time point. Statistically significant differences were found for the M0 and M2 groups as compared to the M1 medias harvested at 8, 12, and 24 hours.

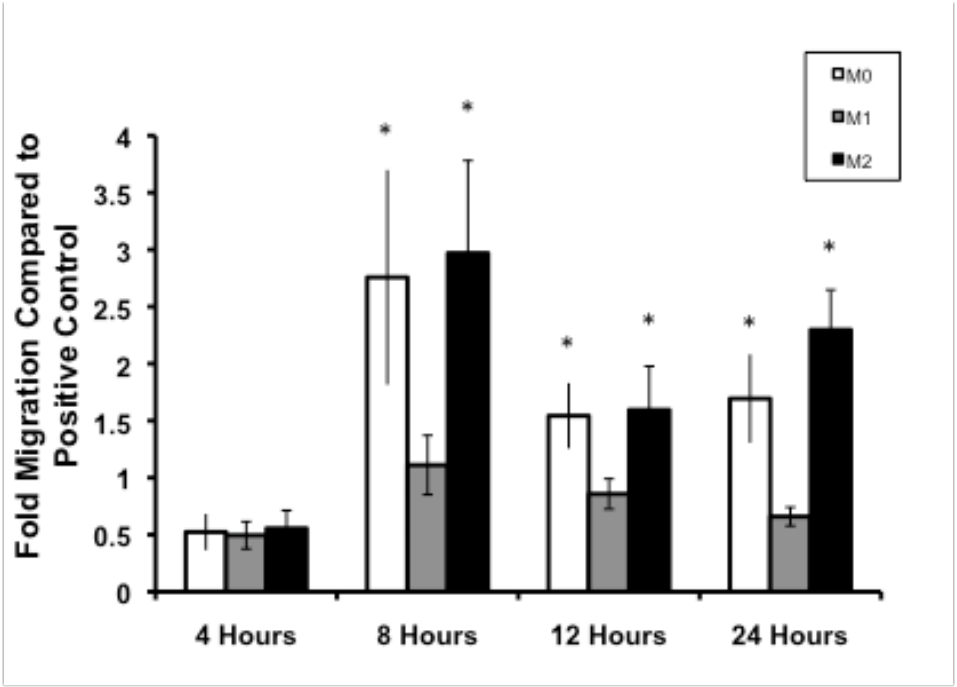


**Figure 43. C2C12 myoblast migration towards culture supernatants from M0, M1, and M2 macrophages at 4, 8, 12, and 24 hours post-implantation. White bar represents M0 supernatants, grey bar represents M1 supernatants, and black bar represents M2 supernatants. * denotes statistical significance, $p<0.05$.**

#### 4.3.2.2 MG-71 Pericytes

Similar to the results obtained for C2C12 cells, no differences in pericyte migration were observed at the 4 hour time point for any of the conditioned medias. At 8 hours it was shown that both M0 and M2 cells caused migration of pericytes which was statistically greater than was observed for M1 cells. A similar result was seen for media conditioned for 12 or 24 hours. The greatest pericyte migration response for any of the conditioned medias was observed for medias which were conditioned for 24 hours. M2 conditioned media was observed to cause statistically greater migration of pericytes than was M0 conditioned media when harvested at 8, 12, and 24 hours.

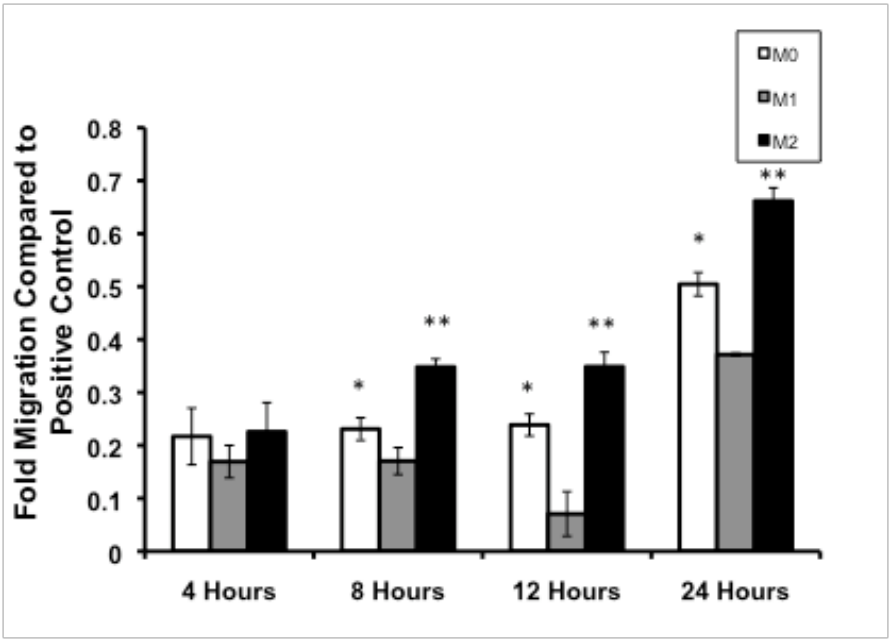


**Figure 44. MG-71 pericyte migration towards culture supernatants from M0, M1, and M2 macrophages at 4, 8, 12, and 24 hours post-implantation. White bar represents M0 supernatants, grey bar represents M1 supernatants, and black bar represents M2 supernatants. * denotes statistical significance as compared to M0, $p<0.05$. ** denotes statistical significance as compared to both M0 and M1, $p<0.05$.**

## 4.4 DISCUSSION

The present study examined the effects of the presence of a cellular component within a scaffold derived from extracellular matrix or chemical crosslinking used in its production upon the polarization of the macrophages participating in the host response following implantation. The study also examined the relationship between macrophage polarization and the host tissue remodeling events until 28 days post-implantation. The results of the study indicate that the presence of a cellular component or the use of chemical crosslinking shifts the macrophage polarization profile towards a more M1, pro-inflammatory phenotype and is associated with a more pro-inflammatory gene expression profile. Further, the results of this study suggest that macrophage polarization is indeed linked to tissue remodeling following implantation of a biologic scaffold.

The mechanisms by which mammals respond to whole organ transplantation are reasonably well understood. Immune recognition of xenogeneic and allogeneic cellular antigens occurs followed by the production of pro-inflammatory mediators, cytotoxcicity, and resultant organ rejection. The mechanisms of the host immune response to acellular biologic scaffolds composed of ECM, either allogeneic or xenogeneic, are neither as well studied nor as well understood. The preparation of an ECM scaffold for regenerative medicine applications involves decellularization of the tissue or organ from which the ECM is harvested (67). The removal of cellular components produces a markedly different type of 'tissue graft' than is typically presented with autogenous, allogenous, or xenogeneic whole organ grafts.

An ECM scaffold consists primarily of the ECM constituent molecules, many of which are known to be highly conserved across species, thus mitigating many of the adverse components of the immune response (7, 86). Studies have shown, however, shown that both

DNA fragments and, in the case of porcine derived ECM scaffolds, Galactosyl-α(1,3)galactose (Gal) epitope are present within ECM scaffolds following the decellularization process (95, 198). The amount of Gal epitope (a molecule known to cause hyper acute rejection in xenotransplants (218, 219)) present within porcine derived ECM scaffolds was found to be insufficient to cause the activation of complement in human plasma (198). Furthermore, despite the presence of these cellular components, many of which are well known for their ability to initiate a host inflammatory/immune response, ECM scaffolds have been shown to elicit constructive tissue remodeling. The decellularization methods used to process ECM scaffolds may alter these molecules such that they can no longer negatively influence the host response or there may be a threshold amount required to alter the host response to an ECM scaffold.

As was shown in Aim 2, and as has been shown elsewhere, the host response following the implantation of an ECM scaffold that has not been chemically cross-linked or seeded with cells is characterized by an immediate and intense neutrophil and mononuclear cell infiltration followed by a shift to primarily mononuclear cells within 72 hours (69, 82). Rapid degradation of the ECM scaffold is followed by replacement with organized, site appropriate functional host tissue (69, 82, 98). Interestingly, although the host response involves a large infiltration of mononuclear cells, an event conventionally associated with inflammation, there is a lack of the usual cytotoxic mediators of inflammation and graft rejection, with resultant formation of a polarized type 2 T lymphocyte (Th2) response (86).

A number of studies have shown differences and, in some cases, improvements in tissue remodeling outcomes when a cellular component has been placed in contact with an ECM scaffolds during or prior to implantation (27, 31, 39). However, the effect of these cells upon the resultant host response remains an open question. A recent study investigated differences in

remodeling of ECM based bioscaffolds with and without cells in a primate model, finding that the presence of cellular content was associated with increased levels of pro-inflammatory cytokines, increased macrophage activation, and a poor remodeling outcome (220). In the present study, it was observed that the presence of a cellular component, either xenogeneic or autologous, altered the host response toward an M1 phenotype compared to the phenotype that was observed with an acellular ECM scaffold alone.

The previous studies, and those published elsewhere, have demonstrated that there were temporal and spatial distribution differences in the neutrophil and mononuclear cell populations that participate in the host response to an implanted ECM scaffold depending on the origin of the ECM as well as the methods used to process the scaffold, and that these differences were related to the downstream tissue remodeling outcome (69). Further investigation these same scaffold materials in the present studies showed that test articles which were chemically cross-linked did not show any significant degradation during the study period following implantation, resulted in a more M1 type macrophage response, and resulted in a host response that was characterized by chronic inflammation. Conversely, non-cross-linked test articles degraded rapidly following implantation, elicited a more M2 type response, and resulted in constructive tissue remodeling of the abdominal wall including organized collagenous connective tissue, islands of skeletal muscle, and blood vessels (96). It is clear from these studies that the phenotype of mononuclear macrophages that participate in the host response to implanted biologic scaffold materials plays an important role in determining the extent of a constructive tissue remodeling outcome versus destructive, scar tissue outcome.

In vitro work performed in the present studies showed that the culture supernatants from all macrophage populations (M0, M1, and M2) were capable of promoting the chemotaxis of

progenitor cell populations (C2C12 and MG-71 pericytes). However, the degree of chemotaxis was shown to differ depending on the cell population investigated. In general, M0 and M2 macrophages were shown to promote greater chemotaxis than did M1 cells. These results parallel those shown in another study which investigated the ability of M1 and M2 macrophages to recruit a mesangioblast population (221). The study showed that the mechanism of chemotaxis was different for M1 and M2 cells. The effects of M0, M1, and M2 effector molecules upon the phenotype and survival of the recruited progenitor cell populations in the long term remains unclear.

## 4.5 CONCLUSIONS

The present study showed that the presence of a cellular component within an extracellular matrix scaffold or the use of chemical cross-liking in scaffold production modulates the phenotype of the macrophages participating in the host response following implantation. It was observed that those test articles that contained a cellular component, even an autologous cellular component, elicited a more M1 type macrophage response and resulted in the deposition of dense connective tissue and/or scarring. A distinct macrophage response was elicited by those test articles which were chemically cross-linked; however, chemical cross-linking was also shown to result in a more M1 (or less M2) type macrophage response. Those test articles that did not contain a cellular component and were not chemically cross-linked, however, were observed to elicit a more M2 type macrophage response and resulted in a more constructive type remodeling response. It was also observed that the macrophage response to one test article did not appear to affect the macrophage response to a second material implanted concurrently within

the same animal. Lastly, in vitro results suggest that M0, M1, and M2 macrophages have distinct paracrine effects upon other cell populations, in this case the chemotaxis of progenitor cell populations, further suggesting distinct roles for macrophage subpopulations in tissue remodeling.

## 4.6 LIMITATIONS AND FUTURE DIRECTIONS

There were several limitations in the present study. A limited number of surface markers were utilized for the characterization of the M1/M2 profile of the macrophages participating in the host response. The choice of markers was mainly due to the limited availability of antibodies specific for M1 and M2 markers in the rat model. It is also recognized that species variations do exist. The markers chosen for this study are known to be highly indicative of M1 or M2 polarization in multiple animal and human models. Multiple studies have shown that CCR7 is highly expressed on M1 polarized cells and that CD163 and CD206 are highly indicative of M2 type anti-inflammatory polarization (141, 222). A limited number of gene expression markers were also used in this study. However, iNOS and arginase expression, used in the unilateral and bilateral studies, are widely viewed as markers of M1 and M2 polarization, respectively. In the bilateral study an expanded set of markers were examined however, the greatest statistically significant differences were observed for IL1β and IL1ra. Additional studies exploring the ways in which ECM scaffolds are capable of modulating the IL1 expression pathway may yield insights into the role of M1 and M2 macrophages in the response to ECM scaffold materials and the ability of ECM scaffolds to promote constructive tissue remodeling.

In the present study, a population of CD68+ macrophages was observed within the wound site, some of which did not stain positive for either M1 or M2 surface markers. These cells may have only just arrived at the site of remodeling and, thus, might not yet have been stimulated to undergo activation or polarization towards an M1 or M2 phenotype. Macrophages that have not yet been polarized towards an M1 or M2 phenotype would not express markers indicative of polarization. Therefore, it is logical to expect that the percentages of CCR7+ and CD163+ cells would not sum to 100%. Perhaps more importantly, it is presently not known what percentage of M1 or M2 cells is required to influence the formation of a scar tissue or constructive tissue remodeling response, respectively (i.e. a threshold effect). It is hypothesized that the ratio of M1:M2 cells may be more important than the absolute number of cells. There is clearly a correlation of the M1:M2 ratio to remodeling outcome in the present study.

Similarly, in the bilateral body wall study, cells expressing various combinations of CD68, CCR7 and CD206 were observed, but not quantified. It is possible that a percentage of the macrophages participating in the host response to ECM scaffolds may not express a fully polarized M1 or M2 phenotype. A recent study showed that cells within the site of ECM mediated tissue remodeling expressed both macrophage and primitive stem cell markers and could be differentiated along all three lineages, suggesting a potentially unique role for macrophages in ECM scaffold remodeling (223). Other studies have shown that myeloid to mesenchymal transition is possible for cells responding to an implanted material, again suggesting potentially unrecognized roles for macrophages in tissue remodeling (224). Additional studies to determine the exact phenotype of the cells observed within sites of ECM mediated remodeling are warranted and will provide additional information on the mechanisms by which ECM scaffolds are capable of promoting constructive tissue remodeling.

In vitro studies showed that M0, M1, and M2 macrophages were capable of causing the chemotaxis of progenitor cell populations. While the recruitment of muscle and vascular progenitor cells to sites of ECM remodeling have been shown in previous studies (225), the role of macrophages in promoting the observed recruitment of progenitor cells in vivo is not yet clear. Additional studies are needed to determine if in vivo macrophage populations possess the same ability as were observed in the present in vitro study. Additionally, the effects of M0, M1, and M2 macrophage populations upon the phenotype and survival of recruited cells has not yet been described.

# 5.0 DISSERTATION SYNOPSIS

The work presented in this dissertation examined the effects of the tissue source and methods used to produce extracellular matrix (ECM) scaffold materials upon the structural and compositional characteristics of the resultant scaffold, the effects of these characteristics upon the ability of the material to support and modulate cell growth *in vitro* as well as to act as an inductive template for the formation of functional site-specific host tissues *in vivo,* and the role of macrophages in determining the ability of an ECM based scaffold material to promote the observed "constructive tissue remodeling" outcome. The major findings for each specific aim are outlined below.

## 5.1 MAJOR FINDINGS

The major findings of the present work were:

**Specific Aim 1:** To determine the effects of tissue source and chemical cross-linking upon the structure and composition of ECM scaffold materials, and to show that these characteristics have effects upon patterns of cell behavior *in vitro*.

- ECM scaffolds derived from each tissue or organ possess a distinct surface ultrastructure and chemical composition
- Certain ECM scaffolds possess a distinct “sidedness” which is related to the function of the tissue or organ of interest
- Chemical crosslinking changes the ultrastructure and chemical composition of the surface of ECM scaffolds
- Differences in the surface characteristics of ECM scaffolds derived from different tissues and organs, or associated with scaffold sidedness, have distinct effects upon the behavior of cells *in vitro*
- ToF-SIMS is a highly sensitive method for the detection and differentiation of the molecular composition of the outermost surface of an ECM scaffold

**Specific Aim 2:** To determine the effects of the presence of a cellular component within an extracellular matrix scaffold and the use of carbodiimide during scaffold production upon the capacity of extracellular matrix scaffolds to elicit a constructive tissue remodeling versus encapsulation or scar tissue type remodeling response in model of rat abdominal wall musculature reconstruction.

**Sub-Aim:** To determine whether the host remodeling response to one ECM scaffold material affects the outcome of the host remodeling response to a second material implanted concurrently in the same animal.

- ECM scaffolds were capable of facilitating constructive tissue remodeling in a model of rat abdominal wall musculature reconstruction

- The presence of a cellular component, even an autologous cellular component, within an extracellular matrix scaffold affects the ability of the scaffold material to facilitate constructive tissue remodeling following implantation
- Chemical crosslinking with carbodiimide affected the ability of an ECM scaffold to facilitate constructive tissue remodeling following implantation
- The host response to one implanted ECM scaffold material did not appear to affect the host response to a second ECM scaffold material implanted in the same animal

**Specific Aim 3:** To show that extracellular matrix scaffolds are capable of altering the default host macrophage response following implantation, and that the modulation of the host macrophage response is related to the ability of the scaffold to promote the constructive versus encapsulation or scar tissue type remodeling responses observed in **Aim 2.**

**Sub-Aim:** To evaluate the effects of polarized macrophages upon the *in vitro* behavior of other cell types.

- Acellular, non-crosslinked ECM scaffolds alter the default host macrophage response following tissue injury
- Macrophage phenotype is related to tissue remodeling outcome
- The ability to modulate the host macrophage response was changed when cells were present or when the scaffold was crosslinked with carbodiimide
- The macrophage response to individual test articles was not observed to affect (or be affected by) the response to other test articles implanted in the same animal

- Macrophage polarization may have an effect upon the tissue remodeling outcome through the induction, or inhibition of chemotaxis

## 5.2 CONCLUSIONS

The work contained within this dissertation describes the effects of tissue source and production methods upon the characteristics of the resulting ECM scaffold material. These characteristics were shown to have distinct effects upon patterns of cell growth *in vitro* as well as the ability of the scaffold material to function *in vivo*. It is clear that an in-depth understanding of the ways in which scaffold characteristics affect the behavior of cells both *in vitro* and *in vivo* is required for the design and production of ECM scaffold materials to be used in the reconstruction of complex three-dimensional tissues and organs. It is also clear that scaffold characteristics have an impact upon the host response elicited by the material following *in vivo* placement. In particular, the phenotype of the macrophages which responds to implanted scaffold materials has been shown to play an important role in determining whether the interaction of the host with the implanted material results in encapsulation, scar tissue formation, or constructive tissue remodeling. A better understanding of the mechanisms which underlie the macrophage behaviors observed in the present work will lead to the design of new biomaterials and strategies for the inductive reconstruction of complex tissues and organs.

# APPENDIX A

# SITE SPECIFIC CONSTRUCTIVE TISSUE REMODELING OF AN EXTRACELLULAR MATRIX SCAFFOLD IN A MODEL OF CANINE TEMPOROMANDIBULAR JOINT MENISCUS RECONSTRUCTION

## A.1 BACKGROUND

Temporomandibular joint (TMJ) disorders (TMD) are a common problem, which affects women up to 9 times more often than men, and usually involves a spatial dislocation and/or a structural defect of the enclosed cartilaginous meniscus (226-229). A variety of procedures, including minimally invasive surgical techniques, have been used to treat TMD. However, meniscectomy is often indicated when the TMJ meniscus is irreparably damaged or if the meniscus prohibits the fluid, smooth movement of the condyle (230-237). Complications arising from meniscectomy without replacement can include articular surface defects, heterotopic bone formation, and joint ankylosis.

The rationale for replacing damaged TMJ menisci with substitute materials is to protect the articular surfaces from degenerative changes and to avoid joint adhesion formation. Alloplastic materials such as Silastic, silicone and Proplast-Teflon, have been used to replace the TMJ meniscus following meniscectomy, but results have been less than satisfactory (238-240).

In some cases, joint pathology has been found to be severe following the placement of such devices. Autograft tissues have been used both as meniscus replacement materials following meniscectomy and as interpositional materials in the treatment of joint ankylosis. Autologous tissue sources such as the temporalis muscle flap, auricular cartilage and dermis have proven to be better options than their alloplastic counterparts. However, the morbidity associated with the graft donor site remains an obvious disadvantage of these options(241-245). Furthermore, fibrosis, or in the case of the temporalis muscle flap, devitalization and necrosis, of autologous tissue grafts has been observed. The ideal graft material for the treatment of TMJ pathology resulting from meniscus abnormalities would provide a substrate for cellular ingrowth and site-appropriate tissue deposition, prevent degenerative changes of the condyle and the fossa, and be readily implanted without the associated morbidity of autologous tissue harvest.

Regenerative medicine approaches to tissue reconstruction often utilize implantable synthetic or naturally derived materials with a goal of inducing the restoration, or regeneration, of the native structure and function of the tissue of interest. Scaffolds composed of multiple forms of allogeneic and xenogeneic extracellular matrix (ECM) have been successfully used as inductive templates for tissue reconstruction in a number of regenerative medicine applications (213). The tissue sources of such ECM scaffolds include the small intestine, urinary bladder, and skin, among others. The typical construct resulting from the processing of these materials consists of flat, two-dimensional, sheet-like shapes, which can limit their potential clinical application (67). Recently, the production of a particulate form of an ECM scaffold for the development of three-dimensional scaffolds has been described (24).

In the present study, a device consisting of particulate ECM derived from porcine urinary bladder (UBM-ECM) was encased within sheets of UBM-ECM to provide a resorbable “pillow”

or interpositional material and an anchoring site while mimicking the shape and size of the native canine TMJ meniscus. The device was implanted in a canine model consisting of either a unilateral TMJ meniscectomy or a bilateral minesectomy with implantation on only one side and the remodeling of the device was assessed at time points of 3 weeks, 1, 2, 3 and 6 months post-implantation.

## A.2 MATERIALS AND METHODS

### A.2.1 Overview

Fifteen female mongrel dogs were subjected to either a unilateral meniscectomy followed by replacement of the meniscus with a UBM-ECM device (n=5) or a bilateral meniscectomy with replacement of the meniscus on only one side, leaving the contralateral side empty (n=10). The UBM-ECM device consisted of particulate UBM-ECM encapsulated between sheets of UBM-ECM forming a “pillow-like” device. At time points of 3 weeks (n=1), 1 (n=1), 2 (n=1), 3 (n=1), and 6 months (n=1 unilateral and n=10 bilateral), animals was sacrificed and the condylar head, temporal fossa, and the UBM-ECM implant were excised and assessed using histologic and immunolabeling methods.

### A.2.2 UBM-ECM Device Preparation

UBM-ECM was prepared from porcine bladders as previously described (1). Briefly, urinary bladders were harvested from market weight pigs immediately following sacrifice. The bladder

tissue was rinsed in water to facilitate the removal of excess urine and the urothelial cell layer. Excess connective and adipose tissue was removed from the serosal surface of the bladder using scissors. The apex of the bladder was removed and the bladder was then split longitudinally from the apical opening to the neck of the bladder forming a rectangular sheet. The tunica serosa, tunica muscularis externa, tunica submucosa, and the majority of the muscularis mucosa were removed by mechanical delamination of the abluminal side of the bladder. The remaining tissue consisted of the basement membrane, tunica propria, and resident cells.

The tissue was then treated in a 0.1% peracetic acid/4% ethanol solution for two hours to initiate decellularization and disinfection of the tissue. Following treatment in the peracetic acid/ethanol solution, the tissue was repeatedly washed in phosphate buffered saline (PBS; pH 7.4) and water to remove cellular remnants and traces of the peracetic acid/ethanol solution and to return the pH of the material to 7.4. The remaining decellularized tissue was stored in water until used and represented the hydrated sheet form of UBM-ECM. A portion of the hydrated sheet form of UBM-ECM was frozen and lyophilized. The dry sheet was cut into smaller pieces and comminuted using a Wiley mill with a #60 mesh screen. The comminuted UBM-ECM represented the particulate form of UBM-ECM.

A hard plastic mold was milled to create an oval-shaped depression with the approximate size of the desired central core of the TMJ device (10 mm x 14 mm oval, 2 mm depth) and a flat surface surrounding the depression to allow for the formation of a “pillow-like” core and a flat anchoring site. Two hydrated sheets of UBM-ECM were then cut to size and placed onto the mold. Following placement, the hydrated sheets were pressed to line the inside of the depression, creating a pocket into which particulate UBM-ECM was packed. Approximately 200-300 mg of the ECM powder was packed into the depression and two hydrated sheets were

cut to size and placed over the top of the powder to create an enclosed core. The constructs were subjected to a vacuum of at least 28 inches Hg until dry, forming a multilaminate construct. Figures 45A and 45B show macroscopic views of the multilaminate UBM-ECM construct.

All constructs were terminally sterilized using ethylene oxide prior to implantation.

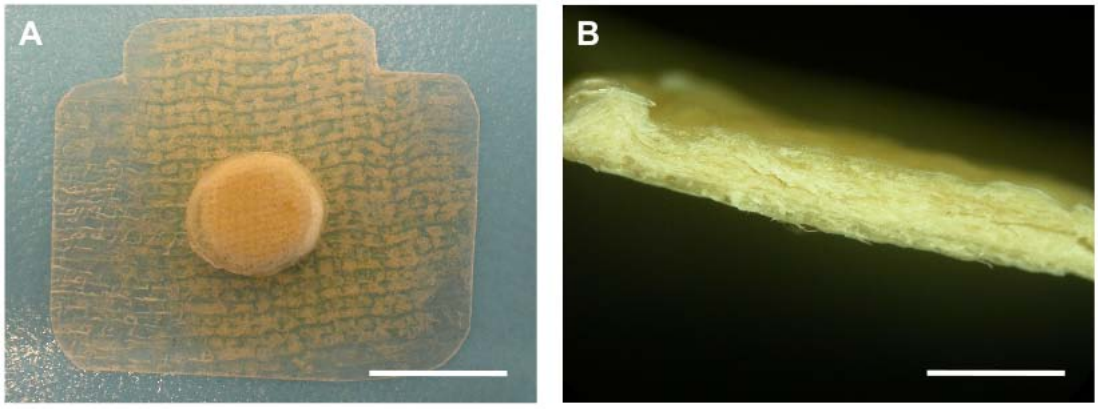


**Figure 45. Macroscopic images of the pre-implantation UBM-ECM device. (A) Whole scaffold, scale bar = 1 cm. (B) Cross sectional view of the "pillow" portion of the device, scale bar = 2.5 mm.**

### A.2.3 Animal Model

Adult female mongrel dogs of approximately 15-20 kg were purchased from Marshall Bio-Resources USA. All animals were examined by a veterinarian prior to surgery and were found to be in good health and all animal procedures were performed in compliance with the 1996 National Institutes of Health "Guide for The Care and Use of Laboratory Animals" and approved by the Institutional Animal Care and Use Committee at the University of Pittsburgh.

### A.2.4 Unilateral Surgical Procedure

All animals were sedated with acepromazine (0.1-0.5 mg/kg body weight) prior to intubation and maintained in a surgical plane of anesthesia with isoflurane (1-5%). The surgical site was shaved then prepared using a betadine scrub prior to the placement of sterile drapes. An incision was made anterior to the tragus, preserving the local innervation and vasculature. The native meniscus was exposed then completely excised.

The UBM-ECM implants were hydrated in sterile saline (0.9%) for approximately 10 minutes prior to implantation as a replacement device for the native meniscus. The implants were placed such that the powder "pillow" was positioned between the temporal fossa and the condylar head. Three holes were created in the temporal fossa and the implants were secured to the temporal fossa using slow resorbing fixation sutures. Fixation sutures were also placed in the anterior and posterior aspects of the implant to adjacent soft tissue. The skin was closed using resorbable suture material. Figure 46 shows images of the surgical procedure.

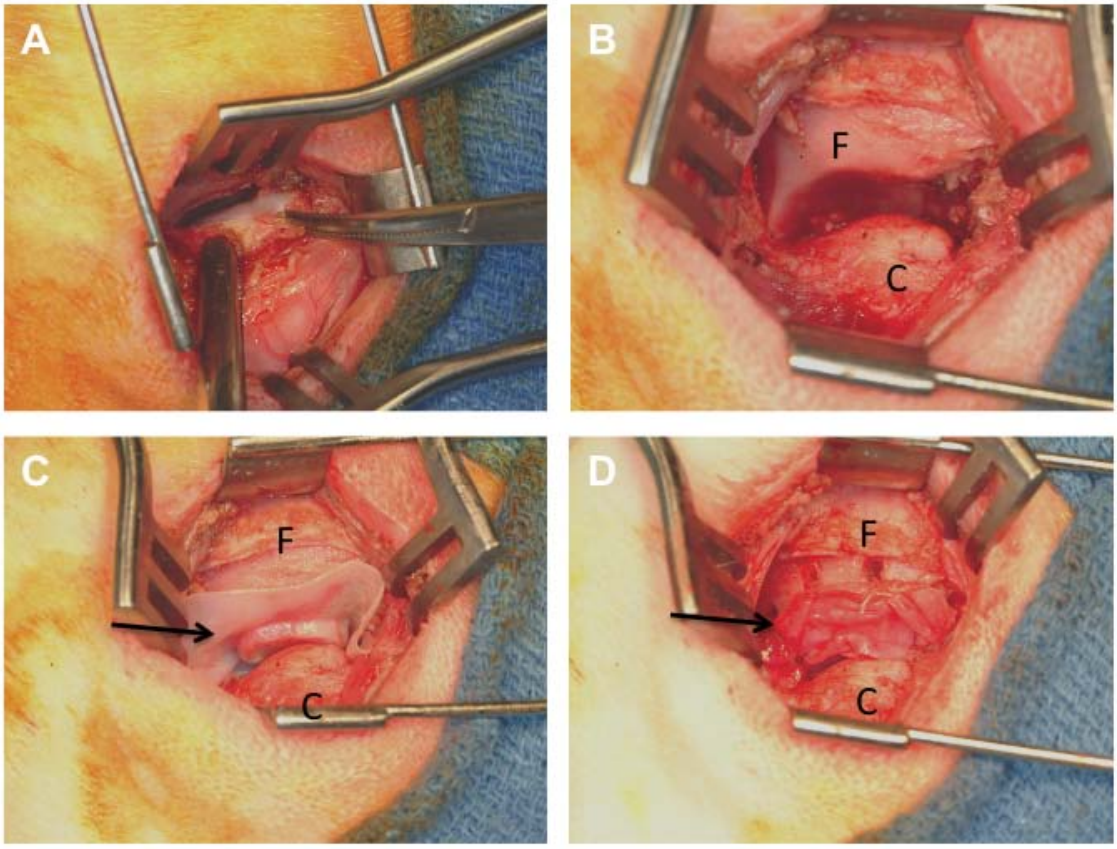


**Figure 46. Surgical procedure. (A) Native meniscus is exposed and isolated. (B) Joint space following removal of the native meniscus. (C) UBM-ECM device placed between mandibular condyle and temporal fossa. (D) UBM-ECM device fixed to fossa with slow resorbing sutures. F = fossa, C=condyle, Arrows = UBM-ECM device.**

### A.2.5 Bilateral Surgical Procedure

The surgical procedures used for the creation of the bilateral defect were identical to those described above for the unilateral defect with the exception that a defect was created on both sides of the canine mandible. One side then underwent reconstruction of the meniscus with the UBM-ECM device and the other was left empty as a control.

### A.2.6 Post Operative Care

Postoperative care was identical for animals which received either the unilateral or bilateral defect. Following the surgical procedure, the animals were recovered from anesthesia, extubated and monitored until resting comfortably in a sternal position. The animals were then monitored and the following parameters were recorded every 3 hours for the first 24 hours post surgery: pulse rate, strength of pulse, capillary refill time, respiratory rate and ability to maintain an open airway, urinary output, and defecation. Body temperature was measured and recorded every 12 hours. The animals were restricted to confinement housing (not more than 2-3 days) until stable, and were then placed in 10x14 ft runs and allowed free movement. Buprenorphine was administered (0.005 – 0.01 mg/kg body weight) for 5 days post operatively and then as needed thereafter for pain management. The dogs were also given Cephalexin (35 mg/kg body weight) for 5 days post-operatively. Animals were fed a soft diet for the first 5-7 days post operatively and were returned to a normal hard diet thereafter.

### A.2.7 Euthanasia and Sample Harvest

On the predetermined date of sacrifice, the animals were sedated with acepromazine (0.1-0.5 mg/kg body weight), anesthetized using isoflurane (5%) and euthanized by intravenous administration of pentobarbital sodium (390 mg/4.5 kg body weight). Following euthanasia, the temporal fossa, the condylar head, and the interpositional material between the structures were excised and fixed in 10% neutral buffered formalin for histologic examination and immunolabeling. Native fossa, condyle, and meniscus tissues were also harvested as control specimens and were treated in identical fashion as the experimental explant tissues.

Animals which were subjected to the unilateral defect were sacrificed at 3 weeks, 1 month, 2 months, 3 months, and 6 months post-implantation (n=1/time point). Animals which were subjected to the bilateral defect were all sacrificed at 6 months post-implantation (n=10). Meniscus tissue from five of the 10 animals sacrificed in the bilateral model were not fixed in formalin, but rather harvested and then subjected to the mechanical and biochemical testing described below.

### A.2.8 Gross Morphologic Examination

At the time of explant, the joint space of all animals was examined for signs of pathology including degeneration of the articulating surfaces of the temporal fossa and mandibular condyle.

### A.2.9 Histologic Evaluation

Formalin fixed tissues were embedded in paraffin, cut into 6 μm sections and mounted on glass slides. Sections were deparaffinized by immersion in xylenes followed by a graded series of ethanol. The slides were stained using hematoxylin and eosin or Herovici's polychrome, and were then dehydrated in ethanol and xylenes prior to coverslipping. The slides were evaluated by light microscopy. Pre-implant UBM-ECM devices were subjected to histologic evaluation using the methods described above.

### A.2.10 Immunolabeling Studies

Sections of the TMJ meniscus tissue were labeled using antibodies specific for CD31 (Neomarkers), CD68 (Dako), smooth muscle actin (SMA, Dako), and calsequestrin (CAL, Abcam) to determine the presence of blood vessels, macrophages, fibroblasts, and skeletal muscle cells, respectively, within the remodeling UBM-ECM implant. Slides were deparaffinized by immersion in xylenes and a graded series of ethanol. Antigen retrieval was then performed by boiling slides in 10 mM citric acid monohydrate (pH 6.0) for 20 minutes. Following antigen retrieval, the slides were exposed to a solution consisting of TRIS buffered saline and 0.05% Tween 20. Slides were then washed in PBS (pH 7.4) three times for a total of 10 minutes and a solution of 3% $H_2O_2$ in methanol was applied for 30 minutes at room temperature to quench endogenous peroxidase activity. Slides were blocked in a solution consisting of 2% normal serum, 1% BSA, 0.1% Triton-X 100, and 0.05% Tween 20 in PBS for 30 minutes at room temperature. Primary antibodies were diluted in the blocking solution (CD31 – 1:250, CD68 – 1:100, SMA – 1:200, CAL - 1:400) and applied to the slides overnight at 4°C. Slides were washed in PBS, and peroxidase conjugated secondary antibodies diluted in blocking solution (CD31 and CD68 - 1:100, SMA – 1:250, CAL 1:400) were applied for 30 minutes at room temperature. The slides were washed in PBS and water prior to development using 4% diaminobenzadine substrate solution. Finally, slides were counterstained using hematoxylin, dehydrated using the reverse of the dewaxing procedure above, and coverslipped for examination under light microscopy.

### A.2.11 Quantification of Histologic and Immunolabeled Images

Changes in the number of cells which were present within the remodeling implants over time was assessed by counting the number of hematoxylin stained nuclei in five 20x images taken from random locations within the bulk of the remodeling devices at 1, 3, and 6 months post-implantation. Nuclei were counted using an automated cell counting algorithm in ImageJ image analysis software (National Institutes of Health, http://rsbweb.nih.gov/ij/). The number of CD31+ vessels in each image was also quantified, as was vessel diameter and the total area occupied by vasculature in each 20x image. Quantification of CD31+ vessels was again performed using image analysis tools available in ImageJ. A student's t-test was used to assess the statistical significance of the results with a $p\text{-value}<0.05$ indicating statistical significance.

### A.2.12 Biomechanical Testing

Mechanical properties of the remodeled UBM-ECM devices explanted from the bilateral defect model were tested using an MTS Insight Mechanical Tester. Briefly, 4 mm cylindrical punches were taken from the center of the samples and placed in a 37°C saline bath prior to testing. A pre-load of 0.1 N was applied for 30 minutes prior to preconditioning, which consisted of 10 cycles between 0-10% strain at a 9%/minute strain rate. Samples were then tested in unconfined compression to 10% strain. Samples were then allowed 30 minutes to reach equilibrium and stress-relaxation behavior was determined. Mechanical properties data obtained for remodeled samples were compared to values obtained both for the pre-implantation UBM-ECM device and for native canine meniscus tissue.

### A.2.13 Biochemical Content Testing

Collagen and GAG contents were determined as a percentage of scaffold dry weight using a hydroxyproline assay and a Blyscan sulfated glycosaminoglycan assay as per manufacturers protocol. Water content was determined as the percentage of water by weight by allowing the tissue to become saturated in a 37°C water bath, measuring the weight of the sample, and then comparing to the weight of the sample following complete lyophilization. All values obtained for collagen, GAG, and water content were compared to values obtained for the pre-implantation UBM-ECM device and for native canine TMJ tissue.

### A.2.14 Statistical Methods

Statistical significance of the mechanical properties and biochemical testing data were determined using a students T-test. P-values of $p<0.05$ were used to determine statistical significance.

## A.3 RESULTS

All of the animals in this study survived the surgical procedure and lived until their predetermined sacrifice date without complication. Appetite and mastication were unaffected.

### A.3.1 Gross Morphologic Findings

Gross morphologic examination showed little to no change in the articulating surfaces of the temporal fossa or the mandibular condyle at any time point following placement of the UBM-ECM device. There were no signs of synovitis, or excess fluid in the joint space. The UBM-ECM device showed progressive remodeling and was replaced with a structure that highly resembled the fibrocartilage of the native TMJ disc by the 6-month post surgical time point. It was not possible to differentiate the original UBM-ECM device from newly deposited host tissue at any of the time points investigated in this study. Figure 47 shows gross morphologic images of the remodeled UBM-ECM constructs explanted at 1, 2, 3, and 6 months. There was a thin film of vascular connective tissue covering the surface of the white firm tissue that represented the remodeled UBM-ECM device. Similar findings were observed in both the unilateral and bilateral reconstruction models.

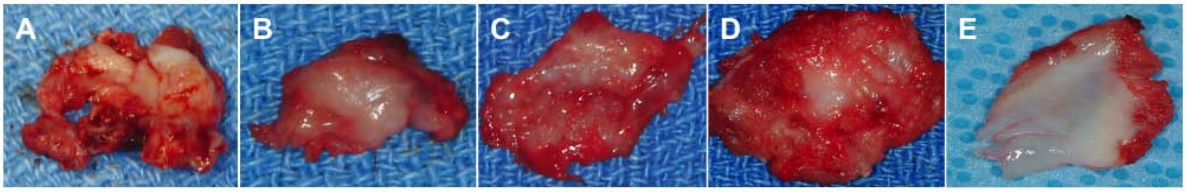


**Figure 47. Macroscopic images of remodeled UBM-ECM device at (A) 1 month, (B) 2 months, (C) 3 months, and (D) 6 months post-implantation. Untreated, contralateral native meniscus (E) is also shown for comparison.**

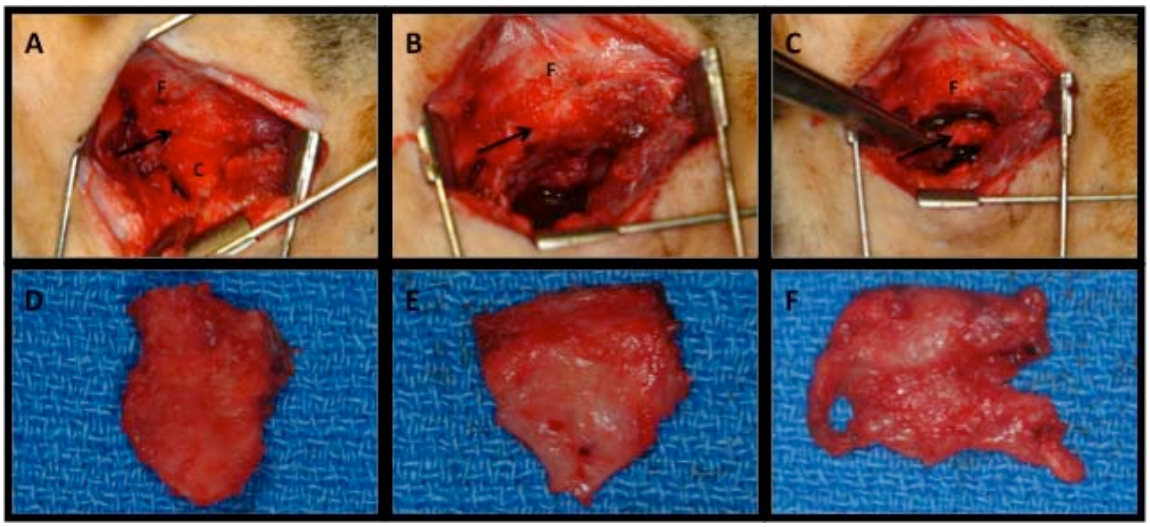


**Figure 48. Gross morphology of the implant site and explanted tissues at 6 months post surgery. (A) Implant site pre-explantation. Fossa (F), condyle (C), and interposed UBM-ECM device are shown. (B) Implant site with condyle removed. Underside of remodeled UBM-ECM device is visible. (C) Removal of UBM-ECM device from implant site. (D) Condyle is shown, note smooth surface appearance and little to no irregularities or pitting. (E) Fossa is shown, note smooth shiny articulating surface. (F) Explanted meniscus is shown. A loose network of vasculature was observed surrounding the explanted tissue.**

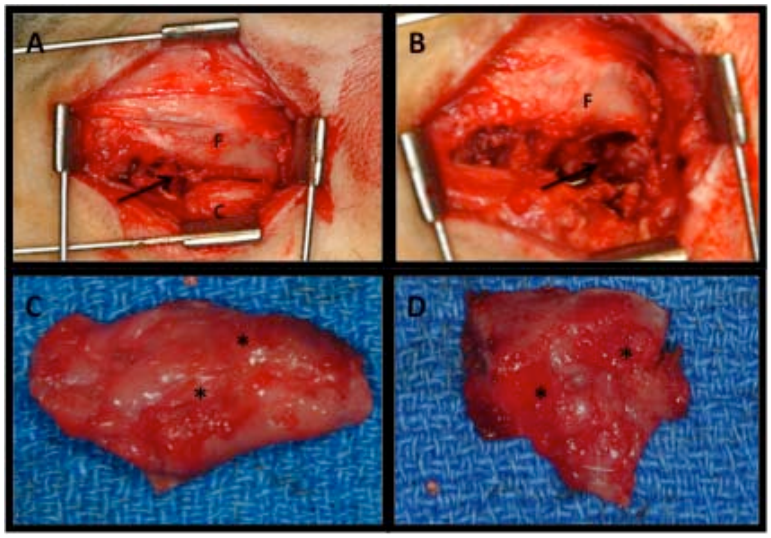


**Figure 49. Control side at explant – six months post surgery. (A) Site of meniscectomy pre-explantation. Fossa (F) and condyle (C) are shown. No interpositional tissue was observed in the control side of any animal. Some fibrotic tissue was observed within the site (arrow). (B) Underside of fossa is shown following explant of the condyle. Fibrotic tissue formation was observed (arrow). (C) Condyle is shown, note irregular surface and pitting (asterisk). (D) Fossa is shown, note irregular surface and pitting.**

### A.3.2 Histopathologic Findings

Histologic evaluation was performed both at the center of the remodeling implant and at the periphery of the implant to determine the bulk morphology of the remodeling device and the degree of integration of the device with the muscular tissues at the peripheral attachment sites.

#### Pre-Implantation UBM-ECM Device

Histologic staining of the UBM-ECM device showed small particles of mature, well-organized collagenous extracellular matrix (UBM-ECM powder) encapsulated within sheets of the same. The particles were randomly oriented and the internal structure of the device was highly porous. The exterior surface of the device was also composed of mature, well-organized

collagenous extracellular matrix and was characterized by a smooth surface and dense structure (UBM-ECM sheets). Figure 50 shows the histologic appearance of the pre-implantation UBM-ECM device.

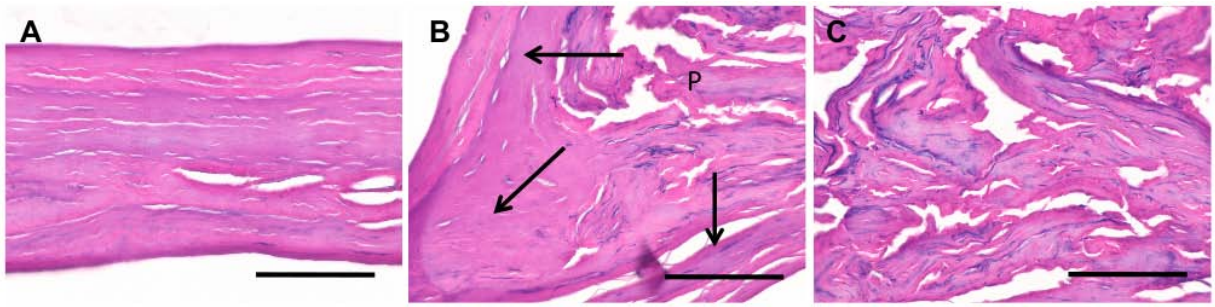


**Figure 50. Microscopic view of pre-implantation UBM-ECM device stained with hematoxylin and eosin. (A) Multilaminate sheet portion of UBM-ECM device, (B) junction between UBM-ECM sheet portion and "pillow" portion of the device, (C) center of "pillow" portion. Arrows = sheet portion, P = powder portion. All images 40X magnification, scale bar = 100um.**

## Remodeled UBM-ECM Device

### Bulk Morphology

At three weeks post-implantation the implanted UBM-ECM device was no longer identifiable and the site of remodeling was characterized by a dense infiltration of predominantly mononuclear cells within newly deposited ECM. Herovici staining showed that the newly deposited ECM was composed of both collagen type I and small amounts of collagen type III.

At one month post-implantation the site of remodeling was characterized by a dense, randomly distributed cellular infiltrate consisting of both mononuclear cells and spindle shaped

cells. There was a decrease in the number of mononuclear cells compared to the three-week time point. Herovici staining indicated that the remodeling site contained both collagen type I and small amounts of collagen type III with an increase in both the density and the degree of organization of the newly deposited collagen type I.

At two months post-implantation the site of remodeling was characterized by an increased number of spindle shaped cells within the remodeling site with a concomitant decrease in the number of mononuclear cells and a decrease in overall cellular density compared to earlier time points. Herovici staining showed that the remodeling site contained both collagen type I and collagen type III with a predominance of collagen type I. The collagen was increased with a morphology that more closely resembled the native TMJ than did the collagen deposited in the remodeling site at the three week or one month time points.

At three months post-implantation the density of the cellular infiltrate within the site of remodeling was greatly decreased compared to all earlier time points. The cell population at the three month time point was characterized by predominantly spindle shaped cells with a small number of randomly distributed mononuclear cells. Herovici staining showed that, as at previous time points, the remodeling site was characterized by a deposition of both collagen type I and collagen type III with a predominance of collagen type I at the three month time point. The density of the collagen type I in the remodeling site was greater than any of the previous time points, and the morphology of the collagen matrix present in the remodeling site at three months highly resembled that of the native TMJ.

At six months post-implantation the remodeling site was characterized by a sparse population of spindle shaped cells within an aligned matrix of collagenous tissue. Herovici staining showed that there were highly organized collagen type I fibers formed within the

remodeling site with interspersed collagen type III fibrils. The morphology of the remodeled tissue at 6 months was almost indistinguishable from that of the native TMJ. Similar results at the 6-month time point were observed for both the unilateral and the bilateral models.

Quantification of the cellularity of the remodeling implants at 1, 3 and 6 months post-implantation (1444.0±229.2, 530.4±27.7, and 347.6±18.3 cells per 20x field, respectively) showed that the number of cells within the remodeling device decreased with time, and was similar to that observed for the native TMJ meniscus by 6 months post-implantation.

Figure 51 shows histologic images of the remodeled UBM-ECM devices at 3 weeks, 1, 2, 3, and 6 months and a quantitative analysis of the cellularity of the remodeling material at each time point.

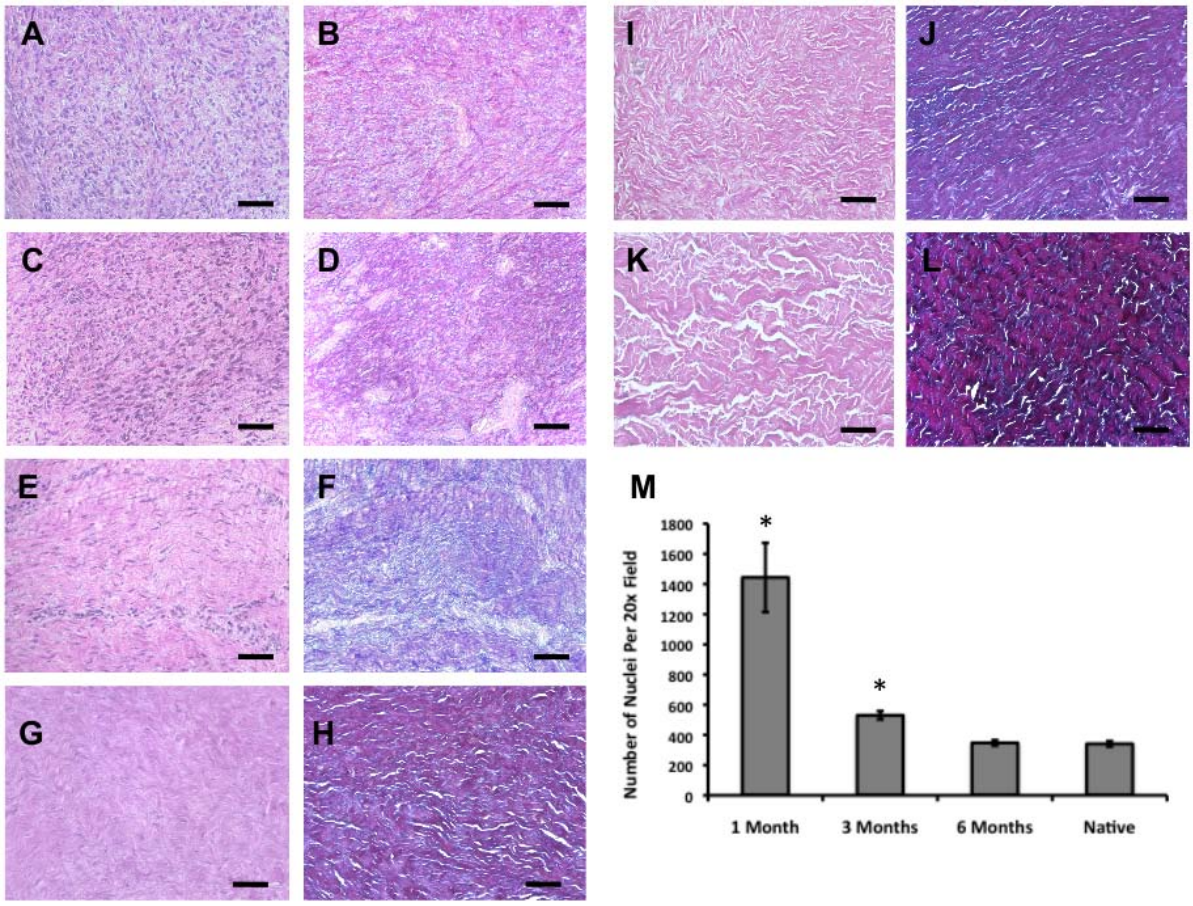


**Figure 51. Microscopic view of hematoxylin and eosin (A, C, E, G, I) as well as Herovici's polychrome (B, D, F, H, J) staining of the central portion of remodeled UBM-ECM devices explanted at 3 weeks (A, B), 1 month (C, D), 2 months (E, F), 3 months (G, H), and 6 months (I, J). Staining of native meniscus is also shown (K, L) for comparison. All images 20X magnification, scale bar = 100 um. (M) Number of nuclei per 20X field. * Indicates values significantly higher than native tissue with $p<0.05$.**

## Peripheral Musculature Attachment Site

Histologic examination showed that the newly deposited ECM within the site of remodeling was well integrated with the native musculature at the periphery of the implanted device as early as one month post-implantation. A dense population of small, dark staining cells was observed adjacent to bundles of skeletal muscle at the interface between the remodeling

UBM-ECM device and native host tissue at one month post-implantation. The degree of integration of the UBM-ECM device with the native host tissue increased with time and ingrowth of host skeletal muscle tissue into the site of remodeling was observed. By six months post-implantation, bundles of skeletal muscle were observed within the site of remodeling and were surrounded by mature, well-organized collagenous extracellular matrix. Muscular ingrowth was observed only at the periphery, and not in the bulk, of the remodeling UBM-ECM device. Similar results were observed in both the unilateral and bilateral model.

Figure 52 shows histologic images of the peripheral attachment site of the remodeled UBM-ECM devices at early (1 month) and late (6 month) time points.

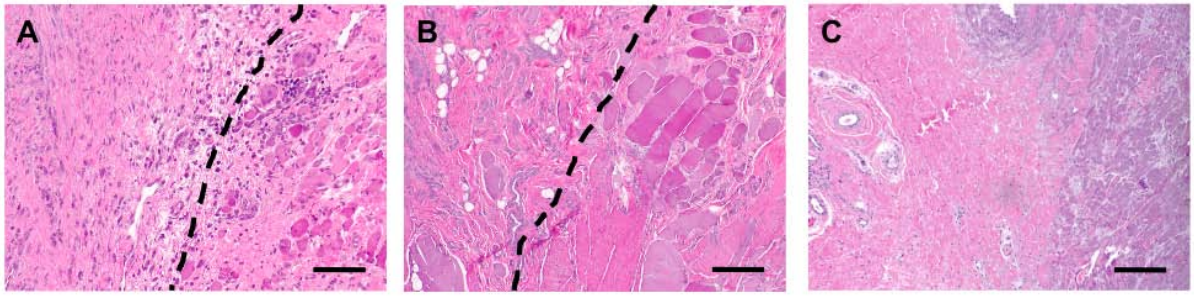


**Figure 52. Microscopic view of hematoxylin and eosin staining of the peripheral attachment sites of the remodeled UBM-ECM explants at (A) 1 month and (B) 6 months. Border between remodeling UBMECM implant and peripheral attachment site denoted by dashed line. Remodeled UBM-ECM device = left of dashed line, peripheral musculature = right of dashed line. Peripheral tissues of the native disc (C) are also shown for comparison. All images 20X magnification, scale bar = 100 um.**

## Articulating Surfaces

Macroscopic and microscopic examination showed that there were no pathologic changes in the articulating surfaces of the condyle or the fossa at any of the time points investigated in this study. That is, the articulating surfaces of the fossa and condyle were characterized by the

presence of smooth, thin fibrocartilaginous tissue which resembled that observed in the contralateral control at all of the time points examined in this study.

Figure 53 shows histologic staining of the articulating surface of the mandibular condyle from contralateral control and from animals at 6 months post-implantation.

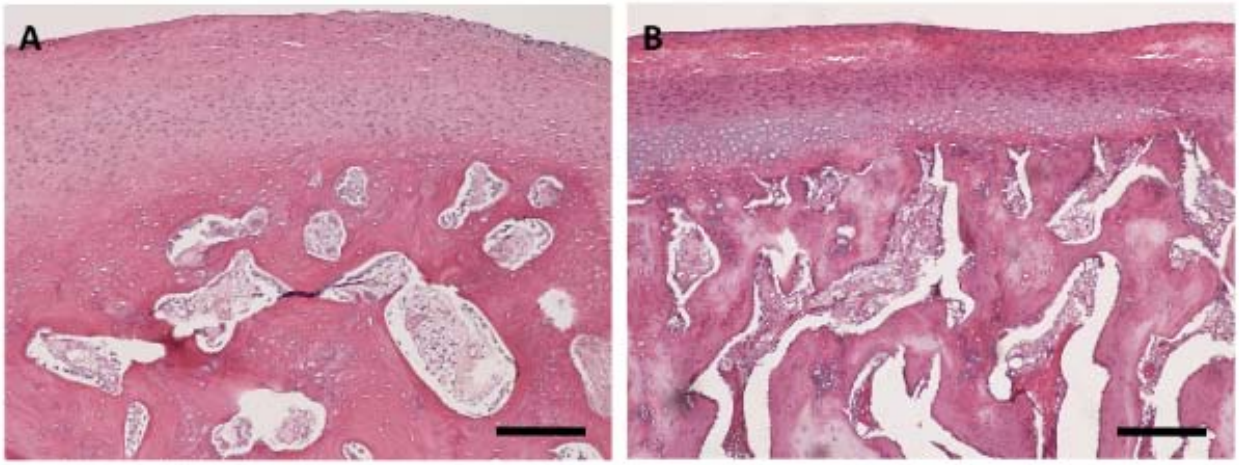


**Figure 53. Microscopic view of hematoxylin and eosin staining of the articulating surface of the mandibular condyle (A) following explant at 6 months. Articulating surface of contralateral control (B) is also shown for comparison. All images are 10X magnification, scale bar = 200 um.**

### A.3.3 Immunolabeling Findings

**CD31**

Immunolabeling for CD31 showed that there were a large number of randomly distributed blood vessels within the site of remodeling at early time points (3 weeks and 1 month post-implantation). Both the number and size of the vessels were decreased by 3 months post-implantation (35.0±8.7 vessels per 20x field, 3.4±0.8% of total image area, 33.0±6.2 μm diameter at 1 months vs. 9.2±0.7 vessels per 20x field, 0.5±0.2% of total image area, 23.3±9.9 μm diameter at 3 months). The number and size of the vessels within the remodeling UBM-

ECM device were further decreased by 6 months post-implantation (5.6±0.5 vessels per 20x field, 0.2±0.1% of total image area, 17.2±5.5 μm diameter) and resembled the vasculature found within the native TMJ meniscus (5.8±0.5 vessels per 20x field, 0.1±0.0% of total image area, 13.5±5.0 μm diameter).

Figure 54 shows sections immunolabeled for CD31 at 1, 3, and 6 months post-implantation and quantitative analysis of the number, area, and diameter of the CD31+ vessels. Similar patterns of CD31 labeling were observed in both the unilateral and bilateral models.

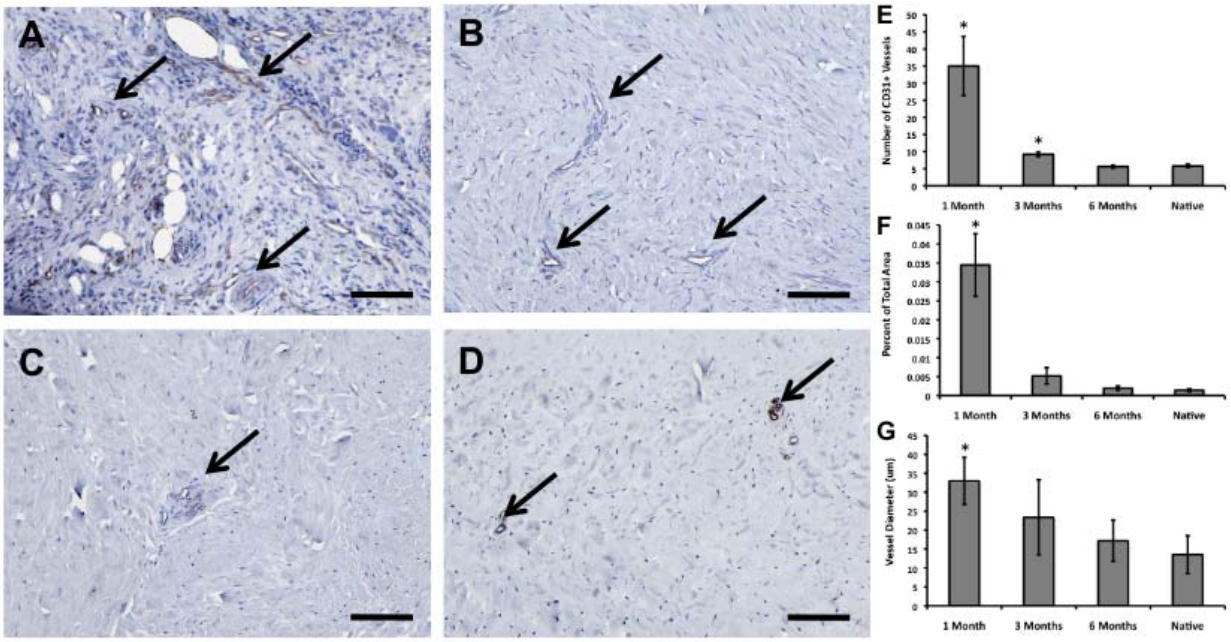


**Figure 54. Microscopic view of CD31 immunolabeling of UBM-ECM devices explanted at (A) 1 month, (B) 3 months, and (C) 6 months. CD31 labeling of (D) native meniscus is also shown for comparison. Arrows indicate examples of positive staining. All images are 20X magnification, scale bar = 100 um. Quantification of the number (E), total area (F), and average diameter (G) of the CD31+ vessels within a 20x field. * Indicates values significantly higher than native tissue with $p<0.05$.**

**CD68**

Immunolabeling for CD68 showed that a large number of mononuclear macrophages were present within the dense cellular infiltrate that was observed during the histologic evaluation of tissue 3 weeks, 1 month, and 2 months post-implantation. The number of CD68+ macrophages decreased with time and few, if any, mononuclear cells were observed by 3 months post-implantation. By 6 months post-implantation, the dense mononuclear macrophage population observed at early time points was replaced by a population of spindle shaped CD68- cells resembling those found in the native TMJ meniscus.

Figures 55A and B show sections immunolabeled for CD68 at early (1 month post-implantation) and late (6 month post-implantation) time points.

It should be noted that the temporal and spatial patterns of angiogenesis and macrophage infiltration seen in this study are similar to those observed in numerous other studies utilizing acellular ECM scaffold materials for tissue reconstruction (69, 100, 166).

**SMA**

Immunolabeling for SMA showed that there were a number of SMA positive cells surrounding the newly formed vasculature as well as throughout the bulk of the remodeling device at 1-month post implantation. By 3 months post-implantation SMA labeling was observed predominantly surrounding the vasculature, with few if any cells labeling positive within the bulk of the remodeling device. A similar pattern of labeling was observed at 6 months post-implantation. The results for the remodeling devices at 3 and 6 months post-implantation were qualitatively similar to those observed for native TMJ tissue.

Figures 55C and D show sections immunolabeled for SMA at early (1 month post-implantation) and late (6 months post-implantation) time points.

**CAL**

Immunolabeling for CAL (a marker of skeletal muscle) showed that there were CAL positive bundles of skeletal muscle at the periphery of the remodeling device as early as 1 month post-implantation. CAL positive bundles of skeletal muscle were also observed at the periphery of the remodeling device at 6 months post-implantation. No immunolabeling for CAL was observed within the bulk of the remodeling device at any time point post-implantation.

Figures 55E and F show sections immunolabeled for CAL at early (1 month post-implantation) and late (6 months post-implantation) time points.

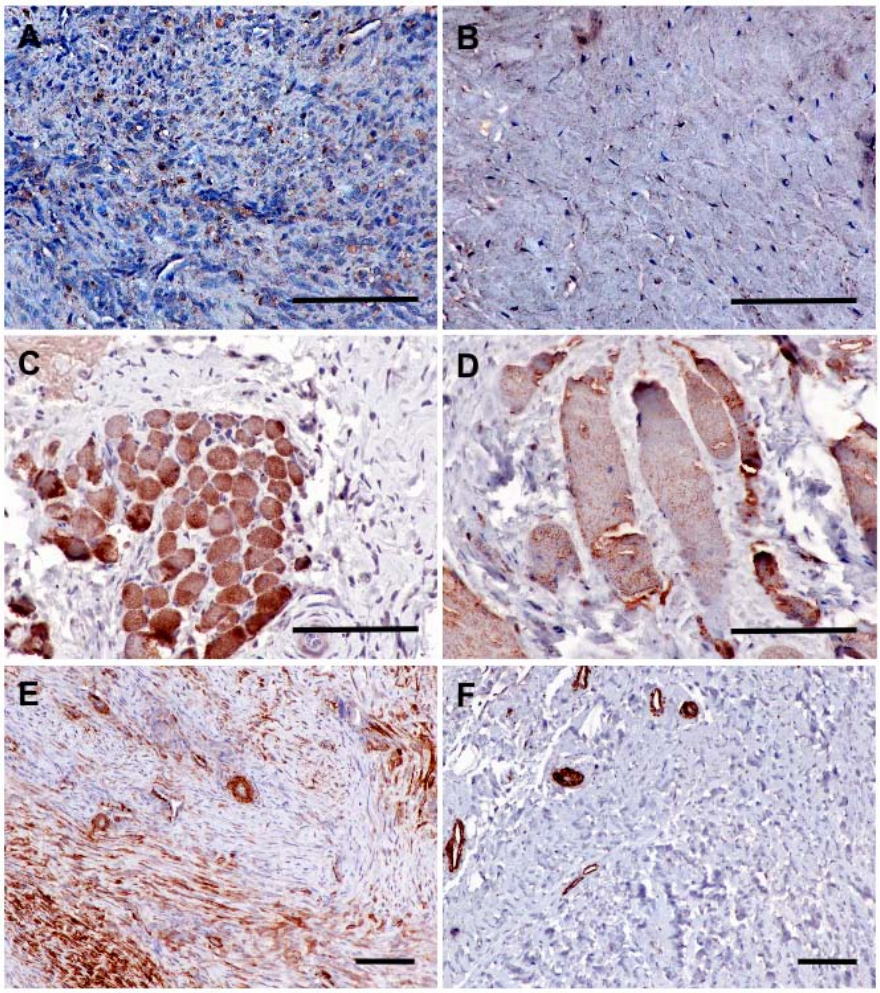


**Figure 55. Microscopic view of immunolabeling of UBM-ECM devices explanted at (A, C, E) 1 month and 6 (B, D, F) months. Immunolabeling for CD68 (A, B), SMA (C, D), and CAL (E, F) are shown. Images A, B, C, and D are 40X magnification, scale bar = 100 um. Images E and F are 20X, scale bar = 100 um.**

### A.3.4 Biomechanical Properties

Biomechanical testing showed that the pre-implantation UBM-ECM device had a significantly higher initial max stress, equilibrium stress, and tangent modulus (16.38±5.78 kPa, 11.29±4.23 kPa, and 179.96±48.29 kPa) than did native TMJ meniscus tissue (2.68±0.57 kPa, 1.46±0.35

kPa, and 23.45 kPa) and a lower percent relaxation (31.38±2.20% vs. 45.35±9.48%). By 6 months post implantation the remodeled tissue had a max stress, equilibrium stress, tangent modulus, and percent relaxation (3.71±1.69 kPa, 1.81±0.65 kPa, and 50.72±32.10 kPa, and 48.10±16.46) which were approaching that of the native meniscus, suggesting that the UBM-ECM device had remodeled and was replaced with tissue which had mechanical properties approaching those of the native meniscus tissue. While the remodeled tissue was observed to have a slightly higher tangent modulus (50.72±32.10 kPa vs. 23.45±6.01 kPa), these differences were not statistically significant and it is likely that the mechanical properties of the remodeling tissue would continue to approach those of the native TMJ meniscus with time.

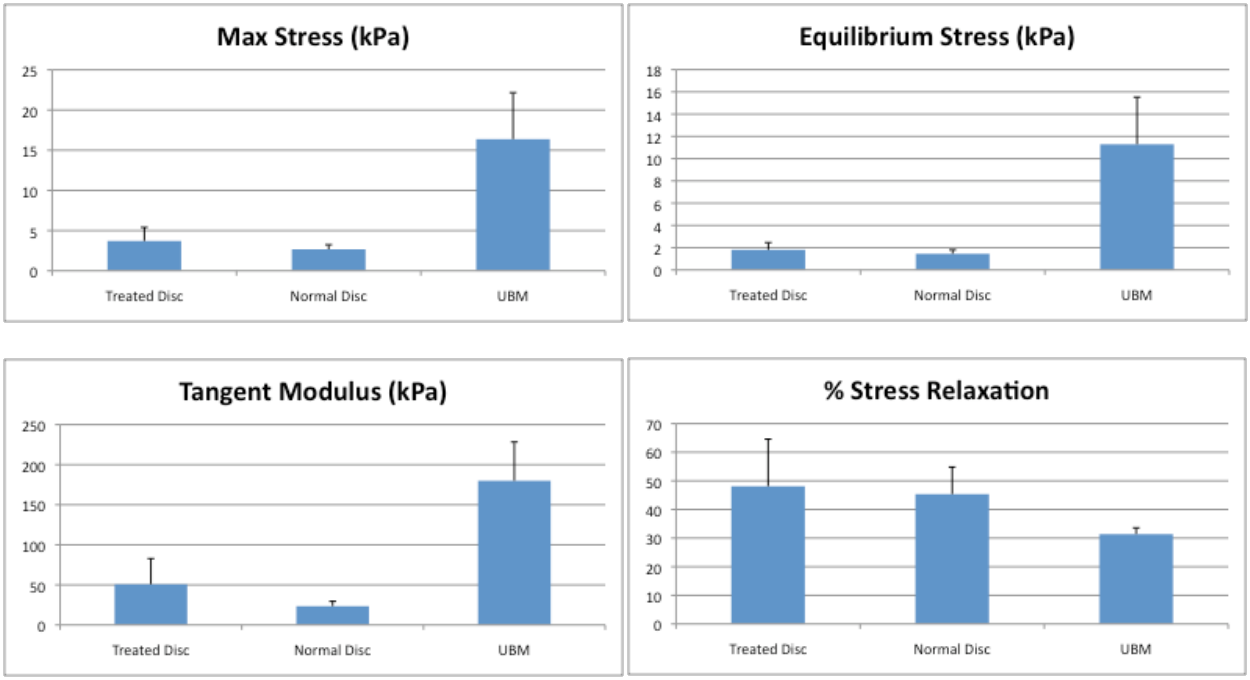


**Figure 56. Max stress, equilibrium stress, tangent modulus, and percent stress relaxation for pre-implantation UBM construct, remodeled UBM construct and native TMJ meniscus.**

### A.3.5 Biochemical Content

Biochemical content testing showed that both the pre-implantation UBM-ECM device and the remodeled host tissue had a collagen content which was similar to that observed in the native meniscus tissues (59.71±29.97%, 60.39±18.68%, and 61.95±17.40%). A similar pattern was observed for water content (69.47±16.72%, 82.54±2.09%, and 77.63±5.26%); however the remodeled UBM-ECM device was found to have a significantly higher GAG content than the pre-implantation device and the native tissue (1.03±0.08% vs. 0.47±0.23% or 0.55±0.11%) No differences were observed for collagen or GAG content between the pre-implantation UBM-ECM device, the remodeled UBM-ECM device at 6 months post-implantation, and the native TMJ meniscus tissue.

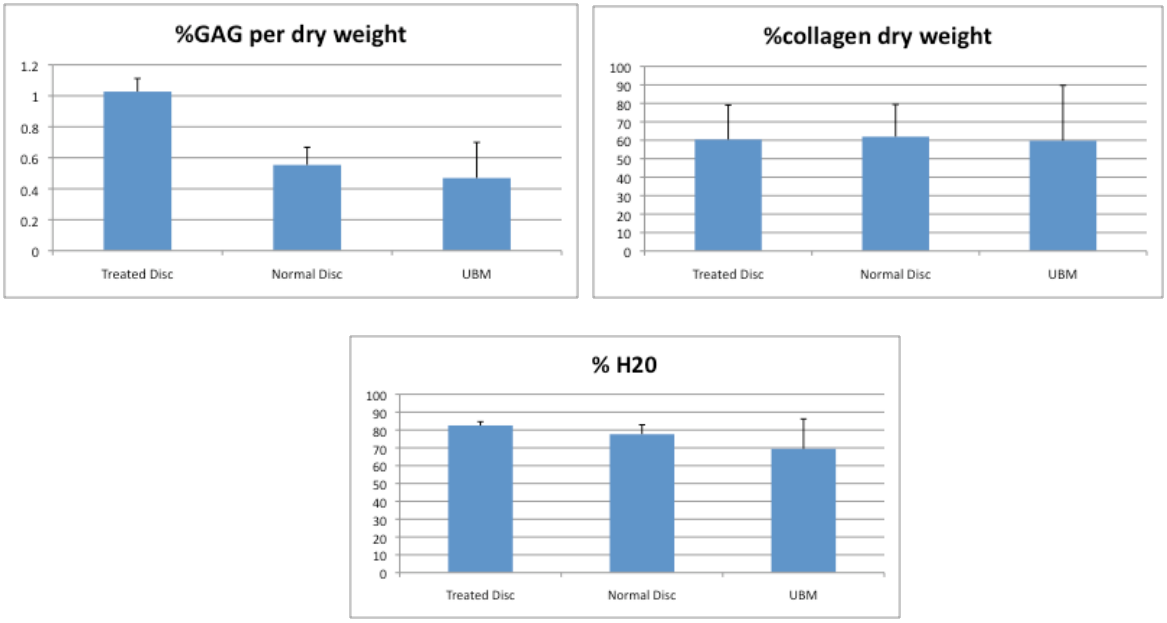


**Figure 57. Biochemical content of pre-implantation UBM construct, remodeled UBM construct and native TMJ meniscus.**

## A.4 DISCUSSION

The results of the present study show that the initially acellular UBM-ECM device acted as an inductive template for constructive remodeling of the TMJ meniscus following meniscectomy. The remodeling of the bulk of the UBM-ECM device was characterized by infiltration of a cell population consisting predominantly of CD68+ mononuclear macrophages and SMA+ spindle shaped cells accompanied by rapid degradation of the scaffold material, deposition of new site-appropriate host-derived tissue, and angiogenesis at early time points changing to a sparse population of SMA- spindle shaped cells and small blood vessels within mature, highly aligned collagen with time. By six months post-implantation, the morphology of the remodeled ECM scaffold site closely resembled that of the native TMJ meniscus both in terms of its shape and size as well as its components, collagen fiber organization, and the makeup and spatial organization of the cell population. The remodeled tissue was shown to be well integrated with the native musculature at the periphery of the implant and host derived CAL+ skeletal muscle tissue was observed at the periphery of the site of tissue remodeling. Additional testing showed that the remodeled tissues possessed both biomechanical properties and biochemical content which was similar to that of the native TMJ meniscus. Further, implantation of the UBM-ECM device was not associated with any pathologic changes in the articulating surface of the fossa or condyle at any of the time points investigated.

Acellular, non-crosslinked ECM scaffolds such as the UBM-ECM used in the present study have been shown to promote a process of constructive remodeling following placement in a wide variety of tissue and organ systems including bone, muscle, nerve, and epithelial tissues among numerous others (19, 20, 26, 29-31, 42, 43, 53, 134, 246). That is, ECM scaffolds have been shown to induce the formation of new, site-appropriate, functional, host tissue that is

arranged in a spatially appropriate pattern for the tissue of interest. This remodeling process is in distinct contrast to the default mechanism of mammalian tissue repair following injury, which generally results in inflammation and scarring with minimal functional recovery. The exact mechanisms by which this ECM mediated tissue specific constructive remodeling occurs are not fully understood. However, a number of factors including mechanical forces, scaffold degradation with concomitant release of bioactive ECM molecules and matricryptic peptides, and the ability of ECM scaffolds to modulate the host immune response are known to play important roles in determining remodeling outcomes (25, 48, 72-74, 76, 78, 83, 84, 86, 96-99, 247).

The present study represents the first report of an intact ECM scaffold material used in an in vivo study of TMJ meniscus replacement. A small number of studies have described the use of intact ECM scaffolds or individual ECM components, such as collagen I, in knee meniscus repair applications with promising results (33, 248-250). Intact ECM scaffolds such as those used in the present study have been shown to retain a large number of tissue specific ECM constituent molecules in a three-dimensional ultrastructure similar to that of the native ECM, and, thus, may offer an advantage over the use of single purified ECM components (1, 251). Further, studies have shown that the molecules that remain following the decellularization of an intact ECM scaffold, such as vascular endothelial growth factor (VEGF), basic fibroblast growth factor (bFGF), and transforming growth factor beta (TGFβ) retain their biologic activity (83).

Degradation products of the ECM are released during a period of rapid scaffold degradation beginning immediately following the implantation of a non-chemically crosslinked ECM scaffold (98). The resultant degradation products have been shown to have chemoattractant activity for of a variety of cells with implications for downstream tissue

remodeling outcomes (74, 76, 78). Chemical crosslinking, a process commonly used during the production of certain ECM scaffolds to increase strength or inhibit the recognition of surface epitope by the host, has been shown to slow or inhibit the degradation of ECM scaffolds and, thus, inhibit the release of the bioactive molecules contained within the scaffold (72). Chemical crosslinking of ECM scaffolds has generally been associated with a process of chronic inflammation and encapsulation of the device within dense collagenous connective tissue as opposed to the constructive and typically functional remodeling outcome which has been observed with non-crosslinked ECM scaffolds. However the exact mechanisms by which chemical crosslinking affects the end outcome of tissue remodeling associated with an implanted ECM scaffold are not completely understood (69).

The non-crosslinked UBM-ECM device used in the present study was rapidly degraded and was indistinguishable from newly deposited host tissue at the three week time point, indicating that scaffold degradation in the TMJ location occurs very rapidly. Rapid degradation of ECM scaffolds has also been observed, and quantified, in other soft tissue locations which experience significant shear or compressive loads; specifically, approximately 50% degradation of non-crosslinked ECM scaffold materials was shown to occur within the first 28 days following implantation in a model of canine Achilles tendon repair (98). Rapid degradation and mechanical loading have both been shown to be critical to the formation of a constructive remodeling response following ECM scaffold implantation (25, 69). A recent study using UBM-ECM as an implantable scaffold material following partial cystectomy in a canine model showed that animals that were prevented from loading the implanted ECM scaffold material via long term catheterization experienced significantly less constructive remodeling than those animals that were allowed to return to normal micturition and, thus, functional loading of the ECM

scaffold following ECM (25). The TMJ meniscus is known to experience both dynamic and static tensile, compressive, and shear forces which occur both during motion and while at rest (252). These constant and diverse forces coupled with the complex synovial fluid milieu may have contributed to the rapid scaffold degradation and concomitant formation and site appropriate spatial arrangement of the newly deposited fibrocartilage, vasculature, and muscle tissue observed in this study. It was not possible, however, to assess the specific contribution of these forces to the tissue remodeling process in the present study. Future studies are planned to address the importance of these factors in the remodeling of UBM-ECM devices in the TMJ location.

Other studies have utilized tissue engineering and regenerative medicine strategies toward the goal of reconstruction of the articulating structures (i.e. mandibular condyle) and the meniscus of the TMJ (253-275). To date, tissue engineering and regenerative medicine studies of the TMJ meniscus have focused primarily upon the characterization of the mechanical and biochemical properties of the disc prior to implantation and the identification of ideal cell sources and scaffolds for the development of tissue-engineered miniscal constructs. While these studies have shown promise, very few have addressed the in vivo implantation of a tissue-engineered construct in the TMJ meniscus location. The present study described the development of a UBM-ECM construct which mimicked the shape and size of the native meniscus and included peripheral anchoring sites for in vivo implantation. When placed in the TMJ location, the device was shown to remodel with a composition and organization that highly resembled the native TMJ meniscus.

## A.5 CONCLUSIONS

The UBM-ECM device described in the present study showed promise as an effective template for TMJ meniscus reconstruction and may represent an “off-the-shelf” solution to TMJ meniscus replacement.

## BIBLIOGRAPHY


1. Brown B, Lindberg K, Reing J, Stolz DB, Badylak SF. The basement membrane component of biologic scaffolds derived from extracellular matrix. Tissue Eng.12:519-26. 2006.

2. Baker SC, Southgate J. Towards control of smooth muscle cell differentiation in synthetic 3D scaffolds. Biomaterials.29:3357-66. 2008.

3. Bissell MJ, Hall HG, Parry G. How does the extracellular matrix direct gene expression? J Theor Biol.99:31-68. 1982.

4. Boudreau N, Myers C, Bissell MJ. From laminin to lamin: regulation of tissue-specific gene expression by the ECM. Trends Cell Biol.5:1-4. 1995.

5. Ingber D. Extracellular matrix and cell shape: potential control points for inhibition of angiogenesis. J Cell Biochem.47:236-41. 1991.

6. Davis GE, Senger DR. Endothelial extracellular matrix: biosynthesis, remodeling, and functions during vascular morphogenesis and neovessel stabilization. Circ Res.97:1093-107. 2005.

7. van der Rest M, Garrone R. Collagen family of proteins. Faseb J.5:2814-23. 1991.

8. Barnard K, Gathercole LJ. Short and long range order in basement membrane type IV collagen revealed by enzymic and chemical extraction. Int J Biol Macromol.13:359-65. 1991.

9. Piez KA. Molecular and aggregate structures of the collagens. In: Piez KA, Reddi AH, eds. Extracellular Matrix Biochemistry. New York: Elsevier; 1984. pp. 1-39.

10. Yurchenco PD, Birk DE, Mecham RP. Extracellular Matrix Assembly and Structure: Academic Press; 1994. pp. 1.

11. Bonewald LF. Regulation and regulatory activities of transforming growth factor beta. Crit Rev Eukaryot Gene Expr.9:33-44. 1999.

12. Kagami S, Kondo S, Loster K, Reutter W, Urushihara M, Kitamura A, et al. Collagen type I modulates the platelet-derived growth factor (PDGF) regulation of the growth and expression of beta1 integrins by rat mesangial cells. Biochem Biophys Res Commun.252:728-32. 1998.

13. Roberts R, Gallagher J, Spooncer E, Allen TD, Bloomfield F, Dexter TM. Heparan sulphate bound growth factors: a mechanism for stromal cell mediated haemopoiesis. Nature.332:376-8. 1988.

14. Dejana E, Colella S, Languino LR, Balconi G, Corbascio GC, Marchisio PC. Fibrinogen induces adhesion, spreading, and microfilament organization of human endothelial cells in vitro. J Cell Biol.104:1403-11. 1987.

15. Macarak EJ, Howard PS. Adhesion of endothelial cells to extracellular matrix proteins. J Cell Physiol.116:76-86. 1983.

16. Causa F, Netti PA, Ambrosio L. A multi-functional scaffold for tissue regeneration: the need to engineer a tissue analogue. Biomaterials.28:5093-9. 2007.

17. Alini M, Li W, Markovic P, Aebi M, Spiro RC, Roughley PJ. The potential and limitations of a cell-seeded collagen/hyaluronan scaffold to engineer an intervertebral disc-like matrix. Spine (Phila Pa 1976).28:446-54; discussion 53. 2003.

18. Koh HS, Yong T, Chan CK, Ramakrishna S. Enhancement of neurite outgrowth using nano-structured scaffolds coupled with laminin. Biomaterials.29:3574-82. 2008.

19. Clarke KM, Lantz GC, Salisbury SK, Badylak SF, Hiles MC, Voytik SL. Intestine submucosa and polypropylene mesh for abdominal wall repair in dogs. J Surg Res.60:107-14. 1996.

20. Prevel CD, Eppley BL, Summerlin DJ, Jackson JR, McCarty M, Badylak SF. Small intestinal submucosa: utilization for repair of rodent abdominal wall defects. Ann Plast Surg.35:374-80. 1995.

21. Freytes DO, Badylak SF, Webster TJ, Geddes LA, Rundell AE. Biaxial strength of multilaminated extracellular matrix scaffolds. Biomaterials.25:2353-61. 2004.

22. Badylak SF, Lantz GC, Coffey A, Geddes LA. Small intestinal submucosa as a large diameter vascular graft in the dog. J Surg Res.47:74-80. 1989.

23. Lantz GC, Badylak SF, Coffey AC, Geddes LA, Blevins WE. Small intestinal submucosa as a small-diameter arterial graft in the dog. J Invest Surg.3:217-27. 1990.

24. Gilbert TW, Stolz DB, Biancaniello F, Simmons-Byrd A, Badylak SF. Production and characterization of ECM powder: implications for tissue engineering applications. Biomaterials.26:1431-5. 2005.

25. Boruch AV, Nieponice A, Qureshi IR, Gilbert TW, Badylak SF. Constructive Remodeling of Biologic Scaffolds is Dependent on Early Exposure to Physiologic Bladder Filling in a Canine Partial Cystectomy Model. J Surg Res. 2009.

26. Piechota HJ, Dahms SE, Probst M, Gleason CA, Nunes LS, Dahiya R, et al. Functional rat bladder regeneration through xenotransplantation of the bladder acellular matrix graft. Br J Urol.81:548-59. 1998.

27. Yoo JJ, Meng J, Oberpenning F, Atala A. Bladder augmentation using allogenic bladder submucosa seeded with cells. Urology.51:221-5. 1998.

28. Freytes DO, Martin J, Velankar SS, Lee AS, Badylak SF. Preparation and rheological characterization of a gel form of the porcine urinary bladder matrix. Biomaterials.29:1630-7. 2008.

29. Suckow MA, Voytik-Harbin SL, Terril LA, Badylak SF. Enhanced bone regeneration using porcine small intestinal submucosa. J Invest Surg.12:277-87. 1999.

30. Moore DC, Pedrozo HA, Crisco JJ, 3rd, Ehrlich MG. Preformed grafts of porcine small intestine submucosa (SIS) for bridging segmental bone defects. J Biomed Mater Res A.69:259-66. 2004.

31. Badylak S, Meurling S, Chen M, Spievack A, Simmons-Byrd A. Resorbable bioscaffold for esophageal repair in a dog model. J Pediatr Surg.35:1097-103. 2000.

32. Nieponice A, McGrath K, Qureshi I, Beckman EJ, Luketich JD, Gilbert TW, et al. An extracellular matrix scaffold for esophageal stricture prevention after circumferential EMR. Gastrointest Endosc.69:289-96. 2009.

33. Welch JA, Montgomery RD, Lenz SD, Plouhar P, Shelton WR. Evaluation of small-intestinal submucosa implants for repair of meniscal defects in dogs. Am J Vet Res.63:427-31. 2002.

34. Peel SAF, Chen H, Renlund R, Badylak SF, Kandel RA. Formation of a SIS–Cartilage Composite Graft in Vitro and Its Use in the Repair of Articular Cartilage Defects. Tissue Eng.4:143-55. 1998.

35. Wainwright JM, Czajka CA, Patel UB, Freytes DO, Tobita K, Gilbert TW, et al. Preparation of Cardiac Extracellular Matrix from an Intact Porcine Heart. Tissue Eng Part C Methods. 2009.

36. Ott HC, Matthiesen TS, Goh SK, Black LD, Kren SM, Netoff TI, et al. Perfusion-decellularized matrix: using nature's platform to engineer a bioartificial heart. Nat Med.14:213-21. 2008.

37. Cobb MA, Badylak SF, Janas W, Simmons-Byrd A, Boop FA. Porcine small intestinal submucosa as a dural substitute. Surg Neurol.51:99-104. 1999.

38. Cobb MA, Badylak SF, Janas W, Boop FA. Histology after dural grafting with small intestinal submucosa. Surg Neurol.46:389-93; discussion 93-4. 1996.

39. Badylak SF, Vorp DA, Spievack AR, Simmons-Byrd A, Hanke J, Freytes DO, et al. Esophageal reconstruction with ECM and muscle tissue in a dog model. J Surg Res.128:87-97. 2005.

40. Badylak SF, Kochupura PV, Cohen IS, Doronin SV, Saltman AE, Gilbert TW, et al. The use of extracellular matrix as an inductive scaffold for the partial replacement of functional myocardium. Cell Transplant.15 Suppl 1:S29-40. 2006.

41. Lin P, Chan WC, Badylak SF, Bhatia SN. Assessing porcine liver-derived biomatrix for hepatic tissue engineering. Tissue Eng.10:1046-53. 2004.

42. Kim BS, Yoo JJ, Atala A. Peripheral nerve regeneration using acellular nerve grafts. J Biomed Mater Res A.68:201-9. 2004.

43. Sondell M, Lundborg G, Kanje M. Regeneration of the rat sciatic nerve into allografts made acellular through chemical extraction. Brain Res.795:44-54. 1998.

44. Prevel CD, Eppley BL, Summerlin DJ, Sidner R, Jackson JR, McCarty M, et al. Small intestinal submucosa: utilization as a wound dressing in full-thickness rodent wounds. Ann Plast Surg.35:381-8. 1995.

45. Black AF, Berthod F, L'Heureux N, Germain L, Auger FA. In vitro reconstruction of a human capillary-like network in a tissue-engineered skin equivalent. Faseb J.12:1331-40. 1998.

46. Bello YM, Falabella AF, Eaglstein WH. Tissue-engineered skin. Current status in wound healing. Am J Clin Dermatol.2:305-13. 2001.

47. Mostow EN, Haraway GD, Dalsing M, Hodde JP, King D. Effectiveness of an extracellular matrix graft (OASIS Wound Matrix) in the treatment of chronic leg ulcers: a randomized clinical trial. J Vasc Surg.41:837-43. 2005.

48. Gilbert TW, Stewart-Akers AM, Simmons-Byrd A, Badylak SF. Degradation and remodeling of small intestinal submucosa in canine Achilles tendon repair. J Bone Joint Surg Am.89:621-30. 2007.

49. Zantop T, Gilbert TW, Yoder MC, Badylak SF. Extracellular matrix scaffolds are repopulated by bone marrow-derived cells in a mouse model of achilles tendon reconstruction. J Orthop Res.24:1299-309. 2006.

50. Dejardin LM, Arnoczky SP, Ewers BJ, Haut RC, Clarke RB. Tissue-engineered rotator cuff tendon using porcine small intestine submucosa. Histologic and mechanical evaluation in dogs. Am J Sports Med.29:175-84. 2001.

51. Musahl V, Abramowitch SD, Gilbert TW, Tsuda E, Wang JH, Badylak SF, et al. The use of porcine small intestinal submucosa to enhance the healing of the medial collateral ligament--a functional tissue engineering study in rabbits. J Orthop Res.22:214-20. 2004.

52. Gilbert TW, Nieponice A, Spievack AR, Holcomb J, Gilbert S, Badylak SF. Repair of the thoracic wall with an extracellular matrix scaffold in a canine model. J Surg Res.147:61-7. 2008.

53. Gilbert TW, Gilbert S, Madden M, Reynolds SD, Badylak SF. Morphologic assessment of extracellular matrix scaffolds for patch tracheoplasty in a canine model. Ann Thorac Surg.86:967-74; discussion -74. 2008.

54. Macchiarini P, Jungebluth P, Go T, Asnaghi MA, Rees LE, Cogan TA, et al. Clinical transplantation of a tissue-engineered airway. Lancet.372:2023-30. 2008.

55. Parekh A, Mantle B, Banks J, Swarts JD, Badylak SF, Dohar JE, et al. Repair of the tympanic membrane with urinary bladder matrix. Laryngoscope.119:1206-13. 2009.

56. Gilbert TW, Agrawal V, Gilbert MR, Povirk KM, Badylak SF, Rosen CA. Liver-derived extracellular matrix as a biologic scaffold for acute vocal fold repair in a canine model. Laryngoscope.119:1856-63. 2009.

57. Huber JE, Spievack A, Simmons-Byrd A, Ringel RL, Badylak S. Extracellular matrix as a scaffold for laryngeal reconstruction. Ann Otol Rhinol Laryngol.112:428-33. 2003.

58. Hodde J, Record R, Tullius R, Badylak S. Fibronectin peptides mediate HMEC adhesion to porcine-derived extracellular matrix. Biomaterials.23:1841-8. 2002.

59. Chen F, Yoo JJ, Atala A. Acellular collagen matrix as a possible "off the shelf" biomaterial for urethral repair. Urology.54:407-10. 1999.

60. Bader A, Schilling T, Teebken OE, Brandes G, Herden T, Steinhoff G, et al. Tissue engineering of heart valves--human endothelial cell seeding of detergent acellularized porcine valves. Eur J Cardiothorac Surg.14:279-84. 1998.

61. Borschel GH, Dennis RG, Kuzon WM, Jr. Contractile skeletal muscle tissue-engineered on an acellular scaffold. Plast Reconstr Surg.113:595-602; discussion 3-4. 2004.

62. Hudson TW, Liu SY, Schmidt CE. Engineering an improved acellular nerve graft via optimized chemical processing. Tissue Eng.10:1346-58. 2004.

63. Buinewicz B, Rosen B. Acellular cadaveric dermis (AlloDerm): a new alternative for abdominal hernia repair. Ann Plast Surg.52:188-94. 2004.

64. Armour AD, Fish JS, Woodhouse KA, Semple JL. A comparison of human and porcine acellularized dermis: interactions with human fibroblasts in vitro. Plast Reconstr Surg.117:845-56. 2006.

65. Tischer T, Vogt S, Aryee S, Steinhauser E, Adamczyk C, Milz S, et al. Tissue engineering of the anterior cruciate ligament: a new method using acellularized tendon allografts and autologous fibroblasts. Arch Orthop Trauma Surg.127:735-41. 2007.

66. Cartmell JS, Dunn MG. Development of cell-seeded patellar tendon allografts for anterior cruciate ligament reconstruction. Tissue Eng.10:1065-75. 2004.

67. Gilbert TW, Sellaro TL, Badylak SF. Decellularization of tissues and organs. Biomaterials.27:3675-83. 2006.

68. Valentin JE, Freytes DO, Grasman JM, Pesyna C, Freund J, Gilbert TW, et al. Oxygen diffusivity of biologic and synthetic scaffold materials for tissue engineering. J Biomed Mater Res A. 2008.

69. Valentin JE, Badylak JS, McCabe GP, Badylak SF. Extracellular matrix bioscaffolds for orthopaedic applications. A comparative histologic study. J Bone Joint Surg Am.88:2673-86. 2006.

70. Nieponice A, Gilbert TW, Badylak SF. Reinforcement of esophageal anastomoses with an extracellular matrix scaffold in a canine model. Ann Thorac Surg.82:2050-8. 2006.

71. Anderson JM. Inflammation, Wound Healing, and the Foreign Body Response. In: Ratner BD, Hoffman AS, Schoen FJ, Lemons JE, eds. Biomaterials Science: An Introduction to Materials in Medicine. 2nd ed: Elsivier; 2004. pp. 296-304.

72. Valentin JE, Stewart-Akers AM, Gilbert TW, Badylak SF. Macrophage participation in the degradation and remodeling of extracellular matrix scaffolds. Tissue Eng Part A.15:1687-94. 2009.

73. Brennan EP, Reing J, Chew D, Myers-Irvin JM, Young EJ, Badylak SF. Antibacterial activity within degradation products of biological scaffolds composed of extracellular matrix. Tissue Eng.12:2949-55. 2006.

74. Brennan EP, Tang XH, Stewart-Akers AM, Gudas LJ, Badylak SF. Chemoattractant activity of degradation products of fetal and adult skin extracellular matrix for keratinocyte progenitor cells. J Tissue Eng Regen Med.2:491-8. 2008.

75. Haviv F, Bradley MF, Kalvin DM, Schneider AJ, Davidson DJ, Majest SM, et al. Thrombospondin-1 mimetic peptide inhibitors of angiogenesis and tumor growth: design, synthesis, and optimization of pharmacokinetics and biological activities. Journal of medicinal chemistry.48:2838-46. 2005.

76. Li F, Li W, Johnson S, Ingram D, Yoder M, Badylak S. Low-molecular-weight peptides derived from extracellular matrix as chemoattractants for primary endothelial cells. Endothelium.11:199-206. 2004.

77. Sarikaya A, Record R, Wu CC, Tullius B, Badylak S, Ladisch M. Antimicrobial activity associated with extracellular matrices. Tissue Eng.8:63-71. 2002.

78. Reing JE, Zhang L, Myers-Irvin J, Cordero KE, Freytes DO, Heber-Katz E, et al. Degradation products of extracellular matrix affect cell migration and proliferation. Tissue Eng Part A.15:605-14. 2009.

79. Holtom PD, Shinar Z, Benna J, Patzakis MJ. Porcine small intestine submucosa does not show antimicrobial properties. Clinical orthopaedics and related research.18-21. 2004.

80. Badylak SF, Park K, Peppas N, McCabe G, Yoder M. Marrow-derived cells populate scaffolds composed of xenogeneic extracellular matrix. Exp Hematol.29:1310-8. 2001.

81. Beattie AJ, Gilbert TW, Guyot JP, Yates AJ, Badylak SF. Chemoattraction of progenitor cells by remodeling extracellular matrix scaffolds. Tissue Eng Part A.15:1119-25. 2009.

82. Badylak S, Kokini K, Tullius B, Simmons-Byrd A, Morff R. Morphologic study of small intestinal submucosa as a body wall repair device. J Surg Res.103:190-202. 2002.

83. Chun SY, Lim GJ, Kwon TG, Kwak EK, Kim BW, Atala A, et al. Identification and characterization of bioactive factors in bladder submucosa matrix. Biomaterials.28:4251-6. 2007.

84. Hodde JP, Badylak SF, Shelbourne KD. The effect of range of motion on remodeling of small intestinal submucosa (SIS) when used as an Achilles tendon repair material in the rabbit. Tissue Eng.3:27-37. 1997.

85. Badylak SF, Gilbert TW. Immune response to biologic scaffold materials. Semin Immunol.20:109-16. 2008.

86. Allman AJ, McPherson TB, Badylak SF, Merrill LC, Kallakury B, Sheehan C, et al. Xenogeneic extracellular matrix grafts elicit a TH2-restricted immune response. Transplantation.71:1631-40. 2001.

87. Collins BH, Chari RS, Magee JC, Harland RC, Lindman BJ, Logan JS, et al. Mechanisms of injury in porcine livers perfused with blood of patients with fulminant hepatic failure. Transplantation.58:1162-71. 1994.

88. Cooper DK, Good AH, Koren E, Oriol R, Malcolm AJ, Ippolito RM, et al. Identification of alpha-galactosyl and other carbohydrate epitopes that are bound by human anti-pig antibodies: relevance to discordant xenografting in man. Transpl Immunol.1:198-205. 1993.

89. Galili U, Macher BA, Buehler J, Shohet SB. Human natural anti-alpha-galactosyl IgG. II. The specific recognition of alpha (1----3)-linked galactose residues. J Exp Med.162:573-82. 1985.

90. Oriol R, Ye Y, Koren E, Cooper DK. Carbohydrate antigens of pig tissues reacting with human natural antibodies as potential targets for hyperacute vascular rejection in pig-to-man organ xenotransplantation. Transplantation.56:1433-42. 1993.

91. Daly K, Stewart-Akers A, Hara H, Ezzelarab M, Long C, Cordero K, et al. Effect of the alphaGal Epitope on the Response to Small Intestinal Submucosa Extracellular Matrix in a Nonhuman Primate Model. Tissue Eng Part A. 2009.

92. Raeder RH, Badylak SF, Sheehan C, Kallakury B, Metzger DW. Natural anti-galactose alpha1,3 galactose antibodies delay, but do not prevent the acceptance of extracellular matrix xenografts. Transpl Immunol.10:15-24. 2002.

93. Derwin KA, Baker AR, Spragg RK, Leigh DR, Iannotti JP. Commercial extracellular matrix scaffolds for rotator cuff tendon repair. Biomechanical, biochemical, and cellular properties. J Bone Joint Surg Am.88:2665-72. 2006.

94. Zheng MH, Chen J, Kirilak Y, Willers C, Xu J, Wood D. Porcine small intestine submucosa (SIS) is not an acellular collagenous matrix and contains porcine DNA: possible implications in human implantation. J Biomed Mater Res B Appl Biomater.73:61-7. 2005.

95. Gilbert TW, Freundb SJ, Badylak SF. Quantification of DNA in Biologic Scaffold Materials. J Surg Res. 2008.

96. Badylak SF, Valentin JE, Ravindra AK, McCabe GP, Stewart-Akers AM. Macrophage Phenotype as a Determinant of Biologic Scaffold Remodeling. Tissue Eng.In Press. 2008.

97. Brown BN, Valentin JE, Stewart-Akers AM, McCabe GP, Badylak SF. Macrophage phenotype and remodeling outcomes in response to biologic scaffolds with and without a cellular component. Biomaterials. 2008.

98. Gilbert TW, Stewart-Akers AM, Badylak SF. A quantitative method for evaluating the degradation of biologic scaffold materials. Biomaterials.28:147-50. 2007.

99. Allman AJ, McPherson TB, Merrill LC, Badylak SF, Metzger DW. The Th2-restricted immune response to xenogeneic small intestinal submucosa does not influence systemic protective immunity to viral and bacterial pathogens. Tissue Eng.8:53-62. 2002.

100. Brown BN, Valentin JE, Stewart-Akers AM, McCabe GP, Badylak SF. Macrophage phenotype and remodeling outcomes in response to biologic scaffolds with and without a cellular component. Biomaterials.30:1482-91. 2009.

101. Guo S, Dipietro LA. Factors affecting wound healing. J Dent Res.89:219-29. 2004.

102. Diegelmann RF, Evans MC. Wound healing: an overview of acute, fibrotic and delayed healing. Front Biosci.9:283-9. 2004.

103. Kumar V, Abbas AK, Fausto N, Robbins SL, Cotran RS. Robbins and Cotran pathologic basis of disease. 7th ed. Philadelphia: Elsevier Saunders; 2005.

104. Clark RA. Fibrin and wound healing. Ann N Y Acad Sci.936:355-67. 2001.

105. Broughton G, 2nd, Janis JE, Attinger CE. The basic science of wound healing. Plast Reconstr Surg.117:12S-34S. 2006.

106. Barrientos S, Stojadinovic O, Golinko MS, Brem H, Tomic-Canic M. Growth factors and cytokines in wound healing. Wound Repair Regen.16:585-601. 2008.

107. Werner S, Grose R. Regulation of wound healing by growth factors and cytokines. Physiol Rev.83:835-70. 2003.

108. Artuc M, Hermes B, Steckelings UM, Grutzkau A, Henz BM. Mast cells and their mediators in cutaneous wound healing--active participants or innocent bystanders? Exp Dermatol.8:1-16. 1999.

109. Adamson R. Role of macrophages in normal wound healing: an overview. J Wound Care.18:349-51. 2009.

110. Sylvia CJ. The role of neutrophil apoptosis in influencing tissue repair. J Wound Care.12:13-6. 2003.

111. Keen D. A review of research examining the regulatory role of lymphocytes in normal wound healing. J Wound Care.17:218-20, 22. 2008.

112. Knighton DR, Hunt TK, Scheuenstuhl H, Halliday BJ, Werb Z, Banda MJ. Oxygen tension regulates the expression of angiogenesis factor by macrophages. Science.221:1283-5. 1983.

113. LaVan FB, Hunt TK. Oxygen and wound healing. Clin Plast Surg.17:463-72. 1990.

114. Gill SE, Parks WC. Metalloproteinases and their inhibitors: regulators of wound healing. Int J Biochem Cell Biol.40:1334-47. 2008.

115. Ratner BD. Biomaterials science : an introduction to materials in medicine. 2nd ed. Amsterdam ; Boston: Elsevier Academic Press; 2004.

116. Anderson JM, Rodriguez A, Chang DT. Foreign body reaction to biomaterials. Semin Immunol.20:86-100. 2008.

117. Horbett TA. The role of adsorbed proteins in tissue response to biomaterials. In: Ratner BD, et al., ed. Biomaterials science: an introduction to biomaterials in medicine. San Diego, CA: Elsevier Academic Press; 2004. pp. 237-46.

118. Wilson CJ, Clegg RE, Leavesley DI, Pearcy MJ. Mediation of biomaterial-cell interactions by adsorbed proteins: a review. Tissue Eng.11:1-18. 2005.

119. Jenney CR, Anderson JM. Adsorbed serum proteins responsible for surface dependent human macrophage behavior. J Biomed Mater Res.49:435-47. 2000.

120. Brodbeck WG, Colton E, Anderson JM. Effects of adsorbed heat labile serum proteins and fibrinogen on adhesion and apoptosis of monocytes/macrophages on biomaterials. J Mater Sci Mater Med.14:671-5. 2003.

121. Hu WJ, Eaton JW, Ugarova TP, Tang L. Molecular basis of biomaterial-mediated foreign body reactions. Blood.98:1231-8. 2001.

122. Dadsetan M, Jones JA, Hiltner A, Anderson JM. Surface chemistry mediates adhesive structure, cytoskeletal organization, and fusion of macrophages. J Biomed Mater Res A.71:439-48. 2004.

123. MacEwan MR, Brodbeck WG, Matsuda T, Anderson JM. Monocyte/lymphocyte interactions and the foreign body response: in vitro effects of biomaterial surface chemistry. J Biomed Mater Res A.74:285-93. 2005.

124. Chen S, Jones JA, Xu Y, Low HY, Anderson JM, Leong KW. Characterization of topographical effects on macrophage behavior in a foreign body response model. Biomaterials.31:3479-91. 2010.

125. Wendel HP, Ziemer G. Coating-techniques to improve the hemocompatibility of artificial devices used for extracorporeal circulation. Eur J Cardiothorac Surg.16:342-50. 1999.

126. Sin DC, Kei HL, Miao X. Surface coatings for ventricular assist devices. Expert Rev Med Devices.6:51-60. 2009.

127. Brodbeck WG, Nakayama Y, Matsuda T, Colton E, Ziats NP, Anderson JM. Biomaterial surface chemistry dictates adherent monocyte/macrophage cytokine expression in vitro. Cytokine.18:311-9. 2002.

128. Brodbeck WG, Patel J, Voskerician G, Christenson E, Shive MS, Nakayama Y, et al. Biomaterial adherent macrophage apoptosis is increased by hydrophilic and anionic substrates in vivo. Proc Natl Acad Sci U S A.99:10287-92. 2002.

129. Bota PC, Collie AM, Puolakkainen P, Vernon RB, Sage EH, Ratner BD, et al. Biomaterial topography alters healing in vivo and monocyte/macrophage activation in vitro. J Biomed Mater Res A.95:649-57. 2010.

130. Madden LR, Mortisen DJ, Sussman EM, Dupras SK, Fugate JA, Cuy JL, et al. Proangiogenic scaffolds as functional templates for cardiac tissue engineering. Proc Natl Acad Sci U S A.107:15211-6. 2010.

131. Bartneck M, Schulte VA, Paul NE, Diez M, Lensen MC, Zwadlo-Klarwasser G. Induction of specific macrophage subtypes by defined micro-patterned structures. Acta Biomater.6:3864-72. 2010.

132. VandeVord PJ, Matthew HW, DeSilva SP, Mayton L, Wu B, Wooley PH. Evaluation of the biocompatibility of a chitosan scaffold in mice. J Biomed Mater Res.59:585-90. 2002.

133. Valentin JE, Turner NJ, Gilbert TW, Badylak SF. Functional skeletal muscle formation with a biologic scaffold. Biomaterials.31:7475-84. 2010.

134. Agrawal V, Brown BN, Beattie AJ, Gilbert TW, Badylak SF. Evidence of innervation following extracellular matrix scaffold-mediated remodelling of muscular tissues. J Tissue Eng Regen Med.3:590-600. 2009.

135. Adkisson HD, Milliman C, Zhang X, Mauch K, Maziarz RT, Streeter PR. Immune evasion by neocartilage-derived chondrocytes: Implications for biologic repair of joint articular cartilage. Stem Cell Res.4:57-68. 2010.

136. Ryan JM, Barry FP, Murphy JM, Mahon BP. Mesenchymal stem cells avoid allogeneic rejection. J Inflamm (Lond).2:8. 2005.

137. Cheung CY, Anseth KS. Synthesis of immunoisolation barriers that provide localized immunosuppression for encapsulated pancreatic islets. Bioconjug Chem.17:1036-42. 2006.

138. Cruise GM, Hegre OD, Lamberti FV, Hager SR, Hill R, Scharp DS, et al. In vitro and in vivo performance of porcine islets encapsulated in interfacially photopolymerized poly(ethylene glycol) diacrylate membranes. Cell Transplant.8:293-306. 1999.

139. Gordon S, Taylor PR. Monocyte and macrophage heterogeneity. Nature reviews.5:953-64. 2005.

140. Krishnaraju K, Hoffman B, Liebermann DA. Early growth response gene 1 stimulates development of hematopoietic progenitor cells along the macrophage lineage at the expense of the granulocyte and erythroid lineages. Blood.97:1298-305. 2001.

141. Mantovani A, Sica A, Sozzani S, Allavena P, Vecchi A, Locati M. The chemokine system in diverse forms of macrophage activation and polarization. Trends in immunology.25:677-86. 2004.

142. Mantovani A, Sozzani S, Locati M, Allavena P, Sica A. Macrophage polarization: tumor-associated macrophages as a paradigm for polarized M2 mononuclear phagocytes. Trends in immunology.23:549-55. 2002.

143. Mills CD, Kincaid K, Alt JM, Heilman MJ, Hill AM. M-1/M-2 macrophages and the Th1/Th2 paradigm. J Immunol.164:6166-73. 2000.

144. Mosser DM. The many faces of macrophage activation. Journal of leukocyte biology.73:209-12. 2003.

145. Verreck FA, de Boer T, Langenberg DM, van der Zanden L, Ottenhoff TH. Phenotypic and functional profiling of human proinflammatory type-1 and anti-inflammatory type-2 macrophages in response to microbial antigens and IFN-gamma- and CD40L-mediated costimulation. Journal of leukocyte biology.79:285-93. 2006.

146. Mantovani A, Sica A, Locati M. Macrophage polarization comes of age. Immunity.23:344-6. 2005.

147. Deonarine K, Panelli MC, Stashower ME, Jin P, Smith K, Slade HB, et al. Gene expression profiling of cutaneous wound healing. Journal of translational medicine.5:11. 2007.

148. Kigerl KA, Gensel JC, Ankeny DP, Alexander JK, Donnelly DJ, Popovich PG. Identification of two distinct macrophage subsets with divergent effects causing either neurotoxicity or regeneration in the injured mouse spinal cord. J Neurosci.29:13435-44. 2009.

149. Ruffell D, Mourkioti F, Gambardella A, Kirstetter P, Lopez RG, Rosenthal N, et al. A CREB-C/EBPbeta cascade induces M2 macrophage-specific gene expression and promotes muscle injury repair. Proc Natl Acad Sci U S A.106:17475-80. 2009.

150. Atala A, Bauer SB, Soker S, Yoo JJ, Retik AB. Tissue-engineered autologous bladders for patients needing cystoplasty. Lancet.367:1241-6. 2006.

151. Atala A, Freeman MR, Vacanti JP, Shepard J, Retik AB. Implantation in vivo and retrieval of artificial structures consisting of rabbit and human urothelium and human bladder muscle. J Urol.150:608-12. 1993.

152. Demirbilek S, Kanmaz T, Ozardali I, Edali MN, Yucesan S. Using porcine small intestinal submucosa in intestinal regeneration. Pediatr Surg Int.19:588-92. 2003.

153. Kropp BP, Cheng EY, Lin HK, Zhang Y. Reliable and reproducible bladder regeneration using unseeded distal small intestinal submucosa. J Urol.172:1710-3. 2004.

154. Mantovani F, Trinchieri A, Castelnuovo C, Romano AL, Pisani E. Reconstructive urethroplasty using porcine acellular matrix. Eur Urol.44:600-2. 2003.

155. McCready RA, Hodde J, Irwin RJ, Coffey AC, Divelbiss JL, Bryant MA, et al. Pseudoaneurysm formation in a subset of patients with small intestinal submucosa biologic patches after carotid endarterectomy. J Vasc Surg.41:782-8. 2005.

156. Pu LL. Small intestinal submucosa (Surgisis) as a bioactive prosthetic material for repair of abdominal wall fascial defect. Plast Reconstr Surg.115:2127-31. 2005.

157. Sardeli C, Axelsen SM, Bek KM. Use of porcine small intestinal submucosa in the surgical treatment of recurrent rectocele in a patient with Ehlers-Danlos syndrome type III. Int Urogynecol J Pelvic Floor Dysfunct.16:504-5. 2005.

158. Schultheiss D, Gabouev AI, Cebotari S, Tudorache I, Walles T, Schlote N, et al. Biological vascularized matrix for bladder tissue engineering: matrix preparation, reseeding technique and short-term implantation in a porcine model. J Urol.173:276-80. 2005.

159. Ueno T, Pickett LC, de la Fuente SG, Lawson DC, Pappas TN. Clinical application of porcine small intestinal submucosa in the management of infected or potentially contaminated abdominal defects. J Gastrointest Surg.8:109-12. 2004.

160. Hodde J, Janis A, Hiles M. Effects of sterilization on an extracellular matrix scaffold: part II. Bioactivity and matrix interaction. Journal of materials science.18:545-50. 2007.

161. Hodde JP, Record RD, Tullius RS, Badylak SF. Retention of endothelial cell adherence to porcine-derived extracellular matrix after disinfection and sterilization. Tissue engineering.8:225-34. 2002.

162. Gilbert TW, Stewart-Akers AM, Sydeski J, Nguyen TD, Badylak SF, Woo SL. Gene expression by fibroblasts seeded on small intestinal submucosa and subjected to cyclic stretching. Tissue engineering.13:1313-23. 2007.

163. Sellaro TL, Ravindra AK, Stolz DB, Badylak SF. Maintenance of Hepatic Sinusoidal Endothelial Cell Phenotype In Vitro Using Organ-Specific Extracellular Matrix Scaffolds. Tissue Eng. 2007.

164. Freytes DO, Tullius RS, Badylak SF. Effect of storage upon material properties of lyophilized porcine extracellular matrix derived from the urinary bladder. Journal of biomedical materials research.78:327-33. 2006.

165. Freytes DO, Tullius RS, Valentin JE, Stewart-Akers AM, Badylak SF. Hydrated versus lyophilized forms of porcine extracellular matrix derived from the urinary bladder. J Biomed Mater Res A. 2008.

166. Badylak SF, Valentin JE, Ravindra AK, McCabe GP, Stewart-Akers AM. Macrophage phenotype as a determinant of biologic scaffold remodeling. Tissue Eng Part A.14:1835-42. 2008.

167. Whitson BA, Cheng BC, Kokini K, Badylak SF, Patel U, Morff R, et al. Multilaminate resorbable biomedical device under biaxial loading. J Biomed Mater Res.43:277-81. 1998.

168. Crow S. Sterilization practices: past, present, and future. Todays Or-Nurse.15:43-4. 1993.

169. Brown SA, Merritt K, Woods TO, McNamee SG, Hitchins VM. Effects of different disinfection and sterilization methods on tensile strength of materials used for single-use devices. Biomedical Instrumentation & Technology.36:23-7. 2002.

170. Rasmussen TJ, Feder SM, Butler DL, Noyes FR. The effects of 4 Mrad of gamma irradiation on the initial mechanical properties of bone-patellar tendon-bone grafts. Arthroscopy.10:188-97. 1994.

171. Belu AM, Graham DJ, Castner DG. Time-of-flight secondary ion mass spectrometry: techniques and applications for the characterization of biomaterial surfaces. Biomaterials.24:3635-53. 2003.

172. Jackson JE. A user's guide to principal components. New York: Wiley; 1991.

173. Ushiki T. Collagen fibers, reticular fibers and elastic fibers. A comprehensive understanding from a morphological viewpoint. Arch Histol Cytol.65:109-26. 2002.

174. Brown BN, Barnes CA, Kasick RT, Michel R, Gilbert TW, Beer-Stolz D, et al. Surface characterization of extracellular matrix scaffolds. Biomaterials.31:428-37. 2010.

175. Canavan HE, Graham DJ, Cheng X, Ratner BD, Castner DG. Comparison of native extracellular matrix with adsorbed protein films using secondary ion mass spectrometry. Langmuir.23:50-6. 2007.

176. Wagner MS, Castner DG. Characterization of Adsorbed Protein Films by Time-of-Flight Secondary Ion Mass Spectroscopy with Principal Component Analysis. Langmuir.17:4649-60. 2001.

177. Bettinger CJ, Langer R, Borenstein JT. Engineering Substrate Topography at the Micro- and Nanoscale to Control Cell Function. Angew Chem Int Ed Engl. 2009.

178. Flemming RG, Murphy CJ, Abrams GA, Goodman SL, Nealey PF. Effects of synthetic micro- and nano-structured surfaces on cell behavior. Biomaterials.20:573-88. 1999.

179. Loesberg WA, te Riet J, van Delft FC, Schon P, Figdor CG, Speller S, et al. The threshold at which substrate nanogroove dimensions may influence fibroblast alignment and adhesion. Biomaterials.28:3944-51. 2007.

180. Henry JA, Burugapalli K, Neuenschwander P, Pandit A. Structural variants of biodegradable polyesterurethane in vivo evoke a cellular and angiogenic response that is dictated by architecture. Acta Biomater.5:29-42. 2009.

181. Chang DT, Jones JA, Meyerson H, Colton E, Kwon IK, Matsuda T, et al. Lymphocyte/macrophage interactions: biomaterial surface-dependent cytokine, chemokine, and matrix protein production. J Biomed Mater Res A.87:676-87. 2008.

182. Ivirico JL, Salmeron-Sanchez M, Ribelles JL, Pradas MM, Soria JM, Gomes ME, et al. Proliferation and differentiation of goat bone marrow stromal cells in 3D scaffolds with tunable hydrophilicity. J Biomed Mater Res B Appl Biomater. 2009.

183. Hezi-Yamit A, Sullivan C, Wong J, David L, Chen M, Cheng P, et al. Impact of polymer hydrophilicity on biocompatibility: implication for DES polymer design. J Biomed Mater Res A.90:133-41. 2009.

184. Jansen EJ, Sladek RE, Bahar H, Yaffe A, Gijbels MJ, Kuijer R, et al. Hydrophobicity as a design criterion for polymer scaffolds in bone tissue engineering. Biomaterials.26:4423-31. 2005.

185. Bernards MT, Qin C, Ratner BD, Jiang S. Adhesion of MC3T3-E1 cells to bone sialoprotein and bone osteopontin specifically bound to collagen I. J Biomed Mater Res A.86:779-87. 2008.

186. Hubbell JA, Massia SP, Desai NP, Drumheller PD. Endothelial cell-selective materials for tissue engineering in the vascular graft via a new receptor. Biotechnology (N Y).9:568-72. 1991.

187. Quirk RA, Kellam B, Bhandari RN, Davies MC, Tendler SJ, Shakesheff KM. Cell-type-specific adhesion onto polymer surfaces from mixed cell populations. Biotechnol Bioeng.81:625-8. 2003.

188. Beckstead BL, Santosa DM, Giachelli CM. Mimicking cell-cell interactions at the biomaterial-cell interface for control of stem cell differentiation. J Biomed Mater Res A.79:94-103. 2006.

189. Liu L, Chen S, Giachelli CM, Ratner BD, Jiang S. Controlling osteopontin orientation on surfaces to modulate endothelial cell adhesion. J Biomed Mater Res A.74:23-31. 2005.

190. Mitragotri S, Lahann J. Physical approaches to biomaterial design. Nat Mater.8:15-23. 2009.

191. Rehfeldt F, Engler AJ, Eckhardt A, Ahmed F, Discher DE. Cell responses to the mechanochemical microenvironment--implications for regenerative medicine and drug delivery. Adv Drug Deliv Rev.59:1329-39. 2007.

192. Engler AJ, Carag-Krieger C, Johnson CP, Raab M, Tang HY, Speicher DW, et al. Embryonic cardiomyocytes beat best on a matrix with heart-like elasticity: scar-like rigidity inhibits beating. J Cell Sci.121:3794-802. 2008.

193. Engler AJ, Sen S, Sweeney HL, Discher DE. Matrix elasticity directs stem cell lineage specification. Cell.126:677-89. 2006.

194. Ghosh K, Ingber DE. Micromechanical control of cell and tissue development: implications for tissue engineering. Adv Drug Deliv Rev.59:1306-18. 2007.

195. Bhrany AD, Beckstead BL, Lang TC, Farwell DG, Giachelli CM, Ratner BD. Development of an esophagus acellular matrix tissue scaffold. Tissue Eng.12:319-30. 2006.

196. Baker MJ, Zheng L, Winograd N, Lockyer NP, Vickerman JC. Mass spectral imaging of glycophospholipids, cholesterol, and glycophorin a in model cell membranes. Langmuir.24:11803-10. 2008.

197. Chilkoti A, Schmierer AE, Perez-Luna VH, Ratner BD. Investigating the relationship between surface chemistry and endothelial cell growth: partial least-squares regression of the static secondary ion mass spectra of oxygen-containing plasma-deposited films. Anal Chem.67:2883-91. 1995.

198. McPherson TB, Liang H, Record RD, Badylak SF. Galalpha(1,3)Gal epitope in porcine small intestinal submucosa. Tissue Eng.6:233-9. 2000.

199. Daly KA, Stewart-Akers AM, Hara H, Ezzelarab M, Long C, Cordero K, et al. Effect of the alphaGal epitope on the response to small intestinal submucosa extracellular matrix in a nonhuman primate model. Tissue Eng Part A.15:3877-88. 2009.

200. Livak KJ, Schmittgen TD. Analysis of relative gene expression data using real-time quantitative PCR and the 2(-Delta Delta C(T)) Method. Methods.25:402-8. 2001.

201. Schmittgen TD, Livak KJ. Analyzing real-time PCR data by the comparative C(T) method. Nat Protoc.3:1101-8. 2008.

202. Skene JH, Willard M. Axonally transported proteins associated with axon growth in rabbit central and peripheral nervous systems. J Cell Biol.89:96-103. 1981.

203. Goslin K, Banker G. Rapid changes in the distribution of GAP-43 correlate with the expression of neuronal polarity during normal development and under experimental conditions. J Cell Biol.110:1319-31. 1990.

204. Hoffman PN. Expression of GAP-43, a rapidly transported growth-associated protein, and class II beta tubulin, a slowly transported cytoskeletal protein, are coordinated in regenerating neurons. J Neurosci.9:893-7. 1989.

205. Chen GY, Nunez G. Sterile inflammation: sensing and reacting to damage. Nature reviews. 2010.

206. Lotze MT, Zeh HJ, Rubartelli A, Sparvero LJ, Amoscato AA, Washburn NR, et al. The grateful dead: damage-associated molecular pattern molecules and reduction/oxidation regulate immunity. Immunol Rev.220:60-81. 2007.

207. Allen RA, Seltz LM, Jiang H, Kasick RT, Sellaro TL, Badylak SF, et al. Adrenal extracellular matrix scaffolds support adrenocortical cell proliferation and function in vitro. Tissue Eng Part A.16:3363-74. 2010.

208. Sellaro TL, Ravindra AK, Stolz DB, Badylak SF. Maintenance of hepatic sinusoidal endothelial cell phenotype in vitro using organ-specific extracellular matrix scaffolds. Tissue Eng.13:2301-10. 2007.

209. Brown BN, Fruend JM, Li H, Rubin PJ, Reing JE, Jeffries EM, et al. Comparison of Three Methods for the Derivation of a Biologic Scaffold Composed of Adipose Tissue Extracellular Matrix. Tissue Eng Part C Methods. 2010.

210. Nam KN, Choi YS, Jung HJ, Park GH, Park JM, Moon SK, et al. Genipin inhibits the inflammatory response of rat brain microglial cells. Int Immunopharmacol.10:493-9. 2010.

211. Koo HJ, Lim KH, Jung HJ, Park EH. Anti-inflammatory evaluation of gardenia extract, geniposide and genipin. J Ethnopharmacol.103:496-500. 2006.

212. Koo HJ, Song YS, Kim HJ, Lee YH, Hong SM, Kim SJ, et al. Antiinflammatory effects of genipin, an active principle of gardenia. Eur J Pharmacol.495:201-8. 2004.

213. Badylak SF. Xenogeneic extracellular matrix as a scaffold for tissue reconstruction. Transpl Immunol.12:367-77. 2004.

214. Porcheray F, Viaud S, Rimaniol AC, Leone C, Samah B, Dereuddre-Bosquet N, et al. Macrophage activation switching: an asset for the resolution of inflammation. Clin Exp Immunol.142:481-9. 2005.

215. Stout RD, Suttles J. Immunosenescence and macrophage functional plasticity: dysregulation of macrophage function by age-associated microenvironmental changes. Immunol Rev.205:60-71. 2005.

216. Stout RD, Jiang C, Matta B, Tietzel I, Watkins SK, Suttles J. Macrophages sequentially change their functional phenotype in response to changes in microenvironmental influences. J Immunol.175:342-9. 2005.

217. Crisan M, Yap S, Casteilla L, Chen CW, Corselli M, Park TS, et al. A perivascular origin for mesenchymal stem cells in multiple human organs. Cell Stem Cell.3:301-13. 2008.

218. Parker W, Stitzenberg KB, Yu PB, Pratt VS, Nakamura YC, Farel LS, et al. Biophysical characteristics of anti-Gal(alpha)1-3Gal IgM binding to cell surfaces: implications for xenotransplantation. Transplantation.71:440-6. 2001.

219. Galili U. The alpha-gal epitope (Gal alpha 1-3Gal beta 1-4GlcNAc-R) in xenotransplantation. Biochimie.83:557-63. 2001.

220. Xu H, Wan H, Sandor M, Qi S, Ervin F, Harper JR, et al. Host response to human acellular dermal matrix transplantation in a primate model of abdominal wall repair. Tissue Eng Part A.14:2009-19. 2008.

221. Lolmede K, Campana L, Vezzoli M, Bosurgi L, Tonlorenzi R, Clementi E, et al. Inflammatory and alternatively activated human macrophages attract vessel-associated stem cells, relying on separate HMGB1- and MMP-9-dependent pathways. Journal of leukocyte biology.85:779-87. 2009.

222. Moestrup SK, Moller HJ. CD163: a regulated hemoglobin scavenger receptor with a role in the anti-inflammatory response. Ann Med.36:347-54. 2004.

223. Agrawal V, Johnson SA, Reing J, Zhang L, Tottey S, Wang G, et al. Epimorphic regeneration approach to tissue replacement in adult mammals. Proc Natl Acad Sci U S A.107:3351-5. 2010.

224. Mooney JE, Rolfe BE, Osborne GW, Sester DP, van Rooijen N, Campbell GR, et al. Cellular plasticity of inflammatory myeloid cells in the peritoneal foreign body response. Am J Pathol.176:369-80. 2010.

225. Turner NJ, Yates AJ, Jr., Weber DJ, Qureshi IR, Stolz DB, Gilbert TW, et al. Xenogeneic extracellular matrix as an inductive scaffold for regeneration of a functioning musculotendinous junction. Tissue Eng Part A.16:3309-17. 2010.

226. Rollman GB, Gillespie JM. The role of psychosocial factors in temporomandibular disorders. Curr Rev Pain.4:71-81. 2000.

227. Oakley M, Vieira AR. The many faces of the genetics contribution to temporomandibular joint disorder. Orthod Craniofac Res.11:125-35. 2008.

228. Tanaka E, Detamore MS, Mercuri LG. Degenerative disorders of the temporomandibular joint: etiology, diagnosis, and treatment. J Dent Res.87:296-307. 2008.

229. Farrar WB, McCarty WL, Jr. The TMJ dilemma. J Ala Dent Assoc.63:19-26. 1979.

230. Hall HD, Indresano AT, Kirk WS, Dietrich MS. Prospective multicenter comparison of 4 temporomandibular joint operations. J Oral Maxillofac Surg.63:1174-9. 2005.

231. Nyberg J, Adell R, Svensson B. Temporomandibular joint discectomy for treatment of unilateral internal derangements--a 5 year follow-up evaluation. Int J Oral Maxillofac Surg.33:8-12. 2004.

232. Krug J, Jirousek Z, Suchmova H, Cermakova E. Influence of discoplasty and discectomy of the temporomandibular joint on elimination of pain and restricted mouth opening. Acta Medica (Hradec Kralove).47:47-53. 2004.

233. Vazquez-Delgado E, Valmaseda-Castellon E, Vazquez-Rodriguez E, Gay-Escoda C. Long-term results of functional open surgery for the treatment of internal derangement of the temporomandibular joint. Br J Oral Maxillofac Surg.42:142-8. 2004.

234. McCain JP, Sanders B, Koslin MG, Quinn JH, Peters PB, Indresano AT. Temporomandibular joint arthroscopy: a 6-year multicenter retrospective study of 4,831 joints. J Oral Maxillofac Surg.50:926-30. 1992.

235. Kaneyama K, Segami N, Sato J, Murakami K, Iizuka T. Outcomes of 152 temporomandibular joints following arthroscopic anterolateral capsular release by holmium: YAG laser or electrocautery. Oral Surg Oral Med Oral Pathol Oral Radiol Endod.97:546-51; discussion 52. 2004.

236. Nitzan DW, Samson B, Better H. Long-term outcome of arthrocentesis for sudden-onset, persistent, severe closed lock of the temporomandibular joint. J Oral Maxillofac Surg.55:151-7; discussion 7-8. 1997.

237. Reston JT, Turkelson CM. Meta-analysis of surgical treatments for temporomandibular articular disorders. J Oral Maxillofac Surg.61:3-10; discussion -2. 2003.

238. Westesson PL, Eriksson L, Lindstrom C. Destructive lesions of the mandibular condyle following diskectomy with temporary silicone implant. Oral Surg Oral Med Oral Pathol.63:143-50. 1987.

239. Dolwick MF, Aufdemorte TB. Silicone-induced foreign body reaction and lymphadenopathy after temporomandibular joint arthroplasty. Oral Surg Oral Med Oral Pathol.59:449-52. 1985.

240. Ferreira JN, Ko CC, Myers S, Swift J, Fricton JR. Evaluation of surgically retrieved temporomandibular joint alloplastic implants: pilot study. J Oral Maxillofac Surg.66:1112-24. 2008.

241. Dimitroulis G. The use of dermis grafts after discectomy for internal derangement of the temporomandibular joint. J Oral Maxillofac Surg.63:173-8. 2005.

242. Matukas VJ, Lachner J. The use of autologous auricular cartilage for temporomandibular joint disc replacement: a preliminary report. J Oral Maxillofac Surg.48:348-53. 1990.

243. Meyer RA. The autogenous dermal graft in temporomandibular joint disc surgery. J Oral Maxillofac Surg.46:948-54. 1988.

244. Pogrel MA, Kaban LB. The role of a temporalis fascia and muscle flap in temporomandibular joint surgery. J Oral Maxillofac Surg.48:14-9. 1990.

245. Thyne GM, Yoon JH, Luyk NH, McMillan MD. Temporalis muscle as a disc replacement in the temporomandibular joint of sheep. J Oral Maxillofac Surg.50:979-87; discussion 87-8. 1992.

246. Ota T, Gilbert TW, Badylak SF, Schwartzman D, Zenati MA. Electromechanical characterization of a tissue-engineered myocardial patch derived from extracellular matrix. J Thorac Cardiovasc Surg.133:979-85. 2007.

247. Beattie AJ, Gilbert TW, Guyot JP, Yates AJ, Badylak SF. Chemoattraction of progenitor cells by remodeling extracellular matrix scaffolds. Tissue Eng.doi: 10.1089/ten.tea.2008.0162. 2008.

248. Bulgheroni P, Murena L, Ratti C, Bulgheroni E, Ronga M, Cherubino P. Follow-up of collagen meniscus implant patients: Clinical, radiological, and magnetic resonance imaging results at 5years. Knee. 2009.

249. Buma P, van Tienen T, Veth R. The collagen meniscus implant. Expert Rev Med Devices.4:507-16. 2007.

250. Gastel JA, Muirhead WR, Lifrak JT, Fadale PD, Hulstyn MJ, Labrador DP. Meniscal tissue regeneration using a collagenous biomaterial derived from porcine small intestine submucosa. Arthroscopy.17:151-9. 2001.

251. Brown BN, Barnes CA, Kasick RT, Michel R, Gilbert TW, Beer-Stolz D, et al. Surface characterization of extracellular matrix scaffolds. Biomaterials.31:428-37.

252. Tanaka E, Detamore MS, Tanimoto K, Kawai N. Lubrication of the temporomandibular joint. Ann Biomed Eng.36:14-29. 2008.

253. Grayson WL, Frohlich M, Yeager K, Bhumiratana S, Chan ME, Cannizzaro C, et al. Regenerative Medicine Special Feature: Engineering anatomically shaped human bone grafts. Proc Natl Acad Sci U S A.107:3299-304.

254. Snider GR, Lomakin J, Singh M, Gehrke SH, Detamore MS. Regional dynamic tensile properties of the TMJ disc. J Dent Res.87:1053-7. 2008.

255. Wang L, Lazebnik M, Detamore MS. Hyaline cartilage cells outperform mandibular condylar cartilage cells in a TMJ fibrocartilage tissue engineering application. Osteoarthritis Cartilage.17:346-53. 2009.

256. Singh M, Detamore MS. Tensile properties of the mandibular condylar cartilage. J Biomech Eng.130:011009. 2008.

257. Wang L, Detamore MS. Tissue engineering the mandibular condyle. Tissue Eng.13:1955-71. 2007.

258. Detamore MS, Hegde JN, Wagle RR, Almarza AJ, Montufar-Solis D, Duke PJ, et al. Cell type and distribution in the porcine temporomandibular joint disc. J Oral Maxillofac Surg.64:243-8. 2006.

259. Detamore MS, Athanasiou KA. Evaluation of three growth factors for TMJ disc tissue engineering. Ann Biomed Eng.33:383-90. 2005.

260. Detamore MS, Athanasiou KA. Motivation, characterization, and strategy for tissue engineering the temporomandibular joint disc. Tissue Eng.9:1065-87. 2003.

261. Detamore MS, Athanasiou KA. Structure and function of the temporomandibular joint disc: implications for tissue engineering. J Oral Maxillofac Surg.61:494-506. 2003.

262. Bean AC, Almarza AJ, Athanasiou KA. Effects of ascorbic acid concentration on the tissue engineering of the temporomandibular joint disc. Proc Inst Mech Eng H.220:439-47. 2006.

263. Almarza AJ, Athanasiou KA. Effects of hydrostatic pressure on TMJ disc cells. Tissue Eng.12:1285-94. 2006.

264. Almarza AJ, Bean AC, Baggett LS, Athanasiou KA. Biochemical analysis of the porcine temporomandibular joint disc. Br J Oral Maxillofac Surg.44:124-8. 2006.

265. Detamore MS, Orfanos JG, Almarza AJ, French MM, Wong ME, Athanasiou KA. Quantitative analysis and comparative regional investigation of the extracellular matrix of the porcine temporomandibular joint disc. Matrix Biol.24:45-57. 2005.

266. Almarza AJ, Athanasiou KA. Seeding techniques and scaffolding choice for tissue engineering of the temporomandibular joint disk. Tissue Eng.10:1787-95. 2004.

267. Lumpkins SB, McFetridge PS. Regional variations in the viscoelastic compressive properties of the temporomandibular joint disc and implications toward tissue engineering. J Biomed Mater Res A.90:784-91. 2009.

268. Lumpkins SB, Pierre N, McFetridge PS. A mechanical evaluation of three decellularization methods in the design of a xenogeneic scaffold for tissue engineering the temporomandibular joint disc. Acta Biomater.4:808-16. 2008.

269. Elder BD, Eleswarapu SV, Athanasiou KA. Extraction techniques for the decellularization of tissue engineered articular cartilage constructs. Biomaterials.30:3749-56. 2009.

270. Elder BD, Athanasiou KA. Synergistic and additive effects of hydrostatic pressure and growth factors on tissue formation. PLoS One.3:e2341. 2008.

271. Johns DE, Wong ME, Athanasiou KA. Clinically relevant cell sources for TMJ disc engineering. J Dent Res.87:548-52. 2008.

272. Allen KD, Athanasiou KA. Scaffold and growth factor selection in temporomandibular joint disc engineering. J Dent Res.87:180-5. 2008.

273. Johns DE, Athanasiou KA. Design characteristics for temporomandibular joint disc tissue engineering: learning from tendon and articular cartilage. Proc Inst Mech Eng H.221:509-26. 2007.

274. Johns DE, Athanasiou KA. Improving culture conditions for temporomandibular joint disc tissue engineering. Cells Tissues Organs.185:246-57. 2007.

275. Allen KD, Athanasiou KA. Tissue Engineering of the TMJ disc: a review. Tissue Eng.12:1183-96. 2006.